MODELING, BEHAVIOR AND DESIGN OF COLLAPSE-RESISTANT STEEL FRAME BUILDINGS

By

Honghao Li

A dissertation submitted in partial fulfillment
of the requirements for the degree of
Doctor of Philosophy
(Civil Engineering)
In the University of Michigan
2013

Doctoral Committee:

Professor Sherif El-Tawil, Chair
Professor Krishnakumar R. Garikipati
Assistant Professor Jason P. McCormick
Professor James K. Wight

DEDICATION

To my parents
Shaoguang Li and Fanmei Meng

ACKNOWLEDGEMENTS

During my past five years as a graduate student in the Department of Civil and Environmental Engineering at the University of Michigan, I received help and support from many people. I would like to take this opportunity to express my gratitude towards all of these individuals.

Foremost I would like to acknowledge my academic advisor, Professor Sherif El-Tawil. I cannot make this happen without his instruction, guidance, inspiration, and financial support. He took great amount of time to train me and help me to develop my proficiency as a researcher and instructor gradually. Professor El-Tawil is my teacher, my mentor, and my role model. What I have received from him is not only knowledge, but also spirits which will benefit my entire life. Sincere thanks are given to my dissertation committee members, Professor James K. Wight, Professor Jason P. McCormick, and Professor Krishna R. Garikipati for their kind help and valuable advice.

I would also like to thank my fellow colleagues and friends from the CEE community at the University of Michigan, Dr. Kittinun Sirijaroonchai, Professor Dongjoo Kim, Dr. Supat Suwwanakarn, Professor Chung-Chan Hung, Professor Yasser Alashker, Professor Philip Park, Professor Kay Wille, Jieshi Fang, Julie Fogarty, Sukhoon Pyo, Mo Alkaysi, Professor Mattew Fadden, Xiaohu Fan, Qianru Guo, Qian Zhang, and Yao Zhang, for their support.

Finally, I would like to dedicate this doctoral dissertation to my beloved parents, Shaoguang Li and Fanmei Meng. I love them to death.

TABLE OF CONTENTS

LIST OF TABLES

LIST OF FIGURES

ABSTRACT

MODELING, BEHAVIOR AND DESIGN OF COLLAPSE-RESISTANT STEEL FRAME BUILDINGS

Chair: Sherif El-Tawil

Progressive collapse is a complex process in which failure of a single component leads to collapse of a disproportionately large part of the structural system. Recent building and bridge failures have highlighted the seriousness of such events and generated widespread research interest. The objective of this study is to address current gaps in the progressive collapse research area, focusing specifically on seismically-designed steel frame structures.

Four different types of nonlinear dynamic computational models are created for a prototype 10-story special moment frame building. The models include a 3-D micro-model, 3-D macro-model, planar micro-model and planar macro-model. After calibration and validation, the models are used to conduct a comprehensive study of the effect of various types of modeling approximations on simulated collapse behavior. The numerical results show that accounting for 3-D effects, specifically the floor slab, is critical for accurate collapse modeling. It is also shown that well-calibrated macro-models can be accurate and that the results of planar analyses are not necessarily conservative.

Simulation results suggest that the prototype building is more vulnerable to loss of columns in the upper stories than in the lower ones and is particularly vulnerable to loss of interior gravity columns at all floor levels. The simulation models are used to clarify the role of different structural components and parameters at the various stages of collapse response. The floor slab is shown to contribute significantly to the robustness of the structure, especially at the early stages of collapse; however, it is a double edge sword that can also be detrimental in the final stages of collapse.

Design requirements in the Unified Facilities Criteria published by the US Department of Defense are evaluated using the developed models. Simulations studies show that the Tie Force Method is effective in protecting buildings from progressive collapse and can significantly reduce deformation under column loss scenarios. However, the Dynamic Impact Factor proposed in the document is deemed to be inaccurate and a new energy-based approach is proposed to assess the peak dynamic displacement. The new method is shown to be accurate and reasonably conservative.

CHAPTER 1

INTRODUCTION

1.1 General Introduction

The performance of building structures under abnormal loading conditions, such as blast and vehicle and aircraft impact, is of interest to researchers and engineers because of the possibility for progressive collapse. In ASCE Standard 7-10: Minimum Design Loads for Buildings and Other Structures, progressive collapse is referred to as "*the spread of an initial local failure from element to element, resulting eventually in the collapse of an entire structure or a disproportionately large part of it*". Although the probability of a building structure being subjected to abnormal loads is small, the consequence may be catastrophic. There are many examples in history in which structural failures and collapse of buildings resulted in huge economic damage and extensive loss of human lives.

The first research in progressive collapse was motivated by the partial collapse of Ronan Point Tower in England, caused by a gas explosion in 1968. Since then, several high profile events have fueled interest in this topic, including the 1995 bombing of the Alfred P. Murrah Federal Building in Oklahoma City and the 9/11 event, which led to the collapse of the twin towers of the World Trade Center in New York City and killed nearly 3,000 people. Although many recent studies have been conducted, the field is still nascent and many questions abound about how various types of buildings behave on the

verge of collapse, how the collapse process unfolds, and how to best design buildings to mitigate the potentially catastrophic effects of collapse.

Based on the research that has been conducted to date, there is consensus within the structural engineering community that in order to mitigate progressive collapse, a structure must have one or preferably more of the following attributes: (1) adequate system strength, stiffness, and ductility; (2) enough local strength and ductility to prevent initiation of the collapse process; (3) structural redundancy to provide alternative load paths; and (4) interconnection of structural and nonstructural components to minimize debris projectiles. There is also agreement that common mechanisms that contribute to the progressive collapse resistance of a system can include: (1) catenary action of slabs and beams allowing gravity loads to span adjacent elements; (2) frame action above a damaged column; and (3) support provided by nonstructural elements such as partitions and infills. However, these specific mechanisms have not been adequately studied to date and there is little quantitative information about how they are initiated and for how long they maintain their effectiveness during the collapse process.

1.1.1 SEISMIC DESIGN AND PROGRESSIVE COLLAPSE

There is a notion in the structural engineering community that a seismically designed structure has higher resistance to progressive collapse than one designed without taking into account seismic considerations. The idea is that seismic detailing leads to more ductile structures, which may have a better response during collapse – although this has not been undisputedly proven to date. Recent research has shown that seismic detailing does play some beneficial role in the collapse response of both steel and concrete structures (Khandewal et al., 2008 and Bao et al., 2008). However, Khandelwal et al. (2008) noted that choosing a better layout of moment resisting frames was more influential than using strict seismic detailing in ensuring good collapse resistance. Therefore, research is needed to investigate how seismically designed buildings collapse

under gravity loading, identify what mechanisms are activated during the collapse process and clarify how those mechanisms can benefit from seismic detailing, if at all.

1.1.2 Numerical Modeling of Progressive Collapse

Collapse models can be planar or 3-D. They can also be linear or nonlinear. Linear models are simpler to develop and more convenient, especially that most existing commercial analysis software can solve linear models. However, a critical drawback of linear models is that they cannot capture the progression of structural behavior that occurs during collapse, in particular, the force redistribution that occurs as a result of local nonlinear behavior. Nonlinear models are able to represent the collapse response more accurately than linear models. Geometric and material nonlinearities are necessarily present in this type of problem and both must be adequately modeled to achieve reasonable results.

Collapse models can also be classified as micro-models and macro-models (Khandelwal et al., 2008). A micro-model is a physical-based, high fidelity, continuum finite element model which is able to capture both local and global responses of a structure accurately. The emphasis in the former is on generalized strain and/or generalized stress behavior (for example, curvature and/or bending moment behavior) as opposed to pointwise constitutive response in the latter. Micro models require extensive computational resources and time. In the latter class of models, a combination of beam-column and discrete spring finite elements are used to simulate the overall response of a structure. Macro-models are able to mimic, in a phenomenological sense, the local and global responses of importance to the physical processes being modeled. Macro-models are fast running and fairly simple to build and run. They are therefore suited for use in a design office environment.

The above discussion clearly indicates that a number of critical choices and assumptions must necessarily be made when the collapse response of structures is investigated using

simulation models. The type and extent of modeling assumptions depend on the computational resources available, modeling expertise, and results sought. Systematic studies are therefore needed to determine what minimum level of modeling is required for accurate assessment of collapse potential.

1.1.3 Designing against Progressive Collapse

ASCE 7-10 (2010) is the only mainstream standard in the US that addresses the issue of collapse in some detail. It specifies two design alternatives: a direct design method (the alternate path method), which considers explicit conditions for analysis when specific members are no longer capable of supporting load, and the indirect design method, which includes implicit considerations that would enhance resistance to collapse through provision of minimum levels of strength, continuity and ductility. The provisions to prevent collapse in the Unified Facilities Criteria (DoD 2009), General Services Administration (GSA 2003) as well as the ISC Security Criteria (2001) are based on a similar philosophy to that in ASCE 7-10 (2010), albeit with more detail. Many of the provisions originate from TM5-1300 (1990), which is one of the earliest specifications to deal with collapse resistant design. The GSA (2003) and Unified Facilities Criteria (DoD 2009) criteria, in particular, specify the alternate path method as one of several alternatives, and promote linear and nonlinear analysis techniques to check structural members in the alternate path structure. Both documents are geared towards blast hazards and their primary intent is to protect a building that has lost critical structural members to a blast. The design approaches in the Unified Facilities Criteria (DoD 2009) document vary according to the building occupancy.

Although much research has been done to develop these provisions, their conservatism and effectiveness in protecting buildings from progressive collapse under column-loss scenarios still needs to be evaluated through experimentation and simulation. The DoD guidelines (UFC, 2009), in particular, need refinement because they were modeled after

seismic performance based design guidelines and have yet to be fully adapted for gravity-induce collapse situations.

1.2 Objectives

The overall objective of this dissertation is to use computational structural simulation models, calibrated and validated against available test data and more refined finite element analyses, to investigate the structural robustness of seismically designed steel structural systems subjected to loss of one or more critical structural members. Specific objectives are as follows:

(1) Develop several types of computational models for a seismically designed steel moment resisting frame structure, including a planar micro-model, a planar macro-scale model, a three-dimensional micro-scale model and a three-dimensional macro-scale model.

(2) Investigate the value of modeling 3-D effects, study the effect of making various modeling approximations on system response and determine the minimum level of modeling that is required for accurate assessment of collapse potential.

(3) Use the developed models to quantitatively study the sources of collapse resistance in steel moment resisting system, including the contributions of the slabs, composite action and system-wide frame effects.

(4) Conduct extensive case studies using buildings with different height and structural layouts to verify whether DoD guidelines (UFC, 2009) can protect the building from progressively collapsing after loss of critical load-bearing structural components. Propose new design approach if flaws are found.

1.3 Structure of the Dissertation

This dissertation is comprised of seven Chapters. Chapter 1 provides general information about this study. Chapter 2 reviews the work that has been done related to progressive building collapse. Chapter 3 to Chapter 6 addresses objectives 1 to 4. The final chapter summarizes this study and draws key conclusions. Following is a brief description of these 7 chapters:

Chapter 1: Introduction. General information about this study is provided. Gaps in our understanding of progressive collapse and problems that need to be addressed are outlined. The objective and structure of this dissertation are also highlighted.

Chapter 2: Literature Survey. This chapter discusses the state-of-the-art in collapse-resistant design, modeling and testing, with specific focus on steel and composite steel-concrete structures.

Chapter 3: Numerical Model Development for Progressive Collapse Analysis. Four types of computational models of a seismically designed steel structure are created, including a detailed micro-based model of the full 3-D system, a model of the full 3-D system composed of macro-elements, a micro-based model of a single frame in the system, and a macro-scale model of a single frame in the system. All of the models are calibrated and validated against available test data and more refined finite element analyses.

Chapter 4: Approximations in Progressive Collapse Modeling. The ability of the various types of models developed in Chapter 3 to represent system-wide progressive collapse is discussed in a quantitative manner. The topics considered include: 1) the accuracy of planar simplifications of 3-D system response, 2) the level of conservatism that exists, if any, in planar representations of system behavior, and 3) the ability of models with macro-elements to accurately capture the behavior of a collapsing system.

Chapter 5: Three-Dimensional Effects and Collapse Resistance Mechanisms in Steel Frame Buildings. Building response to loss of internal and external columns in lower, middle and upper floors is investigated. Extensive parametric studies are conducted using the developed 3-D models to investigate the influence of a number of parameters on collapse resistance. Specifically, the sources of resistance that contribute to structural robustness are quantified, including the contribution of the slabs, focusing in particular on the role of composite action between the slab and underlying steel beams, slab membrane action and system-wide frame action.

Chapter 6: Verification of Design Requirements in DoD Guidelines. Three-dimensional macro-based models are used to investigate how effectively the Tie Method proposed in the DoD guidelines (UFC, 2009) enhances collapse resistance. After assessing existing provisions for the calculation of the dynamic increase factor (DIF) used in nonlinear static procedures, a new energy-based method for calculating DIF is proposed and verified using buildings with different heights, connection types, and structural layouts.

Chapter 7: Summary and Conclusions. This study is summarized in this chapter and the conclusions drawn from the research conducted are presented. Recommendations for future research in the area of structural robustness are also presented.

CHAPTER 2

LITERATURE SURVEY

2.1 Introduction

This chapter discusses the state-of-the-art in collapse-resistant design, modeling and testing, with specific focus on steel and composite steel-concrete structures. Several mile stone events in progressive collapse research history are first described in Section 2.2. In Section 2.3, computational models for progressive collapse are reviewed. Specifically, modeling for progressive collapse simulations is discussed in Section 2.3.1. Modeling considerations, including joint models, member models, floor system models, constitutive models of steel, system studies and other simulation technologies are presented in Section 2.3.2 through Section 2.3.8. This is followed by a description of methods for assessment and quantification of structural robustness in Section 2.4 and other analysis methods for progressive collapse in Section 2.5. Experimental studies that have been conducted to investigate progressive collapse behavior are surveyed in Section 2.6. Studies related to probabilistic analysis of progressive collapse are reviewed in Section 2.7. Enhancement of system collapse resistance, including retrofitting and designing against progressive collapse, is discussed in Section 2.8.

2.2 Mile Stone Events

There are several historical events, which have significantly motivated and promoted research in this field. The first interest in progressive collapse research is widely attributed to the 1968 partial collapse of Ronan Point tower in England, where a gas explosion on the 18th floor led to a cascade of failures that destroyed the entire corner of the building (Griffiths et al. 1968). The collapse of the building was attributed to: (1) inadequate redundancy of the structural system; (2) weak connections of floor and wall panels; (3) lack of continuity; and (4) poor energy absorption ability (Nair, 2004). This event prompted numerous studies in the progressive collapse area, including Ferahian (1972), McGuire (1975), Lewicki et al. (1974), McGuire (1975), Leyendecker and Ellingwood (1977), Popoff (1977), Ellingwood and Leyendecker (1978), Ellingwood et al. (1978) and Arora et al. (1980), Gross and McGuire (1983), McConnel et al. (1983), Casciati et al. (1984) and Pretlove (1986). More recently, Pearson and Norbert Delatte (2005) reviewed the investigations of the Ronan Point collapse and confirmed that the building was deeply flawed in both design and construction. The Ronan Point event influenced many countries, including the United States to adopt some form of structural integrity or "robustness" provisions in their design codes and guidelines. However, these remained rudimentary until recent events prompted more detailed and comprehensive guidelines to be developed.

Another event deemed particularly influential in promoting the development of new robustness guidelines is the 1995 bombing of the Alfred P. Murrah Federal Building in Oklahoma City, where a truck bomb explosion resulted in massive damage of the building. The 9-story reinforced concrete building was an office building for the United States government. A transfer girder at the third floor level on the north side of the building, which transferred the weight of 10 building columns to 5 columns down to the ground, was destroyed by the bomb. Girder failure is believed to have precipitated collapse of the building, which killed 168 people and injured 500 more.

The Murrah bombing is undisputedly a classic case of progressive collapse, where loss of a set of reinforced concrete columns precipitated subsequent widespread failure of the building. Corley et al. (1998) published three papers regarding collapse of the Murrah Building. In their first paper, (Mlakar et al. 1998), blast loading and its effect on the building were investigated. The authors claimed that the energy released by the explosion was equivalent to that from the detonation of 1,814 kg of trinitrotoluene (TNT). The blast removed one column directly and the associated air blast led to failures of two more. Slabs were also damaged because of the explosion. The damage caused by the blast, the failure mechanism for the building and engineering details of the building were described in their second paper (Sozen, et al. 1998). The loss of the three columns caused the transfer girder supporting the upper portion of the building to fail promoting further failure. It was found that the building would have collapsed had even a single column been lost. Another conclusion was that use of continuity reinforcement and column shear reinforcement may have reduced the potential for progressive building collapse. The authors proposed recommendations for mitigating progressive collapse in their third paper (Corley et al. 1998), including the use of compartmentalized construction, special moment frames and dual systems for new buildings, and the use of extra structural walls, supplemental supporting frames and column jacketing for existing buildings. One of the key conclusions was that seismic detailing could contribute to the collapse resistance of the structure.

Osteraas (2006) reviewed the blast damage and collapse patterns of the Murrah Federal Building. He claimed that the collapse was a result of the combined effect of the blast, which destroyed one column and large portions of the slabs in the second, third and probably part of the fourth floor, and the structural configuration of the building, which lead to loss of lateral bracing of the other three buckled columns. The author speculated that ductile detailing could have improved the performance of the building subjected to abnormal loads.

From these two tragic events, researchers learned that civil structures need to have enough local strength and ductility to avoid the initiation of progressive collapse.

Furthermore, in order to prevent occurrence of progressive collapse under extreme load events, system strength, stiffness, ductility, structural redundancy and integrity are all critical and must be adequately ensured.

On 9/11/01, the twin towers of the World Trade Center collapsed after each of them was hit by a Boeing 767 jet airliner. The fuel carried by the aircraft caused large fires and 56 minutes after the first impact, the south tower collapsed. The north tower fell half an hour later, after burning for approximately 102 minutes. Nearly 3,000 people lost their lives in this tragedy. The collapse of the twin towers was investigated by many researchers and federal agencies and, even though there is still debate within the structural engineering community about whether the collapse is in fact a true case of progressive collapse, it motivated numerous studies of the event itself and progressive collapse in general. The controversy stems from dispute about whether the parts of the structure weakened by the fires were 'small' with respect to the rest of the structure, i.e. whether the failure was disproportionate to the initiating event.

The investigation conducted by the National Institute of Standard and Technology (NIST) (2005) revealed that the buildings had enough robustness of withstand the impact of the aircrafts and it was a different combination of impact damage and heat-weakened structural components that caused the collapse of the buildings. Furthermore, the report noted that the buildings would likely have survived had the thermal insulation not been widely dislodged by the aircraft impact and subsequent blast.

After analyzing the failure sequences of the twin towers and the key factors that led to their collapse, it was recommended that progressive collapse be prevented in buildings through the development and nationwide adoption of consensus standards and code provisions, along with the tools and guidelines for their use in practice. Specifically, the capability to prevent progressive collapse due to abnormal loads should include: (1) comprehensive design rules and practice guides; (2) evaluation criteria, methodology, and tools for assessing the vulnerability of structures to progressive collapse; (3) performance-based criteria for abnormal load and load combinations; (4) analytical tools

to predict potential collapse mechanism; and (5) computer models and analysis procedures for use in routine design practice.

Bažant and Zhou (2002) conducted a simplified approximate analysis of the overall collapse of the WTC towers. The analysis revealed that failures of columns in a single floor due to long time exposure to fires could induce collapse of the whole building due to the impact of the upper part on lower part of the building. Newland and Cebon proposed a method that they thought could prevent this type of progressive collapse, i.e. by introducing collapse barriers. The collapse barriers, which consisted of foam impact-absorbing material, could arrest the downward traveling stress wave which caused the structural collapse of the WTC towers.

Cherepanov (2006) compared two theories for the WTC collapse, i.e. the theory of progressive failure and the theory of fracture waves. The results obtained by the former contradicted the observed free fall. The latter showed that the WTC towers "disintegrated at the very beginning of each collapse", thus free fall of the building fragments was suggested. Bažant and Verdure (2007) reviewed the mechanisms of the WTC collapse and developed a dynamic one-dimensional continuum model of progressive collapse. The authors argued that crush-down and crush-up phases of one-dimensional progressive collapse must be distinguished. After formulating and solving the differential equations for these two phases, the authors claimed that the duration of the collapse matched well with the proposed model. Another key conclusion of this study was that "if the total energy loss during the crushing of one story exceeds the kinetic energy impacted to that story, collapse will continue to the next story." Once this criterion was satisfied, progressive collapse would progress because of gravity alone.

Another simplified analysis was performed by Seffen (2008). The author investigated the dynamic behavior in the collapse of the WTC using a variable-mass collapse model. One major conclusion was that the collapse was a result of propagation of instability induced by "near free fall" of the upper part of the building. However, Grabbe (2008) did not agree with the results of this analysis, indicating that some of the assumptions made in the analysis did not agree with physical principles, thus the results were inaccurate. Other

studies related to collapse of the WTC include Cheropanov (2008), Szuladzinski (2007) and Bažant et al. (2008). Although there are still controversies about the mechanism behind the collapse of WTC, it is a common view that the twin towers collapsed because of the fire rather than the impact of the aircrafts.

The rate of research on progressive collapse has intensified in recent years, in response to the previously discussed, highly publicized events. Figure 2 – 1 shows that the yearly rate of published papers has increased by an order of magnitude in just the decade after 9/11. While only 20 papers on progressive collapse (including both journal articles and conference proceedings) between 1992 and 2001, a significant increase in the number of published papers can be observed after the 9/11 event. In fact, the number of papers increased by a factor of nearly 23 times in the next decade (2002 to 2012).

The rapid rate of research has been primarily enabled by significant improvements in modeling and simulation tools, computational hardware and structural testing. However, the risk, cost and effort associated with experimental testing, coupled with the consistent message from modelers about the accuracy and fidelity of their simulation tools, has made computational modeling and simulation primary tools in this research area.

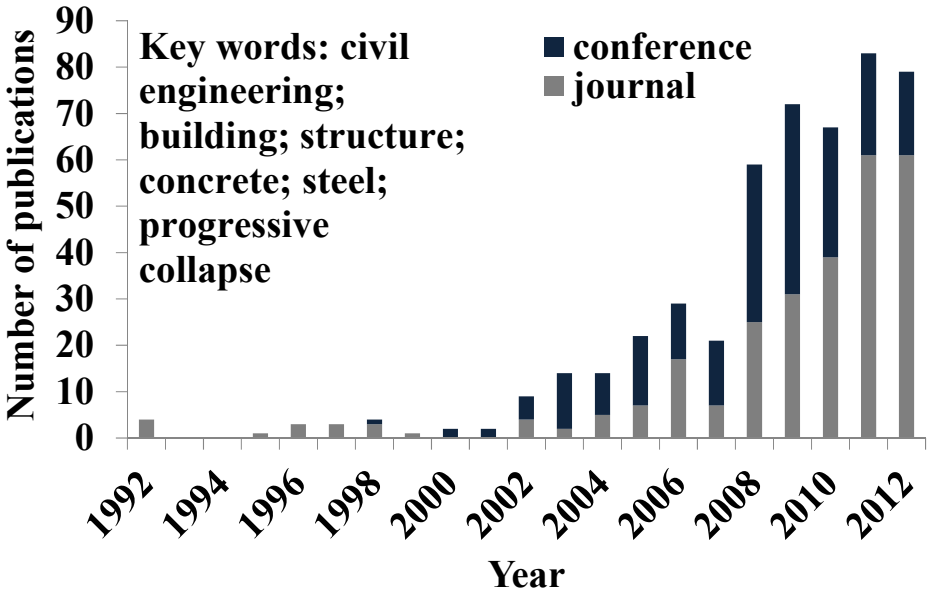

Figure 2 - 1 Statistics for number of published papers on progressive collapse

2.3 Computational Models for Progressive Collapse

Many of the computational models for progressive collapse are direct extensions of models originally developed for earthquake engineering. Following is a discussion of some of the key modeling decisions required to successfully model structures for collapse simulations. The discussion addresses joint models, member models, floor models, constitutive modeling considerations and other modeling techniques that utilize non-standard simulation methods.

2.3.1 Joint Models

Many beam-to-column joint macro-models exist in the literature and can be generally represented as shown in Figures 2 – 2 and Figure 2 – 3 for shear connections and Figure 2 – 4 for moment connections in steel and composite steel-concrete buildings. Unlike joint models that were developed for seismic analysis (Gross 1998, Shen and Astaneh-Asl 2000, Lee and Foutch 2002, Mulas 2004, Zhang and Ricles 2006, Nie et al 2008, Cracia et al 2010, and Hsiao et al 2012), models for collapse analysis must be capable of representing the effect of axial loading and its interaction with shear and flexure.

In the shear connection model of Figure 2 – 2, transfer of forces between the beam and column is achieved through a set of horizontal and vertical springs. Each of the horizontal springs can be assigned properties of a bolt in the shear tab or the binding effect. Binding occurs when the top or bottom of the beam bears against the column flange. Bolt models can be calibrated to account for nonlinear bolt behavior and failure mode, while binding springs are simple contact springs. Shear springs are usually elastic springs since the modeling focus is on catenary action, to which these types of connections are particularly vulnerable. Details about the spring strength and stiffness properties can be found in Sadek et al. (2008), Khandelwal et al. (2009), Sadek et al. (2010) , and Main and Sadek (2012).

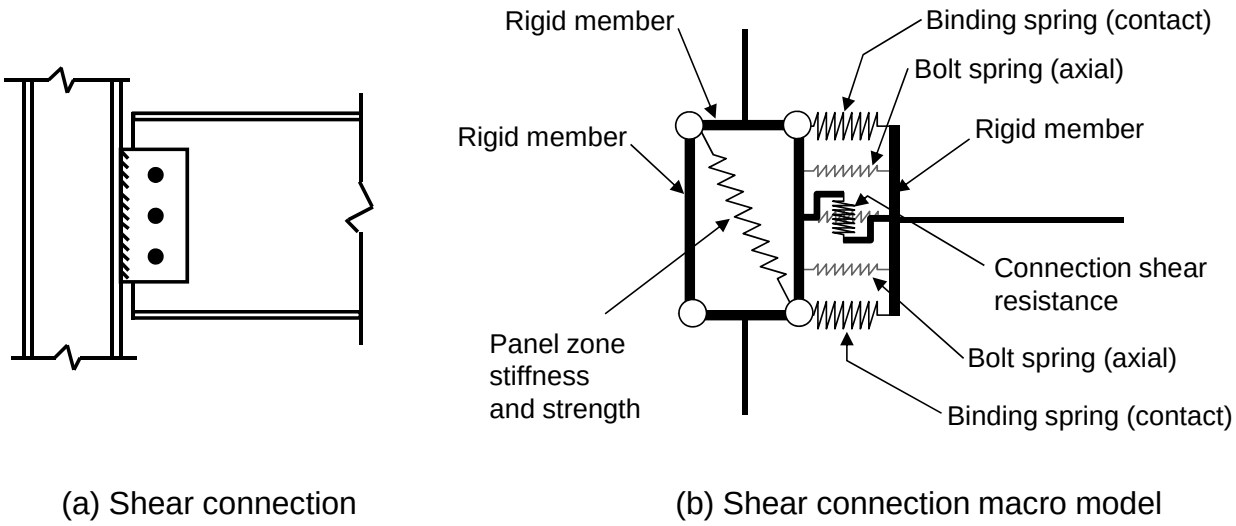

Figure 2 - 2 Shear connection macro-model for steel and composite buildings

Connections undergo large deformations during collapse, and so the vertical and horizontal springs will interact together if they have finite lengths in the model shown in Figure 2 – 2. These interactions can contaminate the model's response, e.g. the elastic shear spring can contribute greatly to the inelastic axial spring. These issues can be eliminated by making the springs zero length, but nevertheless, the model in Figure 2 – 2 assumes that the vertical and horizontal springs act independently. These problems prompted Khandelwal and El-Tawil (2007) to model the connection region as shown in Figure 2 – 3. In this model, the middle member is a beam element with integration points that correspond to individual bolts as shown in Figure 2 – 3(b). The element formulation recognizes the interaction between shear and flexural effects through a user-defined J2 plasticity model developed and implemented by Khandelwal and El-Tawil (2007). The top spring in the model in Figure 2 – 3(a) represents the concrete slab and the bottom spring represents binding. Spring properties are described in Khandelwal and El-Tawil (2007). Variants of the models in Figures 2 – 2 and 2 – 3 have been used by a number of researchers to represent other types of connection including semi-rigid and other types of moment connections. In such models, the springs or beam element represent various connection components, including seat angles, T-sections, etc. (Kim and Kim 2009, Liu et al. 2010, Xu and Ellingwood (2010).

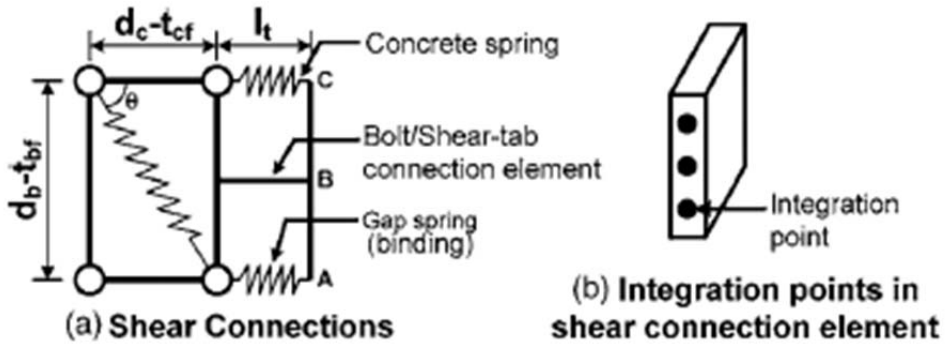

Figure 2 - 3 Connection region in shear connection model (Khandewal et al. 2008)

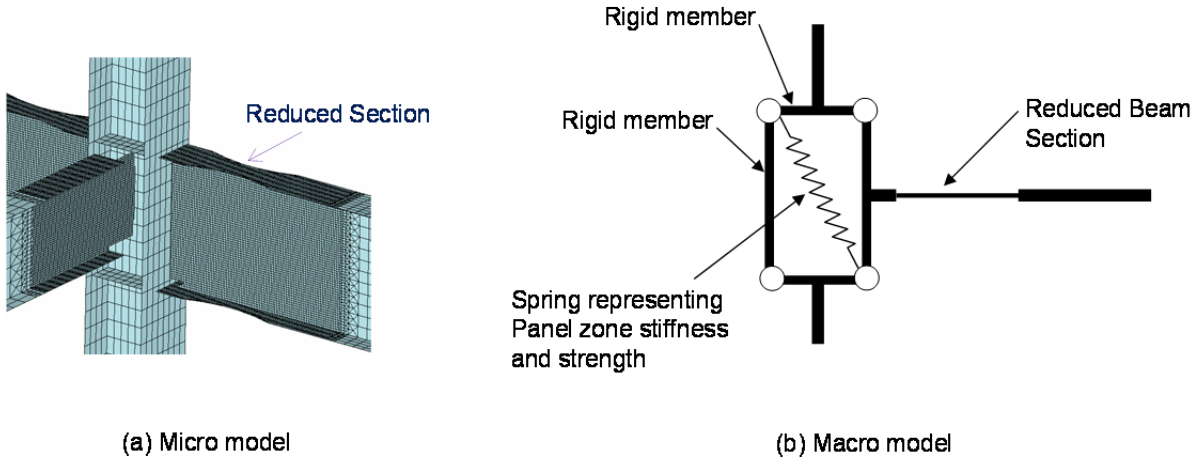

Figure 2 - 4 Modeling of reduced beam connection

Joint micro-models are less common than macro-models, but nevertheless have been used by several researchers. In Li et al. (2012), the shear tab was explicitly modeled via shell element along with the slab and other joint details. The shear tab connection was represented using one single row of shell elements with a thickness equal to that of the beam web. The stress-strain characteristics of these shell elements were derived from the bolt strength and deformation capacity as defined in Sadek et al. (2008). The shear tab model allows the shear tab to be progressively fractured as the failure criteria are reached and elements deleted. In another study, Pirmoz (2011) developed a detailed nonlinear finite element model for a bolted top-seat angle connection with double angles.

Modeling of moment connections is more straightforward than shear connections. A feasible model is shown in Figure 2 – 4. The panel zone in this model (and those in Figures 2 – 2 and 2 – 3) is modeled using a representation that enforces pure shear deformation. This is consistent with past test results of steel subassemblages, where it was observed that the shear stress within the panel is uniformly distributed throughout the column web and that the panel zone region deforms predominantly in pure shear (Krawinkler, El-Tawil Krawinkler 1978 and El-Tawil et al 1999). As shown in Figure 2 – 3 the panel zone model is comprised of 4 rigid bars pinned together at their ends to permit the desired deformation to occur. The stiffness and strength of the panel zone is provided by a diagonal spring joining opposite corners of the panel zone. Details for finding the panel zone spring stiffness and strength can be established using simple engineering principles and data in AISC-Seismic (2010). Sadek et al. (2008) and Khandelwal et al. (2009) also provided equations for finding the panel zone properties. Xu and Ellingwood (2010) noted that panel zone deformations could be neglected in their collapse simulations because of the small imbalance of beam moments due to gravity loads after loss of columns. Li and El-Tawil (2012) ignored the effect of panel zone deformation in their macro-model simulations citing evidence from their previous studies that it did not contribute substantially to behavior.

Besides joint models for steel structures, joint models for reinforced concrete models were also developed. Alath and Kunnath (1995) proposed a macro-based model which was able to account for inelastic shear deformations in the joint region of concrete structure. The connection was modeled using rigid links which could rotate independently based on the fact that the deformation of the panel zone was pure shear. Mitra and Lowes (2007) developed a computational model of reinforced concrete interior beam-column joints. The model was comprised of shear-panel component which represented strength and stiffness due to failure of the joint core, eight bar-slip springs to simulate stiffness and strength loss due to anchorage-zone damage, and four interface-shear springs that simulate reduced capacity for shear transfer at the joint perimeter due to crack opening. The model was calibrated against available experimental data and it

was shown that it could represent well the stiffness and strength response for joints with a wide range of design parameters.

2.3.2 Member Models

Depending on the modeling approach employed, structural members can be modeled using continuum elements or macro-elements. In the former, it is common for steel members to be modeled using shell elements (Khandelwal and El-Tawil 2007, Sadek et al. 2009, Kwasniewski 2010, and Hoffman and Fahnestock 201), although solid elements may be employed when triaxiality is of concern. Karns Karns el at (2006) used solid elements for modeling members. However, the mesh used was not fine enough to adequately capture the effects of stress triaxaility. Although not the main focus of this paper, micro-models of reinforced concrete structures can be found in Pekau and Cui (2006), Tsai and Lin (2008), Bao et al. (2008), Talaat and Mosalam (2009) and Bao and Kunnath (2010).

Macro-scale member models have been successfully used by many researchers. In this approach, beams and columns are represented using beam-column finite elements. Successful beam-column models must employ a large deformation formulation and should ideally sample inelastic behavior at integration points throughout the length and cross-section of the model to accurately capture the spread of inelasticity. The model should also be capable of capturing the interaction between moment, shear and axial catenary loads that commonly occur during progressive collapse analysis. Macro-models of the sort described above have been successfully utilized in the past by many researchers and practitioners for earthquake engineering (Jin and El-Tawil 2005), although most of the modeling effort focused primarily on flexure-only or flexure coupled with axial compressive load, e.g. for modeling brace response, rather than flexure coupled with tensile load which occurs commonly during progressive collapse.

Kaewkulchai and Williamson (2004) presented a beam element formulation and solution procedure for progressive collapse analysis of planar frame structures. The nonlinear beam-column element utilized a lumped plasticity model with inelasticity concentrated at

the element ends and a flexibility-based formulation was applied. Similar models were utilized by Heidarpour and Bradford (2011). Kim and Kim (2009), Kim et al. (2009) and Kim and An (2009) also utilized a macro-scale planar model to investigate the progressive collapse performance of steel buildings with a variety of connection types and investigate the factors that influence progressive collapse.

The majority of the macro models that have been used to date are unable to account for local buckling of steel members. Khandewal et al. (2008) addressed this problem by calibrating their macro-model responses to data from detailed finite-element models of beam-column sub-assemblages. They were able to account for local buckling by using specially calibrated constitutive models, i.e. models that contained softening regimes to mimic local buckling response at the element level. While more accurate than other approaches, this technique is clearly only accurate for the general conditions for which it was calibrated.

2.3.3 Floor System Models

A critical structural part that makes three-dimensional models distinct from planar models is the floor system. Floors make 3-D models more realistic, but are more challenging to represent. Floor decks are generally represented using a collection of beam-column, shell or brick elements.

Sadek et al. (2008) investigated the robustness of a typical concrete deck-steel beam composite floor system with simple shear connections subjected to loss of a center column using computational Finite Element models. The study shed light on the behavior and failure modes of simple shear connections and composite floor systems comprised of such connections. Two reduced modeling approaches for modeling connection behaviors were proposed, i.e. Reduced Component Connection Model and Reduced Coarse Shell Connection Model. Results of the connection sub-assemblage using the two proposed models were compared with those obtained from a high fidelity connection model and good agreement was achieved. The simulation results also revealed that loads were primarily resisted by cable action of the beams after column loss resulting in increasing

tensile forces in the beams and connections that could eventually precipitate failure. The connection models were validated against experimental data. The floor system was modeled as follows: (1) steel columns and beams were modeled using relatively large shell elements and the shear connections were modeled using the reduced coarse shell connection model; (2) the metal deck was modeled using shell elements; (3) concrete slabs were modeled using solid elements; (4) shear studs were modeled using beam elements; and (5) slab reinforcement were modeled using truss elements. Nonlinear static push-down analyses were performed using the proposed model, where the unsupported center column was pushed down under displacement control until the system collapse. In order to investigate the influence of various system components on the system response, the proposed model was exercised as follows: (1) framing only; (2) framing and metal deck; and (3) detailed floor model. The simulation results revealed that the floor deck contributed significantly to the floor system response through diaphragm action to prevent the exterior columns from being pulled inward and membrane action primarily through the reinforcement mesh and steel deck. In addition, it was also indicated that the composite floor system studied would likely not have enough collapse resistance when the floor is subjected to loss of a center column.

Alashker et al. (2010) investigated the progressive collapse resistance of steel-concrete composite floors in which steel beams were attached to columns through shear tabs. The study was conducted using the detailed finite element slab model developed in Sadek et al. (2008) with some modifications in modeling the shear studs, as shown in Figure 2 – 5. The models were calibrated against available experimental data. The models were used to investigate a series of key parameters influencing the robustness of generic composite floors subjected to the removal of a center column, including deck thickness, steel reinforcement and the numbers of bolts in the shear tab connections. Two loading schemes were used in this study: (1) pushing down the center column stub in displacement control; and (2) applying a uniform distributed load to the entire slab and incrementing the load in force control. Nonlinear static analyses were performed using LS-DYNA and the simulation results revealed that the majority of collapse resistance comes from the steel deck. In addition, it was suggested that increasing connection

strength by adding more bolts might not be beneficial in increasing overall collapse strength. It was proposed that the dynamic impact factor of 2.0 could potentially be relaxed and the appropriate value of the DIF depends on the ductility and amount of inelastic action the structure would experience during the column removal scenario.

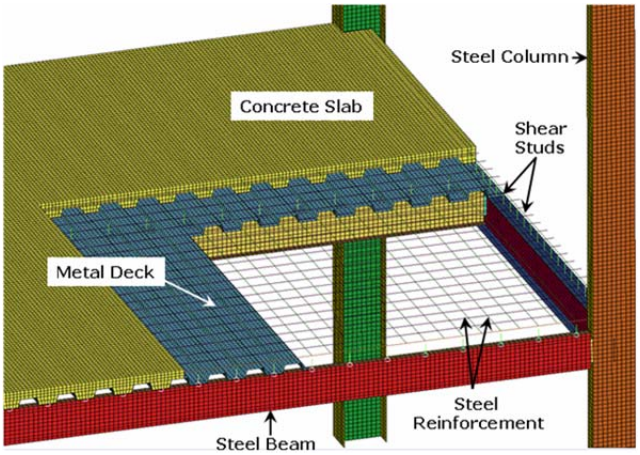

Figure 2 - 5 Detailed finite element model of composite floor (Alashker et al. 2010)

Alashker and El-Tawil (2011) developed a design-oriented model for computing the load-resisting capacity of composite steel-concrete floors subjected to interior column loss on the basis of the premise that floor collapse was resisted by the membrane action developed in the floor slabs and catenary forces developed in the steel beams. A series of simplifying assumptions were made pertaining to the deformed shape of the system, development of failure resisting mechanisms, and overall system behavior. The computation results given by the proposed model were compared with those obtained by a detailed finite element model. It was shown that the model was capable of capturing the effect of influential variables on collapse resistance in spite of the simplifying assumptions made.

Other studies that investigated the influence of floor slabs on structure response under column loss scenarios can be found in Yu et al. (2010) and Williamson and Stevens (2009). Both studies concluded that the floor slab contributes significantly to the collapse resistance of structures.

2.3.4 Considerations for Constitutive Modeling of Steel

Fracture of steel components is one of the most influential factors affecting the collapse resistance of a structural system. Khandelwal and El-Tawil (2007) used a Gurson (1977) model to represent the inelastic, fracture response of steel components. The Gurson (1977) model is porous-plasticity, micro-mechanical material model that accounts for void growth in a steel matrix. Voids are present in because of particles of impurities (carbides and sulphides) that are interspersed in the steel matrix. Fracture is assumed to occur when the void ratio reaches a critical level consistent with rupture. Most other researchers, however, have resorted to classical plasticity models to represent steel behavior. In this approach, fracture is modeled using a simple strain criterion, i.e. an element is deleted once the effective plastic strain reaches some limiting number (Bao et al. 2008, Kwasniewski 2010, Sadek et al 2010, and Alashker et al 2011).

Modeling of ductile fracture of steel requires modeling of softening behavior. Fracture response, i.e. separation, is considered softening response. It is, however, a well-established fact that use of a softening material model in finite element analysis gives results which have first order mesh dependency i.e. the solution does not converge as the mesh becomes finer. This is because of a loss of hyperbolicity (in the dynamic case) or ellipticity (in the static case) of the underlying partial differential equations. Some of the existing techniques used to eliminate mesh sensitivity in micro-models are non-local formulations, gradient based enhancements and visco-plastic formulations. The most commonly used technique for addressing this issue in progressive collapse simulations is to make the material model dependent on element size, i.e. calibrate the used model for a particular element size, say to a steel coupon test, and use the same element size and calibration parameters in the full model (Khandelwal and El-Tawil 2008). Figure 2 – 6 shows an example of the calibration process. The same consideration applies to modeling steel reinforcing bars.

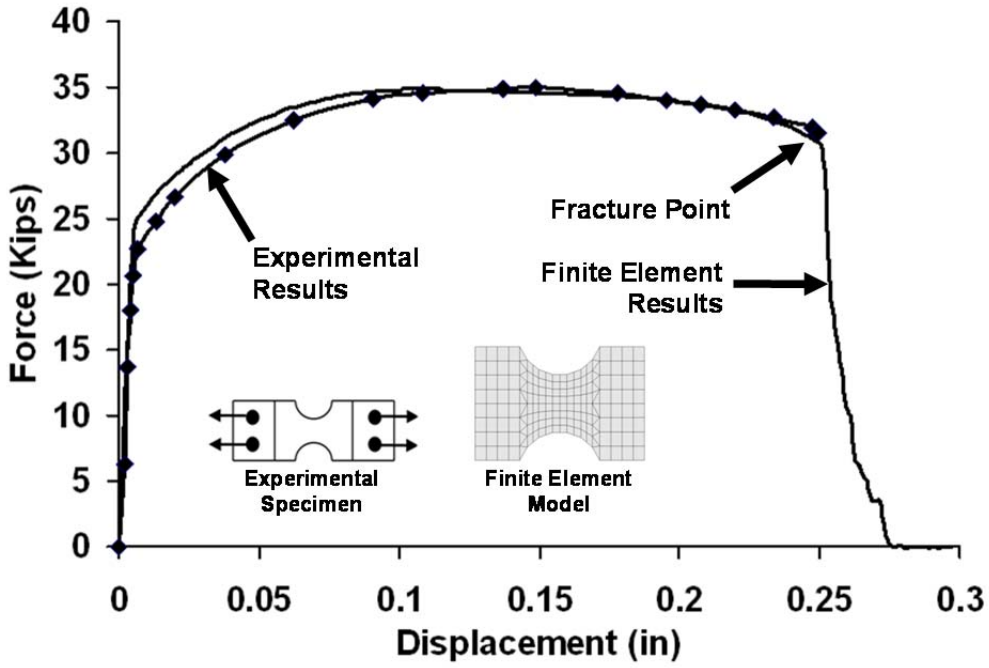

Figure 2 - 6 Calibration of fracture strain using coupon test data (Khandelwal 2008)

2.3.5 System Studies – Planar Models

Kaewkulchai and Williamson (2004) presented a beam element formulation and solution procedure for progressive collapse analysis of planar frame structures. This study shed light on the importance of dynamic load redistribution following the failure of one or more elements and both geometric and material nonlinearity were considered. The proposed nonlinear beam-column element utilized a lumped plasticity model with inelasticity concentrated at the element ends or hinges and a flexibility-based formulation within which the equilibrium of bending moment and axial force along the length of the element was satisfied by using force interpolation functions. The beam-column element also incorporated the interaction of axial force and bending moment and cyclic behavior was captured by using multi-linear force-deformation relationships and the modified Mroz's hardening rule. Large deformation was considered through introduction of a geometric stiffness matrix. A damage index with a value varying from 0 to 1 was used to indicate member failure, through which the effects of stiffness and strength degradation at member hinges were also incorporated. When the value of the damage index of a hinge

reached 1, the hinge was assumed to separate from the structure completely and failure happened. After the failure of an element, the stiffness matrix was updated using a modified member stiffness approach. To illustrate the importance of dynamic effects, the proposed element was used to model a two-bay, two-story frame. Both static and dynamic analyses were carried out and it was concluded that a static analysis may not provide conservative estimates of the collapse potential of frame structures.

A similar work was carried out by Heidarpour and Bradford (2011). They developed a steel beam-column element using a semi-analytical non-discretization numerical methodology and their nonlinear behavior subjected to blast loading was investigated. Although the authors claimed that the developed model could be used in structural analysis and design, for which scenarios of progressive collapse need to be evaluated, the performance of the proposed element still needs to be evaluated under large deformation conditions.

Kim and Kim (2009) utilized a macro-scale planar model to investigate the progressive collapse performance of Reduced Beam Section (RBS), Welded Cover Plated Flange (WCPF), and Welded Unreinforced Flange-Welded Web connections (WUF-W). Two types of steel moment frame buildings, designed for high seismic risk and moderate seismic risk were used in progressive collapse analysis. The buildings are 3 story and 6 stories high with various connection types. In this study, nonlinear planar models which represented the perimeter moment frames of the buildings were used. The panel zones of all types of connections were modeled as rigid and distributed plastic hinge region was incorporated into all types of connections in order to mimic formulation of plastic hinges. The beam and column members were represented by nonlinear beam-column element provided by the OpenSees and second order effect, the interaction between axial force and bending moment reaction could also be considered by using the element. Nonlinear time-history seismic analysis, static push-down analysis and nonlinear dynamic progressive collapse analysis were conducted using the proposed models. It was concluded that although the seismic performance of the three types of connections was

similar, WCPF was the most effective in resisting progressive collapse, especially in structures located in moderate-seismic regions.

Kim and An (2009) investigated the effect of catenary action in the progressive collapse potential of steel moment frames structures using nonlinear planar macro-scale models. The program code OpenSees was used in this study. The beams and columns were modeled using "nonlinear beam column" element and both geometric and material nonlinearity were considered. Nonlinear static push-down analysis of the beam-column sub-assemblage was first conducted. It was shown that the beams could resist significantly larger load when catenary action was considered. Three-story and six-story steel frames with and without braces were then modeled using the proposed modeling approach and both nonlinear static and nonlinear dynamic analyses were performed. It was shown by nonlinear static pushdown analysis that the contribution of catenary action and the progressive collapse potential of structures increased as the number of stories and the number of bays increased. The effect of catenary action also increased as the constraint to lateral movement increased due to braces, for example. The nonlinear dynamic analyses showed that the peak displacement caused by the sudden removal of a column decreased when considering catenary action.

Kim et al. (2009) investigated the progressive collapse resistance of steel moment frames by performing vertical static push-down analysis using planar macro-scale models. OpenSees was used to carry out the analysis. 2-story, 5-story and 10-story steel moment frame with 2-bays in both directions were used in this study and the effects of the number of stories and span length on progressive collapse resistance were investigated through push-down analysis. The analysis revealed that an increase in number of stories and decrease in span length lead to higher progressive collapse resistance. Furthermore, the effects of number of bays were also studies and it turned out that steel frames with larger number of bays were less vulnerable to progressive collapse. By comparing the load-displacement relationships obtained from static push-down analysis with those obtained by incremental nonlinear dynamic analyses, another conclusion was drawn that static

push-down analysis might overestimate the inherent capacity of structures against progressive collapse.

A common problem shared by the above three studies is that no validation studies were carried out, and hence the veracity of the work must be viewed critically.

Khandewal et al. (2008) developed computationally efficient planar macro-models for investigating the progressive collapse resistance of seismically designed steel moment frame buildings. Unlike the models used in the previous studies, the proposed models were calibrated using detailed finite-element models of beam-column sub-assemblages and were able to account for the most important physical phenomena associated with progressive collapse. In the proposed model, the shear connections (Figure 2 – 3) were modeled using two spring elements, which represented the binding effects associated with the bottom beam flange bearing on the column flange, and concrete slab behavior, respectively and a beam element, which had multiple integration points along the height of the cross section corresponding to individual bolts (Figure 2 – 3(b)). The panel zones in both shear and moment connections (see Figure 2 – 3, Figure 2 – 4) were represented by four rigid bars pinned together at their ends, which enforced pure shear deformation, and the stiffness and strength of the panel zone was represented by a diagonal spring. Beams and columns were modeled using Hughes-Liu beam-column elements and the radius cut reduced beam sections in moment connections were represented by a beam element with a length which equal to the length of reduced beam section region but with cross-section properties corresponding to that of the minimum cross section in the reduced section. The behavior of the shear connection model was calibrated against experimental data and the moment connection model was calibrated against data obtained from thoroughly validated micromodel simulations. A J2 plasticity user defined material model which was developed by the author was implemented. The proposed model was fairly simple to build and run and was capable of capturing local behavior such as local buckling and fracture and interaction between moment and axial catenary load that commonly occurr during progressive collapse analysis. The proposed model was used to represent two prototype structures, one was an intermediate moment frame and the other

was a special moment frame, which addressed moderate and high seismic risk, respectively. The performances of both of the structures subjected to sudden removal of columns were investigated by performing nonlinear dynamic analysis using the alternate path method. The simulation results revealed that the special moment frames had a better progressive collapse resistance compared with the intermediate moment frames because of better layout and system strength rather than the influence of improved ductile detailing. Another important conclusion was that the alternate path method was not able to provide information about the reserve capacity of the system and therefore its results should be evaluated carefully.

Khandelwal et al (2009) investigated the progressive collapse resistance of seismically designed steel braced frames using the same modeling approach described above. The moment connections were modeled by rigidly attaching beams and columns to the connection region; brace-to-beam connections were not explicitly modeled because their responses were expected to be elastic; panel zones were not explicitly modeled, either because it was shown that the panel zone behaved elastically under collapse conditions. The shear connections were modeled using two spring elements and a beam element which represented the bolts and shear tab interaction; the shear links were represented by 4 bars pinned together at their ends to permit the desired shear-flexural deformation, within which two bars are rigid and two are elastic, and the stiffness and strength of the link were provided by a nonlinear spring; the beams and columns were modeled using Hughes-Liu beam-column elements. The models were calibrated by comparing model responses to test data and more refined models that were also validated by comparison to test data. Two braced frames: a special concentrically braced frame, which addressed moderate seismic risk and an eccentrically braced frame, which addressed high seismic risk, were modeled using the proposed macro-model and nonlinear dynamic analysis was performed using alternate path method by removing critical columns and adjacent braces, if present. The analysis results revealed that although both systems benefitted from placement of the seismically designed frames on the perimeter of the building, the eccentrically braced frame had better progressive collapse resistance because of improved system and member layouts rather than use of more stringent seismic detailing.

Other work related to progressive collapse analysis of steel structures using planar macro-scale models can be found in Kim and Kim (2009 a, b), Kim et al. (2009), Kim et al. (2011 a, b), Kim and Jung (2011).

Studies in which micro-scale models are used to evaluate progressive collapse potential of civil structures are relatively rare because of the heavy computational load associated with these types of analyses. One of earliest efforts in this direction can be found in Khandelwal and El-Tawil (2007). The authors investigated the collapse behavior of seismic detailed steel special moment resisting frame connections focusing on the effect of catenary action on connection performance under column loss scenarios. In order to investigate a number of key design variables that influenced formation of catenary action in steel special moment resisting frame sub-assemblages, a detailed finite element model of a two-bay steel sub-assemblage with seismic detailing was developed (Figure 2 – 4(a)). The model employed a constitutive model for steel that accounted for ductile fracture. The model was validated against experimental results and was used to model first, fifth, and seventh-story beam-column sub-assemblages of an eight-story special moment resisting frame buildings. The influence of a series of parameters on connection catenary response was investigated, including out-of-plane pulling action imposed by the transverse beam, reduced beam section versus no reduction in beam flange, the yield stress to ultimate stress ratio of steel, beam web connection detail, and the reduction of ductility in the heat affected zone. The simulation results confirmed the ductility of seismically designed special moment frame connections and their ability to deform in catenary mode. It was also shown that the out-of-plane pulling action induced by transverse beams had no adverse effect on system behavior, but connection ductility and strength were adversely influenced by an increase in beam depth and an increase in the yield to ultimate strength ratio and that the beam-to-column detail played an influential role in connection response. Furthermore, it was also observed that subassemblies with reduced beam sections were somewhat stronger and more ductile than corresponding assemblies without RBS. On the other hand, the heat affected zone in beam flanges did not have a significant deleterious influence on system behavior.

The computational models described above are all planar models of steel structures. However, several researchers also dedicated their efforts on development of planar models of reinforced concrete structures to investigate their response subjected to sudden column removal. The details about these models can be found in Pekau and Cui (2006), Tsai and Lin (2008), Bao et al. (2008), Talaat and Mosalam (2009) and Bao and Kunnath (2010).

However, as previously alluded to, planar models have substantial limitations in accurately representing progressive collapse behavior of civil structures. In particular, they cannot account for 3-D effects, especially the effects of slabs. To address this issue, fully 3-D models are needed, of which there are a few cases in the literature.

2.3.6 System Studies – 3-D Models

One of the earliest examples of using 3D models is Ruth et al (2006). In this study, 3D models were used to investigate how conservative the dynamic increase factor provided by the DoD and GSA was. The authors argued that the value of dynamic increase factor provided by both DoD and GSA, which was 2.0, was too conservative, and a dynamic multiplier of 1.5 would be more accurate and efficient. To determine a reasonable dynamic load factor, 11 models for steel moment frame structures were created, including 8 two-dimensional models and 3 three-dimensional models. In order to consider different factors which could affect the value of the dynamic factor, different building geometry parameters were used in these models, such as the number of stories, the number of horizontal bays, the bay dimensions, the member size, foundation constraints and the story height. The author then proposed an approach to obtain a reasonable dynamic multiplier. Dynamic-nonlinear analysis and static-nonlinear analysis with different dynamic multipliers were performed with the proposed models, respectively. A ratio was obtained by dividing a static value by the corresponding dynamic value. Thus, when the ratio reached 1.0, the corresponding multiplier is the dynamic increase value. The results of total plastic rotation, the average plastic rotation and the maximum vertical displacement which were obtained from the two-dimensional and three-dimensional models were compared and plotted. The research revealed that a reasonable value of the

dynamic multiplier was well below 2.0. The author also conducted the same analysis for a reinforced concrete frame, and it turned out the value could be even smaller. However, one of the main shortcomings of the proposed 3D models is that the slabs were not modeled thus the effects of the slabs were not accounted for.

Bae et al. (2008) evaluated the potential of progressive collapse of a cold-formed steel framed structure using three-dimensional analysis, performed according to GSA and DoD guidelines. In another study by Sasani et al (2008), the response of a seven-story reinforced concrete was investigated under column-loss scenarios using the alternate path method. In order to evaluate the potential of development of catenary action and the deformation capacity of the beams of interest, which were the beams bridging over the removed column, an experiment was conducted to investigate the behavior of a 3/8 scaled model of these beams under the event of loss of column. The experiment revealed that even after the fracture of bottom reinforcement, the beams were still be able to carry load and develop large deformation and after that, catenary action was developed in top beam reinforcement. A detailed finite element model which was capable of representing the behavior of the beams of interest was developed and calibrated against the experimental data. The authors also created a three-dimensional finite element model for the structure, which accounted for both material nonlinearity and geometric nonlinearity. In order to obtain high computational efficiency, the beams and columns were modeled with Euler-Bernoulli beam-column elements, except for the beams of interest in different floors and the slabs were represented by shell elements. A hybrid analysis which integrated the two models was performed and the behavior of the structure under one column loss case and a two columns loss case were presented, including a discussion of overall deformations and load redistributions. In the two columns loss case, the DCR method, which was proposed by FEMA, was also applied and it turned out that this method was overly conservative.

Szyniszewski (2009) treated survival probability of a building occupant as a measure of robustness of a 3-storey moment resisting steel framed building, which could be considered as one of the key factors to employ optimization algorithms so that the safest and most economical structural design could be obtained. It was assumed that the ratio of

the collapse floor area to the total floor area was related directly to the probability of an occupant's survival. An approach to calculate the survival probability based on physics based simulations and a theorem of total probability was proposed. The calculation procedure was as follows: 1. the probability of localized damage of the structure under a truck bomb explosion scenario was assessed. The probability was calculated based on the area of "damage zones" around the building. 2. A three-dimensional model was created for the structure and a dynamic nonlinear analysis was performed under the column-loss scenario corresponding to the localized damage postulated before. The area of the collapse floor was estimated and thus the corresponding survival probability of a building occupant could be calculated under that particular scenario. 3. Final probability of the occupant's survival was calculated by employing the total probability theorem. The research estimated the robustness of a moment resisting moment frame from the social point of view. However, the author did not provide any details about the three dimensional model and no calibration work was shown in this paper.

Mohamed et al (2009) investigated the implementation of UFC guidelines to prevent progressive collapse of corner floor panels, whose dimensions exceed the damage limits, under the column-loss scenario. Five three-dimensional models were developed for an 8-storey reinforced concrete building that did not strictly meet the UFC guidelines. The configuration of the models was changed in order to investigate the benefits of different types of braces after notional removal of columns. The simulations revealed that three-dimensional effects were of importance for torsional shear stresses and shear stresses could control the design. On the other hand, braces could reduce maximum bending moments and other internal forced produced by the removed column. However, the author did not discuss the modeling approach or model calibration. Thus, the accuracy of the models is not known.

Main (2009) summarized the development of 3D macro-models for steel moment-frame buildings, which were designed for the purpose of studying progressive collapse of buildings in moderate and high seismic regions. Focus was placed on the modeling of the connections and composite floor systems. However, the simplified slab model was not

validated. The beams and columns were represented by Hughes-Liu beam elements. The connections were modeled with beam elements and discrete spring elements, which were validated against high-fidelity finite element simulations or full-scale test data, depending on the type of the connection. The slab was modeled with a single layer of shell element for simplicity. Some initial simulation results for one prototype building under a column removal scenario were also provided in order to illustrate the model capabilities. Additional simulations that would have illustrated the capacity of the proposed model to represent the behavior of the structure under column-loss scenarios were not provided.

Hoffman and Fahnestock (2011) investigated the progressive collapse behavior of typical multi-story steel buildings with perimeter moment frames and composite steel-concrete floors using three-dimensional nonlinear finite element models. A three-story and a ten-story building were represented and a series of column loss cases were studied by performing nonlinear dynamic analysis. In the models, the beams and columns were modeled using shell elements. The steel deck and concrete slabs were modeled using individual planar layers of shell elements. Shear connections were represented with a component model consisting of nonlinear springs joining each bolt location. Nonlinearities were taken into consideration in the modeling process. A series of conclusions were drawn from the studies: (1) after loss of the corner and perimeter columns with only shear connections, the structure could not survive progressive collapse, although the failure did not propagate; (2) composite flexural response was a significant load redistribution mechanism after column loss; (3) the concrete slab and concrete deck were subjected to inelastic demands as a results of flexural composite action; (4) demands were least severe for perimeter columns within a moment frame but the structure exhibited significant load redistribution for interior column loss scenarios that had no moment connections; (5) building height did not significantly affect progressive collapse of steel frames; and (6) the steel frames which were evaluated in this study demonstrated appreciable robustness. The main drawback of this study is lack of validation studies to validate the accuracy of the proposed models.

Fu (2009) developed two three-dimensional models which represented two 20-storey steel frame buildings, which utilized shear walls and cross bracing to resist lateral loads, respectively, for the purpose of investigating the response of high-rise buildings under column-loss scenarios. The beams and columns were represented by beam elements and the slabs and core wall were modeled by shell elements. Both material nonlinearity and geometric nonlinearity were taken into consideration. In order to validate the proposed model, a two-story frame model was created with the same modeling approach and the results were compared with experimental data. The author argued that the comparison was good and the proposed model was accurate enough to capture the responses of the structure under column-loss scenarios. However, the slab models used were not validated explicitly, neither was the brace model nor the shear wall model. Nonlinear analysis was performed using the two models and several column-loss cases were studied, applying APM. From the results, the author concluded that the dynamic response of the structure under column-loss scenarios was mainly related to the affected loading area, which means the larger the affected loading area was, the more the damage that could be induced. It is going to be shown in this research that this is not an accurate statement. Furthermore, the author also suggested that all the structural members, including beam to column connections, should be designed at least twice the static axial force subjected to the 1.0DL+0.25LL loading condition, although the number has been considered to be too conservative by many researchers. From the comparison of the results, the author also observed that a column removal at a higher level may induce larger vertical displacement than a column removal at ground level.

Fu (2010) used the 3D model proposed in Fu (2009) to conduct parametric studies. The response of the structure was investigated with variations in strength of the structural steel, strength of concrete and reinforcement mesh size. In addition, the author recommended several methods to mitigate progressive collapse including: (1) increase the strength of the steel structural member, because it was observed in the parametric studies that by increasing the strength of the structural elements, the overall deflection of the damaged structure could be reduced; (2) increase the strength of the concrete. However, this effect was limited; (3) decrease the spacing of the grid or provide more

redundancy to the structure; and (4) place more steel mesh, but that is only efficient under deformation large enough to trigger catenary action.

A detailed 3D model representing an 8-storey steel framed structure was developed by Kwasniewski (2010). The details of the model were discussed, including modeling approaches and material models. The model was verified and validated by applying a hierarchical approach with four levels of complexity. Nonlinear dynamic analysis was performed using APM.

2.3.8 Other Simulation Techniques

All of the previously discussed efforts to address collapse behavior were conducted using the finite element method. There are some examples in the literature where techniques other than traditional finite element models were employed to investigate collapse.

Sasani (2009) evaluated the response of Hotel San Diego, which was a six-story reinforced concrete infilled-frame structure subjected to removal of two adjacent exterior columns using three dimensional models developed using the Finite Element Method and Applied Element Method. In the Finite Element model, the beams and columns were modeled with Bernoulli beam elements and plastic hinges were modeled at all possible locations where the reinforcing bars could yield. The slabs and joists were also represented by beam elements which could account for potential nonlinear response of slabs and joists. The infills were modeled in two ways: (1) two dimensional shell elements and (2) compressive struts. In the Applied Element model, beams were modeled with 200 spring triples at each cross section and the same number of springs was used for the cross sections of the columns. Floor joists were represented using the same modeling approach with the beams and slabs between joists modeled using cuboid elements. Reinforcement in all structural members was explicitly modeled. The analytical results were compared with the experimental data and good agreement was achieved. The following results were drawn: (1) three-dimensional Vierendeel action of the transverse and longitudinal frames with the participation of infill walls is the major mechanism for redistribution of loads in the structure; (2) even if the rebars in the beams adjacent to the

removed column did not have proper anchorage, the rebars will not be pulled out; (3) propagation of axial waves required less time than the propagation of flexural waves; as a result, the axial forces in the columns above the removed column reduced to almost zero and then different floors practically moved together soon after column removal; (4) the joints above a removed column in two different floors moved simultaneously with the floor above having slightly smaller displacement due to the loss of axial force in the column connecting the two floors and its corresponding elongation; (5) when the overall deflection was small, struts could not represent the behavior of infill walls reasonably while when the deflection was large, modeling infill walls with struts became more accurate. The response of the structure due to additional gravity loads and in the absence of infill walls was analytically evaluated as well.

In Galal et al (2009), 3-D models, using the Applied Element Method, were created for 18-storey moment resisting frames with different span length for the purpose of investigating the effect of different retrofit strategies on the behavior of the structures. The strategies evaluated were increasing the strength of the beams, increasing the stiffness of the beams, and increasing both strength and stiffness of the beams, subjected to GSA and DoD load combinations, respectively. Nonlinear dynamic analysis was performed applying the Alternate Path Method and 6 column loss cases were studied. The effect of the proposed retrofit strategies on enhancing the response of damaged structures was studied by comparing three performance indicators, which were chord rotation, tie forces and displacement ductility demand in the beams before and after being retrofitted. The effect of the variation of span length on the three indicators was also investigated. From the results of the analysis, equations for calculating the reduction factors of the three indicators, which were the ratios of the three indicators before and after upgrading, were proposed. The author argued that increasing the strength of the beams was more effective than increasing their stiffness for enhancing the behavior of the structures under column-loss scenarios. On the other hand, the reduction factor obtained by increasing both strength and stiffness could be calculated by multiplying the ones obtained through the first two strategies directly. Another important conclusion was that the consequence of the column loss cases under GSA and DoD load combinations could be totally

different thus which load combination was better should be clarified in future research. Furthermore, the author also proposed that the behavior of the structure after sudden removal of the column was affected by the orientation of the columns. The effect of the variation of span length on the three indicators was proportional to the ratio between span lengths to the power to 0.5, 3 and 1, respectively.

Masoero (2010) investigated the response of a reinforced concrete framed structure after the sudden loss of a column. A 3-D model which was comprised of Euler-Bernoulli beam element was developed and simulations were performed applying the discrete element method, in which the structural volume was represented by spheres surrounding each node. Both material nonlinearity and geometric nonlinearity were considered in the analysis. The impact between structural members during collapse was represented by collisions between the spheres. Parametric studies were conducted with variations of cross section sizes of structural members, place of reinforcement and the plastic capacity of material for the purpose of investigating their influence on the mechanisms and consequences of progressive collapse. The author argued that under the condition when only one column was removed, collapse may happen to structures with smaller cross section area but was ductile enough. However, when several columns were removed simultaneously, collapse may also occur in more brittle and stronger structures. The study also revealed that symmetry of the reinforcement could also affect the response of the structure. Structures with symmetric reinforcement were more robust even if they were brittle. On the other hand, after local failures are initiated, the final extent of collapse and the fragment size distribution are closely related to the mechanisms caused by the collision between the structural members. It was shown that collapse could not propagate widely within brittle structures. On the other hand, the fragments are more massive when the structure is more ductile and are independent of the stiffness and strength of the structure.

2.4 Methods for Assessment and Quantification of Structural Robustness

The most widely-used approach to evaluate robustness is the alternate load path method (APM), which is advocated by GSA (2003) and UFC (2009). APM is a threat independent methodology. This means that, rather than consider the triggering event, the collapse resistance of the building system is systematically assessed by removing key structural members and investigating the subsequent ability of the system to bridge over the lost members. While this method is widely used for assessment of robustness, Khandelwal and El-Tawil (2011) pointed out that its primary drawback is that it cannot provide sufficient information about how close the structure is to collapse. For example, a structure could be on the verge of collapse, but could still potentially pass APM.

Izzuddin et al. (2007) proposed a simplified framework to evaluate robustness of multi-story buildings on the basis of APM, which enabled quantification of structural robustness. The main conclusion from this study is that energy absorption capacity, redundancy and ductility cannot be considered as measurement of robustness individually. In contrast, the pseudo-static capacity, which accounted for all of the three parameters, was suggested as a measure of building robustness under column loss scenario. In a companion paper (Vlassis et al. 2007), the application of the proposed framework was demonstrated through case studies, in which a corner column and a peripheral column in the first floor of a steel framed building were removed, respectively. Vlassis et al. (2007) indicated that the tying force requirements alone could not guarantee structural robustness if the ductility demand and supply in the support joints of the affected members were not considered explicitly.

Starossek and Haberland (2008) presented their thoughts on various proposed measures of structural robustness. They indicated that if the initial damage is specified, then the evaluation of robustness depends on the structure, its exposure and vulnerability. In order to promote development of progressive collapse analysis procedures and qualification of robustness indices, Starossek (2007) developed a typology and classification of

progressive collapse based on different mechanisms which may produce progressive collapse. Baker et al. (2008) proposed a framework for robustness assessment based on decision analysis theory employing probabilistic risk analysis. Agarwal et al. (2003) developed a theory of structural vulnerability on the basis of the connectivity of the structural form, which could be used to identify particular failure scenarios that result in progressive collapse.

Using APM, Khandelwal and El-Tawil (2011) proposed "push-down analysis" as a way by which to measure of robustness. Push-down analysis was performed in three ways: (1) uniform pushdown, in which gravity loads on the entire damaged structure were increased proportionately until collapse was triggered; (2) bay pushdown, in which only the gravity loads in the bays which suffered damage were increased proportionately until the system collapsed; and (3) incremental dynamic pushdown, in which the responses of the intact system with increasing gravity loads in the bays of interest were investigated when columns were suddenly removed. Xu and Ellingwood (2011) proposed an energy-based nonlinear static pushdown analysis to predict the dynamic peak response of the system through static analysis. The vulnerability of the structure could be assessed using this method.

The studies surveyed above suggest that there are 4 general ways for measuring robustness: 1) Displacement-based method, in which robustness is describes as the overall deformation of the structure after loss of critical load-carrying members (APM); 2) Force based methods, in which robustness expressed as a ratio of the load carried by the 'damaged' structure to the nominal gravity loads; 3) energy based methods which are based on the Law of Conservation of Energy to assess the vulnerability of structures; 4) methods based on risk analysis, in which the probability of the performance of the structure reaching a certain limit state used as the identification of structural robustness.

It should be mentioned that all of the efforts to date to quantify or categorize robustness have been performed on 2-dimensional structures and ignored three-dimensional effects, which can play a critical role in collapse resistance as previously discussed. While this does not necessarily imply that the measures are problematic, it does suggest that further

research is needed to investigate how influential 3-D effects are on the various measures proposed.

2.5 Other Analysis methods for Progressive Collapse

Some researchers also developed analytical methods other than the methods discussed in the previous sections.

Grierson et al. (2005) proposed a progressive-failure analysis procedure to evaluate the robustness of structures subjected to abnormal loads. The procedure was based on the matrix displacement method of analysis. As with APM, the procedure assumed that initial damage had already happened in the structure and the response of the remaining structure would be evaluated by incrementally applying the gravity loads. In this procedure, the effect of axial force on the bending stiffness of the members was considered. Furthermore, the combined effect of post-elastic bending, shear and axial deformation was also accounted for by the member stiffness matrices, which were updated under incrementally increasing loads though the use of degradation factors. The degradation factors could not only characterize stiffness deterioration but also could identify failure and fracture of members. The impact loads caused by the falling debris was modeled using impact factors. The methodology was also able to account for the unloading effects induced by members disengaging from the structure. Another advantage of this method was that analysis could proceed even after the members broke away and other structural instabilities occurred, such as localized collapse. The procedure was terminated when a globally stable state was reached or progressive collapse to ground level occurred. The author claimed that the procedure could be used to analyze any type of building structures, such as concrete, steel or composite, once the material models were correctly incorporated. Two example planar steel moment frames were analyzed using the procedure.

Chiaia and Masoero (2008) proposed an approach which could assess robustness by means of the tools of Fracture Mechanics. It was shown that the analogy between

progressive collapse and Fracture Mechanics could provide useful tools when analyzing damage propagation. Within this approach, a general energy criterion for damage propagation was provided. The energy criterion was applied to study the dynamic response of simple structures subjected to column loss scenario. Masoero et al. (2010) used the introduced energy criterion and proposed a new approach which was used to evaluate the bearing capacity of reinforced concrete beams with different steel rebars subjected to sudden loss of a single support.

The Mixed Lagrangian Formulation (MLF) is a convenient framework within which the analysis of structures in the elastic and plastic range with large geometric nonlinearity can be considered. Lavan et al. (2009) extended MLF capabilities to account for strength degradation and fracture. The numerical scheme was shown to be stable in terms of the time step size required, even in cases where a sudden fracture happened. Thus, the approach could be used to analyze progressive collapse response. However, this method has not been used to study real structures.

Scott and Fenves (2010) developed an accelerated Newton algorithm based on Krylov subspaces to solve nonlinear equations of structural equilibrium. It was shown that the algorithm could be used to analyze progressive collapse of frames through comparison between progressive collapse responses of a reinforced concrete frame and a steel frame obtained by the proposed algorithm and the Newton-Raphson algorithm.

Naji and Irani (2011) proposed an energy-based simplified procedure for robustness assessment. The progressive collapse response could be obtained by equating external work done by applied loads with internal work done by beams in the bay where the column was removed. The author compared the results obtained by this procedure and nonlinear dynamic analysis, and concluded that the proposed method was accurate enough. However, the approach may be problematic under large deformation condition since both material and geometric nonlinearities are not explicitly considered.

2.6 Experimental Research on Progressive Collapse

Experimental research on progressive collapse is expensive, difficult and dangerous, which has limited the number of studies in this area. Of the few published studies, several were conducted by military organizations. Such studies are typically not thoroughly reported on (at least publically) because of limits on data dissemination, further contributing to the lack of high quality experimental results that can be used for model validation.

Experimental collapse testing that typically falls into two categories: 1) structural system testing, and 2) subassemblage testing. In the former, an entire (usually multi-story) building system is investigated after one or several columns are suddenly removed, either by blasting them away or kicking them out using some other technique, such as projectile impact. In the latter, a connection subassemblage with a missing column is loaded to failure, usually with the objective of studying catenary action. Subassemblage tests are very valuable because they focus attention on an isolated resistance mechanism, allowing it to be studied in detail and enabling thorough validation studies to be conducted. On the other hand, full system tests, while impressive, are: 1) not practical to densely instrument, and 2) represent the outcome of complex interacting processes, whose individual effects are difficult to discern. They are therefore of somewhat limited for validation studies. Also, their expense and size make it difficult to repeat tests to ensure reliability and investigate the effect of variables, further limiting their use. However, they are useful for proof-of-concept exercises.

2.6.1 Full System Testing

One of the first studies in this area was conducted at the University of California, Berkeley. Astaneh-Asl (2001) conducted an experimental test of a one story steel structure in order to investigate progressive collapse resistance of a typical steel structure and floor system subjected to loss of columns. The specimen was a 60 ft by 20 ft one story steel structure with steel deck and concrete slab and wide flange beams and

columns. Two connection types were used: (1) standard shear tab or bolted seat angle under bottom flange and a bolted single angle on one side of web. The column was displaced 19, 24, and 35 inches downward for the first, second, and third subtests, respectively at a rate of 0.25 inches/sec. The bottom of the test column was returned to its original height after each subtest. The test results revealed the following findings: (1) the design dead load and live load could be resisted and the floor could survive progressive collapse due to catenary action of steel deck and girders after removal of the middle perimeter column; (2) the progressive collapse resistance of the structure was limited by the beam-to-column connections at the removed column and progressive collapse could be prevented because of catenary action in the beams and steel deck if the connection bolts did not prematurely fail; (3) the steel deck was effective in redistributing the increased load resulting from the loss of a column; and (4) it was estimated that the catenary action could carry a load of 150 pound per square feet of tributary area.

Sasani et al. (2007) investigated progressive collapse potential of a 10-story reinforced concrete building subjected to sudden loss of an exterior column both experimentally and analytically. Small vertical displacement was observed after the removal of the column. The experimental results revealed that Vinerendeel action of the transverse frame whose exterior column was removed is the major load redistribution mechanism. High modulus of rupture of the concrete is of great importance in reducing overall deflections. Considering this type of load resisting mechanism, proper anchorage of beam and slab bottom reinforcement is important. It was also observed experimentally that the vertical movement of different floors above the removed column is almost the same due to large axial stiffness of the columns. Furthermore, the experimental data also demonstrated large damping effects in the system.

In Sasani and Sagiroglu (2008), the authors presented an experimental evaluation of progressive collapse resistance of a six-story reinforced concrete frame structure subjected to loss of a corner column and an exterior column. As with other related studies, the experimental data revealed that bidirectional Vierendeel action of the transverse and longitudinal frames is the main load resisting mechanism after the loss of the columns.

The contributions of proper anchorage of the reinforcement bars to progressive collapse resistance were emphasized. Furthermore, the author concluded that although not satisfying integrity requirements, progressive collapse is mitigated due to the three-dimensional response of the structure and its redundancy.

Yi et al. (2008) conducted an experimental study to investigate progressive collapse behavior of a reinforced concrete frame subjected to loss of a lower story column. A four bay and three story one-third scale specimen representing a portion of a larger planar frame structure was tested. The author summarized the progressive collapse process as three distinct phases in its response: elastic, plastic, and catenary phases. The experimental results demonstrated that the rupture of the reinforcing steel bars in the floor beams controlled the failure because of progressive collapse of the RC concrete frame structure. An important conclusion is that the force resistance mechanism changes from an elastic mechanism dominated by bending to a beam catenary mechanism dominated by tension, after the plastic mechanism is formed during the collapse process. Furthermore, the experimental results also proved that the static loading method is a viable technique to simulate progressive collapse due to column failure.

Sasani and Sagiroglu (2010) evaluated the dynamic gravity-load redistribution of a 20-story reinforced concrete structure after loss of an interior ground-floor column because of explosion. Progressive collapse was mitigated and since the maximum vertical displacement was small, no damage was observed on the floors above. According to the experimental data, the authors observed that the lower-floor beams and slabs contribute more to load redistribution compared to their counterparts in higher floors. The axial forces in the columns above the removed column dropped much faster than the vertical displacement due to the higher speed of axial wave propagation compared to that of flexural wave propagation. These observations suggest that the whole structure above the removed column contributes to redistribution of the gravity load which was previously carried by the removed column.

In another investigation, Song and Sezen (2009) conducted field studies to investigate the behavior of an actual building that lost an intermediate column. Zheng et al. (2011)

presented an experimental study on the progressive collapse resistance of reinforced concrete frame structures using 1/3 scale specimens. Hunan University, China (Yi et al. 2011) conducted a test to investigate the response of a half-scale, 3-story, 3-bay RC frame subjected to sudden column removal.

2.6.2 Subassemblage Testing

The US General Services Administration commissioned a number of blast tests to investigate the catenary response of various types of steel connections, especially those used in earthquake zones (Karns et al 2007a, 2007b). As shown in Figure 2 – 7, the connection subassemblage was placed in a test rig and then blasted. Collapse loading was then simulated by applying monotonic vertical load to both blast-damaged and non-blast-damaged double-span steel assemblies. Progressive collapse load conditions were simulated by applying monotonic vertical load to both blast-damaged and non-blast-damaged double-span steel assemblies. Four "real world" full scale steel frame beam-column assemblies were subjected to large-scale arena blast tests, and subsequently tests in situ for progressive collapse load conditions. Two additional non-blast-damaged tests articles were subjected to progressive collapse loading alone to establish a performance benchmark, and to simulate possible undamaged upper story levels in a building. Two types of connections were used in the tests: (1) welded unreinforced flange-bolted web connections (WUF-B); and (2) SidePlate moment connections. The test results revealed that: (1) successful performance of a steel frame connection system under earthquake load conditions did not mean successful performance under blast and progressive collapse conditions; (2) conventional steel frame construction could behave in a very ductile manner, even when subjected to the high-strain rates associated with blast loading; (3) conventional steel frame buildings could be an excellent solution for both blast and progressive collapse mitigation as long as the beam-to-column connection geometry was properly configured and detailed to provide significant rotation under large axial tension loads; and (4) the SidePlate connection system was more robust than WUF-B connection system under blast and progressive collapse load conditions.

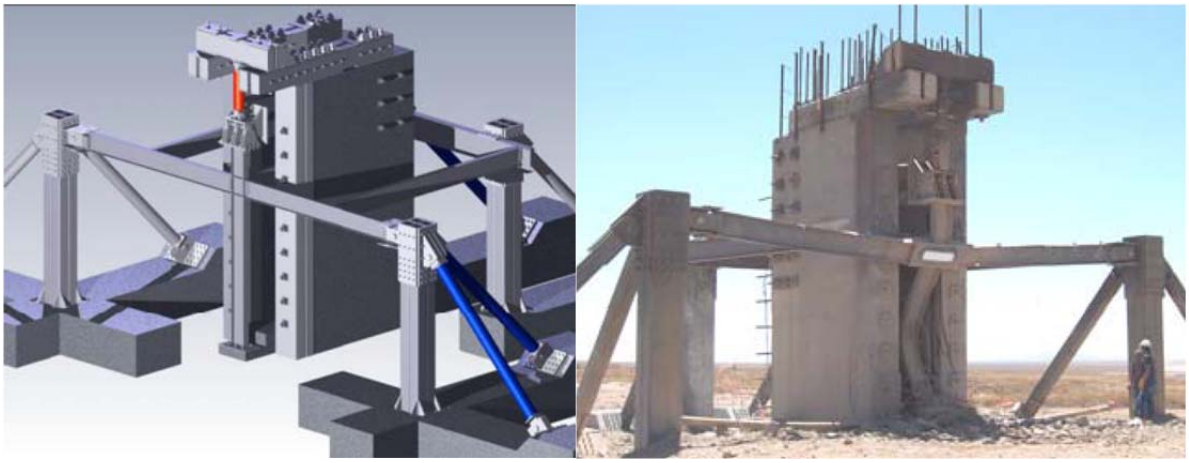

(a) Test setup (b) Connection subassemblage after blast

Figure 2 - 7 GSA connection subassemblage blast tests (pictures from Karns et al 2007a, 2007b)

Sadek et al. (2010) presented an experimental study of two steel-column assemblies, each comprising three columns and two beams under column loss scenarios (Figure 2 – 8). The assemblies used were portions of two seismically design ten-story steel frames and the connections tested were welded unreinforced flange-bolted web (WUF-B) connections and reduced beam section (RBS) connections. The column loss scenarios were simulated by applying incremental vertical displacement to the unsupported stub column until a collapse mechanism developed. It was observed during the tests that both WUF-B and RBS test specimens could develop substantial catenary action and that their rotational capacities under monotonic displacement were about twice as large as those based on seismic test data. It was also shown that the RBS connection was more ductile than the WUF-B one. A companion test series was conducted for reinforced concrete subassemblages (Lew et al 2011). A similar test was conducted by Yang and Tan (2012) to study the behavior of bolted-angle connections subjected to catenary action under column-loss scenarios.

(a) Test setup (b) Close up of fracture in the reduced beam section

Figure 2 - 8 NIST experimental study (pictures from Sadek et al. 2010 ©ASCE)

Choi and Kim (2011) carried out experimental tests to investigate the progressive collapse resistance of reinforced concrete beam-column sub-assemblies designed with and without seismic detailing. Like in the NIST tests by Lew et al (2011), their experimental results revealed that reinforced concrete moment-resisting buildings, which are seismically designed, are more robust when subjected to sudden loss of columns compared with those that are not seismically designed. Tan and Yang (2012) conducted experimental tests to investigate behavior of different types of steel connections in steel frames under column loss scenarios. The test set-up was similar to the one in Sadek (2010).

In order to investigate the structural integrity of steel gravity frame systems, a series of experiments were carried out by the University of Washington, Purdue University of University of Illinois at Urbana-Champaign (Weigand et al. 2012). In these tests, the behavior of single plate shear and bolted angle connections was tested under combined load and large deformations. The tests are still ongoing at the time of this writing. Future studies include investigation of the uniaxial behavior of slabs and steel decking components in both tension and compression, and a complete floor system test.

2.7 Probabilistic Analysis of Progressive Collapse

In stark contrast to earthquake engineering research studies, which commonly account for probabilistic effects, progressive collapse research to date has been almost entirely deterministic. As a result, most collapse-resistant design guidelines are also deterministic. However, uncertainties exist in material properties, loads, and even in the fidelity of the computational modeling tools. Therefore, it is important to take into account reliability and probabilistic risk assessment in progressive collapse research and practice (Ellingwood, 2006).

One of the earliest non-deterministic studies on progressive collapse was conducted by Bennett (1987), who developed formulations for determining the probability of progressive collapse in structures. Ellingwood (2006) discussed methodologies for mitigating risk from abnormal loads and progressive collapse and provided a framework for addressing issues related to low probability/high consequence events in building practice, especially progressive collapse. A mathematical framework for risk analysis for progressive collapse was established, which was able to quantify measures of risk. According to this model, the annual probability of structural collapse due to an event which may lead to progressive collapse is given by

$$P[\text{Collapse}] = P[\text{Collapse}|D]P[D|H]\lambda_H \qquad \text{(Equation 2 – 1)}$$

where H is an extreme event; D is the occurrence of structurally significant local damage; λ_H is the annual mean rate of occurrence of H; $P[D|H]$ is the conditional probability of damage state D, given H; and $P[\text{Collapse}|D]$ is the probability of disproportionate damage or collapse, given damage state D. Equation 3 reveals that appropriate strategies by which to mitigate progressive collapse could involve the following measures: (1) reduction of λ_H by preventing the occurrence of abnormal events through non-structural means, e.g. by social or political means; (2) reduction of $P[D|H]$ by preventing the occurrence of significant local structural damage, e.g. by increasing standoff distance; and 3) reduction of $P[\text{Collapse}|D]$ by increasing system robustness. Since it is difficult

to determine λ_H, the probability of building collapse could be expressed on a scenario basis as follows

$$P[\text{Collapse}|\text{Scenario}] = P[\text{Collapse}|D]P[D|\text{Scenario}] \qquad \text{(Equation 2 – 2)}$$

When the alternate load path method is used in the design process, $P[D|\text{Scenario}]$ is assumed to be unity, i.e. the column is obliterated when the scenario occurs, i.e. which is the basis of the so-called missing column scenario. In this case, $P[\text{Collapse}] \approx P[\text{Collapse}|D]$

Kim et al. (2010) conducted sensitivity studies on the effect of various design parameters for steel buildings after sudden loss of columns, including yield strength of beams, columns and braces, live load, elastic modulus, and damping ratio. Xu and Ellingwood (2011) investigated the behavior of two three-story, pre-Northridge steel moment-resisting frame buildings subjected to loss of columns. Uncertainty in connection strength was considered in the study and the robustness of the two buildings under column loss scenarios was investigated both deterministically and probabilistically using nonlinear dynamic analysis.

Fragilities are common tools used in earthquake engineering for evaluating the probability of a structure or structural component being damaged beyond a certain limit state under various levels of ground shaking. In other word, fragilities can be used to evaluate the "capability of a structural system to withstand a specified event" (Braverman et al. 2003). Fragilities form the basis of probability-based design and performance-based design approaches. They were first used to evaluate the seismic risk of nuclear power plants (e.g. Kennedy et al. 1980, Kaplan et al. 1983, Kennedy and Ravindra 1984, and Braverman et al. 2004). Recently, seismic fragility assessment has been used by many researchers to evaluate the performance of structures under seismic loads, e.g. in Ellingwood et al. (2007) and Koutsourelakis (2010).

In spite of its usefulness in earthquake engineering, there are very few examples of the use of fragility functions in collapse-resistance design. Asprone et al. (2010) proposed a

probabilistic framework for multi-hazard risk analysis considering both seismic-induced collapse and blast-induced progressive collapse. The blast fragility was defined as the conditional probability of progressive collapse under a given blast level as the gravity load increases. Monte Carlo simulation was used to establish the blast-induced fragility curves. A related study was presented by Asprone et al. (2011).

Park and Kim (2010) assessed the progressive collapse potential of steel frames with various types of connections, including WUF-B, RBS, and WCPF, using fragility analysis. Uncertainties in design parameters such as yield strength, live load, and elastic modulus were considered. Fragility curves were obtained by calculating the probability that the vertical displacement at the end of removed column exceeded a certain limit state vs. the increased gravity load after loss of certain column members using the First-Order Second Moment method. Nonlinear static pushdown analysis was used to establish collapse fragilities. Both variation in design variables and correlations between the variables were considered.

One of the reasons why there are so few studies on collapse fragility is that the concept is not as straightforward as it is for earthquake-resistant design. To date, collapse fragility functions lack a clear definition of event intensity, i.e. how strong the event is, since the type of hazard is uncertain and may also be malicious. In contrast, seismic hazard is well documented and can be represented by relatively straightforward intensity measures (peak ground acceleration). Moreover, unlike earthquake engineering, where the seismic event influences the whole structure and not just a portion of it, collapse hazards are localized and their point of application is uncertain.

2.8 Enhancement of System Collapse Resistance

The ultimate goal of progressive collapse studies is to strengthen newly designed structures and retrofit existing structures so that they are not vulnerable to progressive collapse when subjected to abnormal loading conditions. The studies related to these

topics are reviewed herein, including retrofitting strategies and design guidelines against progressive collapse.

2.8.1 Retrofitting strategies

A series of experiments were carried out by Tan and Astaneh-Asl (2003) to evaluate the progressive collapse resistance of typical floor framing systems in steel structures and develop and test a cable-based retrofit technique of steel building floors to prevent progressive collapse. The specimen was a single-story steel floor system with composite concrete floor slab and the beam-to-column connections were typical shear tabs. In order to simulate column loss scenarios, two columns in the middle span of the specimen were designed and constructed as drop columns, whose supports could be removed during the test and a vertical downward displacement applied to them. Three tests were carried out and from the test results, the authors drew the following conclusions: (1) edge distance bolt hole fracture of shear tabs was a prevalent mode failure; (2) the floor slab contributes to progressive collapse resistance significantly through tensile catenary action; (3) the high strength steel cables provided additional strength, stiffness and toughness to resist the progressive collapse and provide an adequate alternate load path for the drop column load; and (4) the proposed retrofit method is efficient and economical in preventing progressive collapse of the tested specimen.

Hayes et al. (2005) discussed whether strengthening for earthquakes can improve blast and progressive collapse resistance of civil infrastructures. In order to answer the question, the Alfred P. Murrah Federal Building, which partly collapsed because of a bomb attack in 1995 was analyzed. A seismic evaluation of the building was first conducted, assuming the building was located in a region of high seismic activity. The analysis results showed that the building was deficient primarily because of poor column reinforcement lap splice details, negative post-yield stiffness due to the absence of seismic detailing, and torsional irregularities caused by the asymmetric shear wall layout. Three strengthening schemes, which were able to improve the seismic performance of the building, were designed for the vulnerabilities found during the evaluation: (1) a pier-

spandrel system, which added two new shear walls on the street side of the building; (2) a new special moment frame, which added a complete new reinforced concrete frame to the street face of the building; and (3) a set of internal shear walls. In addition to these three schemes, the original system was redetailed according to the current provisions. The three strengthening schemes and the redetialed frame were then analyzed when subjected to the same explosion that occurred in 1995. The analytical results reveal that the first two strengthening schemes and the redetailed frame reduced the degree of direct blast-induced damage and subsequent progressive collapse compared with the behavior of the original building. The third strengthening scheme was not as effective in reducing the blast and progressive collapse damage. The authors concluded that for both newly designed and existing building, progressive collapse resistance can be improved further by placing the element that are proportioned and detailed to resist lateral forces on a building perimeter than by placing them in a building's interior.

Orton (2007) investigated the use of carbon fiber reinforced polymer (CFRP) to retrofit existing reinforced concrete beams and provide continuity to reinforced concrete buildings, which may be vulnerable to progressive collapse due to lack of continuity of longitudinal reinforcing steel in the beams. Forty anchorage tests, eight continuity tests, and one catenary model were developed and evaluated. The anchorage tests not only formed the design basis of the CFRP retrofit scheme and ensured that the capacity of a retrofitted beam can be accurately predicted, but also evaluated how carbon fiber anchors improved the use of CFRP sheets to strengthen reinforced concrete members. The anchorage tests consisted of two blocks of concrete connected by a CFRP sheet with or without height transitions. The connected blocks were loaded with a point load at midspan to simulate a beam with preexisting cracks. The continuity tests evaluated the ability of CFRP to provide continuity and reduce vulnerability to progressive collapse. A series of beam-column assemblies with the center column removed and without continuous reinforcing steel were tested and the development of catenary action was studied. In these tests, CFRP was used to provide continuity through both positive and negative moment reinforcement. The experiments revealed that catenary action can only be activated in the negative moment retrofits, although the CFRP retrofit scheme can

increase the capacity of the beam before catenary action is triggered in the positive moment retrofits. In addition, tests were also conducted on a beam with continuous reinforcing steel and a beam strengthened with CFRP to accommodate the double span through flexure. The tests results demonstrated that the former one is not effective in retrofitting concrete beams. Although the latter one limits deflections and provides a higher performance objective, it requires a much great amount of CFRP. In the end, a catenary model based on equations which were developed to characterize the load and deflection relationship of a reinforced concrete beam in catenary action was developed and applied to a 3D model of a reinforced concrete building. From the above results, the author concluded that a CFRP retrofit can reduce vulnerability to progressive collapse in reinforced concrete buildings.

Liu (2009) proposed retrofitting schemes for strengthening shear tab connections. Both theoretical and finite element analyses were conducted and catenary action was investigated in the theoretical study. Two retrofitting schemes were proposed to strengthen shear tab connections. Both schemes were based on the idea of connecting the beam flanges at the connection area to allow carrying higher tensile forces. Catenary action in a truss element was evaluated to examine the effectiveness of the proposed retrofitting scheme. It was shown that the failure load and global deformation increased significantly. To further examine the performance of retrofitted beam-column connections, nonlinear finite element models were developed and used to investigate catenary action, including one-dimensional beam element models, two-dimensional solid element models, and three-dimensional shell element models. All simulations were conducted for both the original and the retrofitted structures. The simulation results demonstrated that the shear tab connections were not capable of developing catenary action because they were too weak. On the other hand, the proposed retrofitting schemes were effective for strengthening the connections.

In other recent efforts, Crawford (2002) presented retrofit schemes suitable for mitigating progressive collapse for multistory buildings. Abbott Galvão Sobreira Lopes (2009) presented potential structural and architectural techniques to design and retrofit buildings

for resistance to blast impact loads as well as progressive collapse. Choi and Chang (2009) claimed that progressive collapse can be prevented by fixing X braces into each span of the top floor. Porte (2009) investigated the effectiveness of a cable-retrofit solution in improving the progressive collapse resistance of existing steel buildings using numerical models. Kim and Shin (2011) proposed retrofit scheme of reinforced concrete frames against progressive collapse using prestressing tendons. Manuel Sanchez Escalera (2011) proposed a retrofit technology which installed thin steel panels into steel building structural frames to enhance the system progressive collapse resistance.

2.8.2 Design against progressive collapse

Many researchers have dedicated their efforts to developing design strategies against progressive collapse. Early examples can be found in Popoff (1977), Leyendecker and Ellingwood (1977), Ellingwood and Leyendecker (1978), Gross and McGuire (1983), and Ettouney et al. (1996). More recent examples can be found in Smilowitz and Tennant (2001), Hamburger and Whittaker (2004), Ellingwood (2005), Byfield (2006), Nair (2006), Wada et al. (2006), Beer and Liebscher (2008), Kim and Park (2008), Starossek and Haberland (2010), and Liu (2011).

Currently, a number of provisions are provided by codes and standards in the United States, such as ASCE Standard 7-10: Minimum Design Loads for Buildings and Other Structures (ASCE, 2010), General Services Administration - Progressive Collapse Analysis and Design Guidelines for New Federal Office Buildings and Major Modernization Projects (GSA, 2003) and Department of Defense (DoD) – Unified Facilities Criteria – Design of Buildings to Resist Progressive Collapse (UFC, 2009).

The only main stream code that addresses progressive collapse in some detail is ASCE Standard 7-10 (ASCE, 2010). Two design alternatives are available: direct design and indirect design. In the former, the resistance to progressive collapse is considered specifically during the design procedure through the Alternate Path Method or Specific Local Resistance Method. In ASCE Standard 7-10 (ASCE, 2010), Specific Local Resistance Method is defined as “A method that seeks to provide sufficient strength to

resist failure from accidents or misuse". In indirect design, resistance to progressive collapse is considered implicitly during the design process through the provision of minimum levels of strength, continuity, and ductility. ASCE Standard 7-10 (ASCE, 2010) emphasizes the importance of general structural integrity in resisting progressive collapse and provides related guidelines.

The purpose of GSA guidelines is to reduce the potential for progressive collapse in newly-designed and existing Federal Office Buildings and to assist in the development of potential upgrades to facilities if required. In this document, the alternate path method is advocated to mitigate progressive collapse. It provides an exemption process and proposes different design approaches for exempt and non-exempt buildings. Both linear procedure and nonlinear procedure are permitted in the guidelines. However, the linear procedure should be used only in low-to-medium-rise buildings, which are below 10 stories high. The document utilizes a flow-chart methodology to determine whether a building needs to be considered for progressive collapse in the design process. The flow chart is shown in Figure 2 – 9. When a Linear Procedure, which is a simplified methodology, is used, appropriate Demand-Capacity Ratios (DCR) have to be used in order to satisfy the acceptance criteria accounting for uncertainties in structural behavior. DCR is defined as the following equation:

$$DCR = \frac{Q_{UD}}{Q_{CE}} \qquad \text{(Equation 2 – 3)}$$

where,

Q_{UD} = Acting force (demand) determined in component or connection/joint (moment, axial force, shear, and possible combined forces)

Q_{CE} = Expected ultimate, un-factored capacity of the component and/or connection/joint (moment, axial force, shear, and possible combined forces)

It is required that the values of DCR should be smaller than 2.0 for typical structural configurations and 1.5 for atypical structural configurations.

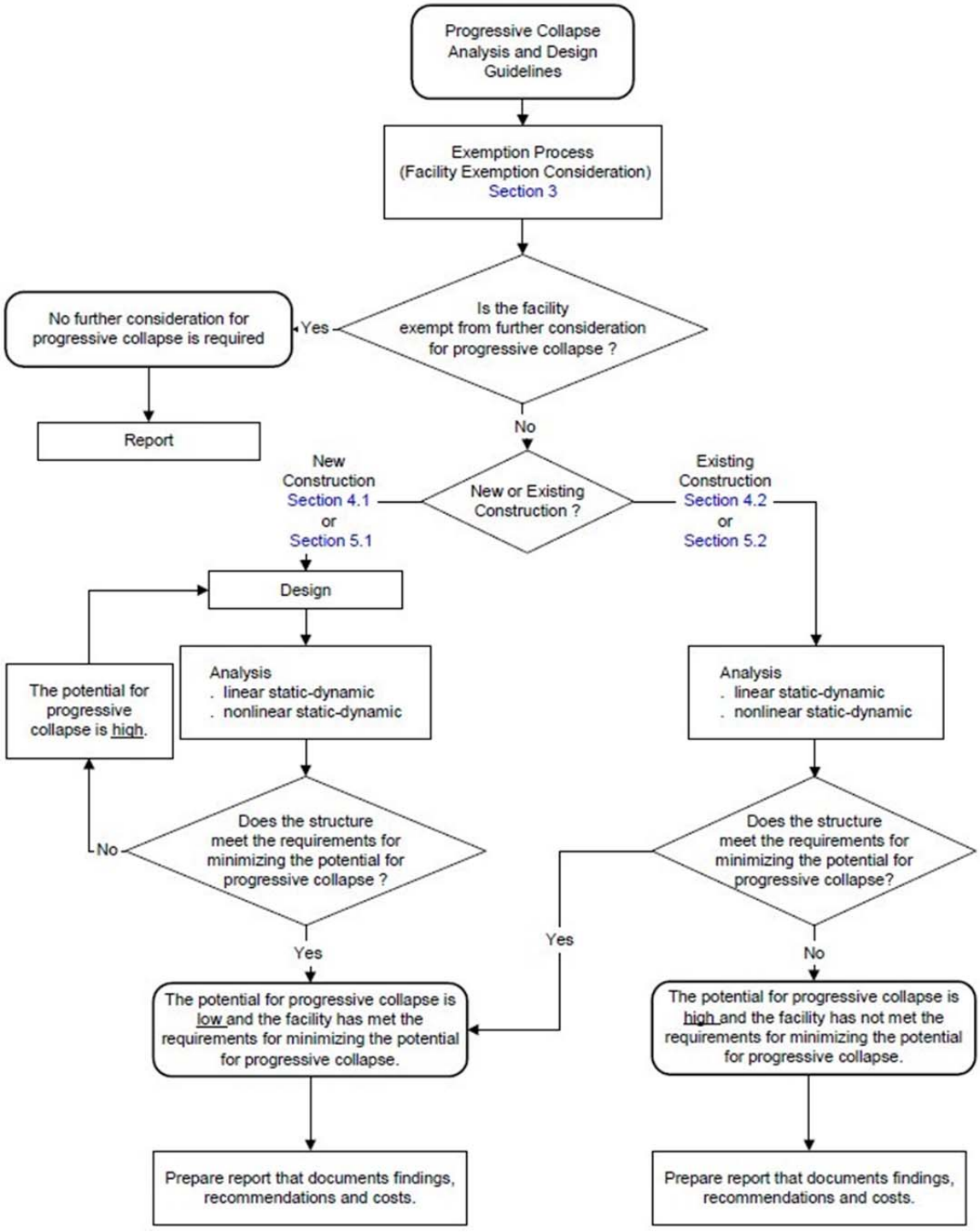

Figure 2 - 9 Overall flow for consideration of progressive collapse (GSA, 2003)

Similar with GSA (2003), UFC (2009) also proposes design strategies for newly designed and existing building against progressive collapse. In this document, design approaches vary according to building occupancy, in other words, "the progressive collapse design approaches are primarily a function of the occupancy of the building". Three design approaches were used, namely, Tie Forces Method, which is an indirect design method, Alternate Path Method and Enhanced Local Resistance Method. The latter two are direct design methods. However, only Tie Forces Method and Alternate Path Method are emphasized and described in detail. In the Tie Forces Method, the continuity, ductility and alternate load paths are enhanced by tying the building together mechanically. The tie forces can be provided by structural elements which are designed using conventional design philosophy under normal loading conditions. There are three horizontal ties, longitudinal, transverse, and peripheral, which must be provided and vertical ties are only required in the columns and load-bearing walls. Figure 2 – 10 showed the tie forces developed in a frame structure. It is required that "unless the structural members and their connections can be shown capable of carrying the required longitudinal, transverse, or peripheral tie force magnitudes while undergoing rotations of 0.20-rad, the longitudinal, transverse, and peripheral tie forces are to be carried by the floor and roof system." The alternate path method can be used when there are not adequate vertical ties in the buildings, but adequate horizontal ties must be present.

Several organizations, such as AISC, ACI and ASCE have developed or are developing model collapse resistance guidelines, which will likely form the basis of future collapse resistance specifications.

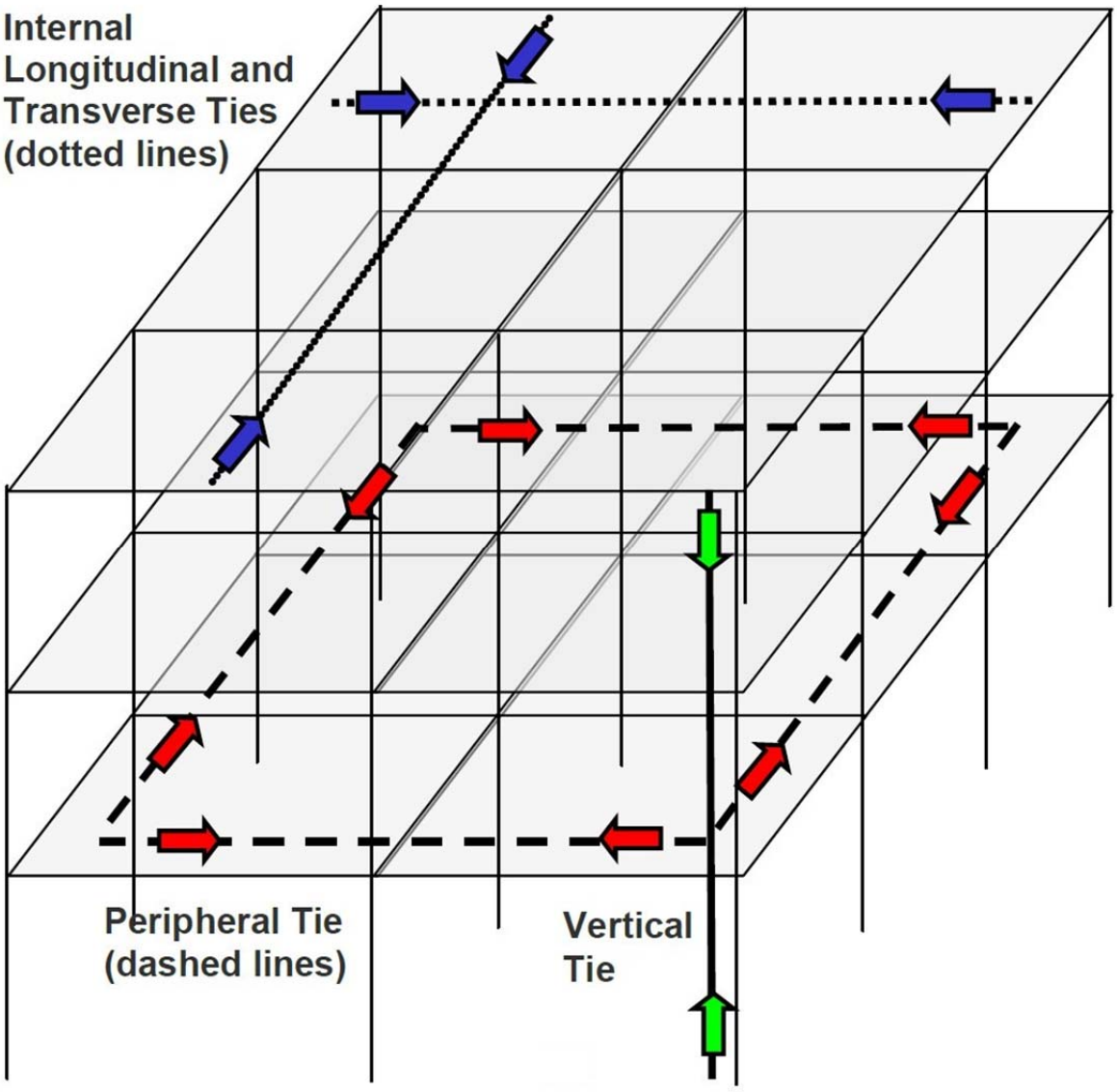

Figure 2 - 10 Tie Forces in a frame structure (UFC, 2009)

CHAPTER 3

PROTOTYPE MODEL DEVELOPMENT

3.1 Introduction

This chapter outlines the development of four types of models of the 10-story prototype building used in this research. The models developed are 1) a detailed micro model of the full 3-D system, termed M1; 2) a model of the full 3-D system comprised of macro-elements for beams, columns and connections and shell elements for the slab, termed M2; 3) a 3-D micro model of a single frame in the system, termed M3; and 4) a macro model of the frame modeled in M3, termed M4. Model M1 is the most sophisticated, while M4 is the least complicated. The former is likely to be used in research studies. While the latter is not permitted by the UFC (2010) guidelines for simulating structural response for a failed column scenario, its simplicity makes it appealing for preliminary, design-oriented computations of robustness. Models M2 and M3 are bracketed in between M1 and M4 in terms of complexity and their ability to accurately represent collapse response.

Details of the prototype structure used in this study are first introduced in section 3.2. Model details are discussed in section 3.3 and validation studies are presented in section 3.4. The chapter is summarized and conclusions drawn in section 3.5.

3.2 Prototype Structure

The National Institute of Standards and Technology (NIST) designed prototype steel framed buildings for the purpose of studying their response to an event which may cause progressive collapse (Liang et al., 2007). The buildings are 10-story office buildings with plan dimensions of 45.7 x 30.5 m and utilize moment-resisting frames as the lateral load resisting system. One of buildings designed by NIST is selected for the study in this work: namely Building 3, located in Seattle, WA, and categorized as Seismic Design Category D, i.e. SDC-D. The building employs Special Moment Frames (SMF) for lateral force resistance. Design details can be found in Liang et al. (2007) and Khandelwal et al. (2008).

Table 3 - 1 Typical beam and column cross sections for moment bays

Floor	Story Height	Column (E-W)	Column (N-S)	Beam (E-W)	Beam (N-S)
1	5.33 m	W24x146	W24x146	W27x94	W24x94
2	4.20 m	W24x146	W24x146	W27x94	W24x94
3	4.20 m	W24x146	W24x146	W27x94	W24x94
4	4.20 m	W24x146	W24x146	W27x94	W24x94
5	4.20 m	W24x131	W24x146	W27x94	W24x94
6	4.20 m	W24x131	W24x117	W27x94	W24x68
7	4.20 m	W24x131	W24x117	W27x94	W24x68
8	4.20 m	W24x117	W24x117	W21x50	W21x44
9	4.20 m	W24x117	W24x117	W21x50	W21x44
10	4.20 m	W24x84	W24x84	W16x26	W16x26

The selected building has a structural system comprised of both moment frames and a gravity system. There are 36 columns, of which 24 belong to moment-resisting bays, while the rest are gravity column. Beams in the gravity system are connected to the columns through shear connections which are comprised of single plate, shear tab connections, that are filet welded to the column and bolted using 22 mm, A325 high strength bolts to 9.5 mm A36 shear tabs. In the moment frames, reduced beam sections (RBS) are used with 50% reduction in RBS flanges. In all moment connections, beams are assumed welded to the columns, to simplify the modeling process. The structural steel used for all beams and columns is A992 (F_y = 345 Mpa). The plan of Building 3 is shown

in Figure 3 – 1(a), while the elevation of the E-W frame on axis 6 is shown in Figure 3 – 1(b). The details of the structural members can be found in Table 3 – 1.

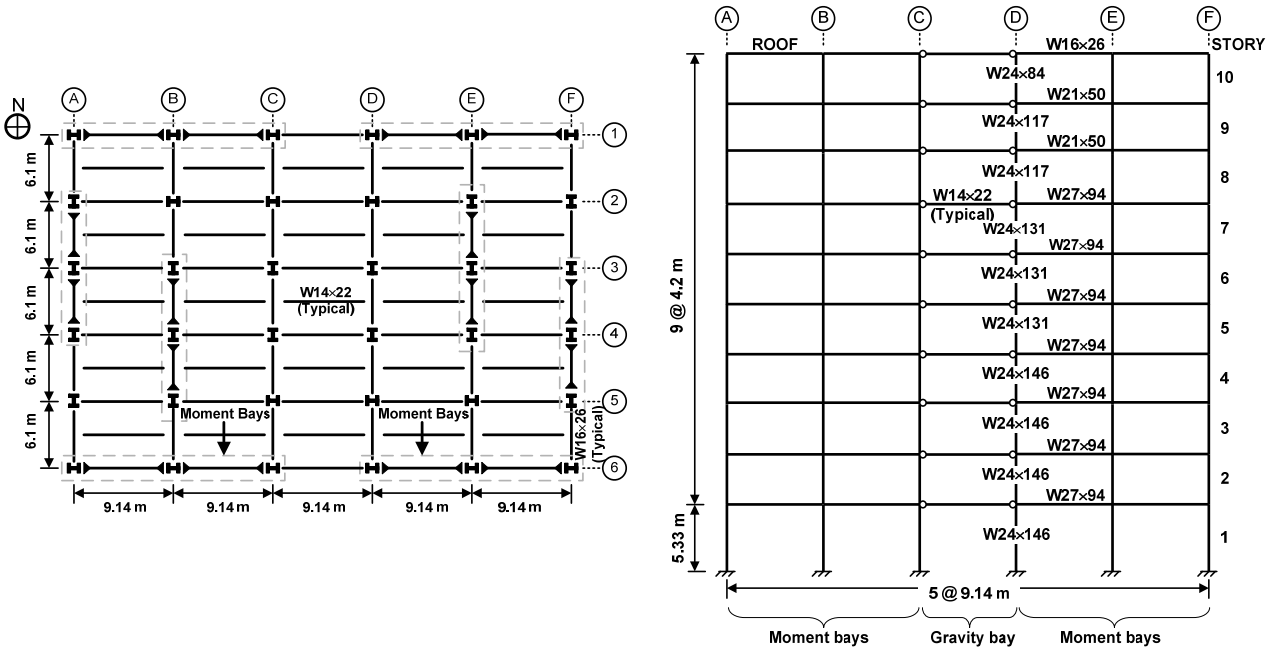

(a) Plan View (b) Elevation View

Figure 3 - 1 The Prototype Building

3.3 Modeling Approaches

The general modeling approach adopted in this study is to model all primary structural elements in the system, within the specific limitations of each model, including all structural members and the connections between them. Since the focus of the study is on nonlinear response, each element's representation permits inelastic response to occur including fracture and separation, where appropriate. To enable realistic simulations of collapse, interpenetration between the various components of each model is prohibited. Therefore, falling components can introduce impact forces on the components with which they come in contact. The simulations are conducted with a single damping parameter

that resulted in mass proportional damping ratios that ranged from 2% to 5%, depending upon the initial dynamic properties of the simulation in question. The simulations are carried out using the explicit finite element code LS-DYNA (Hallquist 2006) running on an AMD Opteron 2435 cluster with 12 CPUs and 24 GB of RAM.

3.3.1 Model M1

- ***General***

Model M1 is a detailed representation of the full 3-D building and is comprised of about 800,000 continuum finite elements. The full 3-D model is shown in Figure 3 – 2. The model accounts for the composite floor, steel beams and columns, as well as the two types of connections that are used to join the columns and beams, i.e. shear tab connections and moment connections. The beams and columns are modeled using fully integrated rectangular shell elements ranging in size from 220 mm to 380 mm. The mesh is refined around connections to ensure that the large strain and stress gradients in such regions are correctly captured. Although the mesh is somewhat coarse to reduce the modeling effort and associated computational demands, extensive mesh size sensitivity studies confirmed that the model produces reasonable results. While more computationally expensive than reduced integration elements, fully integrated elements are employed to ensure that hour-glass modes do not contaminate the simulation results. More details of the model M1 at the connection regions are shown in Figure 3 – 3.

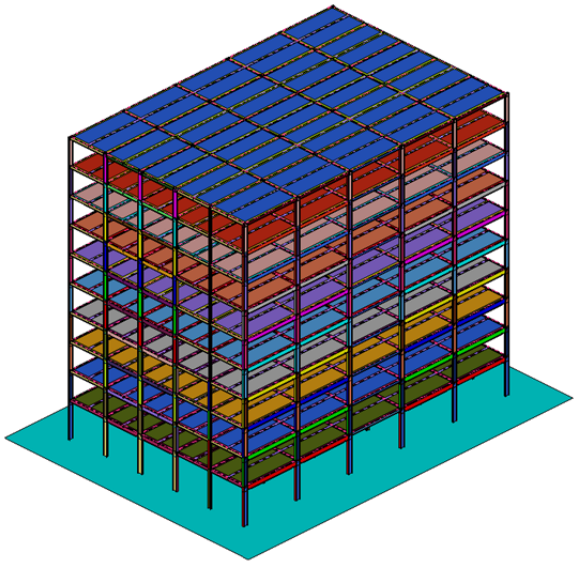

(a) 3-D view

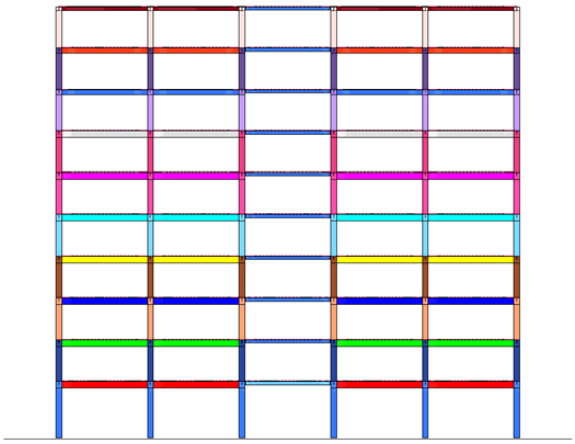

(b) Front view (Column line 1 and 6)

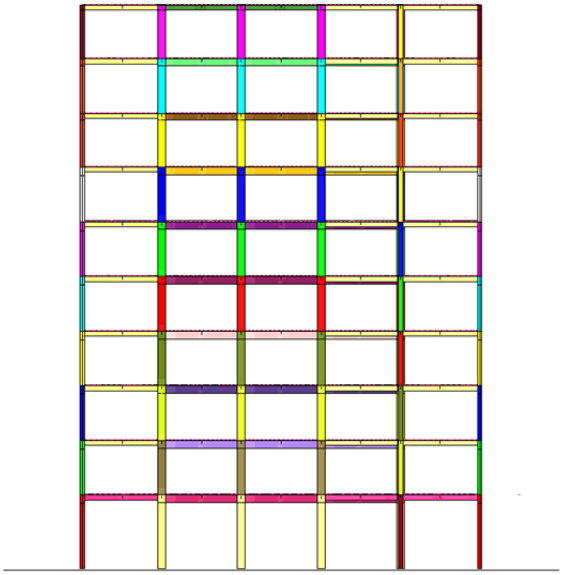

(c) Lateral view (Column line A and F)

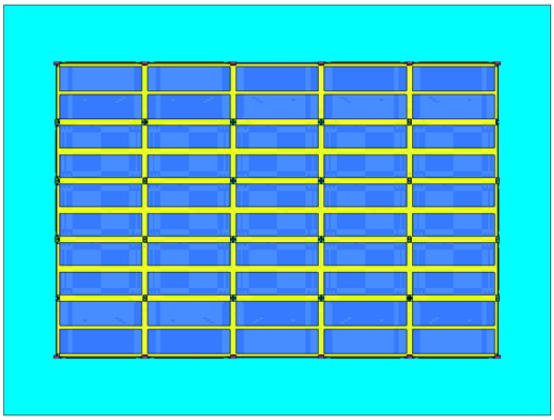

(d) Top view

Figure 3 - 2 Details of Model M1: Full Model

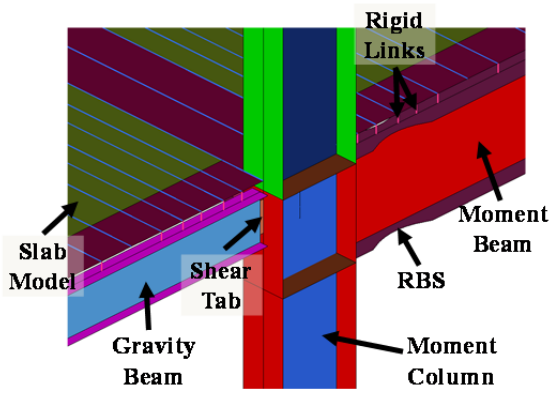

(a) Beam-to-column connection: moment column A2, A4, B3, B5, C1, C6, D1, D6, E2, E4, F3, F5

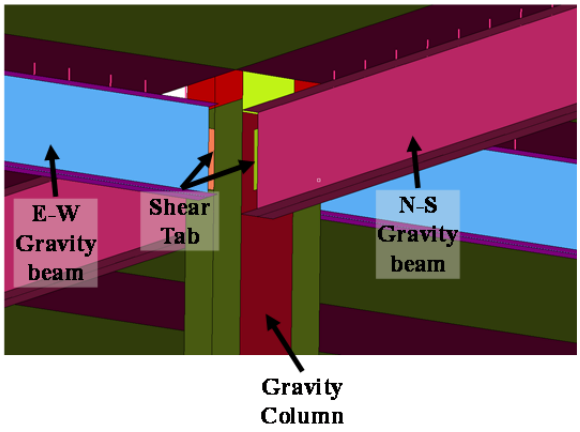

(b) Beam-to-column connection: gravity column B2, C2, C3, C4, C5, D2, D3, D4, D5, E5, F2

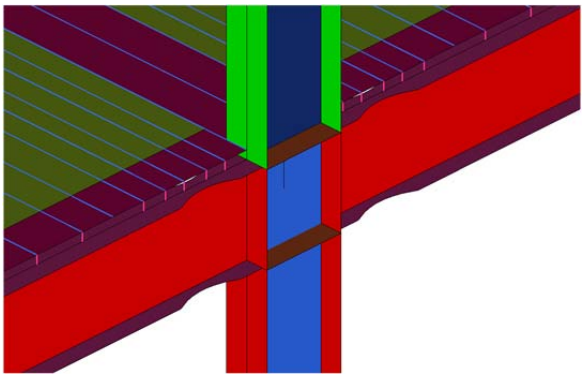

(c) Column-to-beam connection: Column A3, B1, B4, B6, E1, E3, E6, F4

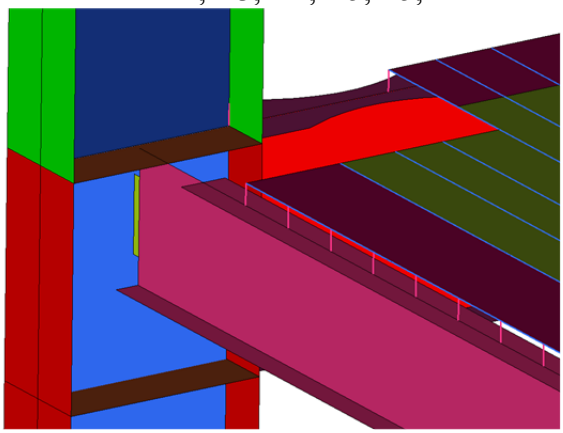

(d) Column-to-beam connection: Column A1, A6, F1, F6

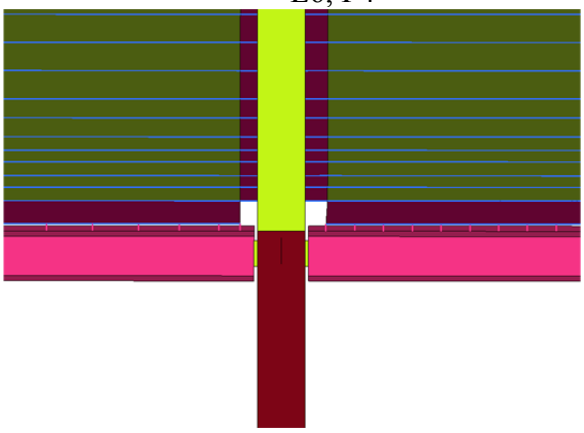

(e) Column-to-beam connection: Column A5, F2

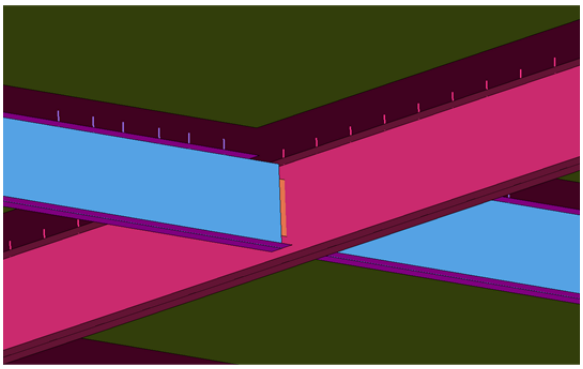

(f) Infill beam-to-gravity beam connection

Figure 3 - 3 Details of Model M1: Connection region

- ***Connections***

Shear tab connections (Figure 3 – 4) are modeled using a single row of shell elements, as shown in Figure 3 – 5. The thickness of the shell elements are set to be equal to the thickness of the beam web. Stress-strain characteristics of these shell elements are derived on the basis of Equations 3 – 15 and 3 – 16 in Section 3.3.2, which will be presented later in this chapter. Beam-to-column moment connections are modeled by connecting beam nodes to the column surface, implying that fractures in the weld zones are precluded. It is reasonable to assume that yielding and subsequent fracture would occur outside of the weld region considering the current stringent requirements on weld quality control (Khandelwal and El-Tawil. 2007).

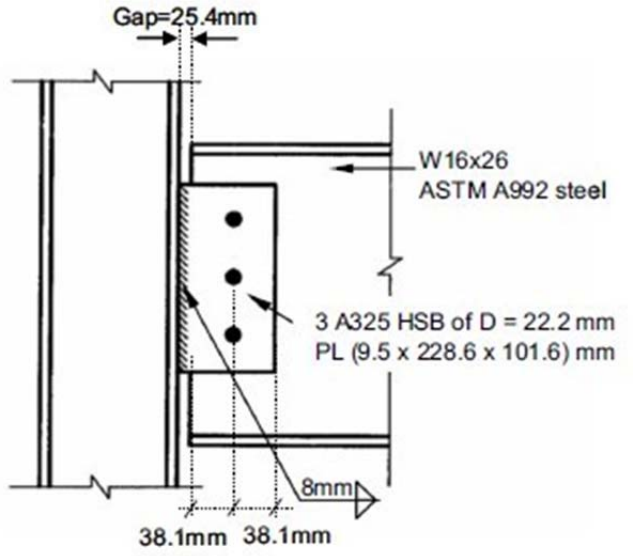

Figure 3 - 4 Single-plate shear connection used in the gravity frames

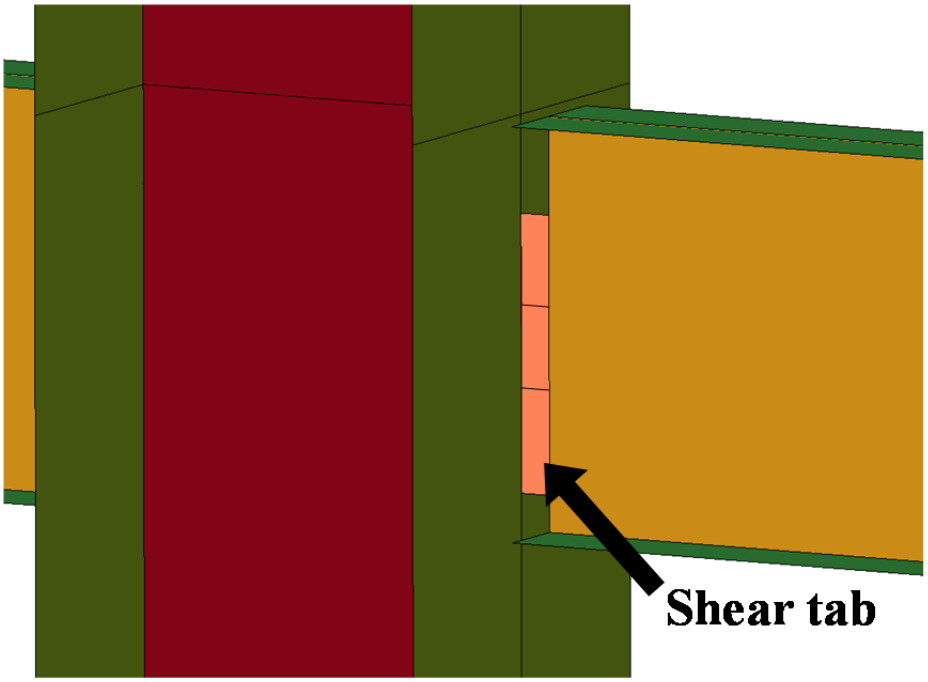

Figure 3 - 5 Model of shear tab

- ***Material model for steel***

A J_2 plasticity model is used to represent the response of steel in all beams and columns. The uniaxial stress strain response is shown in Figure 3 – 7(a). A strain hardening value of 0.5% is assumed and ductile fracture failure is assumed to occur when the plastic strain achieves 0.27 for element sizes that are 25 mm, an approach that was used in previous studies by Khandelwal and El-Tawil (2007), Sadek et al. (2008) and Alashker et al. (2010). Elements that achieve this criterion are removed to represent fracture.

Material model #24 (Piecewise Linear Isotropic Plasticity) in LS-DYNA is selected to represent the steel. In this model, the deviatoric stresses s_{ij} have to satisfy the yield function

$$\emptyset = \frac{1}{2} s_{ij} s_{ij} - \frac{\sigma_y^2}{3} \leq 0 \qquad \text{(Equation 3 – 1)}$$

where $s_{ij} = \sigma_{ij} - \frac{\sigma_{ii}}{3}$ and

$$\sigma_y = \beta[\sigma_0 + f_h(\varepsilon_{eff}^p)] \qquad \text{(Equation 3 – 2)}$$

The parameter β accounts for the strain rate effects. $f_h(\varepsilon_{eff}^p)$ represents the hardening function, in which ε_{eff}^p is the effective plastic strain and

$$\varepsilon_{eff}^p = \int_0^t \left(\frac{2}{3}\dot{\varepsilon}_{ij}^p \dot{\varepsilon}_{ij}^p\right)^{\frac{1}{2}} dt \qquad \text{(Equation 3 – 3)}$$

where $\dot{\varepsilon}_{ij}^p$ is the rate of plastic strain.

During a typical increment, the deviatoric stresses are first updated elastically and the yield function is then checked. If the yield function is satisfied, the deviatoric stresses are accepted as the correct solution. If not, an increment in plastic strain is computed as follows:

$$\Delta\varepsilon_{eff}^p = \frac{\left(\frac{2}{3}s_{ij}^* s_{ij}^*\right)^{\frac{1}{2}} - \sigma_y}{3G + E_p} \qquad \text{(Equation 3 – 4)}$$

where G is the shear modulus, E_p is the current plastic hardening modulus, and s_{ij}^* is the trial deviatoric stress.

Thus,

$$s_{ij}^{n+1} = \frac{\sigma_y}{\left(\frac{3}{2}s_{ij}^* s_{ij}^*\right)^{\frac{1}{2}}} s_{ij}^* \qquad \text{(Equation 3 – 5)}$$

- ***Composite floor***

The composite floor is comprised of a RC slab of thickness 82.5 mm sitting on a steel deck with 76 mm depth and connected to the underlying steel beams via shear studs. Steel reinforcement in the RC slab is 0.06 mm^2/mm in both directions. To avoid the complexity of modeling such a system in detail, e.g. as done in Sadek et al. (2008) and Alashker et al. (2010), a reduced model is employed. As described next, the simplified model is calibrated to model the tensile membrane response of the floor slab. Emphasis is not placed on accurately modeling flexural action, since that diminishes in importance at the large deformation levels that are of interest in this study. The simplified model also does not account for shear stud behavior since the detailed computational studies in Sadek et al. (2008) and Alashker et al. (2010) showed that to be of limited effect on overall response.

As shown in Figure 3 – 6, the floor slab is modeled using fully integrated four-node, isotropic shell elements. An equivalent section shell thickness of 101.5 mm is adopted and the floor slab is connected to the underlying steel beams through rigid links, which are intended to model the physical separation that exists between the center plane of the slab and that of the top beam flange. The uniaxial material response of composite floor elements is based upon the following simplifying assumptions: 1) the concrete slab is the only source for compressive resistance and it has zero tensile strength; 2) the metal deck and steel reinforcement mesh are the source of tensile resistance; 3) the tensile resistance of the steel reinforcement mesh is smeared and acts equally in both directions in the shell model; 4) since the steel deck can only develop resistance along the directions of the flutes, its effect is represented using steel bars attached directly to the shell elements. The area of the equivalent steel bars is taken to be 50% of the area of the steel deck based on calibration to Alashker and El-Tawil (2011). The direct connection between steel bar nodes and shell elements implies that: a) no slip is permitted between the steel deck and the adjacent concrete slab, and b) the steel deck is located at the concrete slab centerline. The latter implication is deemed appropriate given the previously mentioned interest in the floors axial resistance, and not its flexural behavior. The stress-strain response of bars representing the steel deck, as well as the smeared mesh reinforcement, is assumed to be elastic perfectly plastic with yield strength of 248 MPa and a fracture strain of 0.25.

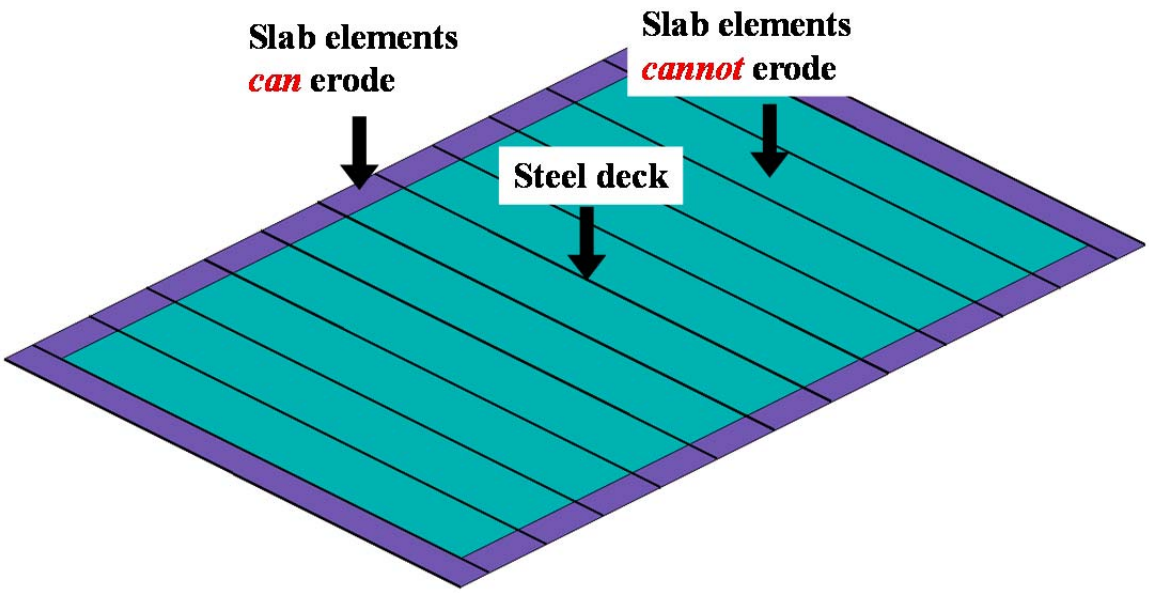

Figure 3 - 6 Composite slab model

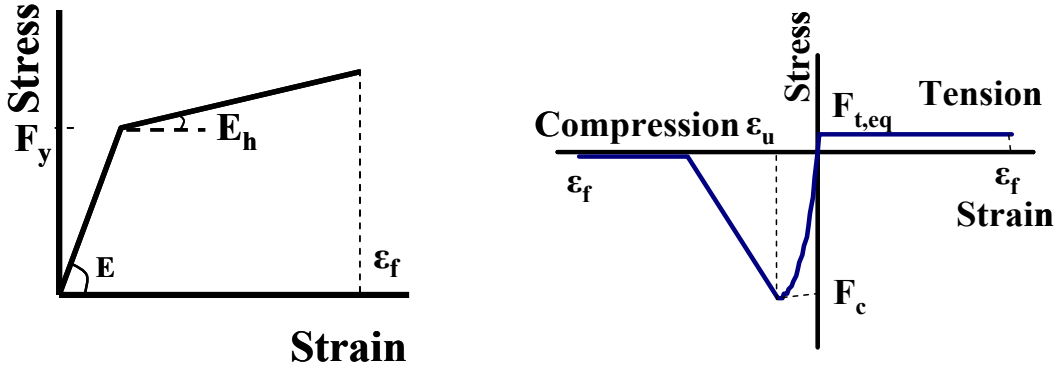

(a) Steel elements

(b) Composite slab elements

Figure 3 - 7 Material models

The nonlinear stress-strain relationship employed for concrete in compression is shown in Figure 3 – 7(b). Concrete compressive strength is taken as 21 Mpa and modulus of elasticity 28 Gpa. The equivalent tensile stress-strain relationship is defined as shown in Equation 1.

$$F_{t,eq}(\varepsilon) = \frac{F_{t,R}(\varepsilon) \cdot A_R}{A_{eq}} \qquad \text{(Equation 3 – 6)}$$

Where; $F_{t,eq}(\varepsilon)$ is the equivalent tensile stress at strain ε; A_{eq} is the equivalent area of the floor element per unit width; $F_{t,R}(\varepsilon)$ are the stress values in the steel reinforcement mesh at strain ε; and A_R is the area of the mesh reinforcement per unit width.

A J_2 plasticity model that can accommodate different tensile and compressive yield responses is used to model the composite slab. The tensile failure criterion for slab elements is taken to be a plastic strain of 0.25 based on calibration to the detailed finite element model in Sadek et al. (2008). This failure criterion is only applied to the shell elements on the periphery of the slab. When these elements achieve the specified plastic failure strain they are eliminated from the model to represent fracture failure of the steel elements in the floor. As the system implodes, falling slabs 'slam' into the slabs underneath them leading to high stress and strain levels, leading to rapid erosion of the entire slab if its elements are permitted to disappear. Therefore, to preserve as much as possible of the mass of the slab as it collapses, only peripheral elements are permitted to be deleted while all other slab elements are not allowed to be eliminated.

The floor model, as described above, is essentially a hybrid micro/macro model because the floor model uses a mixture of shell and bar elements to mimic overall behavior. However, given the predominant effect of the beams, columns and connections, which are modeled using the micro approach, the overall model is still referred to as a micro model.

- ***Formulation of fully integrated shell element***

The shell elements used in Model M1 are fully integrated shell elements, which are not susceptible to hourglassing. The formulation employs a local element coordinate to

account for rigid body motion and satisfy frame invariance of the constitutive relations. The coordinate system is shown in Figure 3 – 8, where it is clear that the local element coordinate system is comprised of three basis vectors. Two of the basis vectors are tangent to the shell mid-surface at the center of the element and the third one is in the normal direction of this surface. The midsurface is defined by the location of the element's four corner nodes. As shown in Figure 3 – 8, the basis vectors $\{e_1^l, e_2^l, e_3^l\}$ can be described as follows:

$$e_3^l = \frac{S_3}{\|S_3\|} \qquad \text{(Equation 3 – 7)}$$

$$\|S_3\| = \sqrt{S_{31}^2 + S_{32}^2 + S_{33}^2} \qquad \text{(Equation 3 – 8)}$$

$$S_3 = r_{31} \times r_{42} \qquad \text{(Equation 3 – 9)}$$

$$S_1 = r_{21} - \left(r_{21} \cdot e_3^l\right) e_3^l \qquad \text{(Equation 3 – 10)}$$

$$e_1^l = \frac{S_1}{\|S_1\|} \qquad \text{(Equation 3 – 11)}$$

$$e_2^l = e_1^l \times e_3^l \quad \text{(Equation 3 – 12)}$$

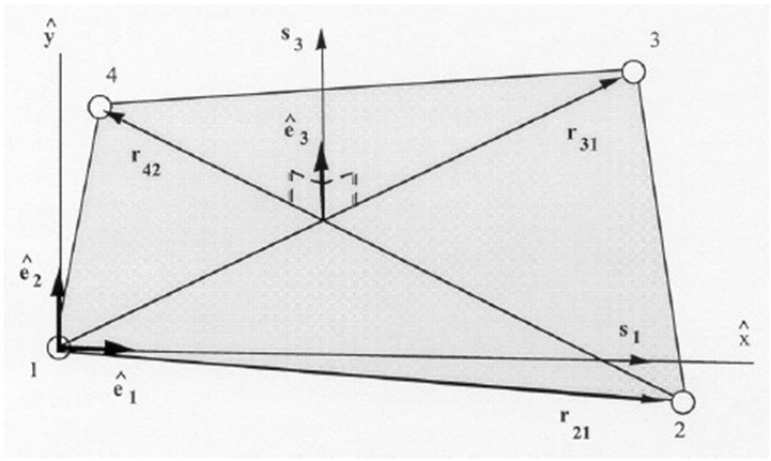

Figure 3 - 8 Element coordinate system (Hallquist, 2006)

The fully integrated shell is derived on the basis of the Hu-Washizu three-field principle, which can be expressed as:

$$0 = \delta\Pi(\vartheta, \bar{D}, \bar{\sigma}) = \int_{\Omega} \delta\bar{D} : \sigma(\bar{D}) d\Omega + \int_{\Omega} \delta[\bar{\sigma} : (D(\vartheta) - \bar{D})] d\Omega - \delta P_{ext} + \delta P_{kin}$$

(Equation 3 – 13)

where ϑ is the velocity, $\bar{D}$ is the assumed strain rate, $\bar{\sigma}$ is the assumed stress, σ is the constitutive update as a function of the assumed strain rate, D is the strain rate computed from the velocity field, and δP_{kin} and δP_{ext} are the virtual power contribution from the inertial and external forces, respectively. Ω denotes the domain of the shell element. The contribution from the internal forces can be decomposed into in-plane and transverse shear parts:

$$0 = \delta P_{int}^{p} + \delta P_{int}^{s} + H^{p} + H^{s} - \delta P_{ext} + \delta P_{kin} \qquad \text{(Equation 3 – 14)}$$

where $\delta P_{int}^{p} = \int_{\Omega} \delta\bar{D}^{p} : \sigma^{p}(\bar{D}) d\Omega$;

$\delta P_{int}^{s} = \aleph\left(\int_{\Omega} \delta\bar{D}^{s} : \sigma^{s}(\bar{D}) d\Omega\right)$, $\aleph$ is the shear correction factor;

$H^p = \int_\Omega \ \delta[\bar{\sigma}^p : (D^p(\vartheta) - \bar{D}^p)]d\Omega$;

and $H^s = \int_\Omega \ \aleph\left(\int_\Omega \ \delta[\bar{\sigma}^s : (D^s(\vartheta) - \bar{D}^s)]d\Omega\right)$.

The kinematics of the element and assumed strain field are calculated on the basis of the material discussed above.

3.3.2 Model M2

- ***General***

Like M1, Model M2 is also a 3-D model. However, beam-column macro elements are utilized instead of continuum elements in the beams and columns. This cuts down greatly on the number of degrees of freedom in the model. The total number of the elements used in this model is 63,600. Figure 3 – 9 shows an overview of the model, while Figure 3 – 10 shows a close up of the various connection regions.

Beams and columns are represented using a Hughes-Liu beam-column element formulation, which was shown to be capable of reasonably representing beam-column structural response by Khandelwal and El-Tawil (2007). However, unlike Khandelwal and El-Tawil (2007), who used a user-defined material model that distinguished between tensile and compressive responses, the model employed herein assumes that the tensile and compressive responses are similar. This was done for the sake of practicality because user-defined models: 1) are more difficult to employ than native material models; and 2) slow down the analysis. Figure 3 – 7(a) shows the general form of the constitutive model employed, where E_h is 0.5% and ε_f is determined based upon calibration studies which will be discussed later in this chapter.

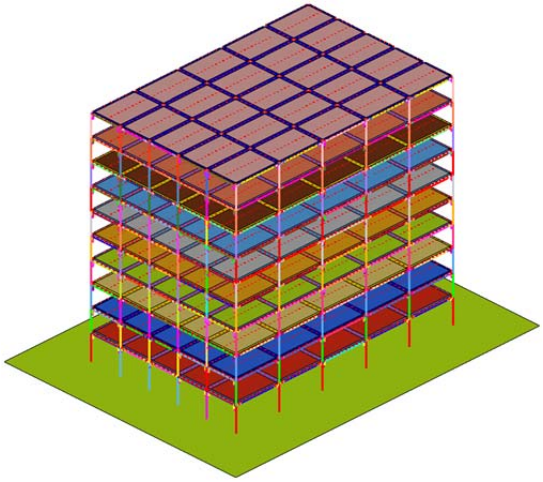

(a) 3-D view

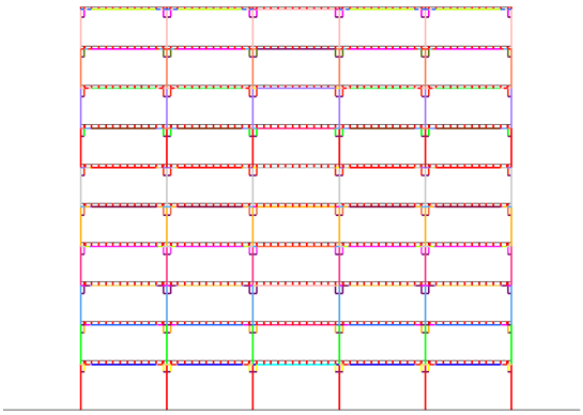

(b) Front view (Column line 1 and 6)

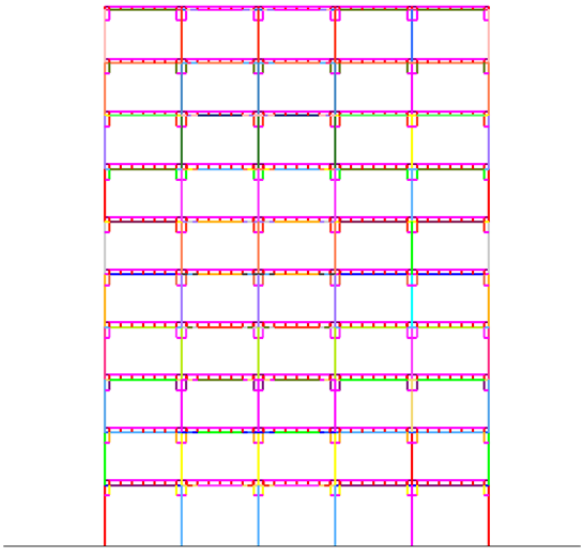

(c) Lateral view (Column line A and F)

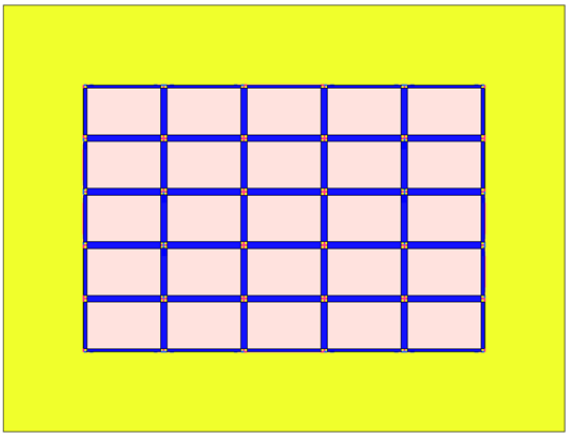

(d) Top view

Figure 3 - 9 Details of Model M2: Full model

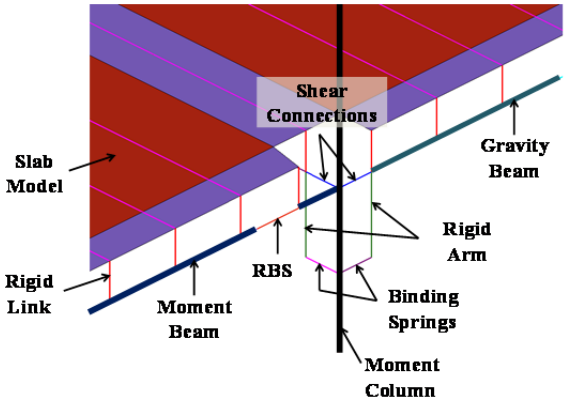

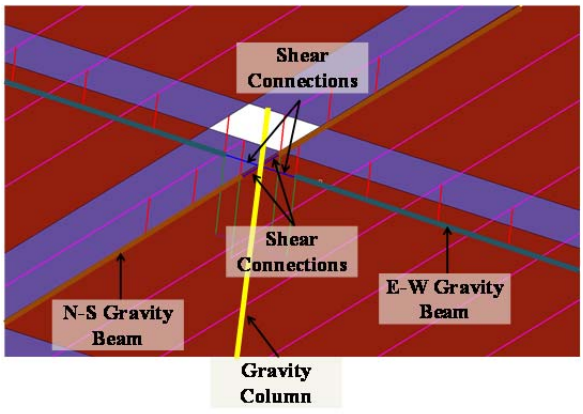

(a) Beam-to-column connection: moment column A2, A4, B3, B5, C1, C6, D1, D6, E2, E4, F3, F5

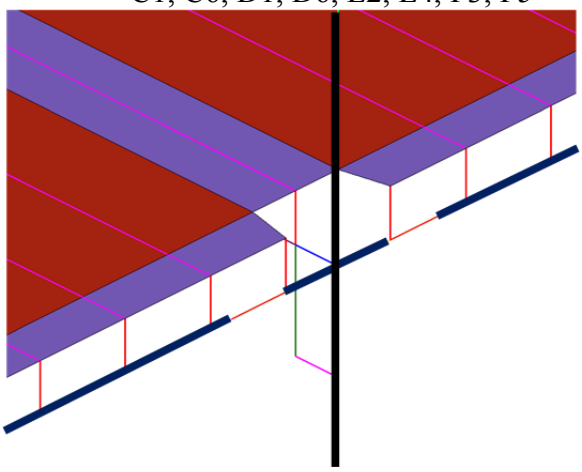

(b) Beam-to-column connection: gravity column B2, C2, C3, C4, C5, D2, D3, D4, D5, E5, F2

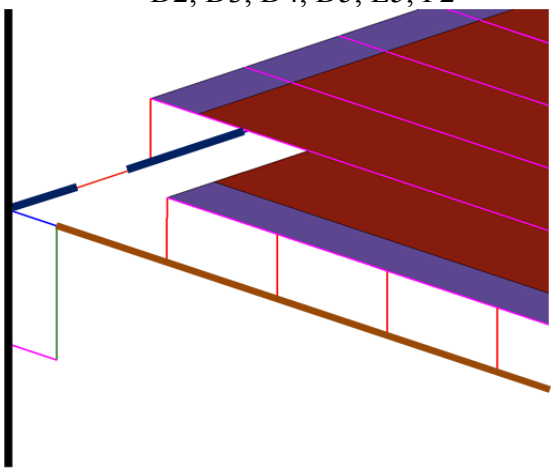

(c) Column-to-beam connection: Column A3, B1, B4, B6, E1, E3, E6, F4

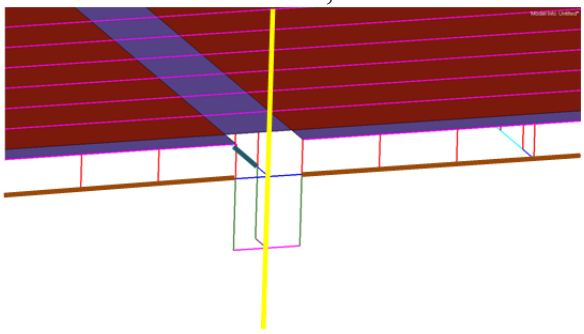

(d) Column-to-beam connection: Column A1, A6, F1, F6

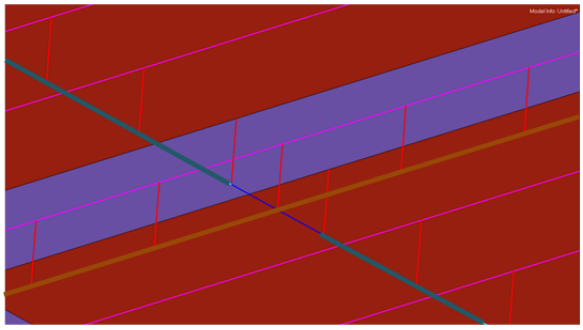

(e) Column-to-beam connection: Column A5, F2

(f) Infill beam-to-gravity beam connection

Figure 3 - 10 Details of Model M2: Connection region

- ***Connections***

The shear tab is modeled by a single beam element, which has integration points that correspond to the location of individual bolts, as shown in Figure 2 – 3(b). The area associated with each integration point is equal to the area of the bolt. The force-deformation response at each of the integration point is shown in Figure 3 – 11.

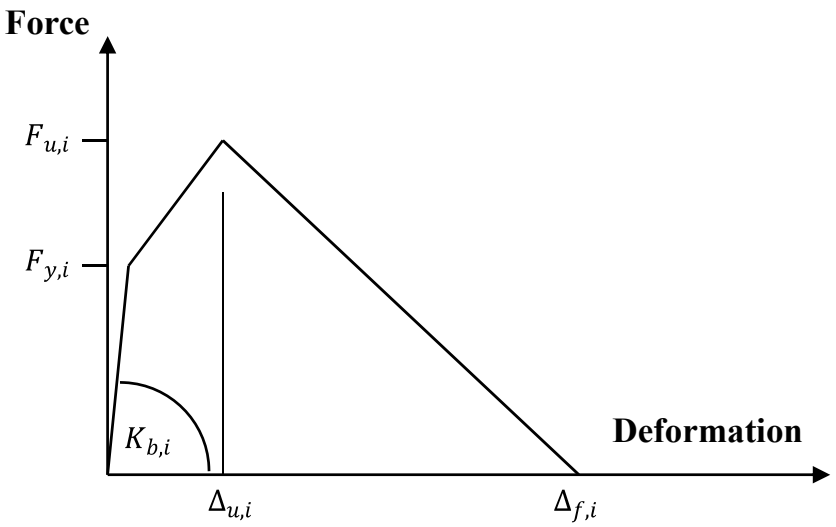

Figure 3 - 11 Force-deformation response of the integration point representing the bolt

Following Sadek et al. (2008) and Khandelwal (2008), the stiffness of an individual bolt, $K_{b,i}$, can be estimated as

$$K_{b,i} = \frac{124550(d_{bg} - 142.2\ mm)}{\sum_i S_i^2}\ \text{kN/mm} \qquad \text{(Equation 3 – 15)}$$

where d_{bg} is the depth (vertical dimension) of the bolt group (mm) and S_i is the distance of each bolt from the center of the bolt group (Figure 3 – 4).

The yield and ultimate forces of each integration point, $F_{y,i}$ and $F_{u,i}$, are calculated based on the governing failure mode or limit state of the connection under axial loading. The possible governing conditions include:

(1) Bolt yield and ultimate capacity in shear with threads excluded;
(2) Block shear yield and ultimate capacity of the web or shear tab;
(3) Tear-out yield and ultimate capacity through the beam web or through the shear tab.

The ultimate deformation $\Delta_{u,i}$ is

$$\Delta_{u,i} = S_{max}\left(0.17 - 0.00014 d_{bg}\right) \quad \text{(Equation 3 – 16)}$$

where S_{max} is the distance from the center of the bolt group to the most distant bolt. $\Delta_{f,i}$ is set to be equal to the edge distance. The integration point fails when the deformation of the integration point reaches $\Delta_{f,i}$ in tension.

The model is calibrated against experimental test data and the results can be seen in Figure 3 – 12. More details can be found in Sadek et al. (2008) and Khandelwal (2008).

A binding spring is used to represent contact between the beam and column flanges, as specified in Khandelwal and El-Tawil (2007). The binding spring had no tensile capacity and a compressive capacity of 1/3 of the plastic axial strength of the adjacent beam, as calibrated from detailed studies. Since the solution scheme is explicit, the solution time is linked to element characteristics. As a ploy to increase the time step, the length of the shear tab is set to an artificially long 381 mm. As discussed later on, the validation studies showed that this assumption yields reasonable results. Unlike the macro model discussed in Khandelwal and El-Tawil (2007), which represents the panel zone, the model employed herein does not include such a detail. While this was done with the explicit objective of simplifying and speeding up the macro models, it was also based on extensive studies (described in Section 3.4.2) that showed that the panel zones did not contribute significantly to the collapse response of the prototype building.

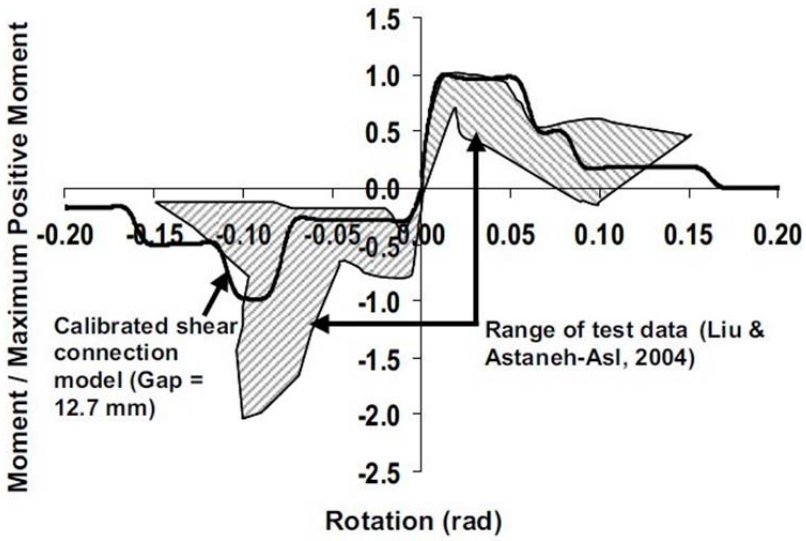

Figure 3 - 12 Comparison between the shear connection model and experimental data (Sadek et al., 2008)

The radius cut reduced beam sections are modeled with a beam element whose cross section is set to the minimum cross section in the reduced section as done in Khandelwal and El-Tawil (2007). Slabs are represented using the method presented for M1, but to simplify the model, the centerlines of beams in both gravity and moment bays are assumed to be located at the same level, which corresponds to the centerlines of the moment beams although the centerlines of the gravity and moment bay beams are located at different levels. Modeling this elevation difference in M2 necessitates the introduction of small elements in the columns. Since these elements can significantly reduce the time step and increase running time, the gravity beams and moment bay beams are assumed to be located at the same level, i.e. the level of the moment beams. Compared to M1, Model M2 is computationally efficient, running 230 times faster than M1. The reduction in computational time is not primarily due to the reduction in number of elements, but rather to the careful sizing of elements within the model to ensure that they yield as large a time step as possible without compromising accuracy.

- ***Formulation of Hughes-Liu beam element***

The Hughes-Liu beam element is used in Model M2 because of its computational efficiency and robustness. The nodes at both ends of the beam element have three translational and three rotational degrees of freedom. The rotational degrees of freedom are treated by defining orthogonal, inextensible nodal fibers. Figure 3 – 13 defines the geometry of a Hughes-Liu beam element.

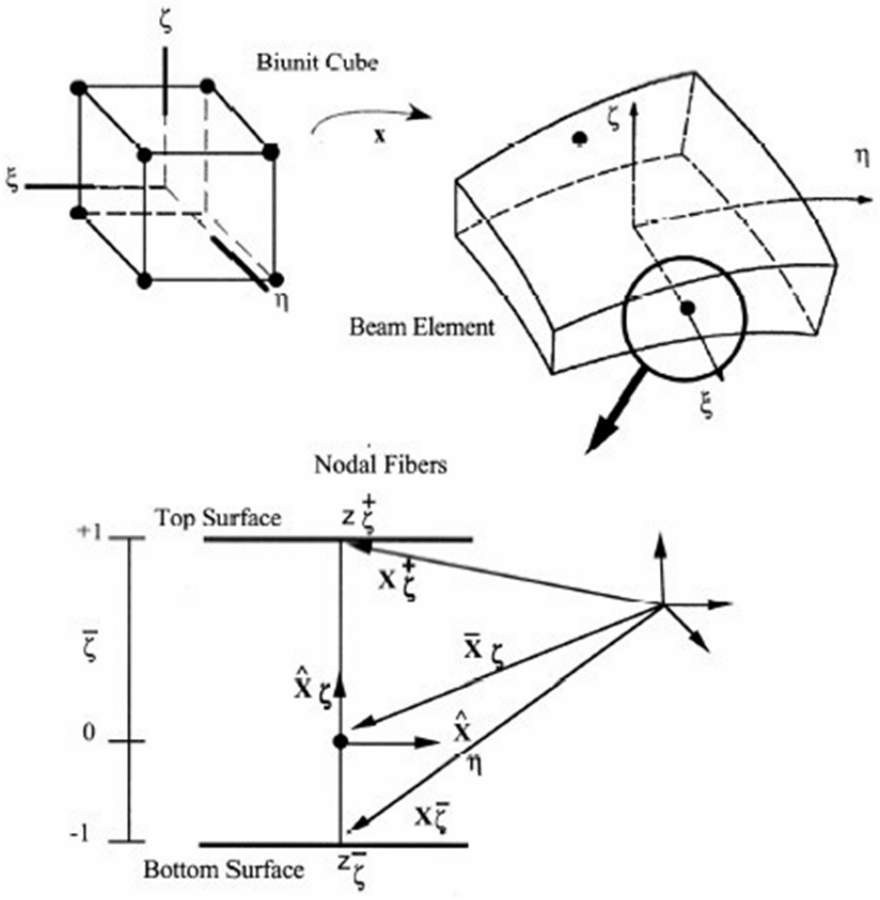

Figure 3 - 13 Geometry of a Hughes-Liu beam element (Hallquist, 2006)

For the arbitrary points on the reference axis which is defined by the two beam nodes, the initial geometry of a Hughes-Liu beam element can be described as follows:

$$x(\xi,\eta,\zeta) = \bar{x}(\xi) + X(\xi,\eta,\zeta) = \bar{x}(\xi) + X_\zeta(\xi,\zeta) + X_\eta(\xi,\eta) \qquad \text{(Equation 3 – 17)}$$

$$\bar{x}(\xi) = N_a(\xi)\bar{x}_a \qquad \text{(Equation 3 – 18)}$$

$$X_\zeta(\xi,\zeta) = N_a(\xi)X_{\zeta a}(\zeta) \qquad \text{(Equation 3 – 19)}$$

$$X_\eta(\xi,\eta) = N_a(\xi)X_{\eta a}(\eta) \qquad \text{(Equation 3 – 20)}$$

In this geometry, x denotes the position vector of a generic point on the beam; ξ determines the location along the axis of the beam and the coordinate pair (η,ζ) defines a point on the cross section. In Equation 3 – 15 and Equation 3 – 16, $\bar{x}$ represents a position vector to a point on the reference axis of the beam, $\bar{x}_a$ is the position vector of the nodal point a, and X is a position vector at point $\bar{x}$ on the axis that defines the fiber directions through that point; N_a denotes a one dimensional shape function associated with node a.

Points off the reference axis are interpolated by using a one-dimensional shape function along the fiber direction, i.e., $X_{\zeta a}(\zeta)$ and $X_{\eta a}(\eta)$ and

$$X_{\zeta a}(\zeta) = z_\zeta(\zeta)\hat{X}_{\zeta a} \quad \text{(Equation 3 – 21)}$$

$$X_{\eta a}(\eta) = z_\eta(\eta)\hat{X}_{\eta a} \quad \text{(Equation 3 – 22)}$$

When the reference axis is located at the center, $z_\zeta(\zeta) = \frac{\left\|x^+_{\zeta a} - x^-_{\zeta a}\right\|}{2}\zeta$ and $z_\eta(\eta) = \frac{\|x^+_{\eta a} - x^-_{\eta a}\|}{2}\eta$ and they are called "thickness functions". The position vectors $x^+_{\zeta a}$ ($x^+_{\eta a}$) and $x^-_{\zeta a}$ ($x^-_{\eta a}$) locate on the top and bottom surfaces, respectively at node a.

With Equation 3 – 15 to Equation 3 – 20, an isoparametric 8-node solid element is degenerated into a 2-node beam geometry.

The beam element displacements are interpolated in the same manner with the geometry, and can be described as follows:

$$u(\xi,\eta,\zeta) = \bar{u}(\xi) + U(\xi,\eta,\zeta) = \bar{u}(\xi) + U_\zeta(\xi,\zeta) + U(\xi,\eta) \qquad \text{(Equation 3 – 23)}$$

$$\bar{u}(\xi) = N_a(\xi)\bar{u}_a \qquad \text{(Equation 3 – 24)}$$

$$U(\xi,\zeta) = N_a(\xi)U_{\zeta a}(\zeta) \qquad \text{(Equation 3 – 25)}$$

$$U_\eta(\xi,\eta) = N_a(\xi)U_{\eta a}(\eta) \qquad \text{(Equation 3 – 26)}$$

$$U_{\zeta a}(\zeta) = z_\zeta(\zeta)\widehat{U}_{\zeta a} \qquad \text{(Equation 3 – 27)}$$

$$U_{\eta a}(\eta) = z_\eta(\eta)\widehat{U}_{\eta a} \qquad \text{(Equation 3 – 28)}$$

where u is the displacement of a generic point, $\bar{u}$ is the displacement of a point on the reference surface, and U is the fiber displacement.

3.3.3 Model M3

Model M3 is a representation of the frame on axis 6 only. The gravity load from the floor system acting on the frame is computed using the tributary area associated with the frame. It is common practice to approximate system response using planar frame response, which is the reason for developing this model. To assure that the frame behaves in a reasonable manner, the top flanges of the beams are prevented from moving out of plane to model the stabilizing influence of the slabs. Model M3 is identical to M1 in all respects except that the slab is not modeled. In fact, M3 was extracted from M1 by deleting all but the pertinent elements associated with the planar frame. Comparisons between M1 and

M3 will shed light on the influence of these assumptions. Model M3 is still a relatively fine model and runs only 36 times faster than Model M1.

3.3.4 Model M4

Like model M3, which is extracted from M1, Model M4 is also extracted from Model M2 and models the frame on axis 6. Also like M3, model M4 does not include a model of the slab and is constrained to undergo planar response. It is very computationally expedient and runs 7,000 times faster than model M1.

3.4 VALIDATION STUDIES

The models presented in this chapter are based on several models that were previously published and validated through comparisons to disparate experimental data and the results of more refined models. (Khandelwal and El-Tawil 2007, Khandelwal et al. 2009, Alashker et al 2010). Following are additional validation studies that together with the previously published studies support the accuracy and suitability of the proposed models to represent collapse response.

3.4.1 Failure Strain for the Macro-Based Models

As was discussed earlier, a bi-linear relationship is used to represent the constitutive response of steel in both macro- and micro- based models. To capture similar failure modes, the failure criteria of the macro-based models, which is the plastic failure strain, is calibrated against more refined micro-based models. Beams with RBS sections, which are used in the prototype building, are modeled using both modeling approaches under the loading scheme shown in Figure 3 – 14. The models of the beams are extracted directly from M1 and M2, respectively. The load-deflection curves obtained from the two models are compared and a trial-and-error process is used until the same failure modes

are obtained. The plastic failure strains for all the beams with different sizes are calibrated in this manner. The cases conducted are listed in Table 3 – 2.

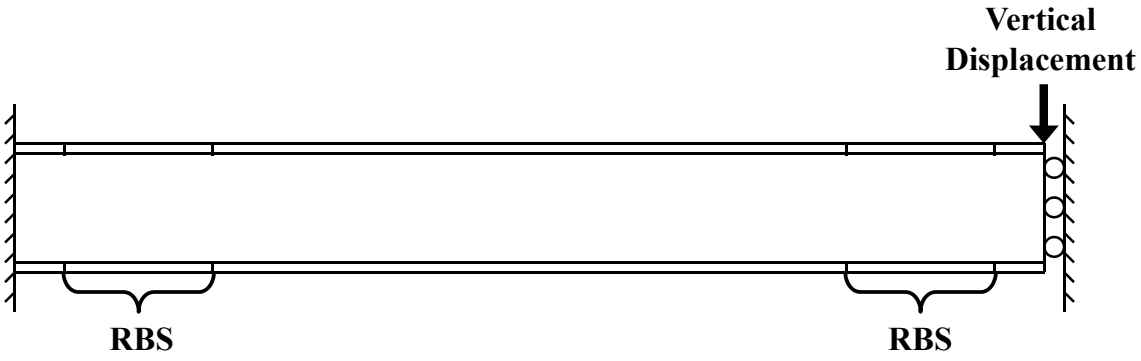

Figure 3 - 14 Loading scheme of the calibration study

Table 3 - 2 Summary of the calibration results: plastic failure strain

Case number	Orientation	Floor range	Beam size	Beam depth	Span length (inch)	Failure strain
1	East-West	1 – 7	W27x94	26.9	360	0.100
2		8 – 9	W21x50	20.8	360	0.113
3		10	W16x26	15.7	360	0.131
4	North-South	1 – 5	W24x94	24.3	240	0.098
5		6 – 7	W24x68	23.7	240	0.097
6		8 – 9	W21x44	20.7	240	0.113
7		10	W16x26	15.7	240	0.128

The comparisons between the macro- and micro- model responses are shown in Figure 3 – 15.

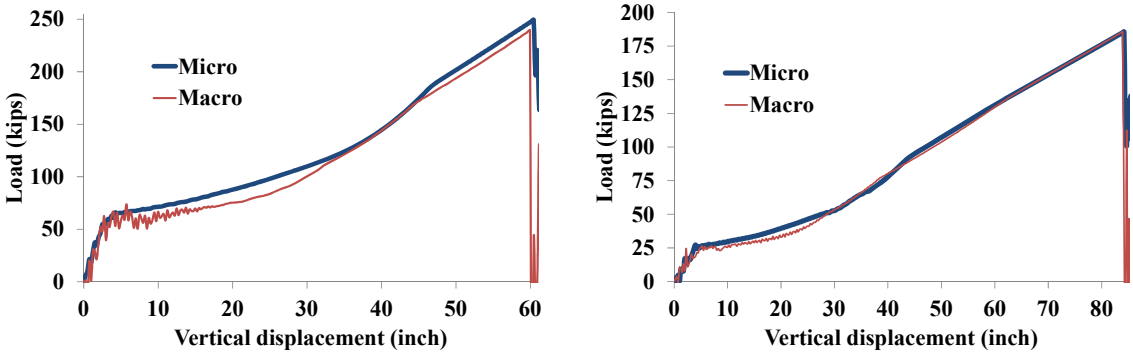

(a) Case 1

(b) Case 2

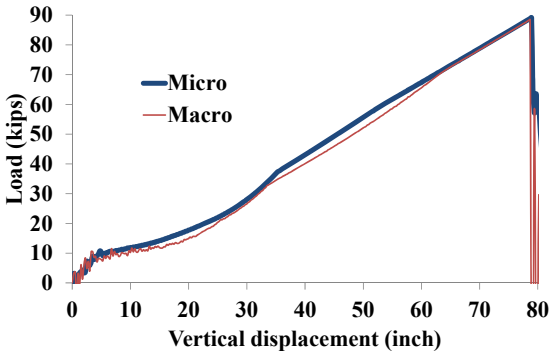

(c) Case 3

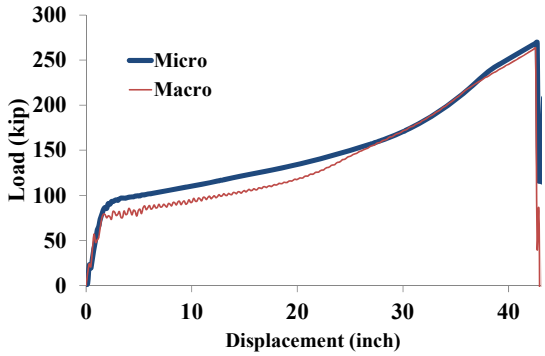

(d) Case 4

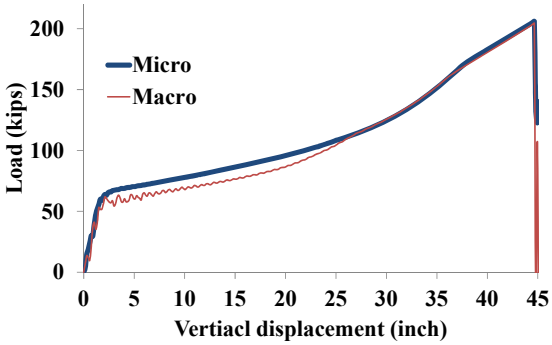

(e) Case 5

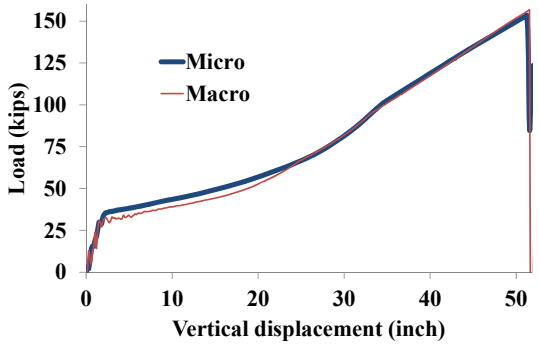

(f) Case 6

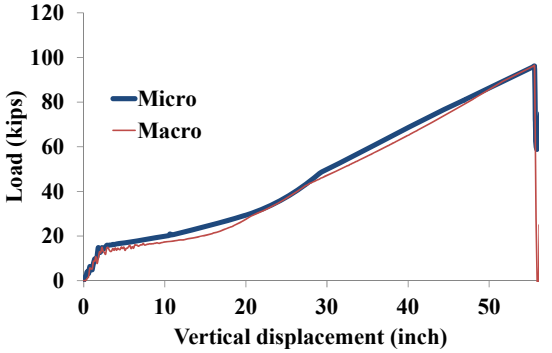

(g) Case 7

Figure 3 - 15 Comparison between macro- and micro- models

The relationship between the beam depth (d_b) and the failure strain (e_f) is plotted in Figure 3 – 16. As in Khandelwal (2008), a linear relationship is obtained and can be expressed as follows:

$$e_f = -0.032d_b + 0.1804 \quad \text{(Equation 3 – 29)}$$

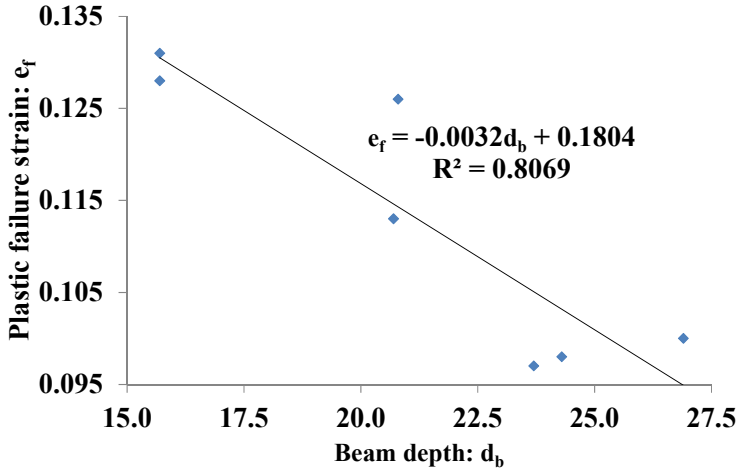

Figure 3 - 16 relationship between d_b and e_f

3.4.2 Effect of the Panel Zone

An important modeling assumption made in this study is that the macro-based models do not explicitly account for the panel zone. To validate this assumption, two types of models are used to represent the behavior of a beam-column subassembly extracted from the 1st floor of the prototype building along the column axis 6. Both models are macro-based models. In the first model, Hughes-Liu beam elements are used to represent the beams and columns. The panel zone is modeled using shell elements for the shear panel, surrounded by four rigid bars pinned together at their ends to permit the desired deformation, i.e. pure shear deformation, to occur. In the other model, the panel zone is not represented. As shown in Figure 3 – 17, the mid-column stud is pushed downward until failure occurs in both models. The column ends are assumed to be fixed.

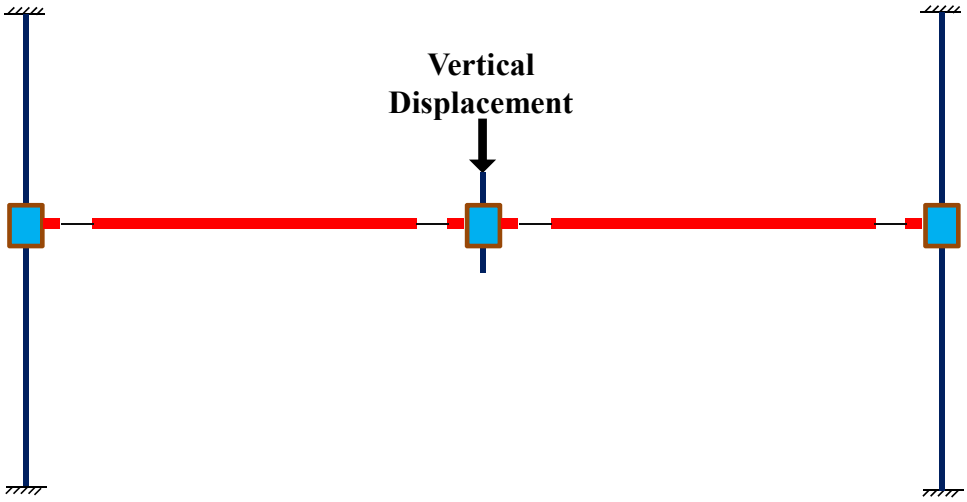

(a) Model considering panel zone

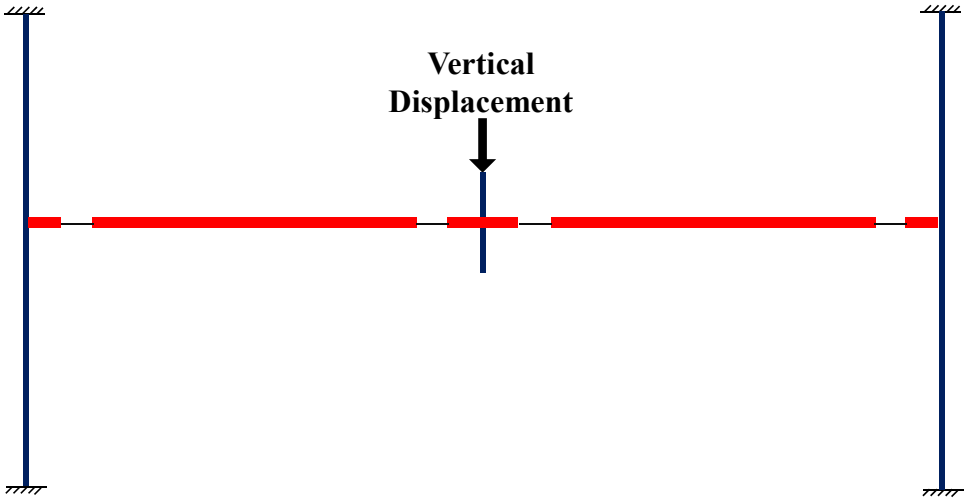

(b) Model ***does not*** consider panel zone

Figure 3 - 17 Models with and without panel zone

The load-deflection curves obtained by the two models are compared in Figure 3 – 18. It is clear from the figure that the responses of both models match very well, suggesting that, for this particular prototype structure, the panel zone can be neglected in the modeling process.

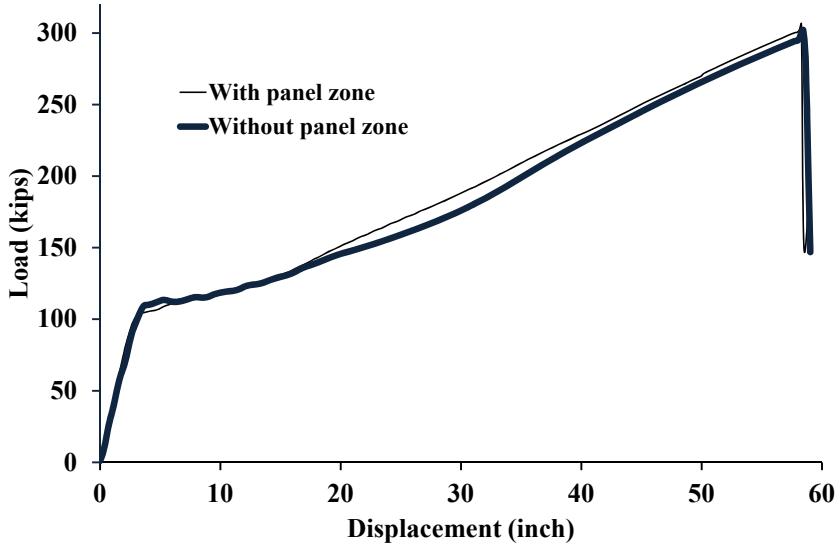

Figure 3 - 18 Comparison between the model with panel zone and without panel zone

3.4.3 Composite Floor Study

Figure 3 – 19 shows a comparison between the responses of a composite floor system modeled using the above-described approach and a detailed model developed by Sadek et al. (2008) and Alashker et al. (2010). Figure 3 – 19(a) shows the level of detail used in Sadek et al. (2008) and that used in this study. The developed model runs in a small fraction of time ($1/300^{th}$) required by the detailed model, but as shown in Figure 3 – 19(b), yields reasonable responses, especially initial stiffness, peak load and even softening behavior. The mode of failure and location of failure initiation also correspond to those observed in the detailed model.

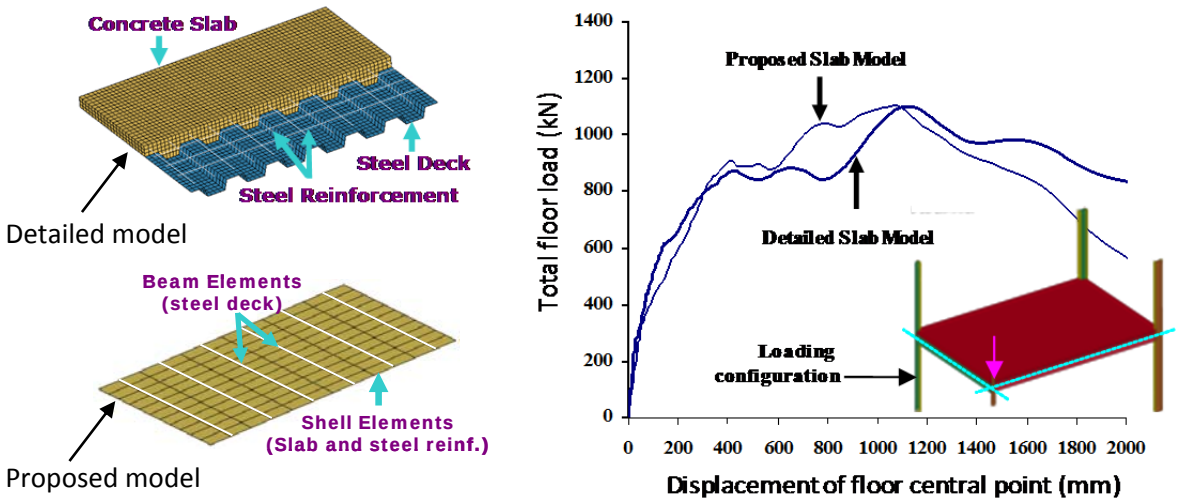

(a) Slab Models (b) Load-displacement response

Figure 3 - 19 Comparison between the proposed slab modeling approach and the detailed model in Sadek et al. (2008)

3.4.4 RBS Beam-Column Assembly Test (NIST 2010)

Sadek et al (2010) carried out experimental tests on beam-column assemblies that are representative of the conditions that occur during collapse. They investigated the response of two types of moment connections by pushing down on the central column in the test assembly depicted in Figure 3 – 20. Their test specimen consisted of two beam spans and three columns. The two exterior columns were prevented from moving horizontally at their ends, while the central column stub was pushed down vertically till failure occurred. One of the two tests was carried out using a reduced beam section (RBS) connection between the beams and columns. The tested sub-assemblage was taken from the prototype building discussed herein and was tested at full scale. Details of the test and test results can be found in Sadek et al. (2010).

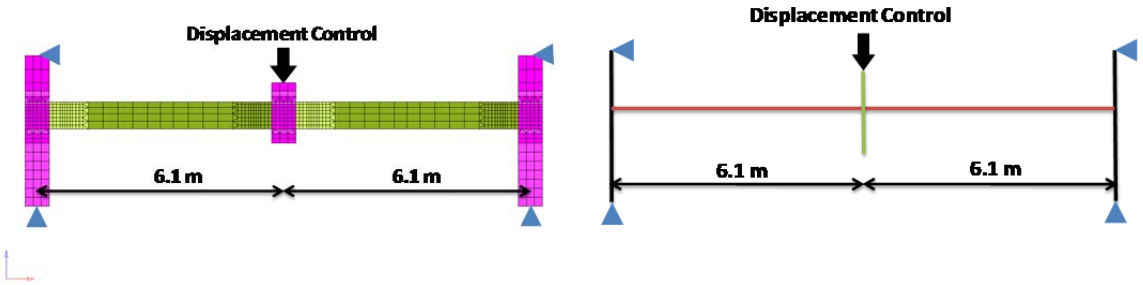

(a) Micro model (b) Macro model

Figure 3 - 20 Micro and macro models of test assembly

For the purposes of validation, the subassemblage is modeled in two ways. The first is based on the approach discussed for Model M1, i.e. using the same element sizes, but measured material properties (Figure 3 – 20(a)). The second is based on the macro-modeling approach discussed for model M2, again using the same element sizes for M2 (Figure 3 – 20(b)) and measured properties of the steel. The sub-assemblage is loaded as the specimen was in the test, i.e. by pushing down on the central column.

As shown in Figure 3 – 21, both models yield good overall load-versus deflection responses, managing to capture the initial slopes, hardening due to catenary action, peak loads, and deformations at failure. The models also capture the observed failure mode well. For example, failure in the M1 model occurred in the small section of the RBS of the beams, as occurred in the test, while failure in the M2 model occurred in the element representing the RBS region, also as observed during the test. Figure 3 – 22(a) shows a comparison between the failure observed in the test and that captured by the M1 simulation, while Figure 3 – 22(b) shows a zoomed in look at the failure region. Clearly both models are capable of capturing overall response well.

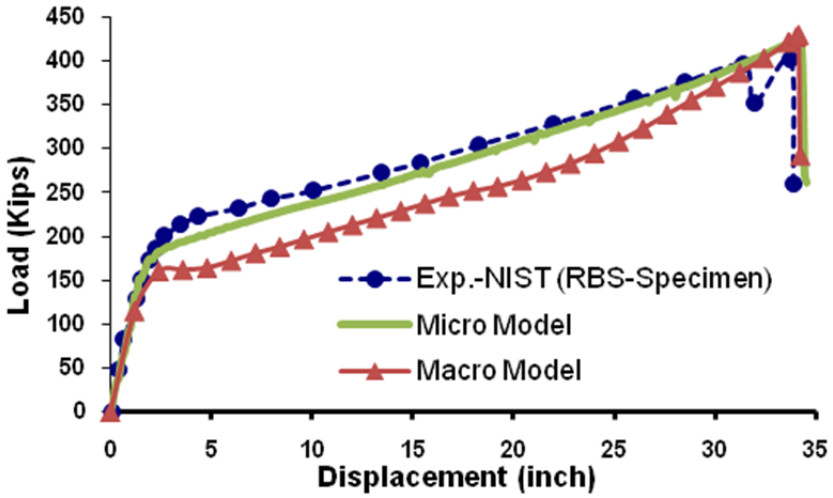

Figure 3 - 21 Comparison between the results of various models and experimental data

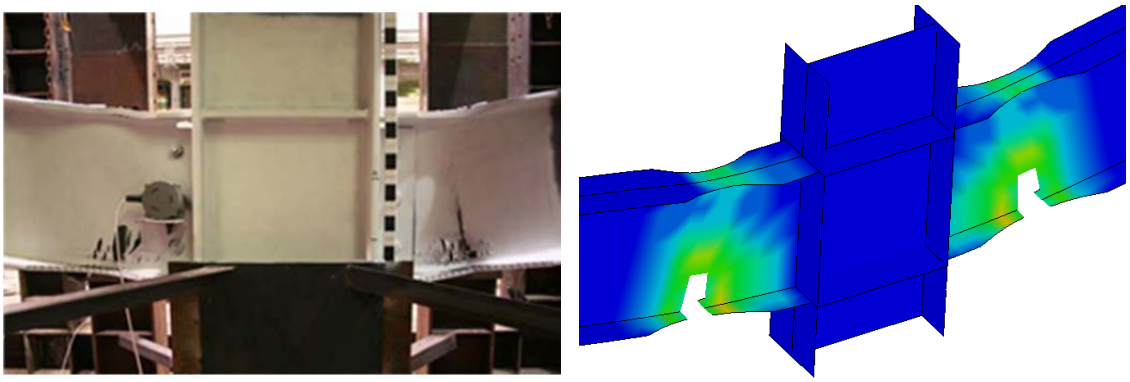

(a) Overall View

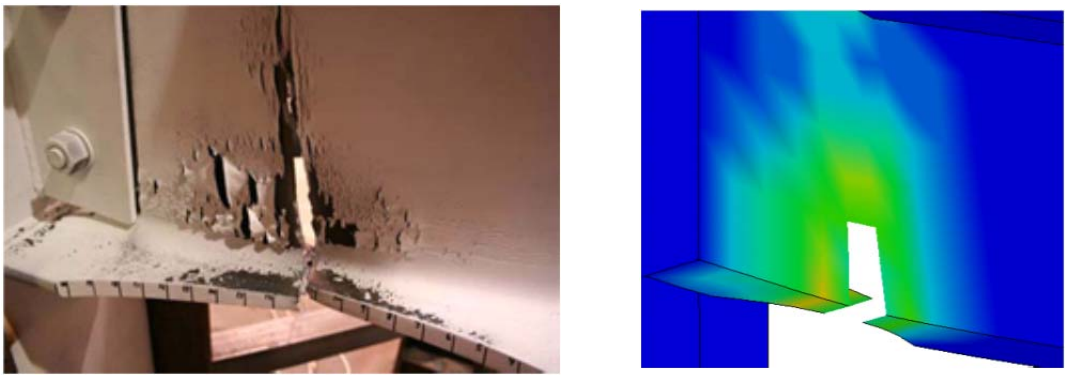

(b) Close up of failure location

Figure 3 - 22 Comparison between experimental and model failure modes

3.5 SUMMARY AND CONCLUSIONS

Four types of computational models with various modeling assumptions are developed in this chapter, including a 3-D micro-based model, M1, a 3-D macro-based model, M2, a 2-D micro-based model, M3, and a 2-D macro-based model, M4. These models are validated carefully against experimental studies and more refined finite element models. The models are able to represent nonlinear and dynamic structural behaviors and are deemed reliable for use in the remaining parts of this study.

CHAPTER 4

APPROXIMATIONS IN PROGRESSIVE COLLAPSE MODELING

4.1 Introduction

This chapter discusses, in a quantitative manner, the ability of various types of models to represent system-wide progressive collapse. Aside from a few studies, e.g. Ruth et al. (2006), this topic has not been studied much in the past and questions abound about: 1) the accuracy of planar simplifications of 3-D system response, 2) the level of conservatism that exists, if any, in planar representations of system behavior, and 3) the ability of models with macro-elements to accurately capture the behavior of a collapsing system. Given the inherent limitations of linear models, the work in this Chapter only focuses on nonlinear response within the scope of the questions listed above.

The responses of the 4 models developed in Chapter 3 to similar collapse initiating events are compared to gain insight into the effects of the various modeling assumptions employed in the models, including: a) the use of macro-elements to mimic behavior instead of using elements that are based on fundamental constitutive relationships, and b) planar versus 3-D representation. Simulation setup and component naming scheme are described in Section 4.2. The effect of macro modeling is discussed in Section 4.3 and Section 4.4 through the comparison between M1/M2 and M3/M4. In section 4.5, responses of the planar models and 3-D models are compared and the effect of planar

versus 3-D modeling is investigated. Implications of the simulation results are presented in Section 4.6. The chapter is summarized and conclusions are drawn in Section 4.7.

4.2 Simulation Setup and Component Naming Scheme

Models M1 through M4 are exercised within an Alternate path method (APM) setting. Each model is first loaded with gravity loads (i.e. dead load plus 25% of the live loads). Once the vibrations associated with the loading process die down, a member of interest such as a column is suddenly eliminated and the model is allowed to respond to the new boundary conditions. The rate of loading employed in this study was tempered by two practical, but conflicting issues: the slowness of Model M1, which necessitated loading the model as quickly as possible to reduce the duration for which the solution is sought; and the need to load the model with gravity loads as slowly as possible to prevent dynamic effects from dominating the response. Many trials showed that an initial loading period of 1 second followed by a wait period of 0.5 seconds yielded a reasonable compromise. Therefore, for simulation involving M1 or comparisons to M1, the initial loading period and wait time are set to be 1.0 second and 0.5 seconds, respectively. While for the other simulations, the initial loading period and wait time are set to be 5.0 second and 7.5 seconds, respectively. The response of each model is tracked by plotting various quantities of interest versus time, e.g. the force in members adjacent to the removed element, or the displacement of adjacent nodes. The progression of failure, if it occurs, is also tracked and recorded. These responses are then compared to corresponding quantities computed from other models to achieve the objectives of the study.

To facilitate the following discussion, beams and columns are designated as E-P-N-X. In this notation, E is the structural element type, where “C” represents columns, “B” represents beams, “I” represents infill beams, “J” represents joints and “S” represents slabs. P is the position of the structural number described by the closest column lines in Figure 3 – 1. N is the story number and X, when designated, is direction (East, West, North, South) as indicated in Figure 3 – 1. For example, C-D6-5 represents the column at

the junction of column lines D and 6 in the 5th floor. B-DE6-2 represents a 2nd story beam in bay DE at column line 6. Designation I-AB34-1 represents a first floor infill beam in the panel bounded by column lines A, B, 3 and 4. J-DE6-10-West means the joint at the West end of beam DE6 on the 10th floor and S-CD56-1 is the first floor slab panel bounded by column lines C, D, 5 and 6.

Six column loss cases are investigated using the 3-D models M1 and M2: first floor exterior moment columns C-D6-1, both C-D6-1/C-E6-1, first floor corner moment column C-F6-1, first floor interior moment column C-E4-1, first floor interior gravity column C-D5-1, and first floor gravity column C-E5-1. Two column cases are investigated using the planar models M2 and M4: C-D6-1 and C-F6-1. Another four column loss cases are investigated using all four models: C-D6-1, C-F6-1, both C-D6-1/C-E6-1, and C-E5-1. Comparisons between the results of M1/M3 or M2/M4 shed light on the effect of the slab and planar versus 3-D modeling. Similarly, comparisons between M1/M2 or M3/M4 highlight the effect of using macro-elements to represent steel frame response. The column loss cases conducted herein are summarized in Table 4 – 1. The location of the removed columns is highlighted in Figure 4 – 1.

Table 4 - 1 Column loss cases

Column loss case	Column removed	Model used	Column type
1	C-D6-1	M1, M2	Exterior moment
2	C-F6-1	M1, M2	Corner moment
3	C-D6-1/C-E6/1	M1, M2	Exterior moment
4	C-E4-1	M1, M2	Interior moment
5	C-D5-1	M1, M2	Interior gravity
6	C-E5-1	M1, M2	Interior gravity
7	C-D6-1	M2, M4	Exterior moment
8	C-F6-1	M2, M4	Corner moment
9	C-D6-1	M1/M3, M2/M4	Exterior moment
10	C-D6-1/C-E6-1	M1/M3, M2/M4	Exterior moment
11	C-E5-1	M1/M3, M2/M4	Interior gravity

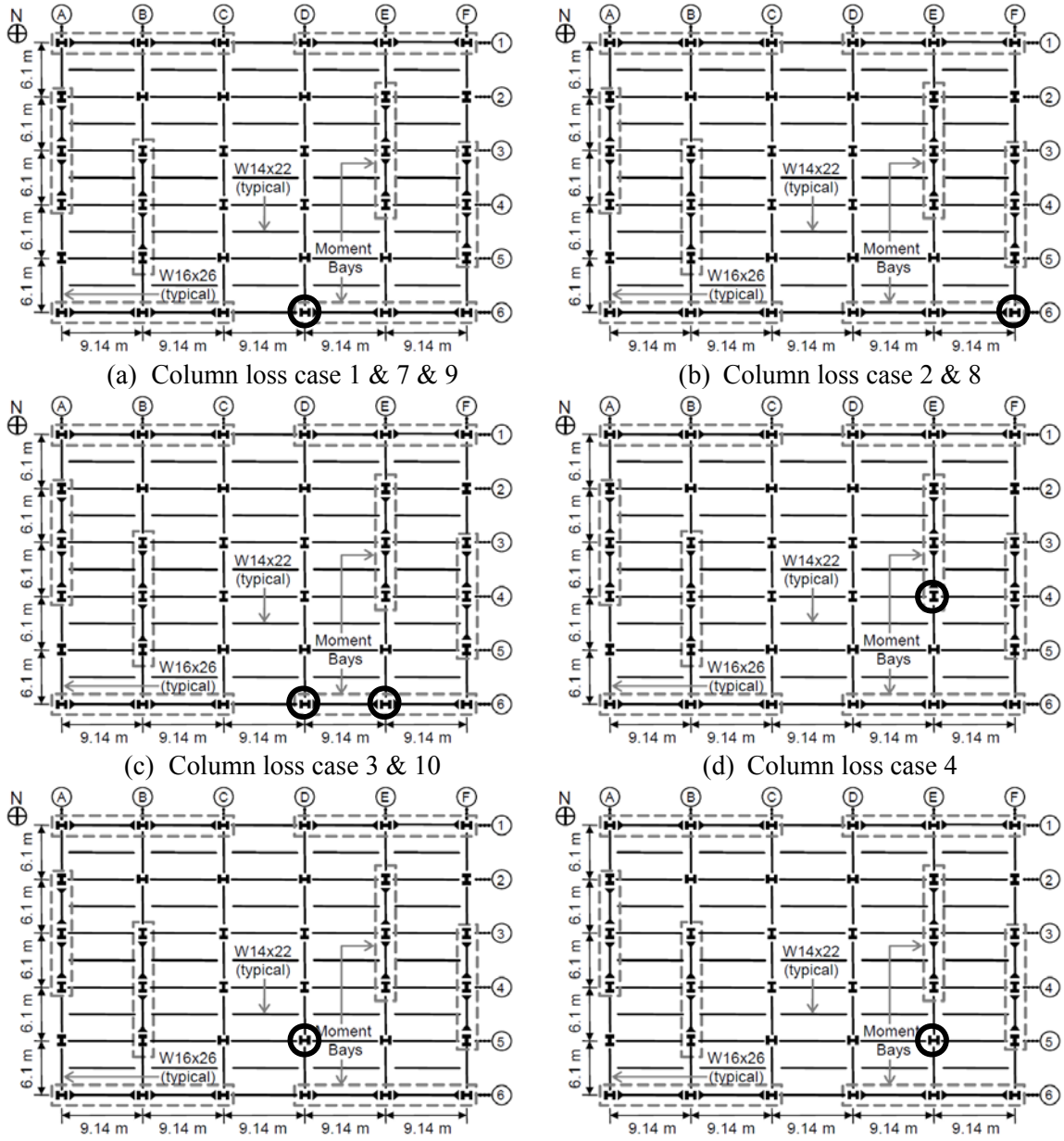

(a) Column loss case 1 & 7 & 9

(b) Column loss case 2 & 8

(c) Column loss case 3 & 10

(d) Column loss case 4

(e) Column loss case 5

(f) Column loss case 6 & 11

Figure 4 - 1 Columns removed

4.3 Effect of Macro Modeling: Comparison between M1 and M2

4.3.1 Column Loss Case 1: C-D6-1

Figure 4 – 2 and Figure 4 – 3 shows a comparison between the responses of models M1 and M2 when column C-D6-1 is suddenly removed. In general, there is good agreement between the results of both models. For example, Figure 4 – 3(a) indicates that the axial forces in the columns adjacent to the removed column develop similar forces in both models. The axial force in the adjacent column C-E6-1 increases from 1555 KN to a peak value of 3596 KN in model M1 and 4022 KN in model M2, which belongs to the same moment frame as C-D6-1. After the vibrations die down, the forces in C-E6-1 become steady at 3150 KN, which is nearly double its original axial force.

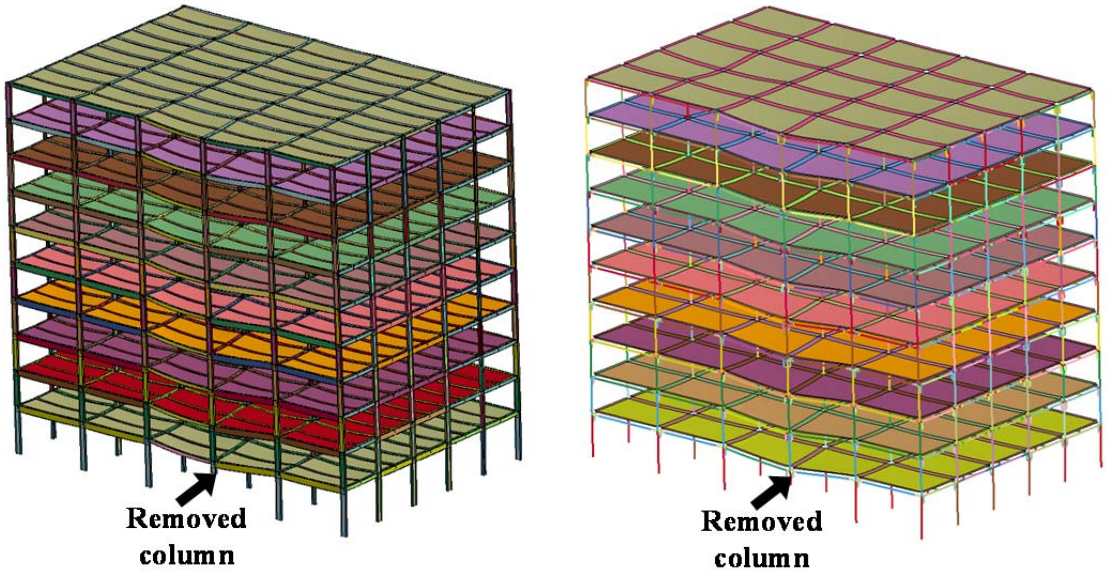

(a) M1 response (displacement magnification factor=10)

(b) M2 (displacement magnification factor=10)

Figure 4 - 2 Overall responses of M1 and M2: Column C-D6-1 removed

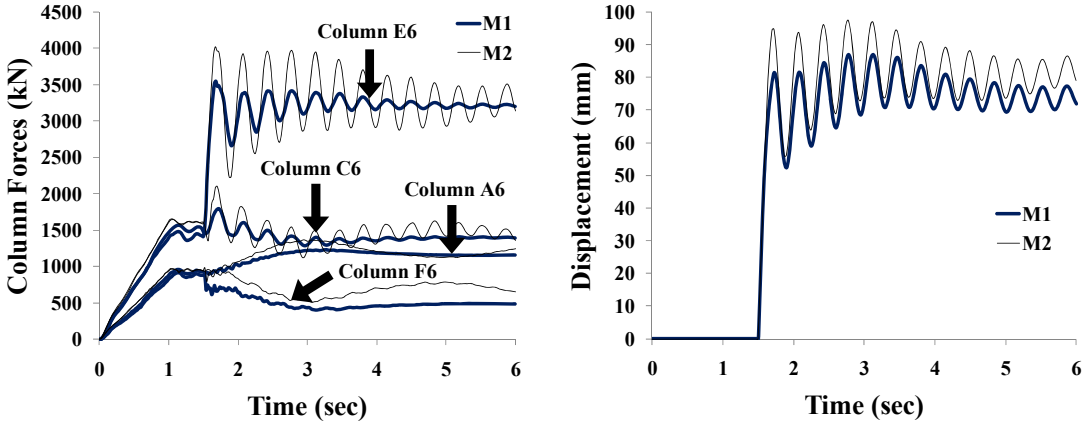

(a) Column axial forces (b) Vertical displacement

Figure 4 - 3 Comparison between M1 and M2 models: Column C-D6-1 removed

Other less substantial force changes occur throughout the frame on axis 6. For example, while columns C-C6-1 and C-F6-1 saw reductions in their axial loads, column C-A6-1 saw an increase in axial force. The observed force redistribution occurs as a result of global frame action that occurs in the moment bays on column axis 6. Removal of column C-D6-1 causes the moment frame spanning columns C-D6-1/C-E6-1/C-F6-1 to lean westwards, which reduces the load on column C-F6-1 and increases the load on C-E6-1 as discussed above. The effect of the leaning action extends through the gravity beams to apply a mild overturning moment on the frame spanning columns C-A6-1/C-CB-6/C-C6-1, which results in an increase in the force in A6 and a corresponding reduction in force in C-C6-1.

Figure 4 – 3(b) shows that the displacements that occur at the location of the removed column match well in M1 and M2. After removal of column C-D6-1, the nodes at the location of the removed column vibrate vertically and reach peak downward displacements of 94.6 mm and 82.2 mm for M2 and M1, respectively. M1 and M2 come to rest at a vertical displacement around 75 mm and 80 mm, respectively, as shown in Figure 4 – 3(b). There appears to be some differences in the dynamic effects captured by both models, e.g. as shown in Figure 4 – 3(a), but the period of vibration, as evident in

Figure 4 – 3, matches well, and the discrepancies are attributed to local differences in the models.

4.3.2 Column Loss Case 2: C-F6-1

The response of both models to removal of corner column C-F6-1 is shown in Figure 4 – 4 and Figure 4 – 5. While there are some differences in the vibration responses, the differences are deemed small and both models correlate reasonably well together. The axial load force of column C-E6-1 in M2 increases from 1,590 KN to reach a peak of 3,447 KN before settling back down at 2,700KN. As shown in Figure 4 – 5(a), Column C-E6-1 is only slightly affected by the removal of column C-F6-1. The column force in column C-D6-1 is reduced after removal of column C-F6-1 because of the global frame action which is also observed in column loss Case 1. The moment frame spanning columns C-D6-1/C-E6-1/C-F6-1 leans west because of loss of column C-F6-1, inducing an overturning moment on that frame, which results in a reduction in column axial force in C-D6-1.

The overall deflections of M1 and M2 are presented in Figure 4 – 5(b) and good agreement is observed. After loss of column C-F6-1, the peak downward displacements of the nodes at the location of the removed column in model M1 and M2 are 47 mm and 55 mm, respectively. After the vibration dies out, the displacements become 45 mm and 46 mm in M1 and M2, respectively. These displacements are more than half of the steady displacement for loss of column C-D6-1, even though structural response is elastic in both cases and the tributary gravity loads carried by column C-F6-1 are half of that carried by column C-D6-1. This is because after loss of column C-D6-1, which is an interior moment column, some resistance is provided by the gravity bay which is adjacent to the removed columns. For corner column C-F6-1, no such resistance is provided by the remaining structural system.

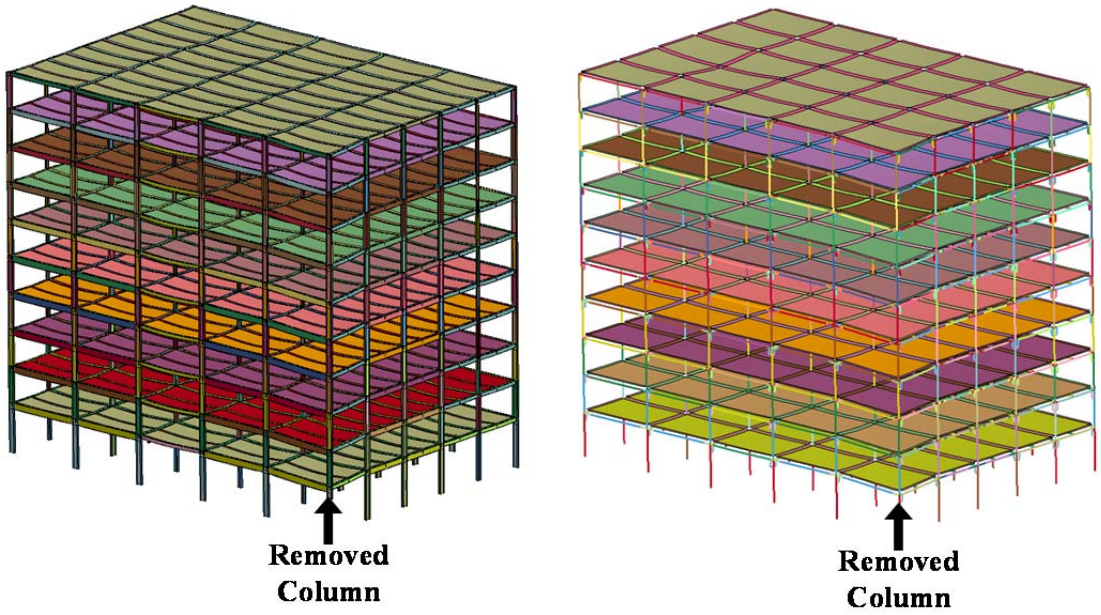

(a) M1 response
(displacement magnification factor=10)

(b) M2
(displacement magnification factor=10)

Figure 4 - 4 Overall responses of M1 and M2: Column C-F6-1 removed

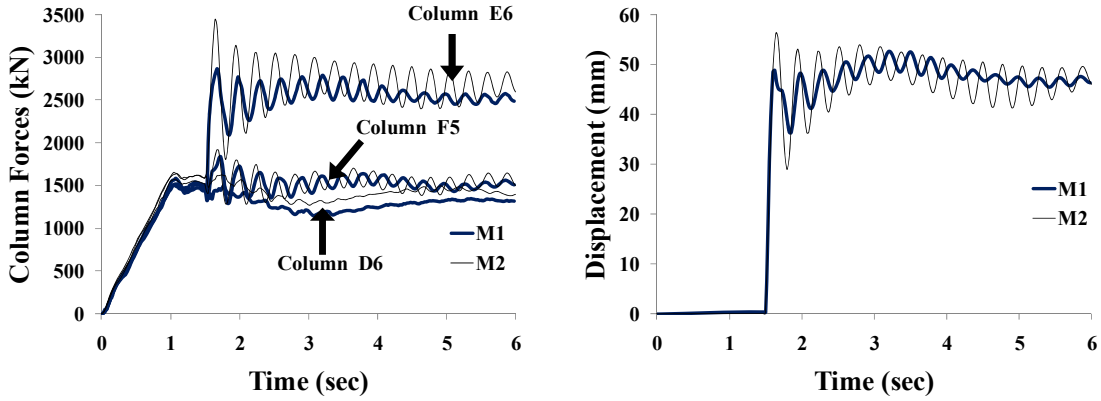

(a) Column axial forces

(b) Vertical displacement

Figure 4 - 5 Comparison between M1 and M2 models: Column C-F6-1 removed

4.3.3 Column Loss Case 3: C-D6-1/C-E6-1

Figure 4 – 6 shows model responses when both C-D6-1/C-E6-1 are removed simultaneously. Both models indicate that collapse will not occur. However, significant damage and large displacements are observed as shown in Figure 4 – 6(b). For example, the peak displacements at the removed columns C-D6-1 and C-E6-1 (in M1) are 538 and 330 mm, settling down at 515 and 327 mm, respectively. In spite of some discrepancies in the computed displacements at C-D6-1 and C-E6-1 (less than 12% difference), both models exhibit the same failure mode, which entails shear connection failures at column C-D6-1 that rapidly propagate from the first up to the top floor (Figure 4 – 7).

Not only is the damage mode well correlated, but the force responses also matched reasonably well, as shown in Figure 4 – 6(a). Both models exhibit significant load redistribution. For example, the force in column C-F6-1 of M1 increases from 930 to 3,135 kN, a 237% increase. Fortunately, this column has sufficient reserve capacity, since it is designed to serve as part of the seismic moment resisting system (see Figure 3 – 1(a)). Because of the large deformation, the changes in axial forces in column C-A6-1 and C-C6-1 are substantial, which is attributed to global frame action.

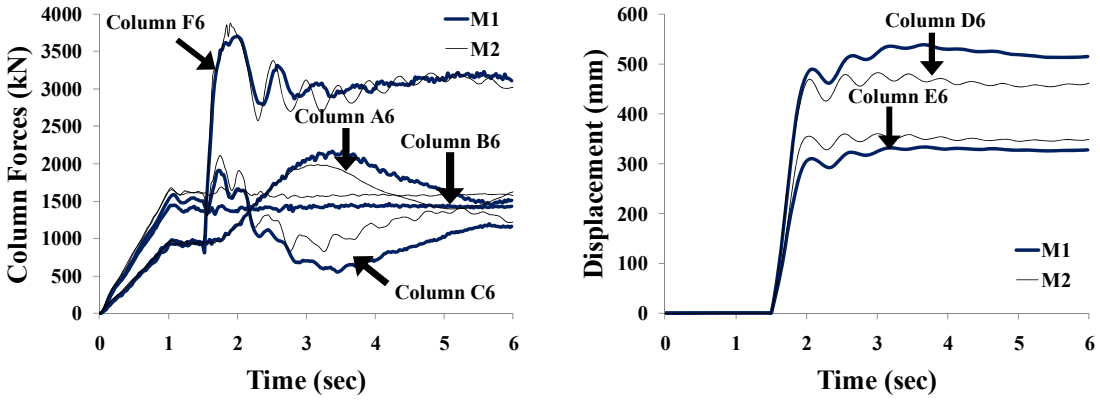

(a) Column axial forces (b) Vertical displacement

Figure 4 - 6 Comparison between M1 and M2 models: Columns C-D6-1/C-E6-1 simultaneously removed

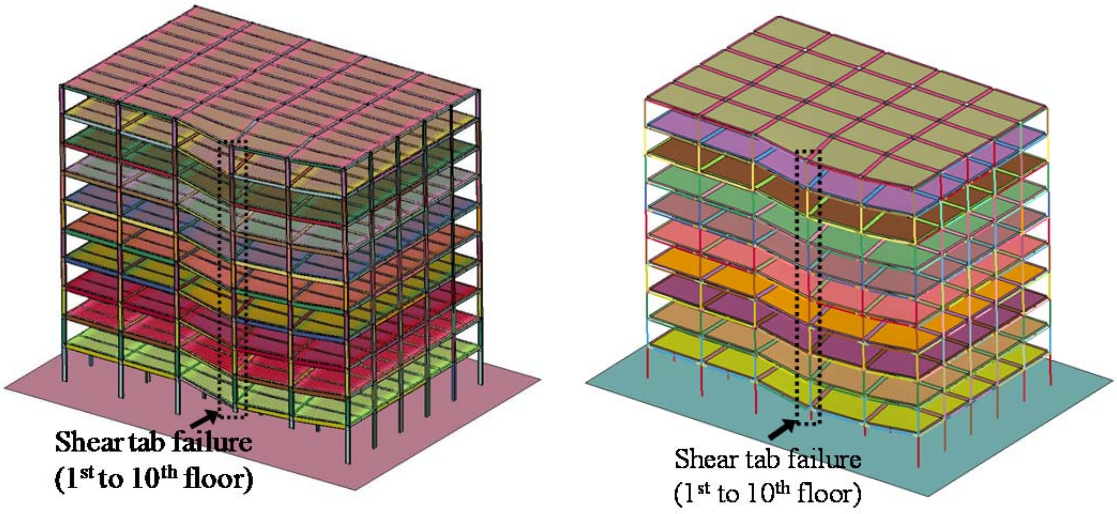

(a) M1 response
(displacement magnification factor=3)

(b) M2
(displacement magnification factor=3)

Figure 4 - 7 Comparison between the failure modes of M1 and M2 after loss of columns C-D6-1/C-E6-1

4.3.4 Column Loss Case 4: C-E4-1

Both M1 and M2 suggest that removal of column C-E4-1, which is a moment frame column, will not lead to collapse. The comparison between the overall response of M1 and M2 are shown in Figure 4 – 8 and good agreement is achieved. Significant force redistribution occurs as shown in Figure 4 – 9(a), but damage is light and permanent deformations are limited as shown in Figure 4 – 9(b). Figure 4 – 9(a) shows that the axial forces in the columns C-E1-1, C-E5-1 and C-E6-1 do not change much, which implies that the load does not redistribute to these columns. These 3 columns are unable to attract additional load because of the low stiffness and strength of their beam-to-column shear connections. The axial force in column C-E3-1 jumps from about 2930 kN to a peak value of 7230 kN and damps out to 6000 kN, which is slightly more than twice the original value. It is clear that the loads are mostly redistributed through frame action in the moment bay spanning columns C-E4-1, C-E3-1 and C-E2-1 (surrounded by dotted lines in Figure 3 – 1). This frame action leads to a reduction in the axial force in column C-E2-1 (Figure 4 – 9(a)) and causes the entire moment frame to lean to the south,

generating a global twisting action on the building. Vertical displacement of the node corresponding to the top of the removed column reaches a peak value of 77.7 mm and reaches steady state at 69.0 mm (Figure 4 – 9(b)).

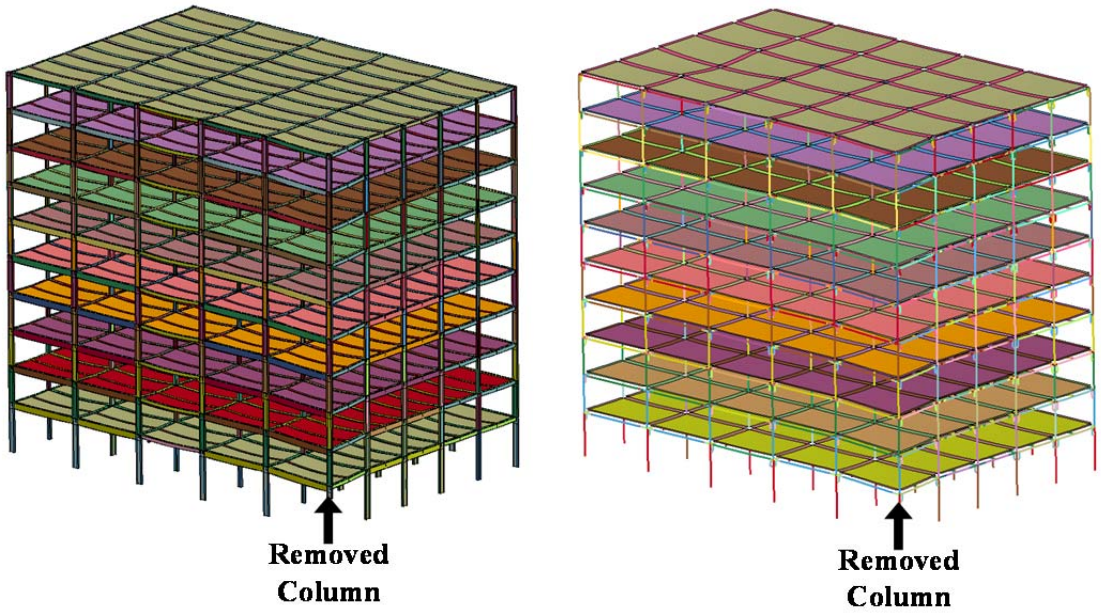

(a) M1 response
(displacement magnification factor=10)

(b) M2
(displacement magnification factor=10)

Figure 4 - 8 Overall responses of M1 and M2: Column C-E4-1 removed

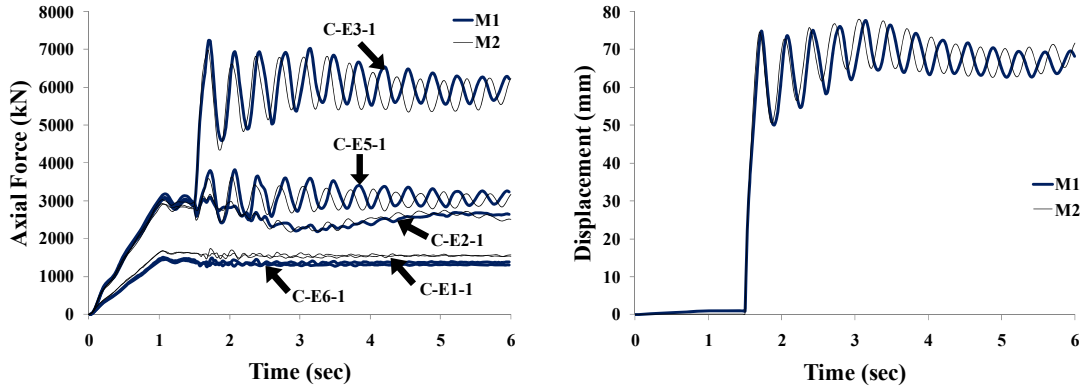

(a) Column axial forces

(b) Vertical displacement

Figure 4 - 9 Comparison between models M1 and M2: removal of C-E4-1

The overall deflection of the system in this case is smaller than the displacement at the node at the top of the removed column when column C-D6-1 is lost, although the tributary area of column C-E4-1 is twice of the tributary area of column C-D6-1 and both C-D6-1 and C-E4-1 are at the edge of a moment frame which have moment connections on one side and shear connections on the other side. The smaller deformation obtained in this case attributes to the smaller span length in the N-S direction.

4.3.5 Column Loss Case 5: C-D5-1

Simulations with both Models M1 and M2 suggest that removal of interior column C-D5-1, which is a gravity column, will lead to progressive building collapse. Figure 4 – 10 shows the progression of damage in both models. Large deformations and severe local damage occur shortly after column removal. The first failures in both models occur in the shear connections attached to C-D5-1 followed, almost simultaneously, by failure of the corresponding shear connections in floors above. Shear connections to C-D4-1 and C-D6-1 fail shortly after, again starting at the bottom floor and propagating rapidly upwards, followed by shear connections of infill and gravity beams in the panels adjacent to the removed column. Connection damage is followed by extensive fracture in the steel deck and mesh reinforcement in the slabs adjacent to B-D56-1 through B-D56-10 in slab panels S-CD56-1 through S-CD56-10. At this point, both models start to deviate from one another, although the subsequent general trends are still similar. Slab fractures between column lines C and D eventually spread beyond the collapse-initiation area, travelling from South to North. Almost in parallel, slabs between column lines D and E experience a similar progression of failures. However, an important difference is that, instead of pulling in only the peripheral gravity beams, the collapsing slab pulls on the entire moment frame spanning columns C-D6, C-E6 and C-F6. The out-of-plane pulling action destabilizes the frame, leading to a global buckling type response that precipitates severe and wide spread damage to the remainder of the system. Continued building implosion is promoted by the impact of falling debris.

4.3.6 Column Loss Case 6: C-E5-1

Like C-D5-1, removal of column C-E5-1 leads to progressive collapse. Similar C-D5-1, collapse is initiated by failure of 1st floor shear connections adjacent to the removed column. This is quickly followed by vertical propagation of shear connection failures along column C-D5 and failures of shear connections at columns C-E4 and C-E6. Slab failure initiates in the adjacent bays causing the slab to fracture along column line E in a south-to-north direction eventually leading to buckling of columns C-E6 followed by C-D6 and later column C-F6. Buckling of column C-D6 causes shear connections attached to it to fail at multiple stories, which precipitates slab failures in the bay bounded by column line C and D, propagating in the south-to-north direction. Falling slabs slam into the standing adjacent bays leading to widespread damage. The collapse sequence captured by both models M1 and M2 compares reasonably well, as is shown in Figure 4 – 11. The fact that consistently good agreement is obtained suggests that M2 is reasonably capable of capturing the propagation of collapse.

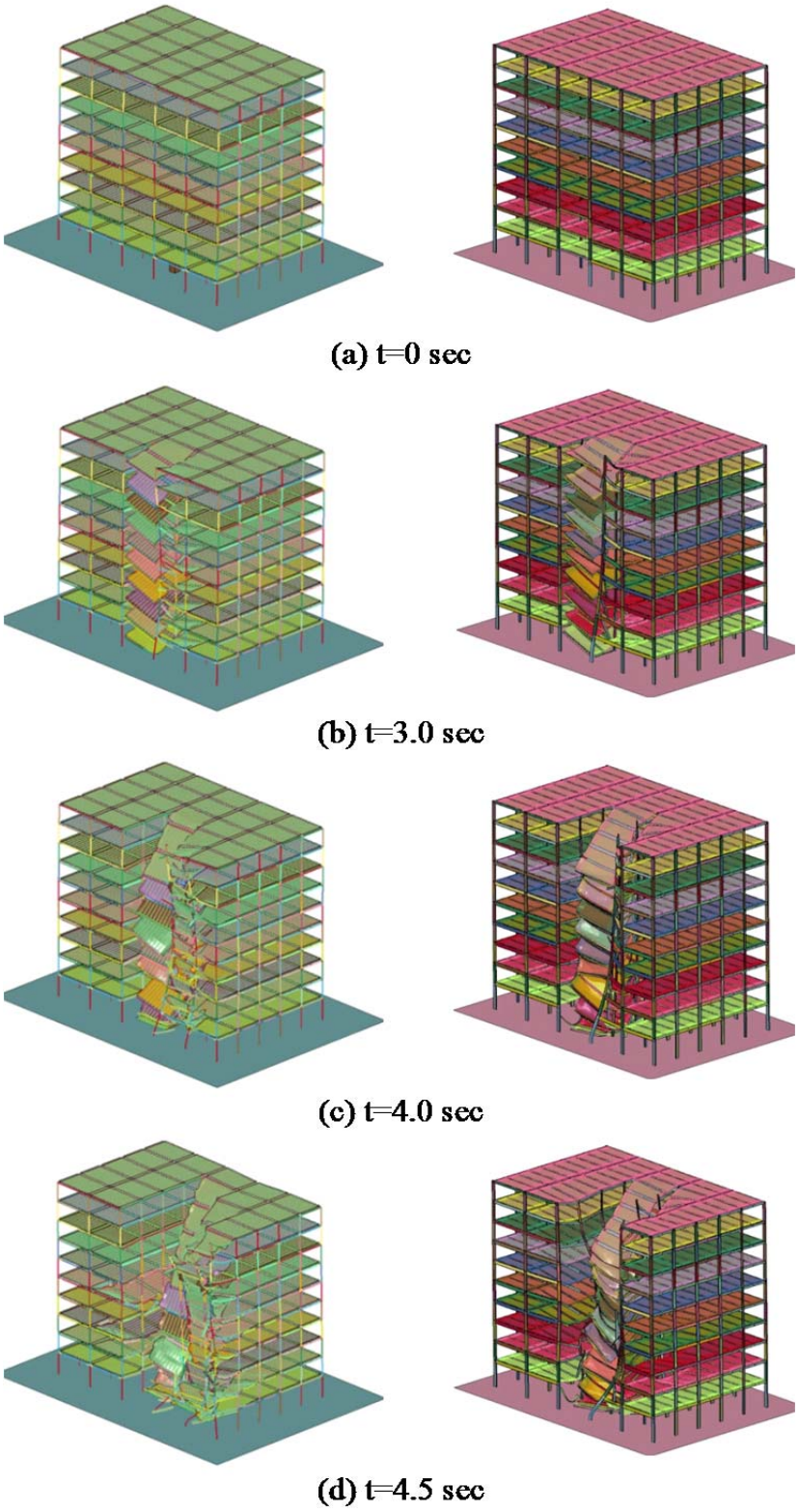

Figure 4 - 10 Comparison between the collapse modes of M1 and M2: removal of C-D5-1

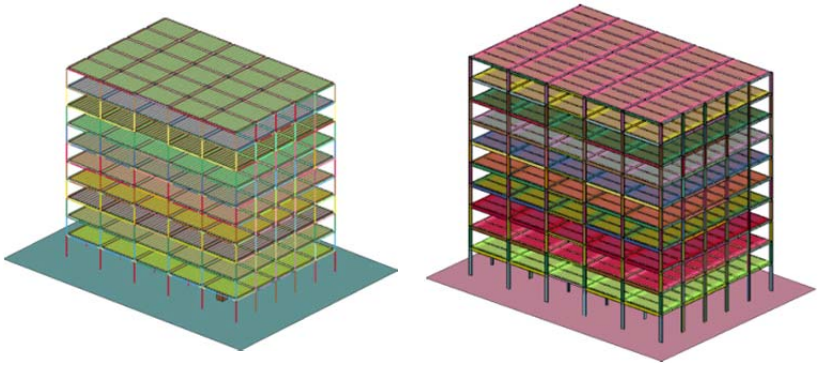

(a) t=0 sec

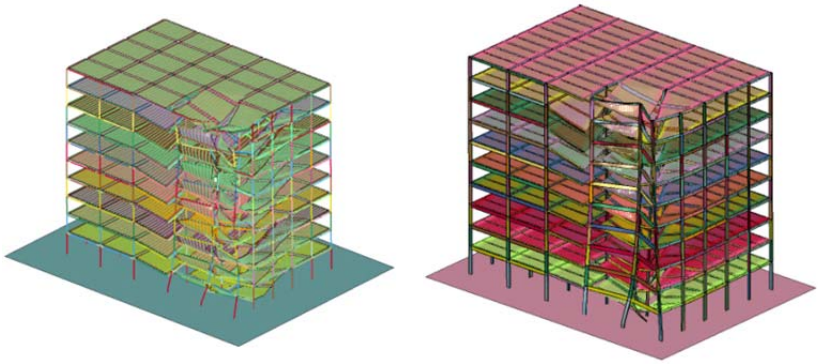

(b) t=3.0 sec

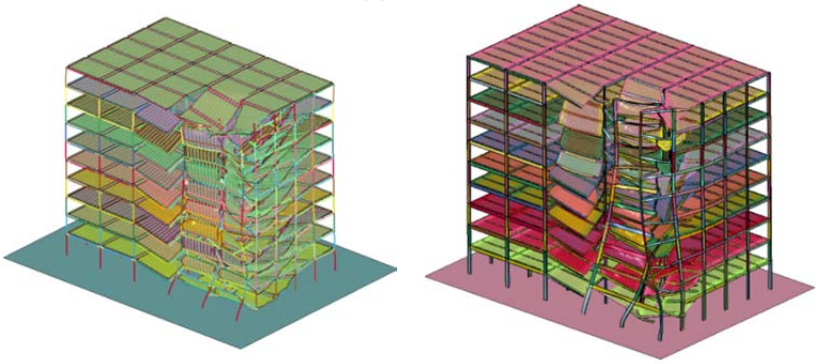

(c) t=4.0 sec

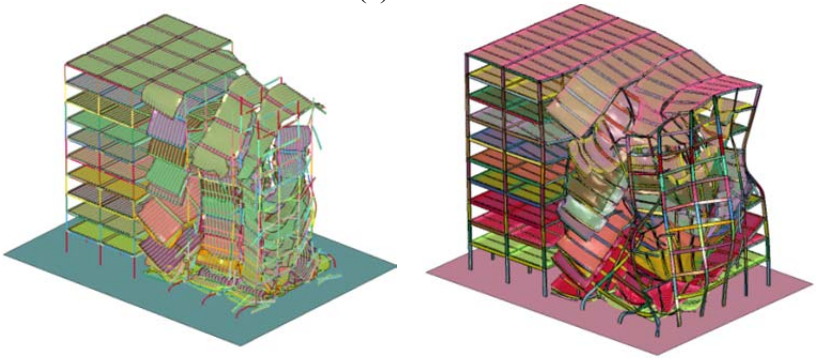

(d) t=5.0 sec

Figure 4 - 11 Comparison between the collapse modes of M1 and M2: removal of C-E5-1

4.4 Effect of Macro Modeling: Comparison between M2 and M4

The comparisons between the responses of planar models M2 and M4 after loss of column C-D6-1 and C-F6-1 are shown in Figure 4 – 12 and Figure 4 –13, respectively. In both cases, progressive collapse does not occur. Models M2 and M4 correlate well together. Both models match in their ability to simulate the force redistribution associated with column removal and the displacements that occur as a result.

4.4.1 Column Loss Case 7: C-D6-1

The force distribution after loss of column C-D6-1 is shown in Figure 4 – 12(a). The axial force in the column C-B6-1 is almost identical before and after loss of C-D6-1. The axial force in C-A6-1 increases and the axial force in C-F6-1 decreases because of the "global frame action" induced by the leaning of the moment frame after loss of column C-D6-1. The axial force in column C-E6-1 changes from 1440 kN to a peak value of 4220 kN and becomes steady at 3280 kN in M2, which is a little larger than twice the original value. This is also a result of the "global frame action" because the structure leans to the west after loss of column C-D6-1. The peak displacements at the node corresponding to the top of the removed column captured by M3 and M4 are 151 mm and 169 mm, respectively and the steady state displacements are 130 mm and 138 mm, which is much larger than what is obtained from 3-D models (Figure 4 – 12(b)).

4.4.2 Column Loss Case 8: C-F6-1

From Figure 4 – 13(a), significant force redistribution occurs after loss of column C-F6-1. Changes in axial forces in column C-A6-1, C-C6-1, and C-D6-1 occur because the structure leans to the East after loss of column C-F6-1. The axial force in the adjacent column C-E6-1 increases from 1470 KN to a peak value of 3450 KN in model M3 and 3620 KN in model M2. After the vibrations die down, the force in C-E6-1 becomes steady at 2530 KN, which are a little more than 1.5 times of its original axial force

because of the global frame action. Figure 4 – 13(b) shows that the displacements that occur at the location of the removed column match well in M3 and M4. After removal of column C-F6-1, the nodes at the location of the removed column vibrate vertically and reach peak downward displacements of 62 mm and 73 mm for M3 and M4, respectively. M3 and M4 come to rest at vertical displacements around 49 mm and 55 mm, respectively, as shown in Figure 4 – 13(b) (approximately 12% difference).

Only the results of these two cases are shown herein because extensive damage occurs after loss of columns C-D6-1 and C-E6-1 simultaneously, which will be discussed later.

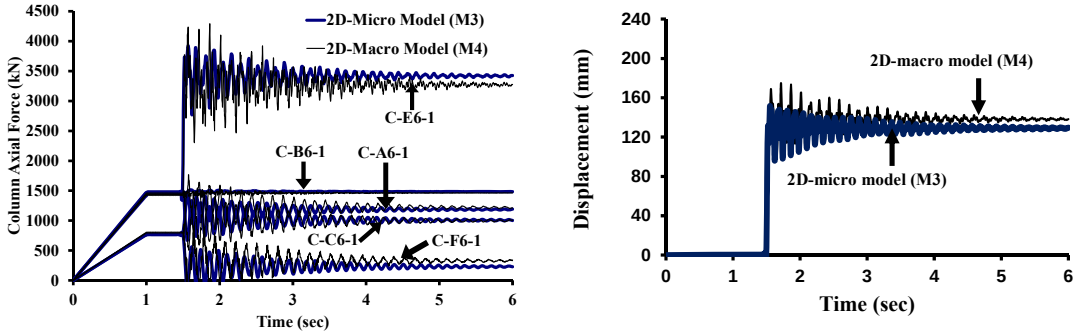

(a) Column axial forces (b) Vertical displacement

Figure 4 - 12 Comparison between models M3 and M4: removal of C-D6-1

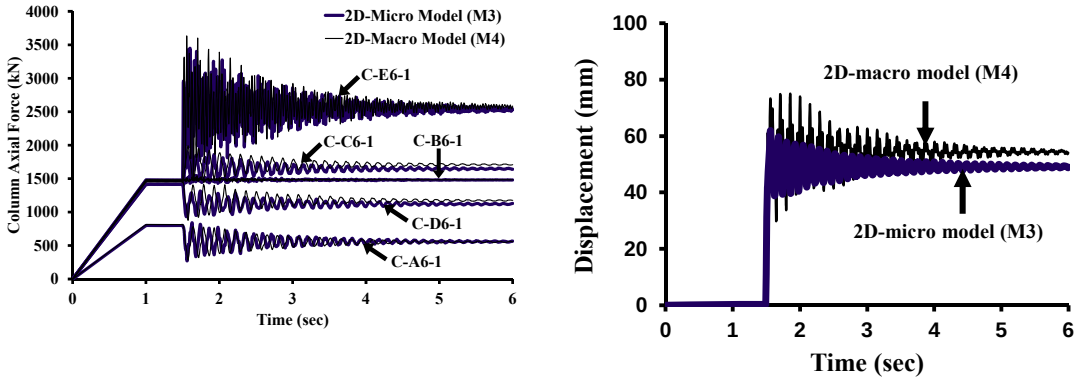

(a) Column axial forces (b) Vertical displacement

Figure 4 - 13 Comparison between models M3 and M4: removal of C-F6-1

4.5 Planar Versus 3-D Modeling

4.5.1 Column Loss Case 9: C-D6-1

Figure 4 – 14 shows the effect of removal of exterior Column C-D6-1. Clearly, there are substantial differences between the M1/M3 responses, which are attributed to the slab and other 3-D effects captured by Model M1 but not M3. These effects appear to play a key role in reducing the overall deflections and promoting load redistribution. For example, the vertical deflection under column C-D6-1 reduces from 128.6 mm in Model M3 to 68.3 mm in Model M1, a 47% reduction (Figure 4 – 14(b)). The compressive force in Column C-C6-1 is less affected by column removal, losing only 70 kN in the M1 case versus 479 kN in the M3 case, which highlights again the role of the slab in promoting load redistribution (Figure 4 – 14(a)).

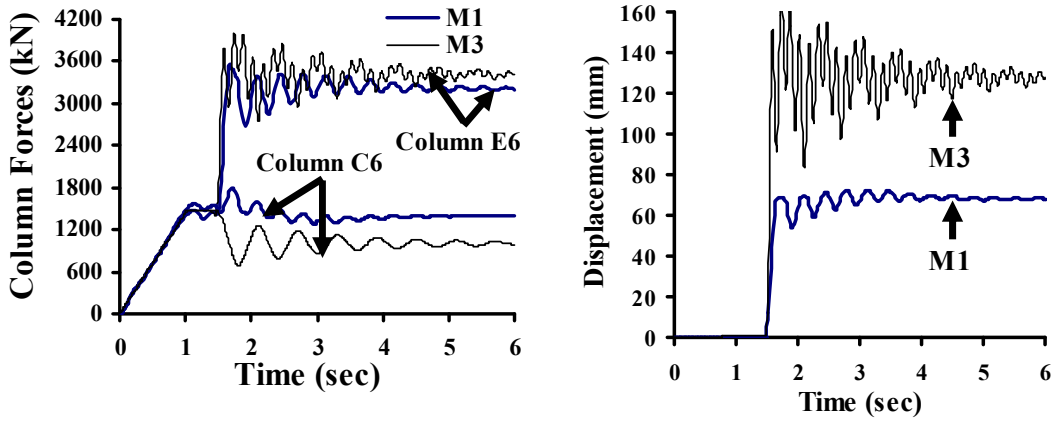

(a) Columns axial forces (b) Vertical displacement

Figure 4 - 14 Comparison between models M1 and M3: Column C-D6-1 removed

The comparison between the responses of model M2 and M4 is shown in Figure 4-15. The same trends observed for M1/M3 are also seen in this comparison for both deformation and load distribution.

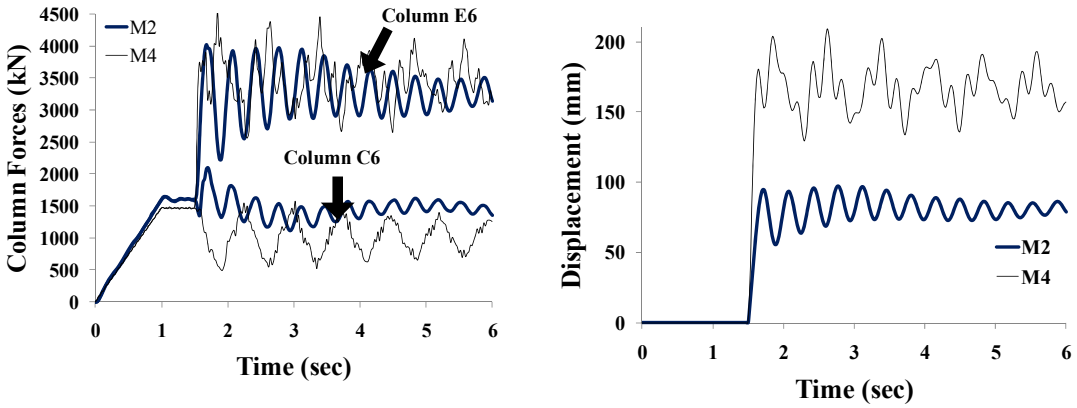

(a) Columns axial forces (b) Vertical displacement

Figure 4 - 15 Comparison between models M2 and M4: Column C-D6-1 removed

4.5.2 Column Loss Case 10: C-D6-1/C-E6-1

Great differences are evident between the M1 and M3 models when Columns C-D6-1 and C-E6-1 are simultaneously removed. The axial force in column C-F6-1 and the displacements above the removed columns C-D6-1 and C-E6-1 are shown in Figure 4 – 16. As shown in Figure 4 – 17, Model M3 predicts failure of the system, while M1 shows a controlled response in spite of failure of one of the shear tab connections in bay CD. Like M1, failure in M3 initiated at the shear tab connection in bay CD, adjacent to column D6, at the first floor. However, unlike M1, shear tab connection failures propagate rapidly upwards all the way to the top floor. At that point, the moment frame spanning columns C-D6-1/C-E6-1/C-F6-1 becomes unbalanced because it is effectively supported on only one intact column, i.e. C-F6-1, and the frame collapses. A similar comparison is captured by M2 and M4.

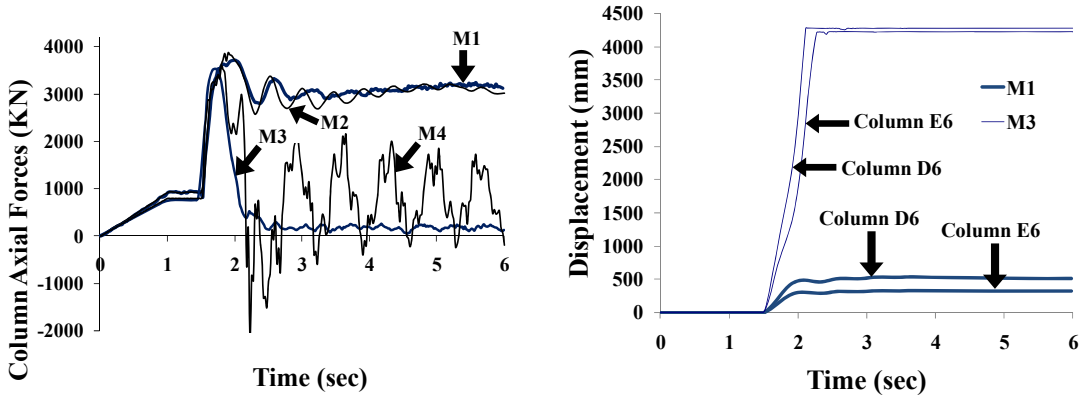

(a) Axial force in column F6 (b) Vertical displacement

Figure 4 - 16 Comparison between models M1 and M3: Column C-D6-1/C-E6-1 simultaneously removed

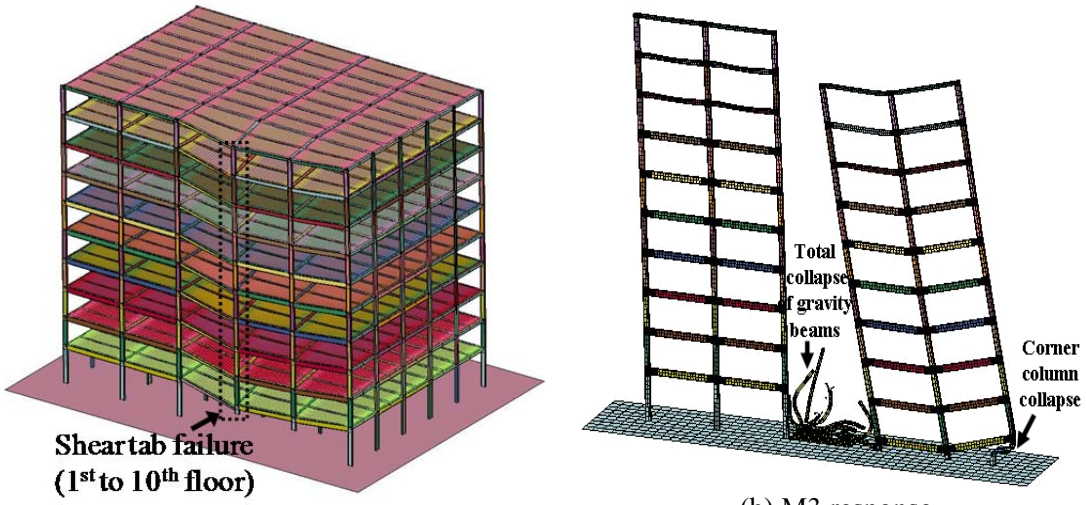

(a) M1 response
(displacement magnification factor = 3)

(b) M3 response
(displacement magnification factor = 1)

Figure 4 - 17 Responses of models M1 and M3 when column C-D6-1 and C-E6-1 are simultaneously removed

4.5.3 Column Loss Case 11: C-E5-1

Figure 4 – 18 presents a comparison between the response of model M1 and M4 after loss of column C-E5-1. Significant differences can be observed. Progressive collapse occurs

after loss of C-E5-1 in model M1, as discussed in section 4.3.6. However, planar analysis of the frame on axis E (using Model M4) predicts localized bay failures in the bays adjacent to the removed column. Similar comparisons are obtained for M2 and M3.

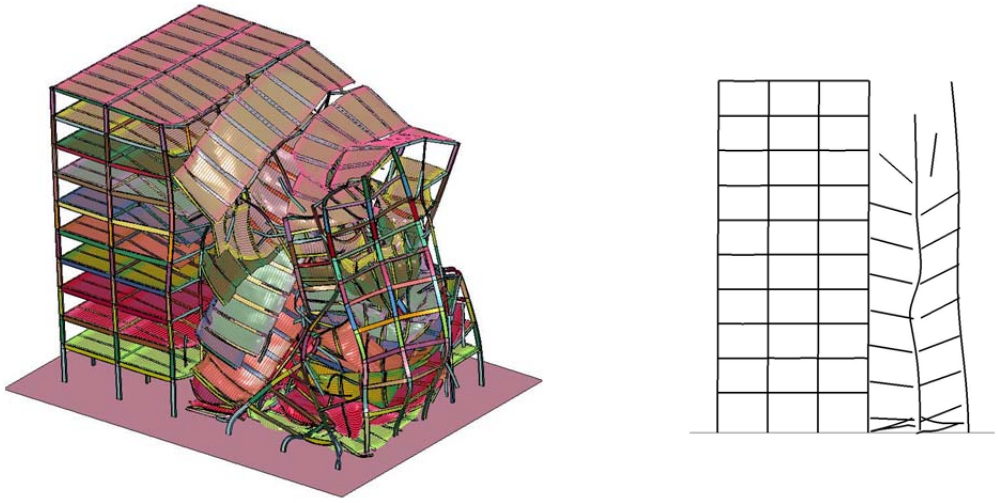

(a) M1 (at 6.50 sec) (b) M4 – Frame on Axis E (at 1.75 sec)

Figure 4 - 18 Comparison between deformed shapes of models M1 and M4: Column C-E5-1 removed

4.6 Implications of Simulation Results

The above discussions indicate that Models M1 and M2 compare favorably in terms of their predictions for force redistribution, displacements, and the general process of failure propagation. The same can be said of the M3/M4 comparisons. The favorable comparison between the detailed models (M1 and M3), both of which can explicitly capture local instability, global buckling, and fracture effects, and the macro models (M2 and M4) that simulate those effects in a phenomenological manner, reflects the success of the macro modeling strategies for the particular case discussed in this study. In other words, well calibrated macro-models can be relied upon for reasonable accuracy when modeling progressive collapse.

The simulation studies show that there are distinct differences between the results of the planar and 3-D models. The 3-D models are considered more realistic than the planar models in that they can capture the effects of the slab and its interaction with the other frame members. Through comparisons of 3-D models with planar models, it turns out that these effects are significant. When failure is not imminent, e.g. as shown in Figure 4 – 14 and Figure 4 – 15, it appears that the slab reduces the deformations that occur and leads to a reduction in the forces that are redistributed to adjacent columns. This can be clearly seen in Figure 4 – 14(a), where column C-E6-1 in Model M3 sees a larger increase in load than in Model M1, whereas Column C-C6-1 sees a larger decrease in Model M3 than in Model M1. In other words, the slab collaborates with the moment frames to temper the force redistribution that happens when members are removed. The effect of the slab is discussed in greater detail in Chapter 5.

When failure is predicted, planar models may overestimate the vulnerability of a structure. In the studies presented herein, the planar models predicted failure when columns C-D6-1 and C-E6-1 were simultaneously removed. However, the 3-D models showed that failure was arrested and did not propagate. On the contrary, it is possible that planar models may actually underestimate the extent of the vulnerability of a structure. Specifically, it is feasible that planar models that have localized bay failures may focus the attention of an analyst on the localized nature of the failure, whereas a 3-D analysis of the problem may lead to much more widespread failure because of 3-D effects. An example of such a situation is loss of interior gravity columns, where a planar frame analysis may suggest localized bay failure, but a full 3-D analysis may uncover the potential for system wide collapse (column loss case 11 in section 4.5.3). Additional cases are described in Chapter 5, such as column loss case 5, 6, 11 and 12 in Table 5 – 1. This implies that the 3-D simulation predicts more widespread collapse than that predicted by the planar analysis and therefore it is not possible to state with certainty that planar models are always conservative.

Another dimension to the comparison between planar/3-D and micro versus macro models is the computational effort that needs to be expended to achieve an analysis.

Table 4 – 2 shows a summary of the computational statistics for all 4 models for simulation of 6-seconds of real time. All runs were conducted with 12 CPUs. Clearly, Model M1 is very computationally expensive, running for 208,564 sec. Compared to M1, Model M2 is computationally efficient, running 230 times faster than M1. The reduction in computational time is not primarily due to the reduction in number of elements, but rather to the careful sizing of elements within the model to ensure that they yield at large a time step as possible without compromising accuracy. While Model M4 is the fastest, it runs in 30 sec or 1/7,000th the time needed by M1. The trend in Table 4 – 2 is: macro is 1 to 2 orders of magnitude faster than micro, while planar is 1 to 2 orders faster than 3-D. Clearly, there are huge computational benefits to be gained by using models such as M4. As shown in this chapter, such models are reasonably reliable; however, their limitations must be thoroughly understood before their results can be employed.

Table 4 - 2 Statistic for Various Models

Model Number	Number of Elements	Time (sec)
M1	766935	208564
M2	62554	903
M3	32600	5854
M4	1048	30

4.7 Summary and Conclusions

The models developed in Chapter 3 are employed to investigate the effect of some commonly employed approximations in collapse modeling, including macro versus micro modeling and planer versus 3-D modeling. A series of column loss cases are conducted and the ability of all four models to predict collapse response is compared. Comparisons between M1/M2 or M3/M4 showed that the macro and micro models produce generally similar responses.

A key conclusion that can be drawn from this study is that there are significant computational benefits to be gained by using models such as M2 or M4 in lieu of the

others. The simulations in this chapter show that planar representations can lead to reasonable modeling of behavior, especially when failure is not predicted. However, the limitations and implications of their results must be thoroughly understood. For example, as highlighted in this chapter, planar models tend to see higher deformations and greater force redistribution because the effect of the slab is not accounted for. Moreover, when failure is predicted, planar analysis significantly overestimated the extent of the vulnerability for the case considered. It is, however, not possible to generalize this statement since, at the other extreme, planar analysis may also underestimate vulnerability, e.g. by predicting localized bay failure that could propagate to a progressive collapse in a 3-D model. These conclusions suggest that a full 3-D analysis, in spite of its computational cost, may be the only sure way to rigorously investigate system robustness.

CHAPTER 5

THREE-DIMENSIONAL EFFECTS AND COLLAPSE RESISTANCE MECHANISMS IN STEEL FRAME BUILDINGS

5.1 Introduction

From the literature survey in Chapter 2, it is clear that there is growing consensus that accounting for 3-D effects is necessary for accurate and meaningful progressive collapse modeling. This trend is highlighted by the recent requirement in the DoD (2009) guidelines that specifies that only 3-D models should be used for robustness evaluations. However, in spite of the growing realization that 3-D effects may be important, there has not been a systematic study to show how important they actually are. There has also not been adequate study of what collapse resistance mechanisms are activated just before and during collapse and how well they can be captured by planar and 3-D models. To address these outstanding issues, simulations are conducted in this chapter to assess the influence of a number of parameters on collapse response. The objective is to quantify the sources of resistance that contribute to structural robustness, including the contribution of the slabs and frame action. The 3-D macro-model M2, described in Chapter 2, is used to conduct the simulations and its results are contrasted with the results of planar model, M4, to highlight the effects of accounting for 3-D behavior.

System response due to loss of columns in the upper stories is first presented in Section 5.2. The effects of the slabs are discussed in Section 5.3. Sections 5.4 and 5.5 examine the sources of resistance provided by the slab, focusing in particular on composite action between the floor slabs and the steel beams and membrane action in the slabs, respectively. Frame action in moment-resisting system is addressed in Section 5.6 and the chapter summary and conclusions are presented in Section 5.7.

5.2 System Response to Column Removal in Upper Stories

A number of column loss cases are considered to study the robustness of the prototype building, focusing on the loss of upper floor columns. The upper floor column removal cases conducted are listed in Table 5 – 1. These locations correspond to first floor column removal cases shown in Table 4 – 1 and Figure 4 – 1 in Chapter 4. Therefore, the study in this Chapter is complementary to the Chapter 4 study.

Table 5 - 1 Column removal cases in Chapter 5

Column loss case	Column removed	Column type
1	C-D6-5	Exterior moment
2	C-F6-5	Corner moment
3	C-D6-5/C-E6-5	Exterior moment
4	C-E4-5	Interior moment
5	C-D5-5	Interior gravity
6	C-E5-5	Interior gravity
7	C-D6-10	Exterior moment
8	C-F6-10	Corner moment
9	C-D6-10/C-E6-10	Exterior moment
10	C-E4-10	Interior moment
11	C-D5-10	Interior gravity
12	C-E5-10	Interior gravity

While there are many column loss studies in the literature, the vast majority have focused on first floor column loss and not higher floor column loss as is done herein. The upper floor column loss scenarios are compared with corresponding first floor column loss scenarios outlined in Chapter 4 to highlight the effect on system response of column loss

location along the height. As was done for first floor columns studied in Chapter 4, the alternate path method is used in the simulations presented in this Section.

5.2.1 Removal of 5th Floor Exterior Columns

Removal of 5th floor column C-D6-5 results in a response that is similar to that which occur when 1st floor column C-D6-1 is removed. The only difference is that the displacement at the location of the removed column increases from 82 mm to 107 mm (a 30% increase). Similar results are observed for column C-F6-5, where the deflection at the removed column location increases from 47 mm for 1st floor column removal to 57 mm (a 21% increase). The load redistribution mechanism is fairly simple in this case, with much of the unbalanced load finding its way to C-E6-5 through frame action in the frame spanning columns D6, E6 and F6. The axial force in C-E6-5 increases from 950 kN to a peak value of 2,010 kN and becomes steady at 1,550 kN.

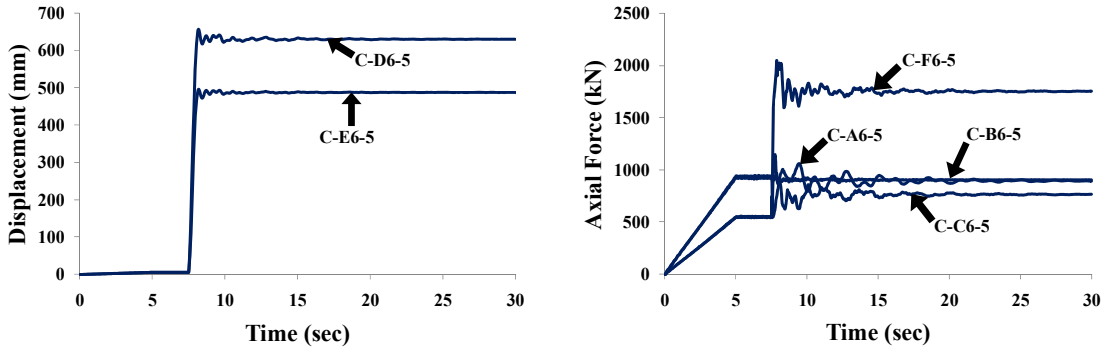

(a) Column axial forces (b) Vertical displacement

Figure 5 - 1 Response of M2: removal of C-D6-5 & C-E6-5 simultaneously

As with their 1st floor counterparts, collapse does not occur after simultaneous removal of columns C-D6-5 and C-E6-5 although severe local damage and significant deformations occur, as shown in Figure 5 – 1. Compared with the corresponding 1st floor column loss case, the displacement at the top of column C-D6-5 increases from 538 mm to 630 mm (a 17% increase) and the deflection at the other column increases from 330 mm to 488 mm

(a 48% increase). As shown in Figure 5 – 2, progression of damage is similar to the first floor case, i.e. failure of shear connections connecting beams B-CD6 to column D6, travelling from the floor in which the columns are removed up to the top floor.

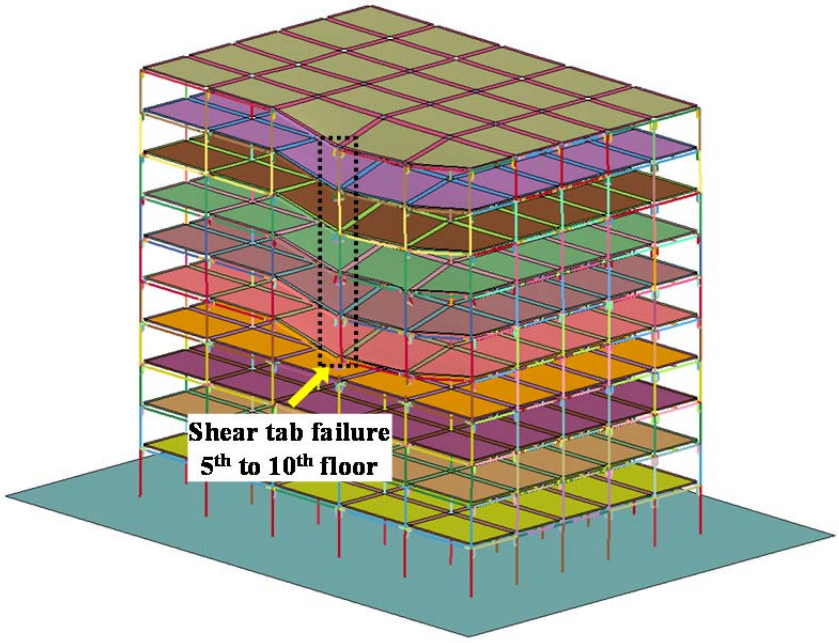

Figure 5 - 2 Failure mode: removal of column C-D6-5/C-E6-5 (displacement magnification factor =3)

5.2.2 Removal of 5th Floor Interior Columns:

Like C-D5-1, loss of interior column C-D5-5, which is also a gravity column, causes progressive collapse of the structure. The progression of failure above the 5th floor is generally similar to the process observed when C-D5-1 is removed. What is different in this case is that falling slabs from the higher floor levels causes damage to progress downwards (below the 5th floor) and to the East as shown in Figure 5 – 3. Similar behavior is observed for loss of column C-E5-5.

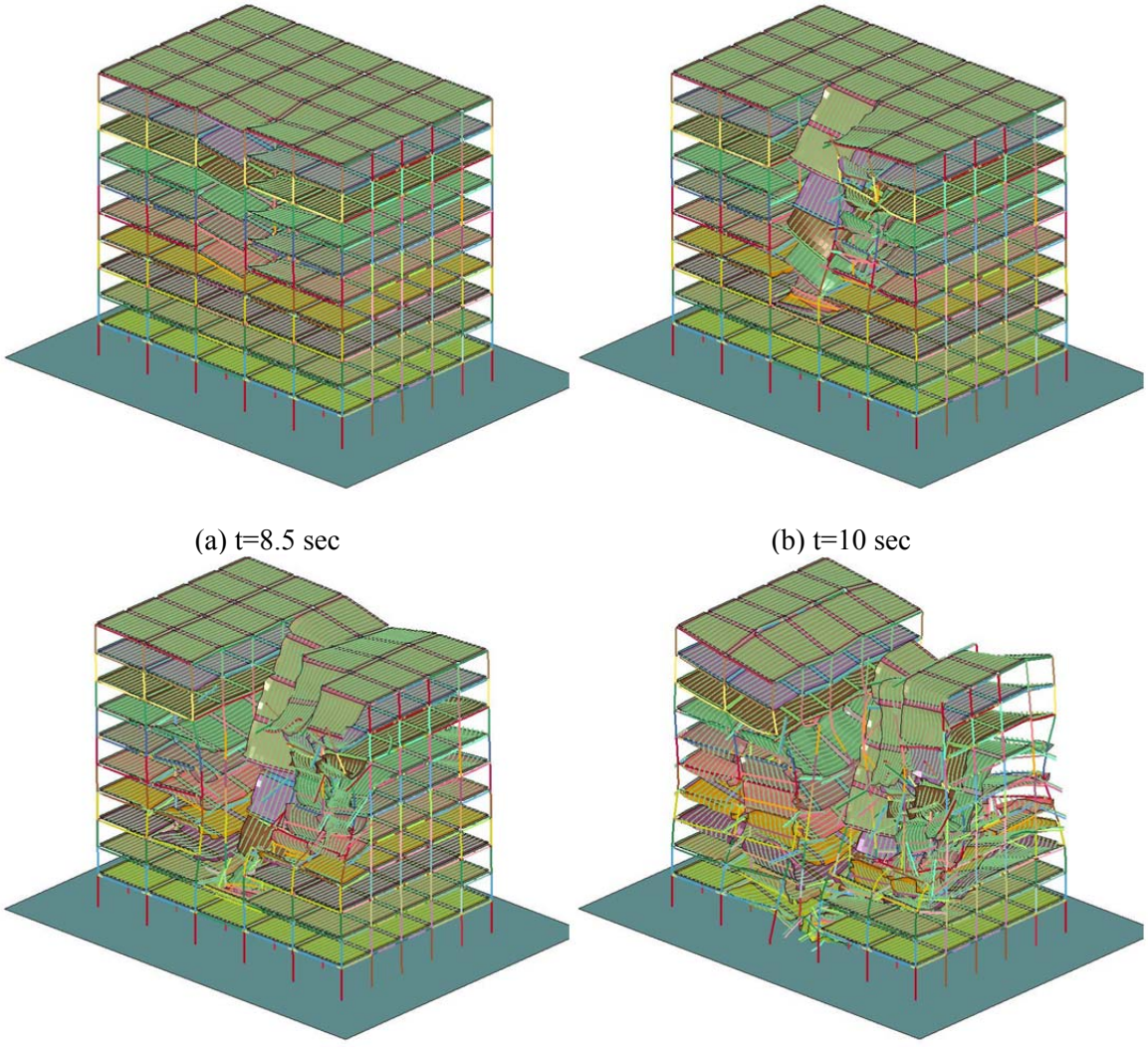

(a) t=8.5 sec (b) t=10 sec

(c) t=11 sec (d) t=12 sec

Figure 5 - 3 Response of M2: removal of C-D5-5

Collapse does not occur when column C-E4-5, which is a moment column, is lost. The behavior is similar to that computed for the first floor counterpart. As observed for exterior columns, frame action in the moment bay plays a critical role in redistributing forces, mostly to column C-E3 (Figure 5 – 4).

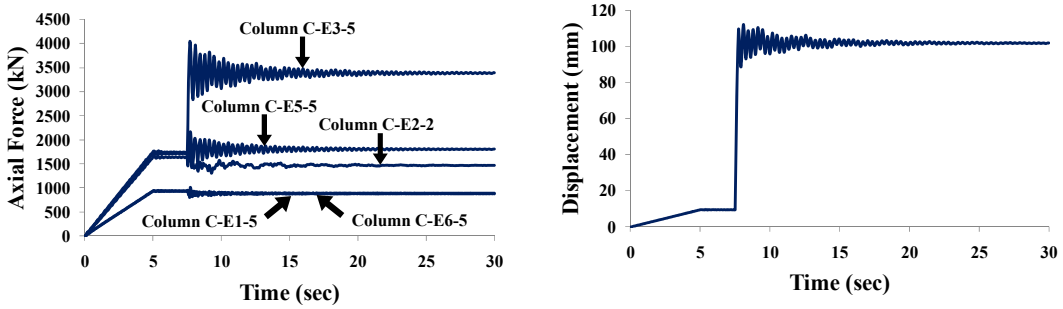

(a) Axial force in column F6 (b) Vertical displacement

Figure 5 - 4 Response of M2: removal of C-E4-5

5.2.3 Removal of 10th Floor Exterior Columns:

Removal of column C-D6-10 results in localized damage as shown in Figure 5 – 5. The observed damage is more extensive than that observed for corresponding columns at the 1st or 5th floors. The cause of damage can be seen in Figure 5 – 5, which shows that two beam spans (B-CD6-10 and B-DE6-10) are involved in resisting collapse along with their adjacent slab panels. As the deformation level increases when the column is lost, both beams mobilize a catenary mechanism in the East-West direction. However, the tensile resistance of the mechanism is limited by the tensile strength of the shear connections at the ends of beam B-CD6-10. Slab membrane action helps although it is limited because the metal deck flutes are aligned in the North-South direction. Combined, the resistance mechanisms in the beam and slab are unable to support the load and resist local failures. The slamming effect of the slab appears limited in this case because: 1) the roof carries smaller loads than lower slabs, and 2) the falling slab is smaller in area than in other cases.

Simultaneous removal of exterior columns C-D6-10 and C-E6-10 precipitates progressive collapse (Figure 5 – 5). Compared to the corresponding first and fifth floor cases, major differences are observed when both C-D6-10 and C-E6-10 are simultaneously removed. In the first and fifth floor situations, collapse is arrested, although significant damage and large displacements are observed as previously discussed. The failures are initiated by the fracture of shear connections attached to B-CD6-10 followed by the fracture in the steel

deck and mesh reinforcement in the slab panel S-CD56-10. Shortly after that, the reduced beam section of B-EF6-10 fractures, leading to failures in slab panel S-EF6-10. The failures propagate from South to North between column lines C to F. The falling slabs slam onto the floor beneath causing damage to propagate downwards and laterally to the East because of the asymmetry of the collapse mode. The damaged and sagging slab between column lines D and E eventually pulls on columns C-D6, C-E6 and C-F6 bending them inward about their weak axis, leading to buckling of the entire facade of the building in that location and extensive subsequent damage.

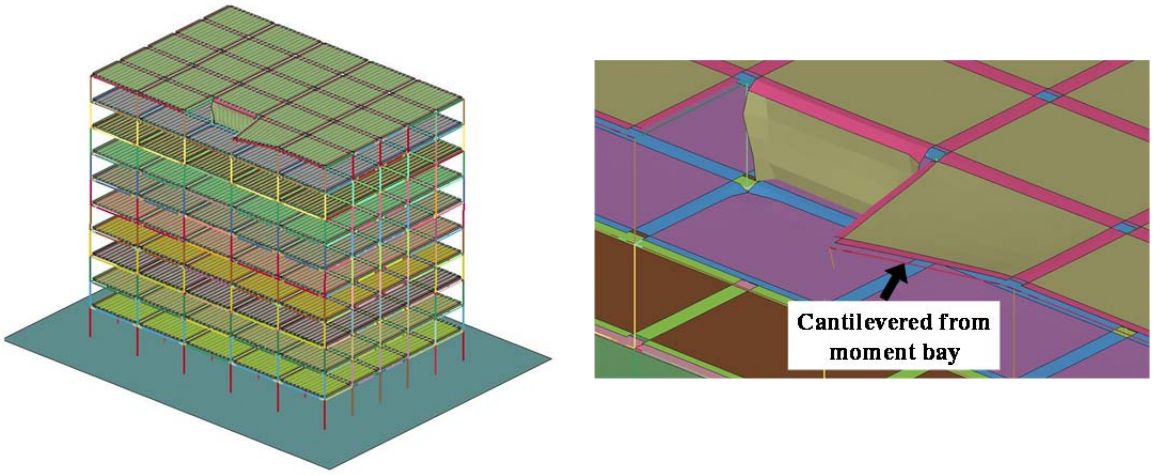

(a) Global response (b) Zoom in at damaged area

Figure 5 - 5 Response of M2: removal of C-D6-10

Removal of C-F6-10 resulted in behavior that is similar to removal of corresponding 1st and 5th floor columns, although the deflections are much higher in this case because the system cannot benefit from frame action that occurs above the removed column in the 1st and 5th floor cases. On the other hand, the sizes of the structural elements are also smaller than those in the 1st and 5th floor. Membrane action in the slab coupled with catenary action in beams B-EF6-10 and B-F56-10 plays an important role in preventing complete collapse of the local slab panel.

5.2.4 Removal of 10th Floor Interior Columns:

Like the corresponding case at the 5th floor, removal of C-D5-10 leads to progressive collapse, primarily driven by the inability of lower floors to support the weight of falling slabs from higher levels.

Figure 5 – 6 shows the response of the model to loss of column C-E4-10. Compared to removal of C-E4 columns at lower floors, removal of this particular column results in much deflection (peak deflection is 673 mm, steady state is 657 mm) and extensive gravity connection damage; 2 of the 3 shear connections to the column stub of the removed column fail, i.e. J-DE4-10-East and J-E45-10-North. However, like the other cases, collapse is eventually arrested. The moment frame spanning columns C-E2, C-E3 and C-E4 is not as effective in supporting the lost load carrying capacity as with lower floors, since it is unable to develop full frame action above the top floor column. This is also manifested in more uniform force redistribution to surrounding columns, whereas columns in the moment bays play a key role in force redistribution in lower floors.

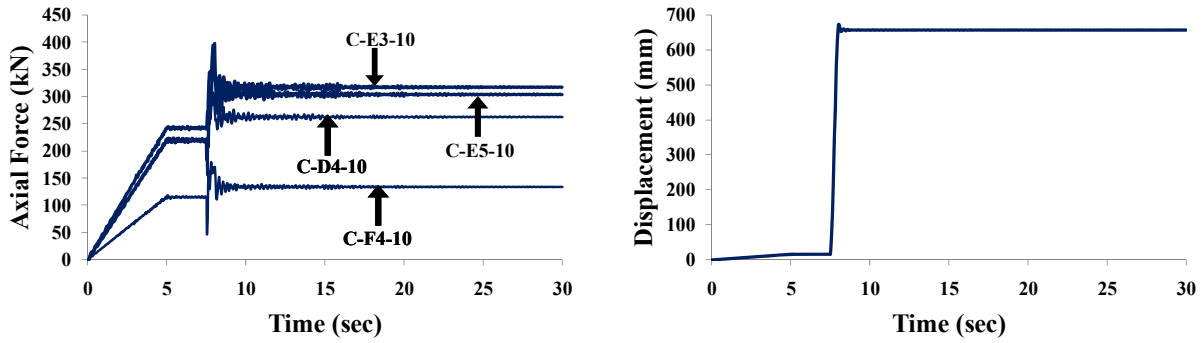

(a) Column axial forces

(b) Vertical displacement

Figure 5 - 6 Response of M2: removal of C-E4-10

Removal of gravity column C-E5-10 does not result in collapse, even though removal of its counterparts in lower floors leads to progressive collapse. The local slab is, however, on the verge of collapse and there is extensive local damage and substantial deformation.

The failure mode is shown in Figure 5 – 7. The top of the removed column drops 1069 mm below its original location, as shown in Figure 5 – 8(d). Figure 5 – 8(a), Figure 5 – 8(b) and Figure 5 – 8(c) illustrate the column forces in the columns adjacent to the removed columns on column lines D, E and F, respectively. It can be seen that most of the loads, if not all, are transferred to C-E4-10 and C-E6-10. The axial force in C-E4-10 changes from 227 kN to a peak value of 381 kN. After the vibrations damp out, the value became 329 kN. The axial force in C-E6-10 increases from 117 kN to a maximum 285 kN and the steady value was 227 kN. Damage is concentrated in the area adjacent to the removed column and pertains to failure in shear connections and yielding in large parts of the slab steel. The reason that collapse is mitigated in this case but occurs in the cases when C-E5-1 and C-E5-5 are removed is that the loads applied on the roof are smaller than the loads on the lower floors.

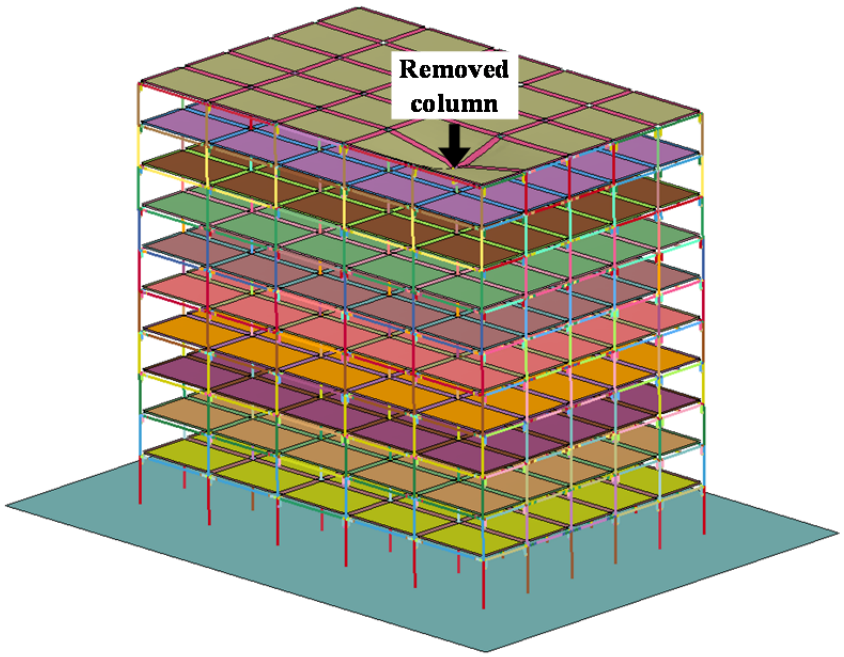

Figure 5 - 7 Overall response of M2: after removal of C-E5-10 (Displacement magnification factor = 2)

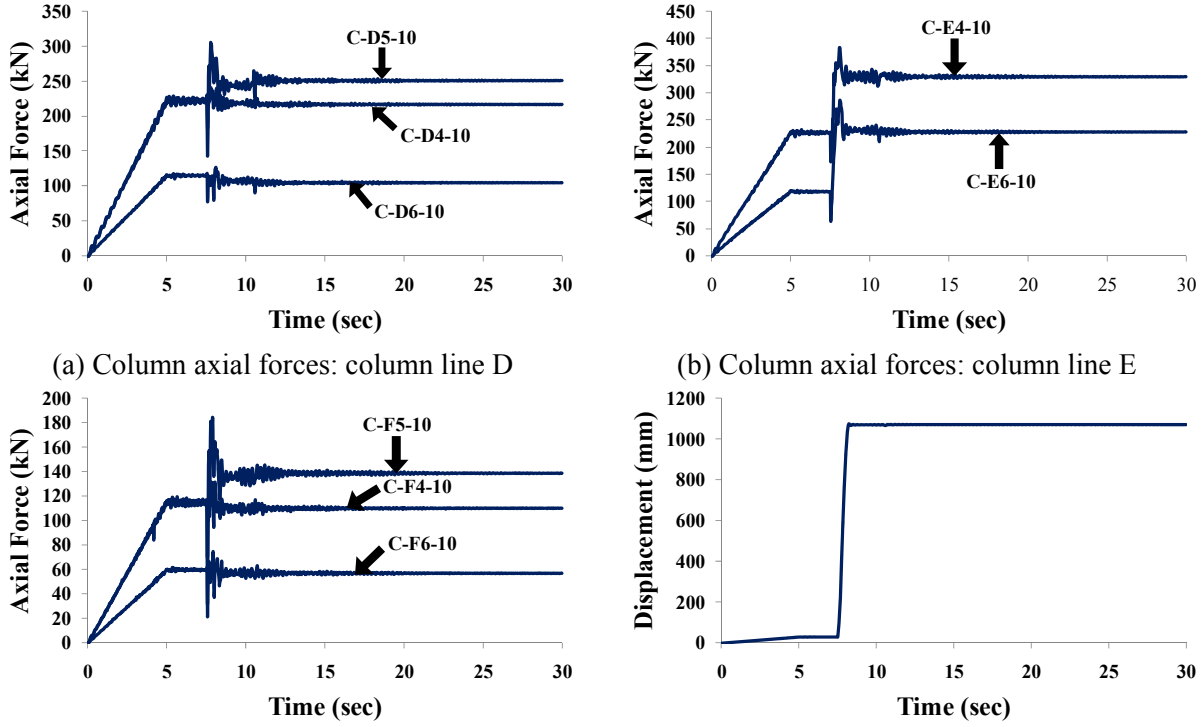

(a) Column axial forces: column line D

(b) Column axial forces: column line E

(c) Column axial forces: column line F

(d) Vertical displacement

Figure 5 - 8 Response of M2: removal of C-E5-10

5.2.5 Summary of System Response Simulations

Table 5 – 2 summarizes system responses for the various column loss scenarios. It can be inferred from the table and the discussion above that the results of the column removal study shows two general trends: 1) the prototype building is more vulnerable to loss of columns in the upper stories than in the lower ones, and 2) the building appears to be particularly vulnerable to loss of interior gravity columns at all floor levels. The former result is evident in the increase in displacement at the removed column and worsening outcome (e.g. collapse versus no collapse) that occurs as columns are removed at higher floors. The only exception is column E5, which as discussed before, survived because of lower roof loads. This somewhat counter intuitive result is attributed to the fact that column loss in lower floors can mobilize more of the structure above it to survive than column loss in upper floors. The latter trend is in accord with observations made in Sadek et al. (2008) and Alashker et al. (2010).

Table 5 - 2 Displacement at removed column (steady state) for various column loss cases

Column Position	1st floor	5th floor	10th floor
D6	82	107	***PC*[2]**
D6/E6	457/348	630/488	***C*[1]**
F6	47	57	***PC*[2]**
D5	***C*[1]**	***C*[1]**	***C*[1]**
E4	69	102	657
E5	***C*[1]**	***C*[1]**	1069

[1]Progressive Collapse
[2]Partial collapse limited to 10th floor

5.3 Global Effect of the Slab

In this section, simulations are conducted using model M2 and a modified M2 model without the slab, designated M2-NS (where NS stands for no slab). In M2-NS, it is necessary to keep a small set of peripheral slab elements in each panel in order to maintain the stability of the beams, which will undergo premature lateral torsional buckling if they are left completely unsupported, as shown in Figure 5 – 9(b).

The comparisons in Chapter 4 showed that there are substantial differences between the response of planar and 3-D models. It is hypothesized that the slabs are the source of this difference, however that could not be clearly discerned from the simulations conducted in that Chapter. To clarify the role of the slab in 3-D response, comparisons are made between models M2, M2-NS, and model M4. Tables 5 – 3 and 5 – 4 illustrate these comparisons. Table 5 – 3 lists all cases in which collapse is mitigated in the 3-D models. In it, the steady state displacements of the node corresponding to the top of the removed column, computed from various models, are compared. Table 5 – 4 presents cases in which collapse could not be arrested in the 3-D models and describes how the models respond during the collapse process.

Table 5 - 3 Comparison between the responses of the 3D models with and without slabs: progressive collapse is prevented

Column-loss case	Deformation after column loss (steady state)		
	Model M2 (mm)	Model M2-NS (mm)	Model M4 (mm)
C-D6-1	69.3	108.1	109.0
C-E6-1	26.4	32.1	33.3
C-F6-1	45.7	51.8	53.3
C-E4-1	65.5	196.1	collapse

An examination of Table 5 – 3 shows that the deformations captured by M2-NS are always larger than those captured by M2 and, in fact, are very close to those captured by M4, although slightly smaller. The only exception is when column C-E4-1 is removed, which leads to collapse in M4 (representing the frame on axis E), but not in M2 or M2-NS. However, the displacement in M2-NS reaches 196 mm, which is 3 times the value in M2. Comparisons between M2 and M2-NS results clearly show that the slab is exerting much 3-D influence. However, there appears to be other significant sources of 3-D resistance, e.g. attributed to out-of-plane structural members, which help arrest collapse in M2-NS versus M4 when column C-E4-1 is eliminated. It is also possible that some composite action between steel beams and the remaining peripheral slabs enhance the resistance preventing outright collapse when C-E4-1 is removed.

Table 5 - 4 Comparison between the responses of the 3D models with and without slabs: progressive collapse occurs

Column-loss case	Response of the model	
	Model M2	Model M2-NS
C-D5-1	Full structure collapse	Partial collapse
C-E5-1	Full structure collapse	Partial collapse
C-D6-1/C-E6-1	Collapse mitigated	Partial collapse

Table 5 – 4 reveals that the existence of the slabs is not always beneficial. In cases where D5 or E5 are individually removed, full progressive structural collapse occurs in M2, but not M2-NS, which suffers only partial collapse around the eliminated column. Clearly, the presence of the slab helped promote progressive collapse in these cases. In contrast,

when C-D6-1/C-E-16 are removed simultaneously, partial collapse also occurs in M2-NS, but collapse is mitigated in M2.

The simulation results discussed in this section shed light on the complex role of the slab in resisting collapse. The results show that when a column in a moment bay is lost and the structure does not collapse, the moment bay containing the removed column will lean towards the location of the removed column. The moment bay will therefore push or pull on adjacent bays in the plane containing the affected moment bay causing the entire frame to also lean in that direction. This effect is equivalent to applying an additional lateral force on to the frame, which results in force redistribution in the columns in the moment bay. In addition, since the slabs are stiff in plane, they tend to maintain their rectangular shape, which can lead to global torsional effects.

Figure 5 – 9 shows the comparison between the top views of the deformed shape of the models with and without the slabs after loss of C-E4-1. The dark lines indicate the outline of the undamaged structure. The global torsional effect is evident in Figure 5 – 9(a) and it is clear that the slabs force other moment bays in the system to be mobilized to resist collapse, e.g. the frame on axis F. It can also be seen that the greatest lateral displacement demands may not occur in the frame containing the removed column. In this particular case, the frame on axis F experiences the largest lateral displacement leading to substantial force redistribution in that frame. For example, after loss of C-E4-1, the steady state axial force in C-F5-1 increases from 1470 kN to 1980 kN, whereas the force in F3 decreases from 1470 kN to 935 kN.

Figure 5 – 9(b) shows that for model M2-NS, the frame containing C-E4-1 suffers the greatest lateral deformation. Other frames are also being mobilized, but force redistribution in surrounding frames is not as severe as when the slab is present because the other three frames containing moment bays in the N-S direction hardly deform laterally. Also evident from a comparison between Figures 5 – 9(a) and 5 – 9(b) is that a much larger lateral displacement occurs in the frame on axis E in M2 versus M2-NS, which clearly demonstrates the effective role of the slab in this situation.

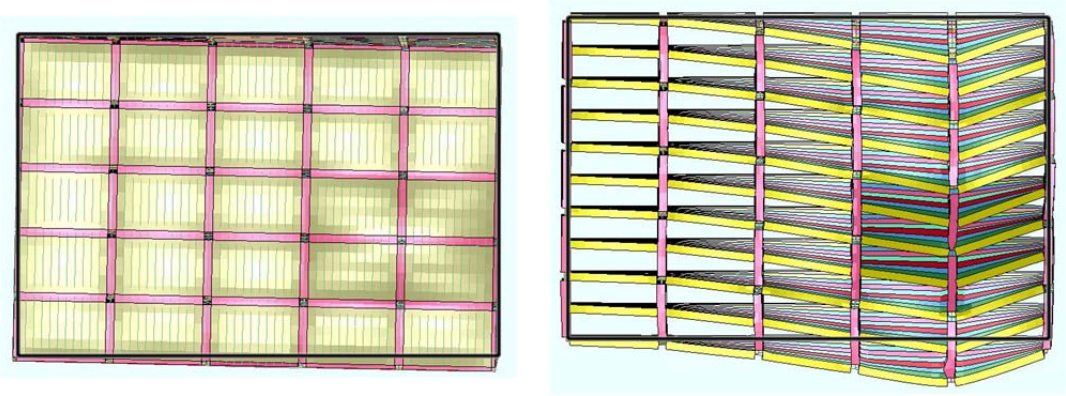

(a) Deformed shape of M2 (displacement magnification factor=20)

(b) Deformed shape M2-NS (displacement magnification factor=20)

Figure 5 - 9 Comparisons of top views of M2 and M2-NS subjected to loss of E4

5.4 Role of Flexural Composite Action in Collapse Resistance of Steel Frame Buildings

In order to investigate the role of flexural composite action (FCA) in collapse resistance under column loss scenarios, a series of nonlinear dynamic analyses are performed using model M2, and a variation of M2, designated M2-NC. The variant M2-NC is identical to M2 except that slab-beam composite action is eliminated in the slab panels which are adjacent to the removed column(s). This is achieved by permitting unrestricted slippage along the beam direction between the slab and beam nodes of the shear stud elements, as shown in Figure 5 – 10. Other degrees of freedom are not released to ensure lateral stability of the beams. Three first floor column loss cases are considered: removal of C-D6-1, C-D6-1/C-E6-1 simultaneously, and C-E6-1.

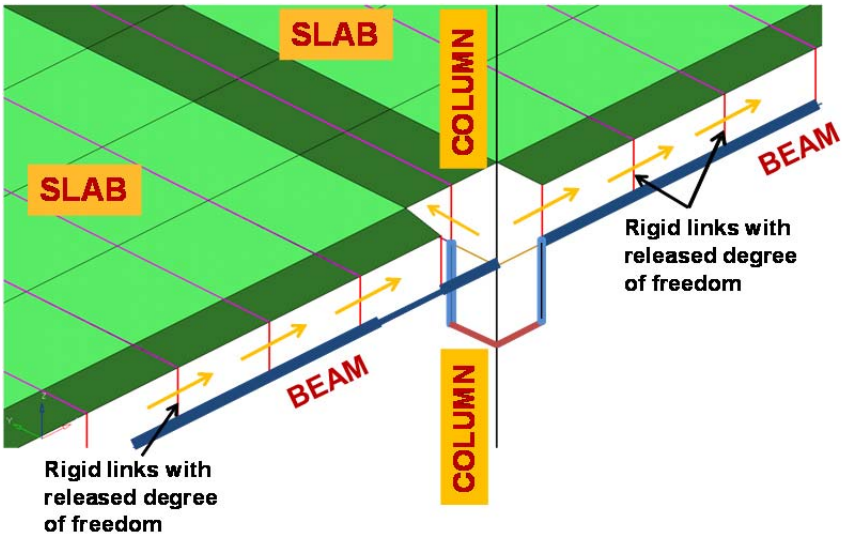

Figure 5 - 10 Model details of M2-NC

Table 5 – 5 shows comparisons between the deflection at the removed columns for models M2 and M2-NC. The table shows that there are substantial differences between the responses of the two models. For example, after loss of column C-D6-1, the vertical displacement of the node corresponding to the top of the removed column is 82 mm in M2 and 129 mm in M2-NC, a 57% increase. For C-E6-1, the deflection of model M2-NC is 40 mm, which is 38% greater than that in M2 (29 mm). In other words, when collapse is arrested, FCA will significantly reduce deflections compared to situations in which FCA is eliminated.

Table 5 - 5 Deflection at lost columns

Column-loss case	Overall deflection after column loss (steady state)	
	M2 (mm)	M2-NC (mm)
C-D6-1	82	129
C-E6-1	29	40
C-D6-1/C-E6-1	457/348	*Progressive Collapse*

When both C-D6-1/C-E6-1 are simultaneously removed, great differences are evident between M2 and M2-NC. Specifically, collapse is arrested in the former, but progressive

collapse occurs in the latter. Clearly, M2 is significantly damaged, as evinced by the large displacements; nevertheless, collapse does not propagate as it did in M2-NC. An interesting observation pertaining to M2 is that local slab damage around the column prevented force transfer between the slab and beam, which, in turn, prevented flexural composite action from being mobilized in the first floor beam B-DE6-1. However, FCA continues to be developed in beams in floors 2 through 10 (B-DE6-2 through B-DE6-10).

The above discussion suggests that FCA between the steel beam and slab can play an important role in resistance against collapse. To quantitatively investigate the contribution of composite action to collapse resistance, the amount of composite action mobilized when a column is removed is computed. The horizontal shear force V' transferred between a beam and slab is defined as:

$$V' = \sum_{i=1}^{N} V_i \qquad \text{(Equation 5 – 1)}$$

In Equation 5 – 1, V_i represents the shear force in a shear stud, computed by subtracting the axial forces in the two adjacent beam elements; N is the number of the shear studs in a the beam segment along which the stud shear forces are in the same direction. A factor, α, which represents the degree of utilization of composite action is defined as follows:

$$\alpha = \frac{V'}{\sum_{i=1}^{N} Q_i} \qquad \text{(Equation 5 – 2)}$$

where Q_i is the shear strength capacity of a shear connector. The number of shear studs and their spacing (assumed uniform) in the gravity bays are computed assuming that full composite action is provided. For convenience, the configuration of shear studs in moment beams is assumed identical to that used for gravity beams, although allowance is made for protected areas in which shear studs are not permitted (ANSI/AISC 358-10). The calculation of V' and V_i is shown in Figure 5 – 11 schematically.

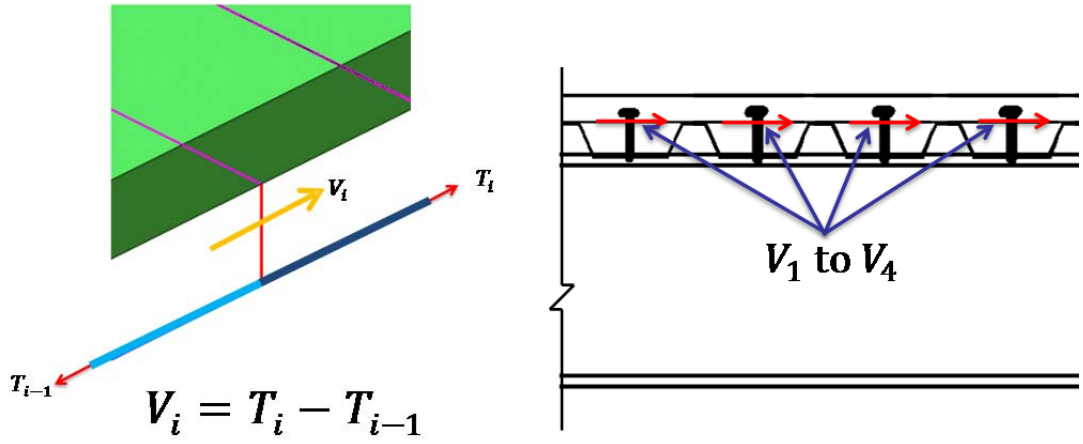

(a) Calculation of V_i (b) Calculation of V'

Figure 5 - 11 Calculation of V' and V_i

The values of the FCA factors are calculated for several column-loss cases including removal of (1) C-D6-1, (2) C-E6-1, (3) C-F5-1 which are peripheral exterior moment columns; and (4) C-E4-1, which is an interior moment column. The values of α before and after loss of the columns are then compared, as shown in Figure 5 – 12 to Figure 5 – 15. Only the sub-structure around the removed column is shown for convenience and clarity. In the first two cases, the removed columns belong to a moment bay which spans along column line 6 in the E-W direction, which is perpendicular to the flutes of the steel decks, whereas the columns which are removed in case 3 and case 4 are located in the moment bays in N-S direction, which is parallel to the flutes of the steel decks.

In case 1, before C-D6-1 is removed, the FCA factors of the gravity beams B-CD6 from the first floor to the top floor range from 10%-12%. The corresponding numbers range between 6%-8% for moment beams B-DE6, as shown in Figure 5 – 12(a). The FCA factors of the gravity beams are larger than those of moment beams, which is reasonable because gravity beams are smaller and are intended to mobilize composite action under service loads (DL + ¼ LL in this case). After loss of C-D6-1, the system drops 82 mm at the location of the removed column. Column loss causes α of the gravity beams to

increase slightly to about 12%-15% (Figure 5 – 12(b)). However, for the beams along the moment frame, α increases substantially as shown in Figure 5 – 12(b), reaching as high as 51%. The sharp increase in α along the moment beams, suggests that that those beams play a much larger role than the gravity beams in resisting collapse, which is expected given the weak shear connections attaching the gravity beams to the rest of the structural system.

In case 2 (removal of C-E6-1), since beams B-DE6 and B-EF6 are moment beams in the moment bays spanning columns C-D6, C-E6 and C-F6, the α factors for these beams are almost symmetric about columns C-E6 before and after column C-E6-1 is removed (Figure 5 – 13). The values of α in beams B-DE6 and B-EF6 increase from a range of 5% - 8% to a range of 9% (top floor) - 28% (bottom floor) after the column is removed, indicating composite action is indeed mobilized, but not heavily (Figure 5 – 13). The displacement is small (only 29 mm) indicating that the demand on the system is mild, which is expected given the high strength and stiffness of the structural members of the moment bay.

As in case 1, the α factors of the gravity beams in cases 3 (removal of C-F5-1) and 4 (removal of C-E4-1) are larger than those for the moment beams before loss of the column, as shown in Figure 5 – 14 and Figure 5 – 15, respectively. Before column loss, higher FCA factors occur in the gravity bay in case 4, which represents an interior case, than in case 3, which represents an exterior case, because the loads are higher on the intermediate system than on the edge one. In case 3, the maximum α factor for the gravity beams is 10% and in case 4, it is 20%, before column loss. The latter is larger than the former because it is associated with interior panels, where the beams carry more tributary area than in the external panels. After column loss, the moment bay for case 4 sees a sharp rise in α (up to 46%) as composite action is mobilized to support the load shed by the removed column (see Figure 5 – 15). In contrast, case 3 (edge situation) sees a more modest increase in α in the moment bays because the load demands are less.

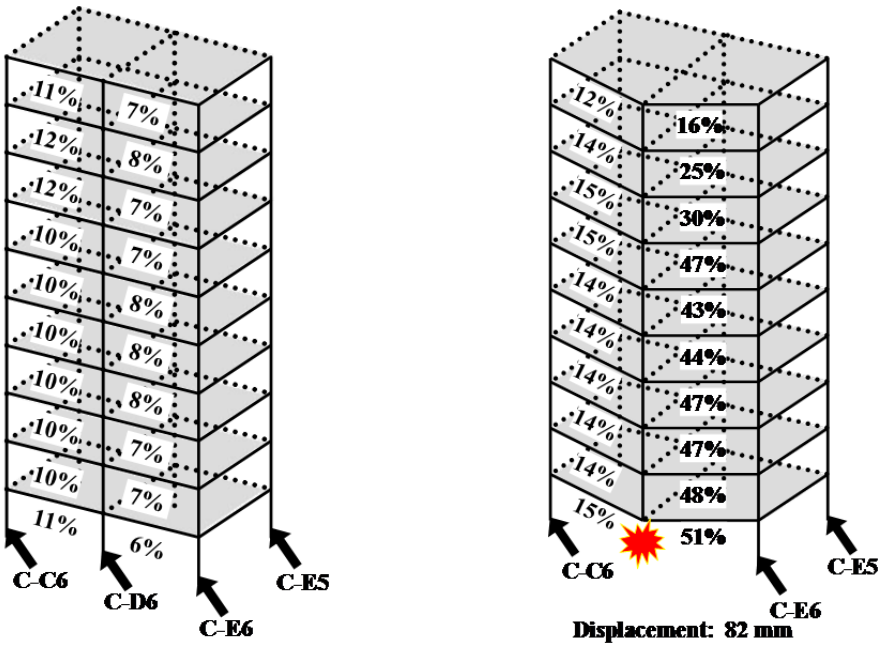

(a) Before removal of column (b) After removal of column

Figure 5 - 12 Composite action factor: removal of column D6

Further analysis of the results suggest that beams along the same axis spanning the removed column resist loads as a long beam instead of two adjacent beams, which generates compression in the slab around the removed column. If the column is removed by a blast, then the blast could also damage the slab, preventing it from carrying compression, thereby compromising the ability of the system to develop FCA.

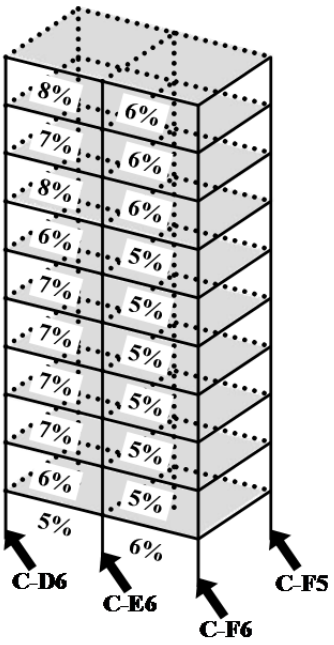

(a) Before removal of column

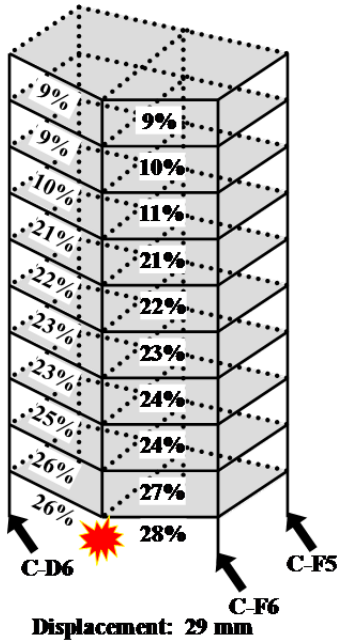

(b) After removal of column

Figure 5 - 13 Composite action factor: removal of column E6

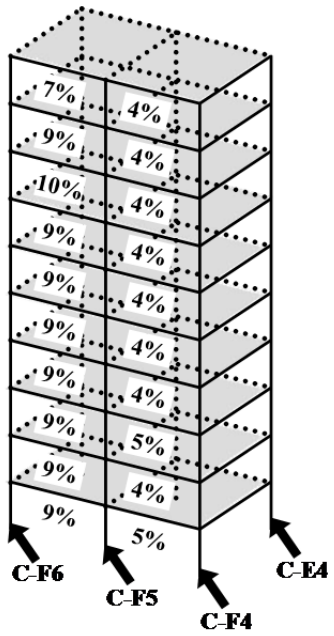

(a) Before removal of column

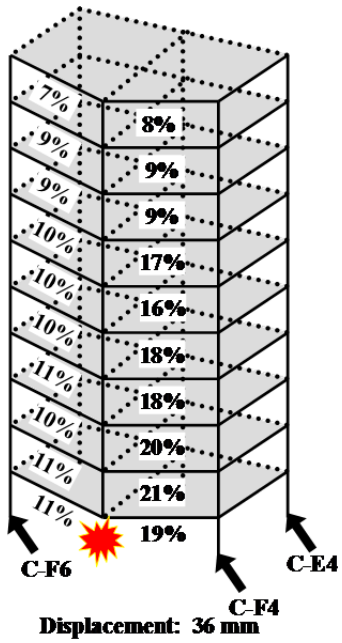

(b) After removal of column

Figure 5 - 14 Composite action factor: removal of column F5

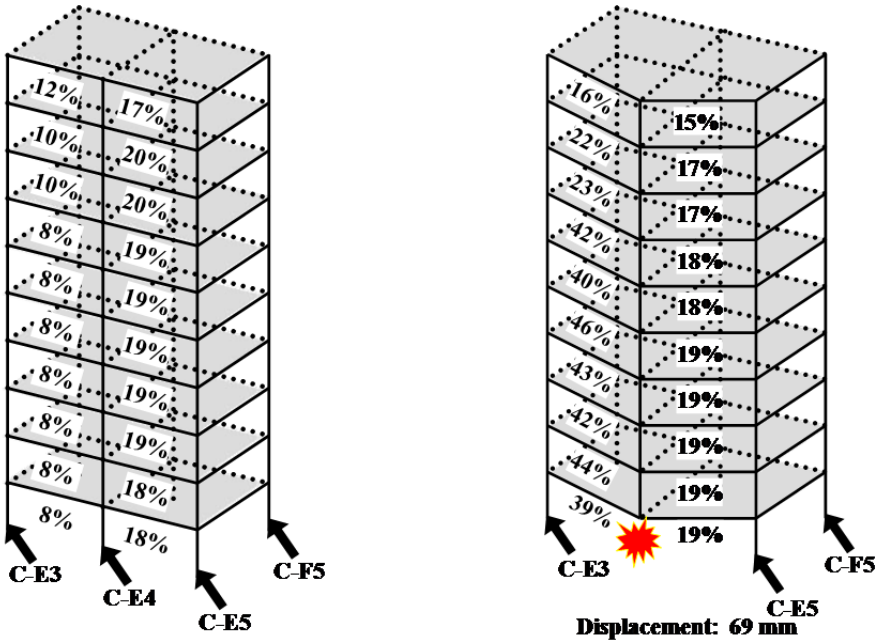

Before removal of column After removal of column

Figure 5 - 15 Composite action factor: removal of column E4

Simulations of scenarios involving removal of gravity columns such as C-E5-1 or C-D5-1 indicate that progressive collapse will occur in both models M2 and M2-NC - in spite of the presence of FCA in the former. For model M2, FCA in the beams is lost as local damage occurs in the slab or connections (because force cannot be transferred from the slab to the beam) as collapse progresses. This observation suggests that composite action may not be able to play a role in the final stages of collapse because of widespread slab damage at that stage of response.

To demonstrate the diminishing role of FCA at impending collapse for removal of column C-D5-1, consider Figure 5 – 16, which shows the evolution of various response parameters versus the load factor, β. The load factor is defined as

$$\beta = \frac{\text{Applied Loads}}{\text{Nominal gravity loads}} \qquad \text{(Equation 5 – 3)}$$

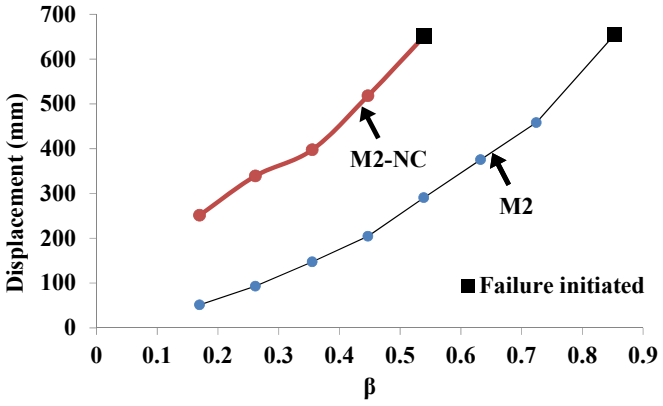

(a) Displacements at removed column

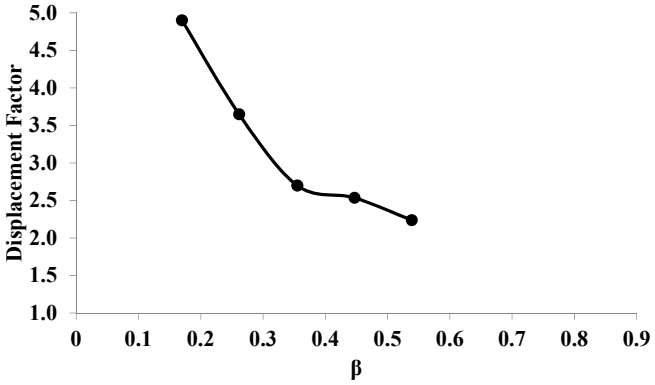

(b) Displacement factor

Figure 5 - 16 Results of incremental dynamic push down analysis: M2 vs. M2-NC subjected to loss of C-D5-1

Each point on the curves in Figure 5 – 16(a) represents a separate simulation in which the applied load is scaled by β i.e. an incremental dynamic analysis (IDA) as defined in Khandelwal and El-Tawil (2011). It has already been shown earlier that loss of C-D5-1 leads to progressive collapse. Therefore, the values of β used here are smaller than 1.0. Figure 5 – 16(a) shows that failure occurs in M2 and M2-NC after β reaches critical values of 0.86 and 0.54 in M2 and M2-NC, respectively. It is clear that the system is much weaker without composite action, in this case, 37% weaker. The benefit of FCA at lower load factors is evident in Figure 5 – 16(b), which plots the ratio of the displacement of M2-NC to M2 versus β. Clearly, FCA results in a much higher deflection in M2-NC compared to M2. However, as the load factor grows, this ratio decreases rapidly from 4.96 at β = 0.17 to 2.1 at β = 0.54, which suggests that the effects of composite action diminish as the system becomes more heavily loaded and approaches collapse.

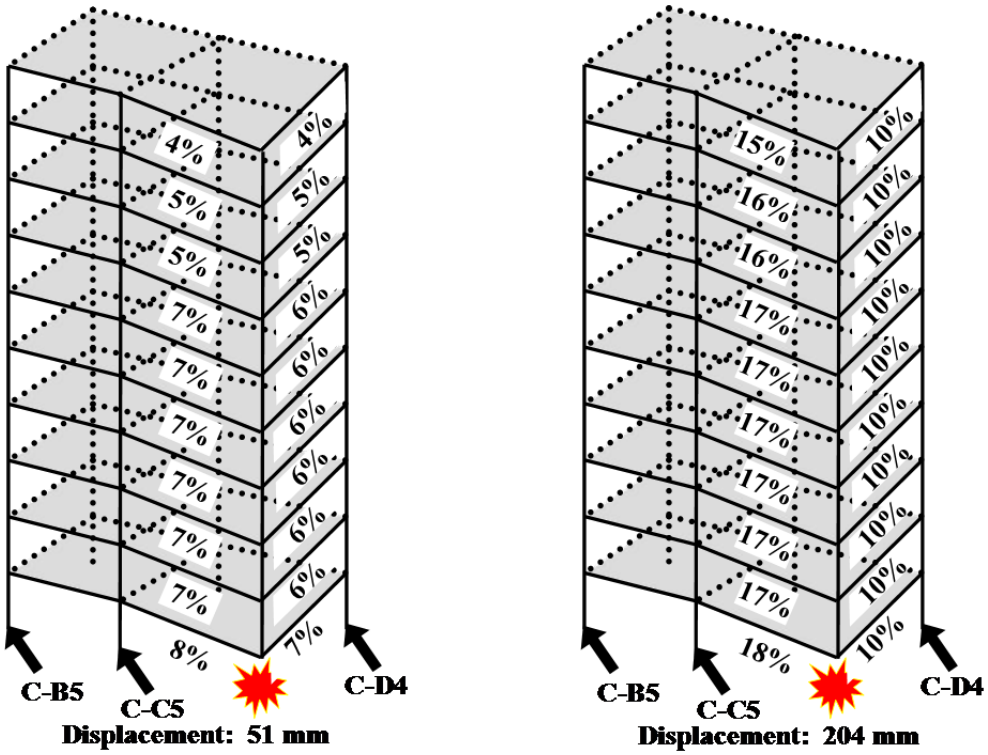

(a) β = 0.17

(b) β = 0.45

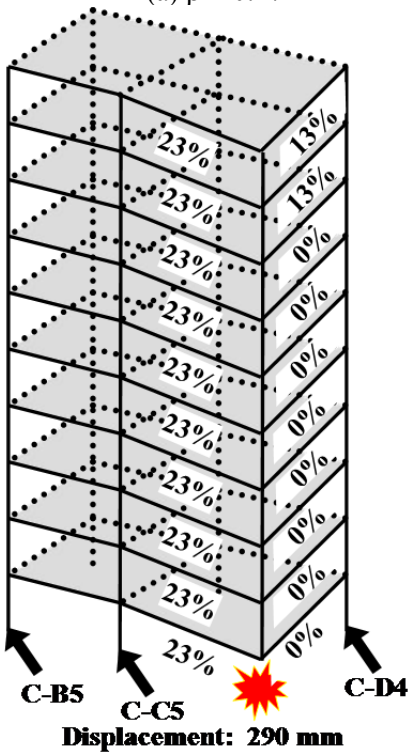

(c) β = 0.54

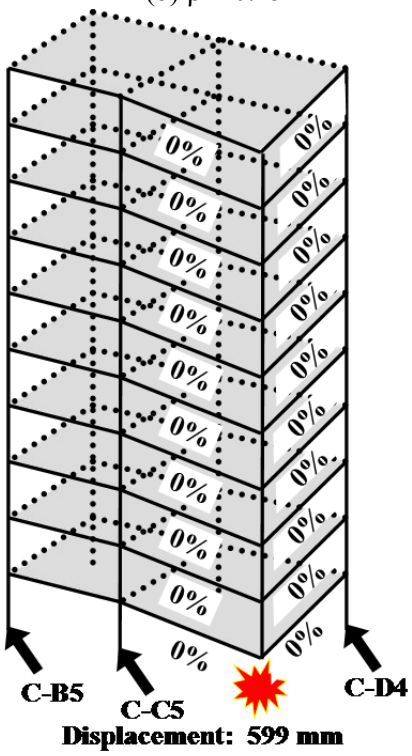

(d) β = 0.82

Figure 5 - 17 FCA factor: removal of C-D5-1 under various loading conditions

The α values are calculated for β = 0.17, β = 0.45, β = 0.54, and β = 0.82 and are shown in Figure 5 – 17. Because of the symmetry of the system, only the FCA factors in beams B-CD5 and B-D45 are shown. From the figure, it can be seen that when β = 0.17, α values are small, ranging from 4% to 8% in beams B-CD5 and 4% to 7% in beams B-D45 (Figure 5 – 17(a)). These values increase to 15% to 17% in beams B-CD5 and 10% in beams B-D45 when β = 0.45 (Figure 5 – 17(b)). When the load factor reaches 0.54, although the α factors in beams B-CD5 are still increasing, the α factors in beams B-D45-1 to B-D45-8 drop sharply to zero as slab damage occurs in the connection region and composite action is lost (Figure 5 – 17(c)). Composite action is completely eliminated in the slab panels surrounding the removed column when β = 0.82 (recall that failure occurs at β = 0.86), as shown in Figure 5 – 17(d). At this stage, collapse resistance is primarily provided by catenary action.

5.5 Role of Slab: Membrane Action

By comparing the responses of 2-D and 3-D models under the same column-loss scenarios, Alashker et al. (2011) argued that the slab plays an important role in determining structural responses under column-loss scenarios. In situations when failure was not imminent, they noted that the presence of the slab tended to create new load paths that mitigated the effect of sudden column loss. Alashker et al. (2010) pointed out that membrane action in the slab could also be detrimental to overall integrity of the system under certain conditions, e.g. destabilizing critical columns leading to buckling and additional progressive damage. This can be seen clearly in Figure 5 – 18. After loss of interior gravity column C-E5-1, failures start to propagate and the slabs pull column C-D6-1, C-E6-1, and C-F6-1 to bend inward and eventually buckle, leading to collapse of the collapse of bay CD, DE, and EF, after which the entire structure collapses.

Loss of column C-E5-10 is considered to demonstrate the influence of slab membrane action. The 10^{th} floor column is selected to eliminate the effect of any framing action from the structural members above. As previously discussed in Chapter 4 and the

previous sections, although major collapse occurs when the corresponding columns at the 5th and 1st floors are removed, the structure survives this case because roof loads are smaller than regular floor loads by 13%. The tensile forces per unit width developed in the slab panels surrounding the removed column are shown in Figure 5 – 19. The figure shows that large membrane forces develop in the NS direction, which is parallel to the direction of the flutes of the steel decks. On the other hand, much smaller forces develop in E-W direction. These results are in accord with Alashker et al. (2010). In this case, the development of membrane action and successful anchorage to the compression ring prevents complete collapse of the floor.

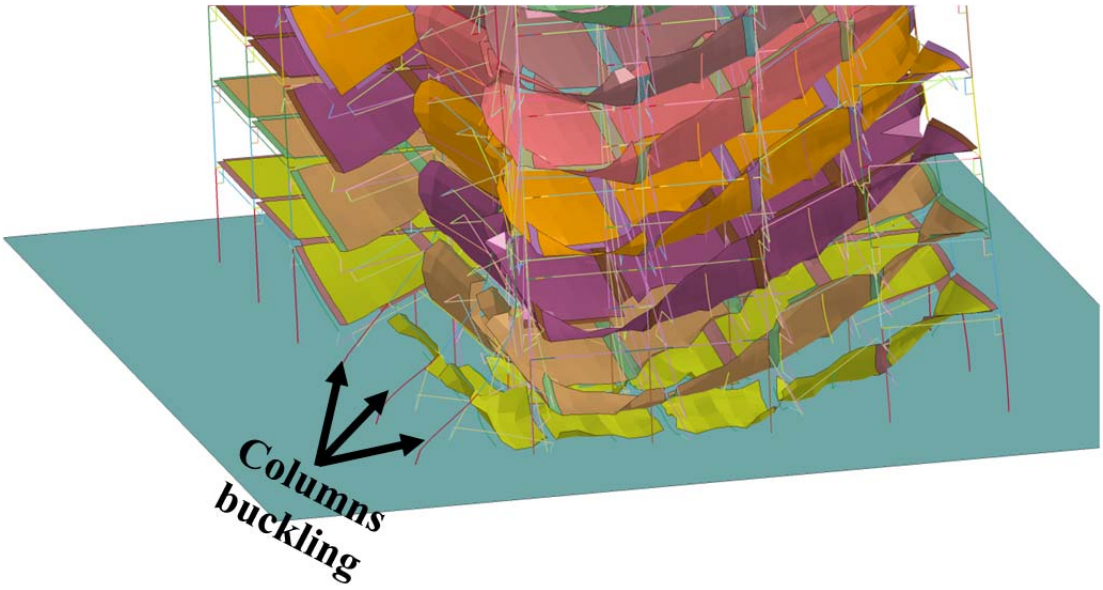

Figure 5 - 18 Bucking of column C-D6-1, C-E6-1, and C-F6-1 after loss of column C-E5-1

The simulations conducted in this study suggest that the tensile strength of the slab, attributed to the steel deck and reinforcing mesh, plays a key role in determining the robustness of the structure. To illustrate this point, a series of IDAs are performed using model M2 and M2-RT-X, where RT denotes reduced slab tensile strength and X represents the fraction of the tensile strength available. For example, M2-RT-20% indicates the tensile strength of the slab in this model is only 20% of the nominal one.

The responses of models M2, M2-RT-20%, M2-RT-40%, M2-RT-60% and M2-RT-80% under various loading conditions for removal of column C-D5-1 are compared to the full model results in Figure 5 – 20.

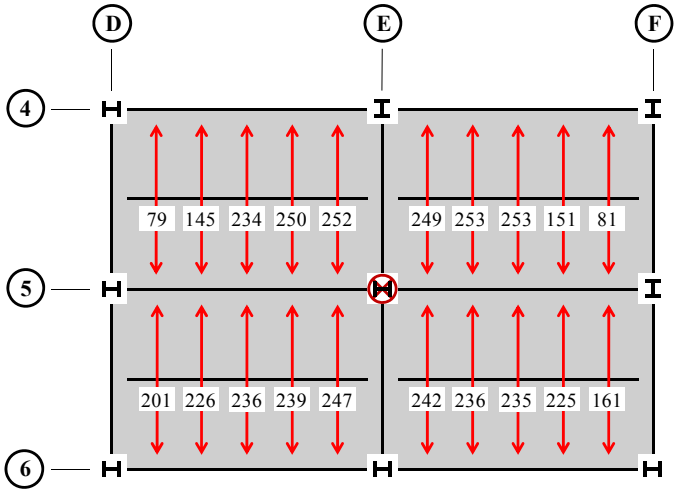

(a) Slab tensile force: N-S direction

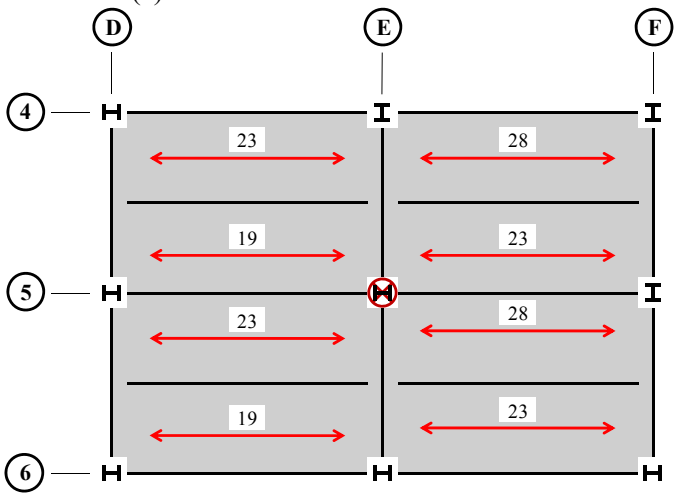

(b) Slab tensile force: E-W direction

Figure 5 - 19 Tensile forces in the slab (kN/m): removal of C-E5-10

Figure 5 – 20(a) illustrates the displacement at the removed column obtained from the suite of M2-RT models as β increases. Figure 5 – 20(b) shows the ratio of the displacement at the removed column as computed from M2-RT models versus the

original M2 model (termed displacement factor in Figure 5 – 20(b)). It is clear from Figure 5 – 20 that when the value of β is small (less than 0.35), the displacements captured by M2 and the various M2-RT models are close to each other. This suggests that the collapse resistance at this stage is primarily provided by flexural action in the beams and slabs and composite action between them. However, as β increases, larger displacements occur in the models with lower slab strength compared to M2. This is attributed to an increase in membrane action mobilization as the structure approaches collapse.

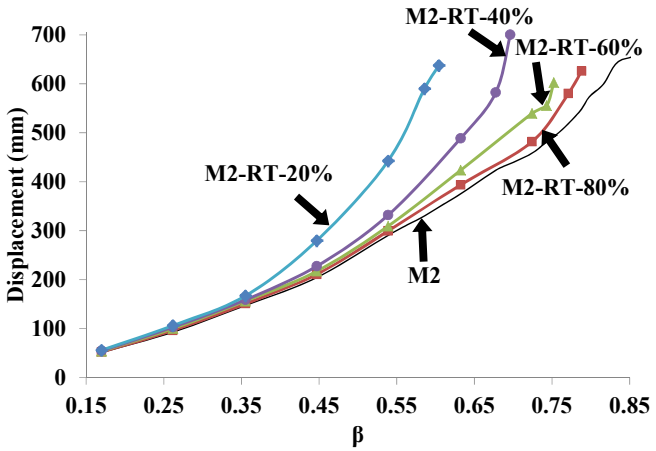

(a) Comparisons of displacements

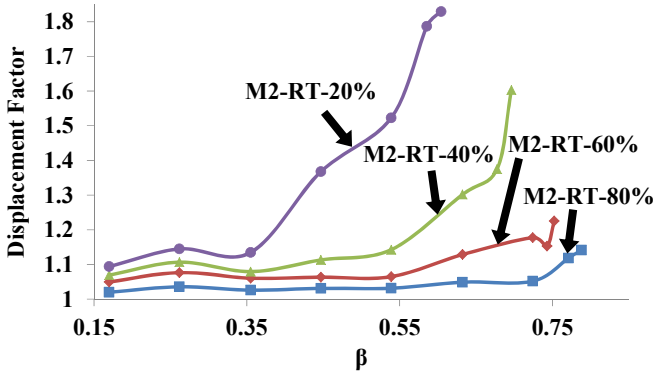

(b) Comparisons of displacement ratios

Figure 5 - 20 Comparison between the responses of Models M2 and M2-RT

Section 5.4 has shown that FCA will likely not play a role in the final stages of collapse in large deformation situations. From a series push-down analysis, it can be observed that

the final mechanism that contributes to the collapse resistance is the slab membrane action. In Figure 5 – 21, it can be observed that the load factor at failure β_{FL} is proportional to the fraction of the tensile strength available. Since in all of these analyzes, the structure collapses at almost the same displacement (around 700 mm), the tensile strength of the floor slab will decide how much load the structure can actually support. The relationship between β_{FL} and the D_{RT} can be generalized as the following equation for the particular structure under study:

$$\beta_{FL} = 0.30D_{RT} + 0.57 \quad \text{(Equation 5 – 4)}$$

where D_{RT} is represent the fraction of the tensile strength available.

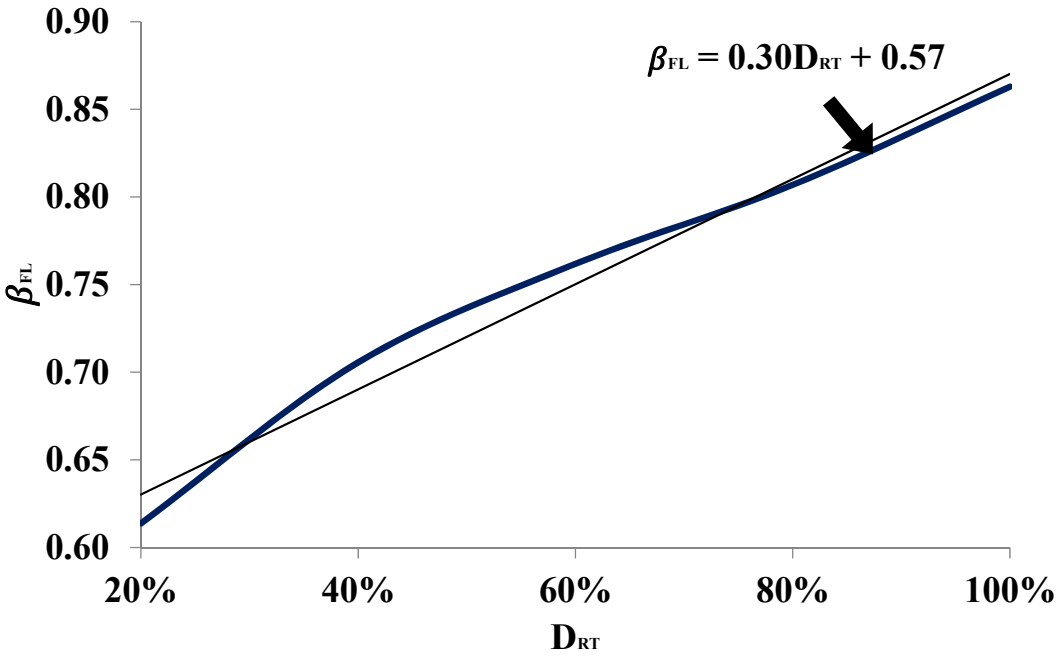

Figure 5 - 21 Relationship between D_{RT} and β_{FL}

The results described above quantify and confirm that the role of composite action in resisting progressive collapse is to reduce the deformation in the earlier stages of loading and the role of membrane action is to carry the gravity loads in the final stages of collapse. This trend can be clearly observed in Figure 5 – 22, which plots the displacement factors (ratio of displacement obtained from M2 to that computed from M2-NC or M2-RT) when column C-D5-1 is deleted.

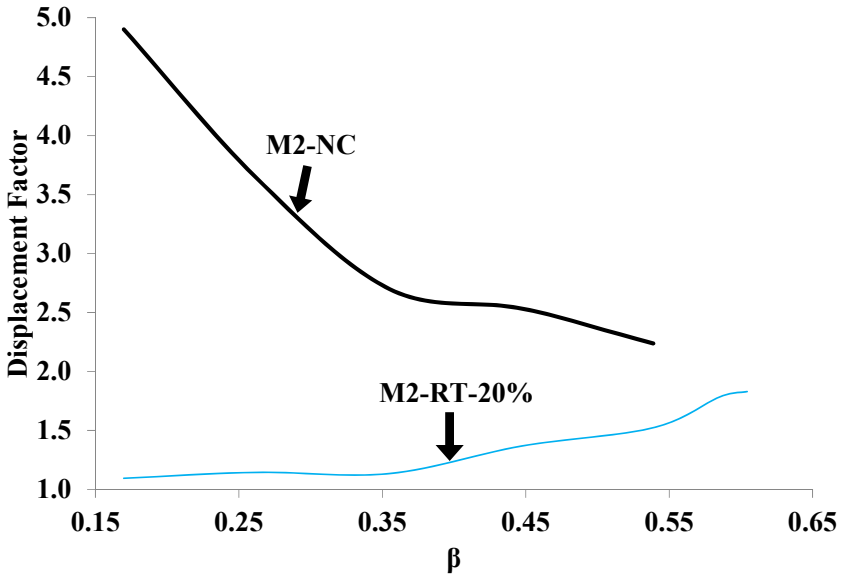

Figure 5 - 22 Comparisons of displacement factor for M2-NC and M2-RT-20% under various loading states

5.6 Frame Action in Moment-Resisting System

The previous sections discussed the role of flexural composite action and membrane action in resisting progressive collapse under column loss scenarios. In the vicinity of the moment bays, another key source of resistance to progressive collapse under column loss scenario is frame action. Frame action is defined as the resistance to collapse attributed to the moment frame system above the removed column.

Since frame action will also mobilize FCA and floor catenary action during the various stages of collapse, planar Model M4 is used to focus attention on only frame action and isolate its contribution in this study. An incremental push down analysis, similar to that discussed in Section 5.4 and Section 5.5, is performed for removal of C-E6-1. Figure 5 – 23 shows the distribution of axial forces developed in the beams in bays DE and EF after column loss when $\beta = 1.0$, $\beta = 1.5$, $\beta = 2.0$, $\beta = 2.5$ and $\beta = 2.9$. A positive sign means the beam is under tension and a negative sign means the beam is under compression.

Under normal loading conditions ($\beta = 1.0$), as shown in Figure 5 – 23(a), the axial forces in the beams B-DE6-1 and B-EF6-1 are 71 kN and 75 kN, respectively. The axial forces in beams B-DE6-2 to beams B-DE6-6 and B-EF6-2 to B-EF6-6 are small compared to the ones in the first floor beams, ranging from only -7 kN to 8 kN. The sign of the axial forces in the beams changes at the 7th floor. The axial forces in the beams B-DE6-7 and B-EF6-7 are -53 kN and -52 kN, respectively. The beams in the 9th and top floor are also in compression. The distribution of the axial forces is reminiscent of the normal stress distribution along the cross-section in a deep beam subjected to positive bending moment, indicating that bay DE and bay EF acts somewhat like a deep beam spanning the two bays and bridging over the removed column.

In the first three cases, the vertical displacements are 36 mm, 74 mm, and 166 mm, respectively. The deformations in all of these cases are not large enough to signify mobilization of substantial catenary action. In these situations, frame action is accomplished through Vierendeel action, i.e. the loads are resisted by flexural action in the main frame members.

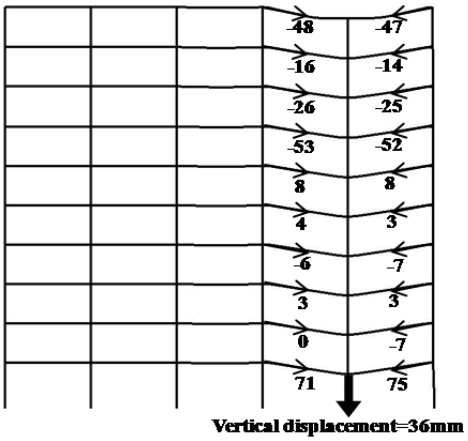

(a) $\beta = 1.0$

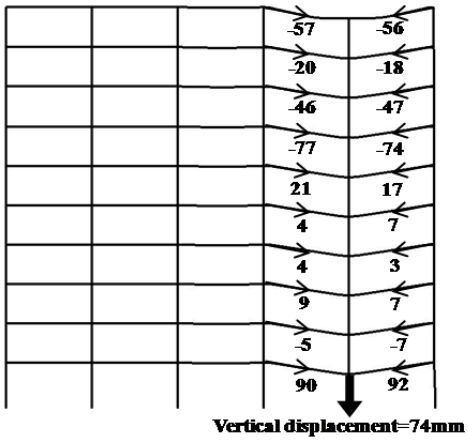

(b) $\beta = 1.5$

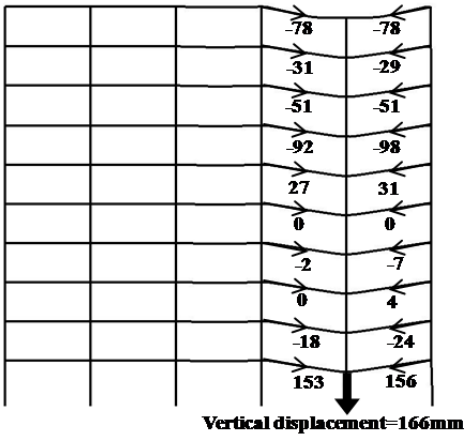

(c) $\beta = 2.0$

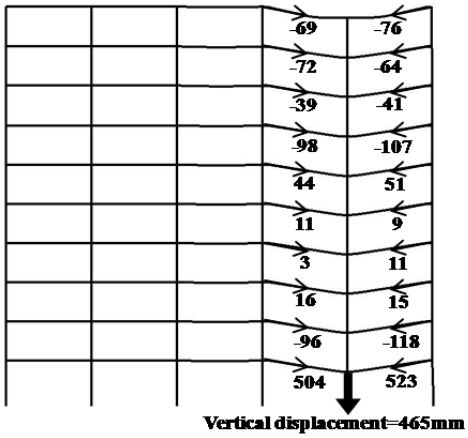

(d) $\beta = 2.5$

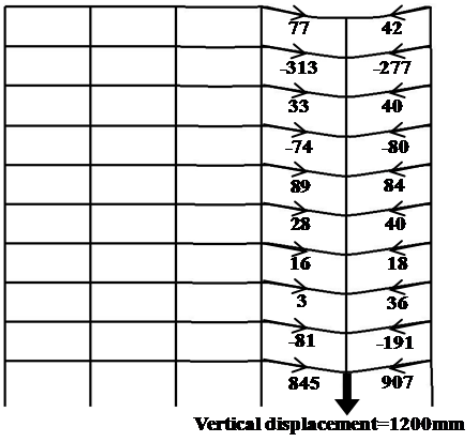

(e) $\beta = 2.9$

Figure 5 - 23 Axial forces in the beams: removal of C-E6-1 (M4)

The highest load cases, where $\beta = 2.5$ and $\beta = 2.9$, represents response close to and at impeding collapse, respectively. The displacement of the node corresponding to the top

of the removed column is 465 mm and 1200 mm, respectively and the plastic rotations in all beams are very high, in excess of 0.07 radians in the latter case, which is considered a threshold value for triggering catenary action (Hamburger et al 2004). Under such large overall deformation, flexural action in the beams cannot be the reason the frame is supporting the applied load. Moreover, there are large compression forces in some beams in the upper levels and tension in some beams at the lower levels, again reminiscent of deep beam action. Clearly, the resistance mechanism is now different from what was mobilized at lower loads, i.e. a combination of axial forces in the beams and flexure in the columns.

5.7 Summary and Conclusions

In this chapter, the inelastic collapse response of the prototype building is investigated using planar and 3-D nonlinear models with the objective of identifying the sources of collapse resistance and quantifying 3-D effects. System responses for 5^{th} and 10^{th} floor column removals were first presented and discussed. Parametric studies were conducted to provide insight into the contributions of composite action between steel beams and composite floor system, slab membrane action, and system frame action.

Simulations with column loss at various floors suggest that the building can be more vulnerable to loss of columns in the upper stories than in the lower ones. This result stems from the fact that column loss in lower floors mobilizes more of the structure above it to survive than column loss in upper floors. Debris resulting from column loss in higher floors can also be very damaging and was observed to precipitate progressive collapse. The current concern by many researchers regarding first floor columns is understandable given the threat of vehicle bombs. However, the substantial reduction in column size in upper floors makes these columns vulnerable to suitcase or backpack bombs and therefore they should be routinely considered in vulnerability assessment.

Composite action between the slab and the underlying steel beams was found to be particularly influential. It was shown to reduce deflections when collapse was not imminent and even warded off progressive collapse in one situation that would have led to collapse had composite action not been mobilized. However, it was also shown that composite action can be lost in the final stages of collapse as the slab is damaged due to large deformation demands. Under such conditions, membrane action takes over and becomes a dominant player in the final stages of collapse. However, the simulations conducted herein suggest that membrane action is a double edged sword. It can help increase the resistance of the building to collapse, but once a threshold is exceeded and the building continues to collapse, membrane action can help promote progressive collapse by pulling on and damaging other components of the structure. Design for collapse accounting for membrane action therefore becomes a balancing act, weighing the potential benefits of membrane action on one hand, and its detrimental effects on the other.

CHAPTER 6

ASSESSMENT OF DESIGN REQUIREMENTS IN DOD GUIDELINES

6.1 Introduction

The most comprehensive design requirements in the US addressing progressive collapse in new and existing buildings can be found in the Unified Facilities Criteria (UFC 2009) published by the US Department of Defense (DoD guidelines). One of the techniques permitted for designing against collapse is the Tie Force Method (TFM). This is an indirect technique, permitted under certain occupancy conditions, in which structural robustness is assured by promoting structural continuity, ductility, and structural redundancy. Robustness is achieved by specifying the minimum amount of tensile forces and their locations that must be provided to 'tie' the structure together. Another concept promoted by the provisions is the dynamic impact factor (DIF), which is used to predict the dynamic behavior of a building by simply magnifying its corresponding static response by DIF. The TFM procedures traces its origins to British engineers involved in the 1968 Ronan Point incident, while the DIF provisions were recently proposed by Ruth et al. (2006). Both sets of provisions have yet to be thoroughly evaluated using fully 3-D models, which is the objective of this Chapter

The prototypes structures that are used in this study are first introduced in Section 6.2 and modeled in Section 6.3. General information about TFM is provided in Section 6.4 and

the TFM provisions are evaluated through case studies in Section 6.5. DIF provisions are assessed in Section 6.6 and a newly proposed energy-based approach for assessing peak dynamic displacement is proposed in Section 6.7. The accuracy of the new method is evaluated and its applicability in a design office environment is discussed. The Chapter is summarized in Section 6.8 and some conclusions are drawn from the presented data.

6.2 Prototype Structures

6.2.1 General Information

Three additional prototype structures are used in this Chapter besides the NIST building described in Chapter 3 to ensure that the analytical results obtained herein are generally applicable. The prototypes are selected so that they cover different structural layouts, types of connections, and heights. The three buildings are selected from the SAC model buildings in FEMA-355C (FEMA, 2000), which were designed for the purpose of investigating the seismic performance of moment-resisting frame structures. They were designed for the Boston area using pre-Northridge connection configurations. This set of buildings consists of a three-story, a nine-story and a twenty-story building and are designated as SAC-3, SAC-9, and SAC-20, respectively. These configurations are chosen because they represent typical steel framed office buildings designed for low-seismic risk, to contrast with the NIST building, which represents common steel framed office buildings designed for high seismic risk.

Design details of the three new buildings can be found in Foley et al. (2007) and Hoffman (2010), but are repeated here for completeness. The structural systems of these three buildings are comprised of moment frames and a gravity system. Like the NIST building, these buildings utilize moment resisting frames as the primary lateral load resisting system and simple shear connections are used in the gravity system. However, standard beam-to-column welded connections are used in these buildings, unlike the NIST building, in which reduced beam sections were used in the moment frames.

A composite floor is used for the floor system, comprised of a 3" thick RC slab sitting on a 2" tall 19 gauge steel deck. The composite floor is connected to the underlying steel beams using shear studs and 6x6-W1.4x1.4 welded wire mesh reinforcement is used in the RC slab. Concrete compressive strength f_c' is taken as 4,000 ksi, the modulus of elasticity $E_c = 4{,}000$ ksi, and Poisson's ratio $\nu = 0.15$. The structural steel used for all beams and columns is A992 ($F_y = 50$ ksi).

The floors are assumed to carry a total dead load of 83 psf, including the loads from the decks, slab and additional flooring/ceiling loads, mechanical, electrical and plumbing, and partitions. The design live load is assumed to be 50 psf. While the roof carries a total dead load of 63 psf and the design live load is also 50 psf. In the original design, each of these three buildings has a penthouse on the roof level, which may result in higher local loads. However, these loads are neglected in this study to avoid discontinuities in loading as done in Hoffman (2010).

6.4.2 Three-story Building (SAC-3)

The three-story building (SAC-3) has a plan dimension of 180' × 120". The building spans six bays in East-West direction and four bays in North-South direction. The total height of the building is 39'. The moment connections are indicated by little triangles at the beam ends. Beams in the gravity system are connected to the columns through shear connections that are composed of single-plate, shear tab connection that are filet welded to the column and bolted using three 7/8", A325 high-strength bolts to 3/8" A36 shear tabs. The floor plan and the size of the gravity beams are shown in Figure 6 – 1. It can be seen that the moment frames are all placed on the perimeter of the structure. The elevation view of the frame on column line A and the frame on column line 5 are shown in Figure 6 – 2. The size of the moment beams are also shown in this figure. Figure 6 – 3 presents the column schedule of the three-story building and the size of the columns is also shown in this figure.

6.4.3 Nine-story Building (SAC-9)

The nine-story building (SAC-9) has a plan dimension of 150’ × 150”. The building has five bays in both East-West direction and North-South direction. The total height of the building is 122’. The shear connections used in the gravity system of SAC-3 are used in this building as well. The floor plan and the size of the gravity beams are shown in Figure 6 – 4. It can be seen that the moment frames are all placed on the perimeter of the structure and are identical on all four sides. The elevation view of the frame on column line A and the frame on column line 5 are shown in Figure 6 – 5. The size of the moment beams are also shown in this figure. Figure 6 – 6 presents the column schedule of the nine-story building and the size of the columns is also shown in this figure.

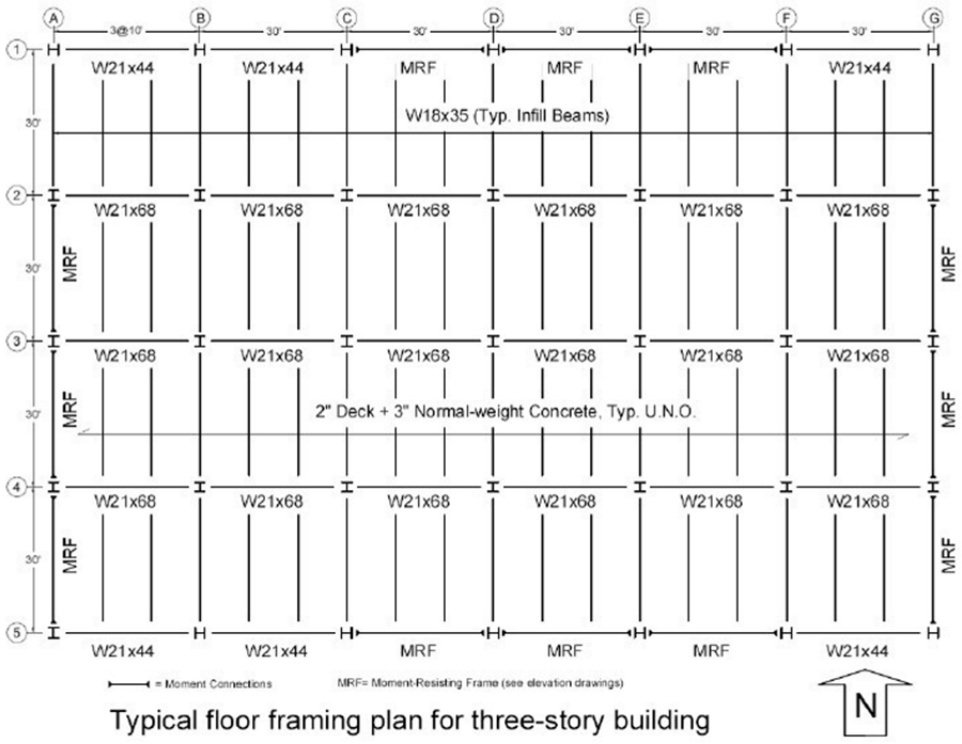

Figure 6 - 1 SAC-3: plan view (Hoffman, 2010)

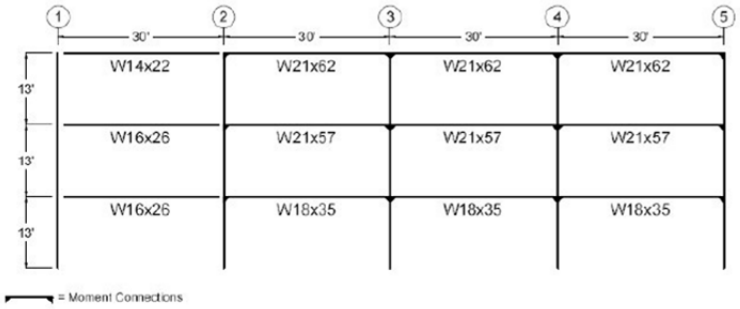

Perimeter frame along columns lines A and G looking East

(g) Elevation view: N-S

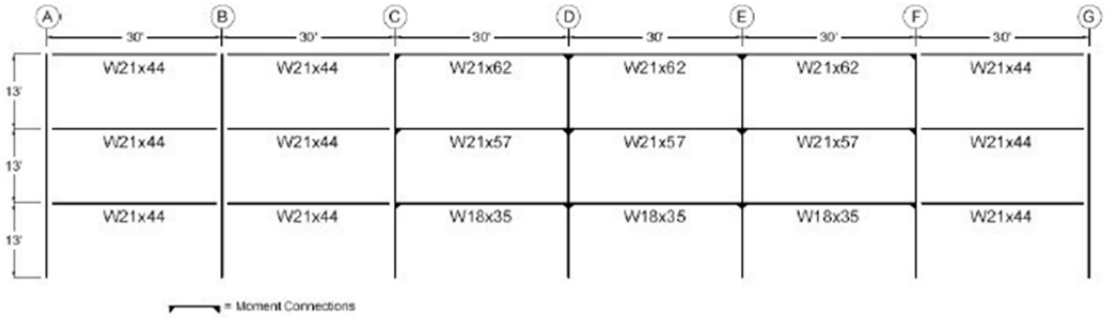

Perimeter frame along columns lines 1 and 5 looking North

(h) Elevation view: E-W

Figure 6 - 2 SAC-3: elevation view

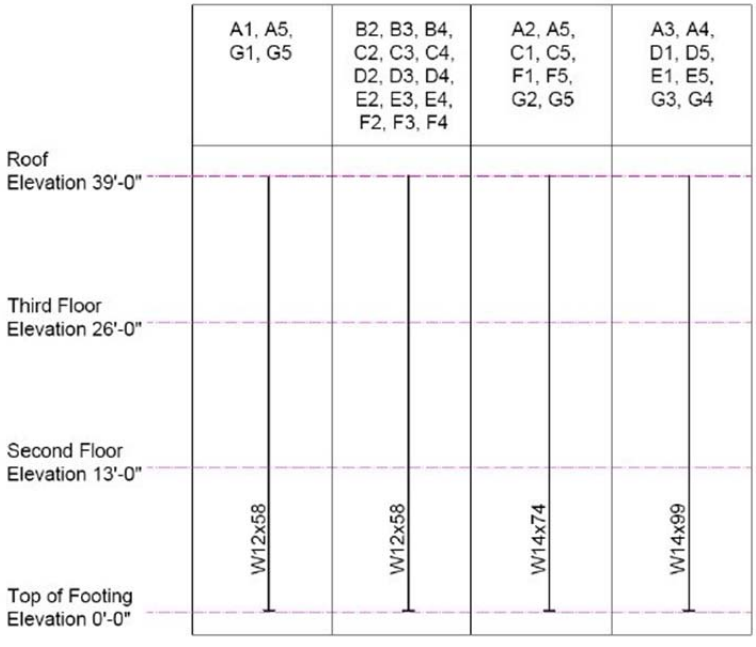

Figure 6 - 3 SAC-3: column schedule

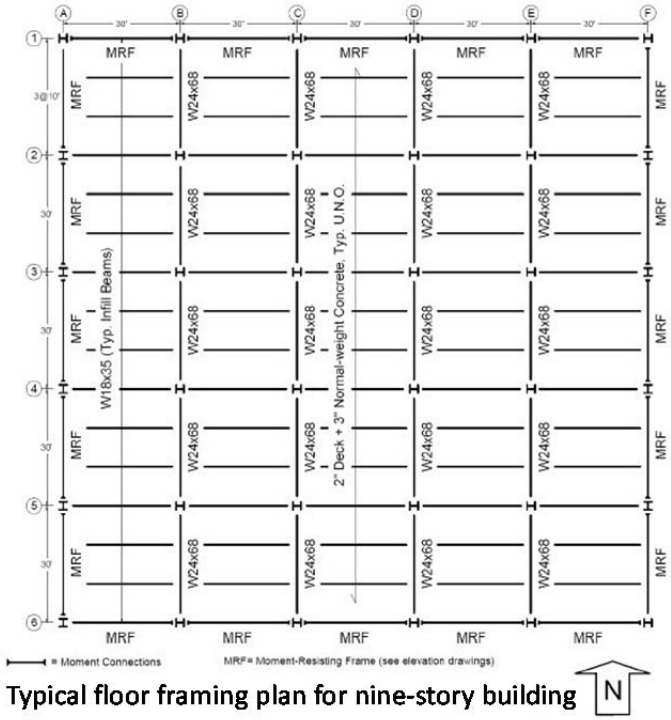

Figure 6 - 4 SAC-9: plan view

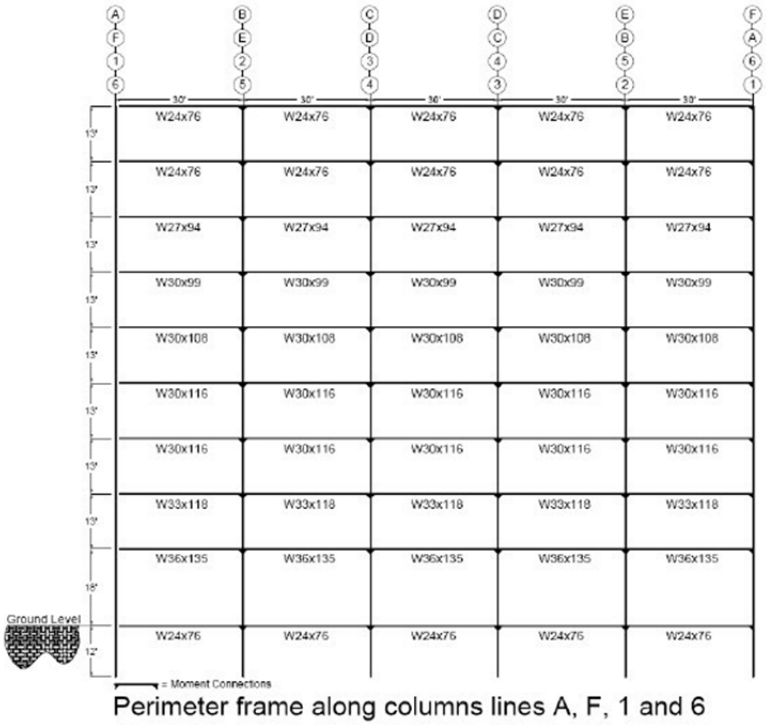

Figure 6 - 5 SAC-9: Elevation view

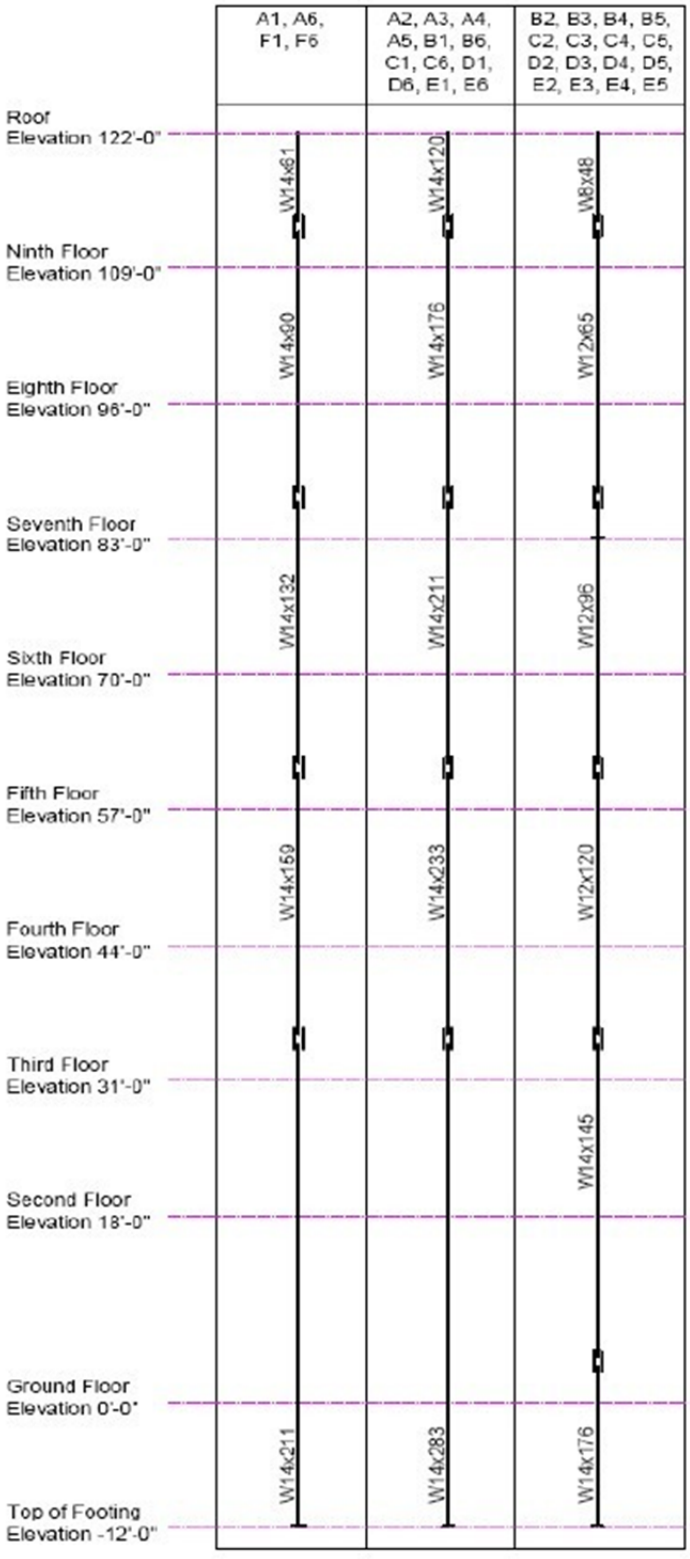

Figure 6 - 6 SAC-9: Column schedule

6.4.4 Twenty-story Building (SAC-20)

The twenty-story building (SAC-20) has a plan dimension of 100’ × 120’. The building has five bays in both East-West direction and North-South direction. The total height of the building is 249’. The shear connections used in this building are the same as those used in SAC-3 and SAC-9 in East-West direction of the gravity system. However, an additional bolt is added to the shear connections in the gravity beams in North-South direction since these beams span longer distances and carry more loads. The floor plan and the size of the gravity beams are shown in Figure 6 – 7. The size of moment beams is listed in Table 6 – 1. It can be seen that the moment frames are all placed on the perimeter of the structure. The column schedule of the nine-story building and the size of the columns is also shown in this Figure 6 – 8.

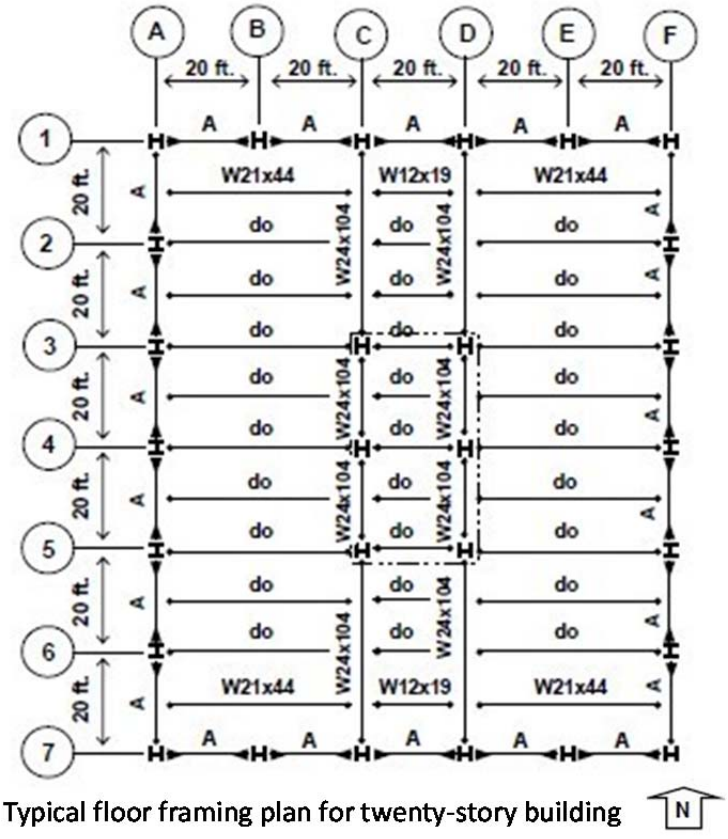

Figure 6 - 7 SAC-20: Plan view

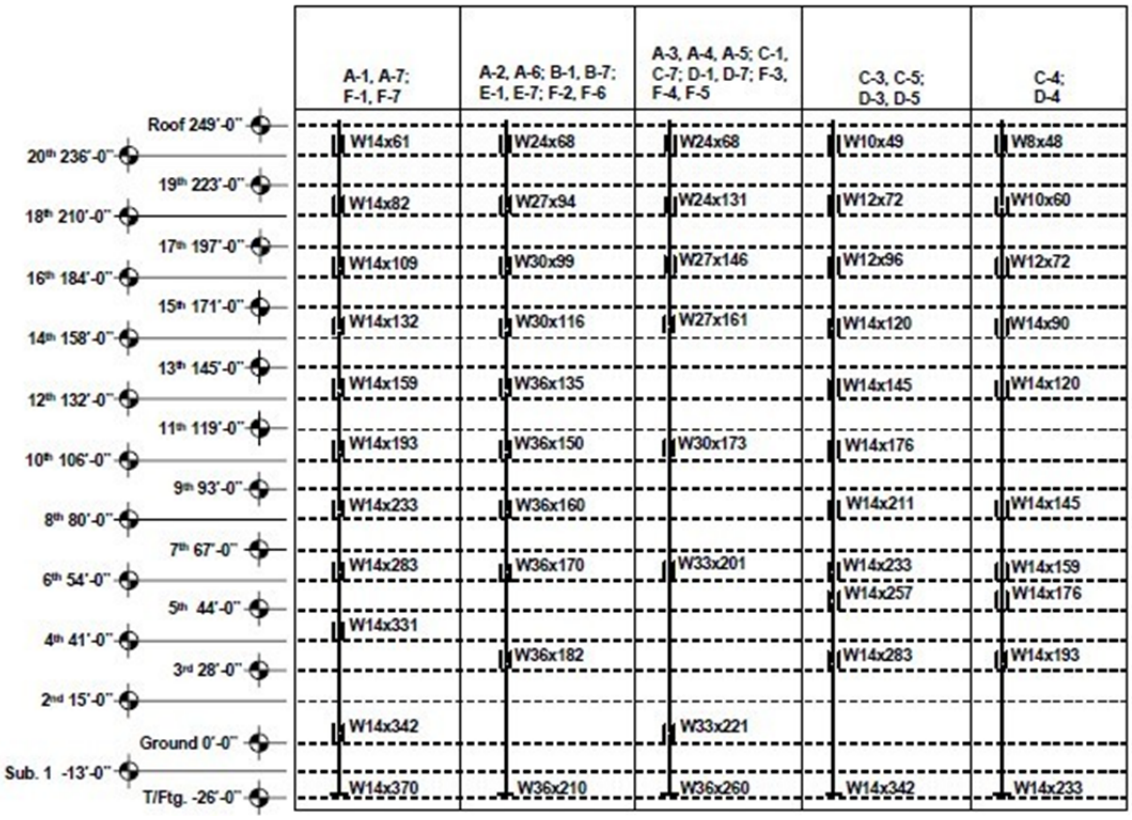

Figure 6 - 8 SAC-20: column schedule

Table 6 - 1 Size of moment beams of the twenty-story building

Floor range	Section
1 – 6	W36x150
7 – 8	W36x135
9 – 11	W33x130
12 – 13	W33x118
14	W30x116
15	W30x108
16	W30x99
17	W27x94
18	W27x84
19	W24x68
20	W18x35

6.3 Modeling Approaches

Model M2 which is described in Chapter 3 is used in this chapter to represent the structural system of the NIST building. In order to evaluate the performance of the SAC buildings under column loss scenarios, macro-based, three-dimensional models are developed for SAC-3, SAC-9, and SAC-20 using the same modeling approaches used for M2. These models are designated as M2-SAC-3, M2-SAC-9, and M2-SAC-20, respectively. These models are shown in Figure 6-9. Like M2, both material and geometric nonlinearities are accounted for in the three SAC models. The beams and columns are represented using a Hughes-Liu beam-column element formulation. The shear tab is modeled by a single beam element, which has integration points that correspond to the location of individual bolts. The floor slab is modeled using fully integrated four-node isotropic shell elements with an equivalent section shell thickness of 3.5". The floor slab is connected to the underlying steel beams using rigid links. The steel deck is modeled using truss elements attached directly to the shell elements in the direction of the flutes. Like M2, the centerlines of the gravity and moment bay beams are located at the same level to eliminate the small elements introduced by the differentials between the centerlines of the gravity and moment bay beams, to increase the time step and reduce running time.

The Alternate Path Method (APM) is used in the dynamic analyses and the naming scheme of the structural components discussed in Chapter 4 is employed in this Chapter.

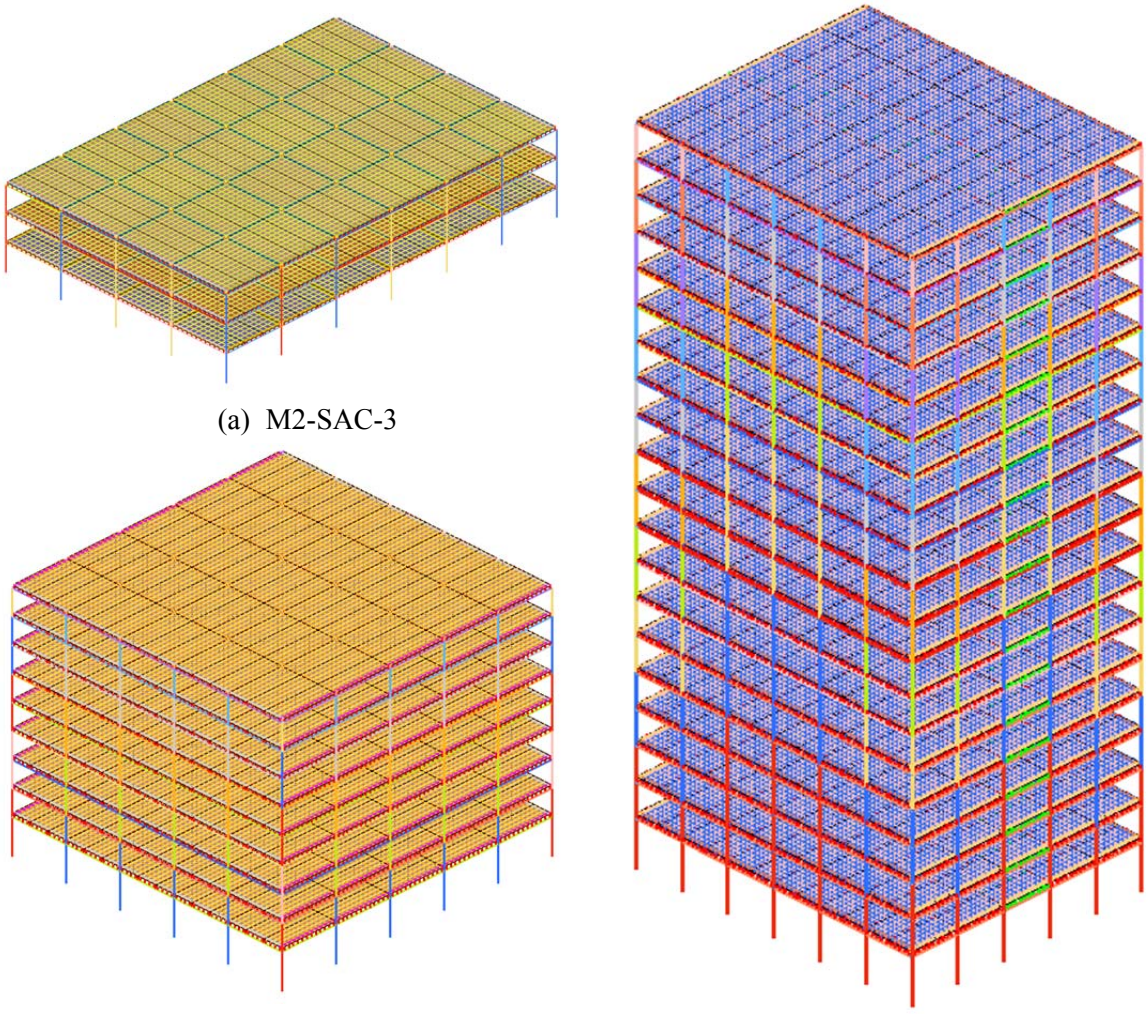

(a) M2-SAC-3

(b) M2-SAC-9

(c) M2-SAC-20

Figure 6 - 9 Details of full 3-D models for SAC-3, SAC-9, and SAC-20

6.4 Tie Force Method (TFM): General Information

Tie force method is an indirect design approach advocated by the DoD guidelines with the objective of "*enhancing continuity, ductility, and development of alternate load paths*" (UFC, 2009). There are two types of ties: horizontal ties and vertical ties, and both can be proportioned using methods provided in the DoD guidelines. According to the DoD guidelines, there are three types of horizontal ties that must be provided by the structural system: longitudinal, transverse, and peripheral. For framed structures, the floor and roof

system should carry the required longitudinal, transverse, and peripheral ties if the beams, girders and spandrels cannot be proven capable of carrying the tie force while undergoing a 0.20-rad rotation.

The required tie strength F_i in the longitudinal or transverse direction is

$$F_i = 3W_F L_1 \quad \text{(Equation 6 – 1)}$$

Where

$W_F = 1.2D + 0.5L$ is the uniform floor load

L_1 = greater of the distances between the centers of the columns, frames, or walls supporting any two adjacent floor spaces in the direction under consideration.

The origin of the above equation is simple. The beams or floor system bridging two spans with span length of L can be modeled as a simply supported beam subjected to uniformly distributed load w, as shown in Figure 6 – 10. After loss of the middle support, simulating the column loss scenario, the deformed shape of the system can be modeled as a parabola, as shown in Figure 6-11.

Assume that the middle support drops 10% of the combined span (i.e. 0.1 x 2L = 0.2L) and that the origin of the coordinate system is located at the middle of the two-span beam. The equation used to describe the deformed shape is therefore:

$$Y = \frac{0.2}{L} X^2 \quad \text{(Equation 6 – 2)}$$

Where

Y is the deformation of the system at a certain point

X is the distance between the point and the middle support

Differentiating Equation 6-2, the slope of the deformed shape is

$$\frac{dY}{dX} = \frac{0.4}{L}X \qquad \text{(Equation 6 – 3)}$$

Therefore, at the end support, the slope is 0.4 and the tie forces are

$$F_T = \frac{wL}{0.4} = 2.5wL \qquad \text{(Equation 6 – 4)}$$

The coefficient of 2.5 in Equation 6-4 is rounded up to 3.0 in the UFC criteria (DoD 2009).

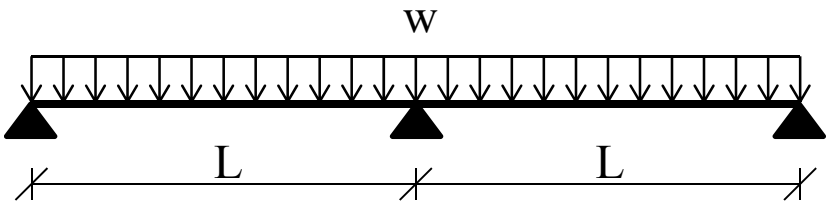

Figure 6 - 10 Two span beams before loss of the middle support

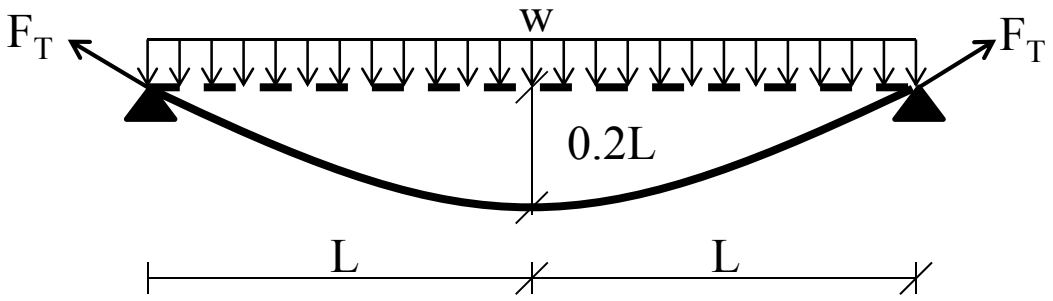

Figure 6 - 11 Two span beams after loss of the middle support

In order to "*provide adequate development or anchors at corners, re-entrant corners or changes of construction*" (UFC, 2009), peripheral ties have to be placed within 3 ft (L_P) of the edge of a floor or roof. As previously stated, the peripheral ties have to be carried by the floor and roof system unless the beams, girders, or spandrels could be shown to be capable of carrying the peripheral tie force while undergoing a 0.20-rad rotation.

In this case, the required tie strength

$$F_P = 6W_F L_1 L_P \qquad \text{(Equation 6 – 5)}$$

Where L_P=3 ft

According to ASCE 41: Seismic Rehabilitation of Existing Buildings (ASCE, 2007), the plastic rotation angles for RBS connections and WUF connections cannot reach 0.20. Khandewal and El-Tawil (2007) also illustrated that the beam end rotations for these two types of connections cannot fulfill this requirement. Previous simulation studies with the NIST building showed that the shear connections employed failed before reaching 0.2 radians. According to the simulations in Chapter 4 and 5 and the data from Sadek et al. (2008), the NIST building is vulnerable to collapse after loss of a gravity column. Since the shear connections used in the SAC buildings are the same as the ones used in the

NIST building and the floor systems are weaker than the NIST buildings, it can be reasonably inferred that the gravity system in these three building cannot achieve this requirement, either. Therefore, the floor system has to carry the entire required tie forces in the types of buildings considered in this work.

For the vertical ties, the DoD guidelines require that "*the vertical ties must have a design strength in tension equal to the largest vertical load received by the column or wall from any one story, using the tributary area and the floor load* W_F"(UFC, 2009).

6.5 Tie Force Method: Case Studies

6.5.1 NIST Building

1. Calculating W_F

Dead load: 76 psf

Live load: 100 psf

$$W_F = 1.2D + 0.5L = 1.2 \times 76 + 0.5 \times 100 = 141.2 \text{ psf} \quad \text{(Equation 6 – 6)}$$

2. Tie force calculation

The calculated values of the required tie forces F_{demand} are compared with the tie forces that can be developed in the current floor system F_{supply}. The results are shown in Table 6 – 2.

Table 6 - 2 Tie forces comparison: required & available

Type of Tie	Orientation	L_1 (ft)	F_{demand}	F_{supply}
Peripheral/transverse (kips)	N-S	20	50.83	42.85
Peripheral/ longitudinal (kips)	E-W	30	76.25	5.76
Interior/transverse (kips/ft)	N-S	20	8.47	14.28
Interior/longitudinal (kips/ft)	E-W	30	12.71	1.92

It can be seen from Table 6 – 2 that the slab system of the NIST building cannot provide the required horizontal ties. Since the tensile strength of steel members will always larger than their compressive strength (governed by buckling), the systems is considered to have sufficient vertical ties.

3. Additional slab reinforcement used to develop required ties forces

To develop the required tie forces in the floor system, additional reinforcement needs to be placed in the slabs. It is assumed that the reinforcing bars used here are ASTM grade 60 reinforcing steel with a minimum specified yield strength of 60 ksi. The strength reduction factor ∅ and over-strength factor required by the DoD guidelines are taken as unity when calculating the design yield capacity of the steel rebar. Rebar detailing requirements can be found in the DoD guidelines and are not elaborated here.

When calculating the additional slab reinforcement needed to develop the required tie forces, four different cases are considered. The purpose of considering these different cases is to investigate the effectiveness of the Tie Force method under different loading conditions and design requirements. The calculation results are shown in Table 6 – 3 to Table 6 – 6.

- Case 1: Consider the contribution of the steel deck and reinforcing mesh to the tie forces and use the unreduced live load.
- Case 2: Neglect the contribution of the steel deck and reinforcing mesh to the tie forces and use the unreduced live load.

- Case 3: Consider the contribution of the steel deck and reinforcing mesh to the tie forces and use the reduced live load.
- Case 4: Neglect the contribution of the steel deck and reinforcing mesh to the tie forces and use the reduced live load.

The reduced live load is calculated according to ASCE 7-10 (ASCE, 2010). Although only the load combination without live load reduction (Table 6-2) was used to demonstrate that the tie forces in the NIST building cannot satisfy the UFC requirements, the same conclusion can be drawn even if live load reduction is considered because the tensile strength perpendicular to the direction of the flutes of the steel deck is limited. This can be seen by inspection of Tables 6 – 3 through 6 – 6. The layout of the reinforcing bars for Case 2 is illustrated in Figure 6 – 12. The layout of the reinforcing bars calculated for the other cases are similar, and are not shown here to conserve space.

Table 6 - 3 Slab reinforcement needed to developed required tie forces: Case 1

Type of Tie	Orientation	Required ties	Reinforcement type
Peripheral/transverse	N-S	7.98 kips	#4
Peripheral/longitudinal	E-W	70.49 kips	#10
Interior/transverse	N-S	Sufficient	N/A
Interior/longitudinal	E-W	10.79 kip/ft	6 #7 between columns

Table 6 - 4 Slab reinforcement needed to developed required tie forces: Case 2

Type of Tie	Orientation	Required ties	Reinforcement type
Peripheral/transverse	N-S	50.83 kips	#9
Peripheral/longitudinal	E-W	76.25 kips	#11
Interior/transverse	N-S	8.47 kip/ft	10 #6 between columns
Interior/longitudinal	E-W	12.71 kip/ft	10 #6 between columns

Table 6 - 5 Slab reinforcement needed to developed required tie forces: Case 3

Type of Tie	Orientation	Required ties	Reinforcement type
Peripheral/transverse	N-S	enough	N/A
Peripheral/longitudinal	E-W	55.26 kip	#9
Interior/transverse	N-S	Enough	N/A
Interior/longitudinal	E-W	8.52 kip/ft	5 #7 between columns

Table 6 - 6 Slab reinforcement needed to developed required tie forces: Case 4

Type of Tie	Orientation	Required ties	Reinforcement type
Peripheral/transverse	N-S	40.68 kips	#8
Peripheral/longitudinal	E-W	61.02 kips	#10
Interior/transverse	N-S	6.78 kip/ft	7 #7 between columns
Interior/longitudinal	E-W	10.17 kip/ft	7 #7 between columns

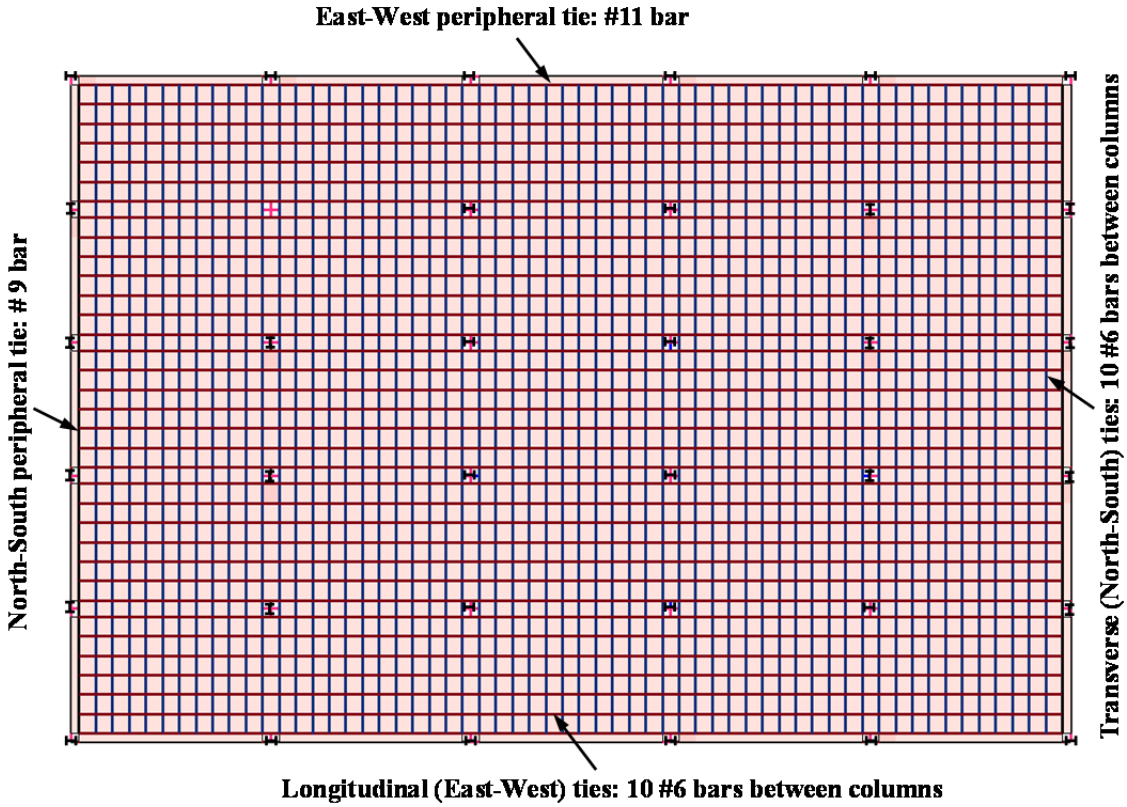

Figure 6 - 12 Layout of additional slab reinforcement

4. Performance of the NIST building with adequate tie strength

After calculating the required tie capacities and corresponding reinforcement according to the DoD guidelines, a set of new models with revised slab reinforcement are developed. The model name is appended with ATF to signify that adequate tie forces are provided, e.g. M2-ATF. The rebars in the modified models are modeled using truss elements directly attached to the slabs. Like the steel deck, these additional rebars are also assumed

to be placed at the concrete centerline. This assumption is reasonable since the flexural behavior of the floor system is not as important as the tensile strength for collapse mitigation. The material property of the rebar is represented using a plastic-kinematic model (material model type 3 in LS-DYNA) and an elastic-perfectly plastic relationship is used. The elongation at fracture of the rebar used is based on Table 3 – 4 in Wight and MacGregor (2009) and is listed in Table 6 – 7.

Table 6 - 7 Fracture elongation of rebars

Reinforcement type	Fracture elongation (%)
#4	9
#7	8
#8	8
#9	7
#10	7
#11	7

The new model is used in a series of nonlinear dynamic analysis using the alternate path method to investigate the adequacy of the Tie Force method. The responses of model M2 and modified model M2-ATF are compared under the same column loss scenarios. Three loading conditions are employed in M2-ATF, which are (i) Designed loading: 1.2DL+0.5LL (141.2 lb/ ft^2 for Cases 1 and 2 and 113 lb/ ft^2 for Cases 3 and 4); (ii) NIST loading, , which is a lower level of gravity loading defined in Main and Sadek (2012): $1.05DL+LL_{survey}$ (LL_{survey} = 10.9lb/ft^2) (90.7 lb/ ft^2); and (iii) GSA loading: $1.0DL+0.25LL_0$ (101 lb/ ft^2). Under each loading conditions, the loads are applied gradually within 5 seconds, followed by a wait period of 2.5 seconds, in order to eliminate dynamic effects. After that, a key element, such as a column is removed by deleting it instantaneously.

Three first floor column loss cases are considered first – loss of column C-D4-1, C-D5-1 and C-E5-1, all of which are interior columns. The comparisons are presented in Table 6-8.

Table 6 - 8 Comparisons between M2 and M2-ATF subjected to different design schemes

Column lost	Loading condition	M2 (mm)	M2-ATF (mm)			
			Case 1	Case 2	Case 3	Case 4
C-D4-1	i	***PC***[1]	968	777	724	602
	ii	690	531	478	541	480
	iii	791	605	528	623	536
C-D5-1	i	***PC***[1]	1016	838	782	705
	ii	***PC***[1]	558	498	583	502
	iii	***PC***[1]	646	559	674	576
C-E5-1	i	***PC***[1]	998	826	745	612
	ii	***PC***[1]	533	470	551	475
	iii	***PC***[1]	618	523	633	535

[1]***PC***: Progressive collapse

Table 6 – 8 shows the deflection at the location of the removed column for the various scenarios considered. Progressive collapse, when it occurs, is designated as *PC*. Clearly, *PC* occurs in original model M2, but does not occur in any of the revised models M2-ATF. It can therefore be concluded from Table 6 – 8 that the tie force method proposed in the DoD guidelines protects this particular building against progressive collapse under column loss scenarios. Although model M2 does not collapse after loss of column C-D4-1 when load combinations ii and iii are applied, adequate tie strength (in model M2-ATF) reduces the deformation significantly. The maximum reduction is 31%. In all of the other cases, the deformation given by M2-ATF is significantly below the maximum failure displacement, which is about 1300 mm as discussed in Alashker and El-Tawil (2010). Therefore, tie forces play a critical role in reducing system displacement when a column is lost.

Another six first floor column loss cases are conducted to further gain insight into the effect of the additional tie strength to the response of the structure subjected sudden column removal, including (1) removal of exterior moment column C-D6-1; (2) removal of exterior moment column C-E6-1; (3) removal of exterior columns C-D6-1 and C-E6-1 simultaneously; (4) removal of exterior gravity column C-A5-1; (5) removal of corner moment column C-F6-1; and (6) removal of interior moment column C-E4-1. The locations of the removed columns are shown in Figure 6 – 13.

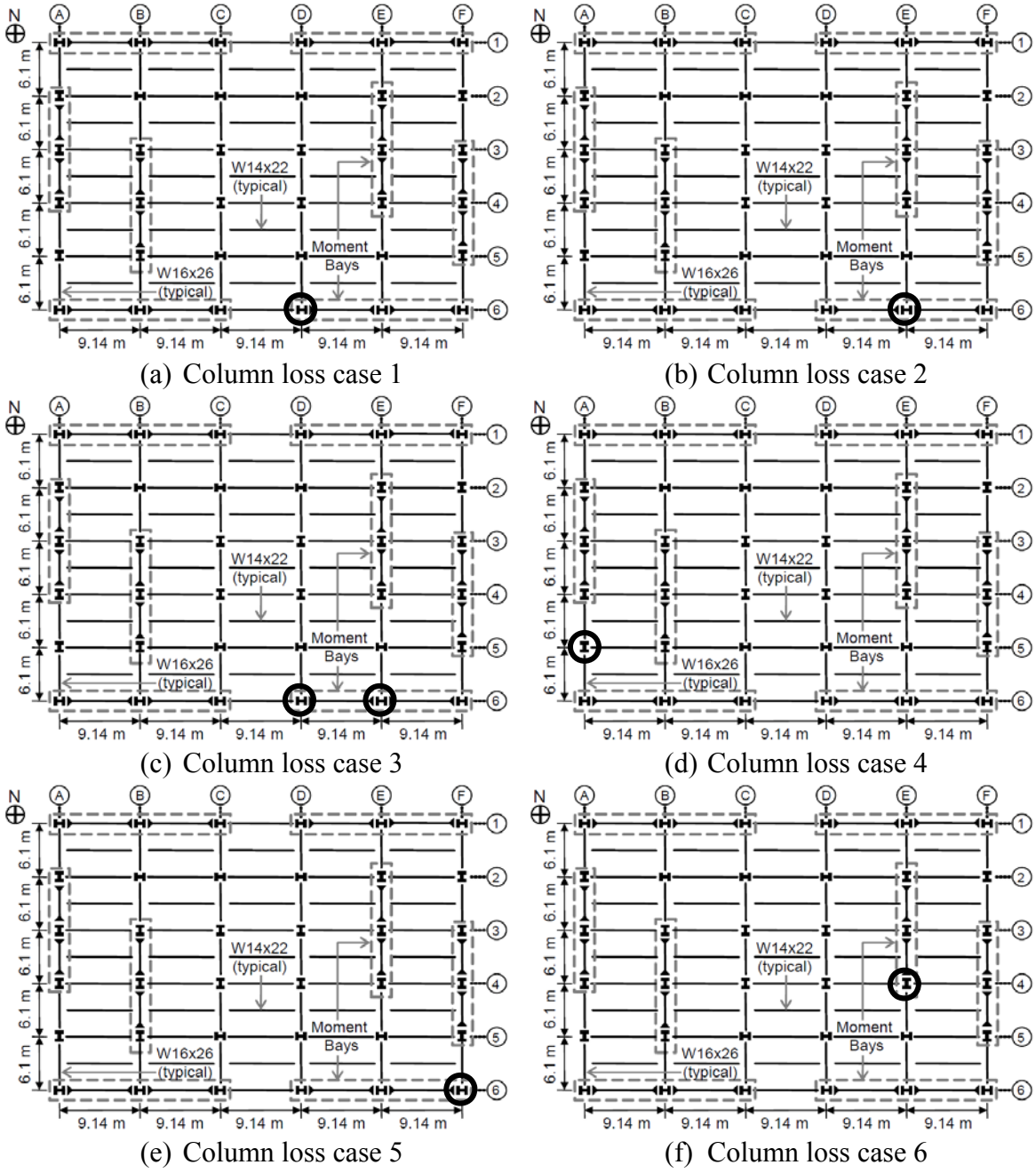

(a) Column loss case 1 (b) Column loss case 2

(c) Column loss case 3 (d) Column loss case 4

(e) Column loss case 5 (f) Column loss case 6

Figure 6 - 13 Locations of the removed columns: NIST building

The responses (permanent deformation) of model M2 and M2-ATF under similar column loss scenarios are compared in Table 6-9 for Case 4 and load combination iii. It can be seen from Table 6 – 9 that in the cases when moment column(s) is (are) removed, the effect of the additional tie reinforcement is limited. The maximum difference between

M2 and M2-ATF is 11% and the minimum difference is only 3%. The reason is that the deformation of the structure subjected to loss of a moment column is so small that membrane action in the slabs is not mobilized. Moreover, the contribution of the additional reinforcement to composite action is also limited. Therefore, it is not surprising that the differences between the responses of M2 and M2-ATF are small. The effects are obvious when the deformation is large, such as loss of column C-A5-1, which is an exterior gravity column. As observed earlier, the additional reinforcement plays an important role in resisting progressive collapse and reducing the deformations.

Table 6 - 9 Comparison between M2 and M2-ATF: collapse is prevented

Column loss case	Column type	M2 (mm)	M2-ATF (mm)	Difference (%)
C-D6-1	Exterior moment	82	74	11
C-E6-1	Exterior moment	29	28	4
C-D6-1/C-E6-1	Exterior moment	457/348	417/317	10/10
C-A5-1	Exterior gravity	709	506	40
C-F6-1	Corner moment	47	43	9
C-E4-1	Interior moment	69	66	5

6.5.2 SAC Buildings

Since the slab system of the SAC buildings is similar to the NIST building, it is clear that the original design will not have sufficient tie strength. In redesigning the slab system, the contribution of the steel deck and reinforcement mesh are not considered to contribute to the tie force strength and the live load is not reduced when calculating W_F. The calculated required tie forces for the Boston buildings are presented in Table 6 – 10.

Table 6 - 10 Required tie force for the Boston buildings

Required Ties	SAC-3		SAC-9		SAC-20	
	E-W	N-S	E-W	N-S	E-W	N-S
Longitudinal/transverse (kip/ft)	10.84	10.84	10.84	10.84	14.45	7.224
Peripheral (kip)	65.0	65.0	65.0	65.0	86.69	43.34

The same calculation results are obtained for SAC-3 and SAC-9 because the loads are the same and the distance between the columns are also the same for these two buildings. ASTM grade 60 reinforcing steel is used and both strength reduction and over-strength factors required by the DoD guidelines are taken as unity. The calculation results are shown in Table 6 – 11.

Table 6 - 11 Additional reinforcement needed to develop required tie strength for the Boston buildings

Building	Type of tie	orientation	Reinforcement between columns (area)	Yield capacity of tie
SAC-3	Longitudinal	E-W	7 # 8 (5.53)	11.6 kip/ft
	Transverse	N-S	7 # 8 (5.53)	11.6 kip/ft
	Peripheral	E-W	#10 (1.27)	76.2 kip
	Peripheral	N-S	#10 (1.27)	76.2 kip
SAC-9	Longitudinal	E-W	7 # 8 (5.53)	11.6 kip/ft
	Transverse	N-S	7 # 8 (5.53)	11.6 kip/ft
	Peripheral	E-W	#10 (1.27)	76.2 kip
	Peripheral	N-S	#10 (1.27)	76.2 kip
SAC-20	Longitudinal	E-W	7 # 8 (5.53)	16.59 kip/ft
	Transverse	N-S	4 # 8 (3.16)	9.48 kip/ft
	Peripheral	E-W	#11 (1.56)	93.6 kip
	Peripheral	N-S	#8 (0.79)	47.4 kip

The revised models are developed on the basis of the calculation results in Table 6 – 11. The responses of model M2-SAC and M2-SAC-ATF under the same column loss scenarios are compared for all of the three SAC buildings. 12 column loss cases are conducted for SAC-3, 9 column loss cases are done for SAC-9, and 8 column loss cases are conducted for SAC-20. Only single-column loss cases are considered herein and the column-loss cases conducted are listed in Table 6 – 12.

To facilitate referral to various configurations, the column loss cases are designated as SAC-X-N. In this notation, X is the height of the building in stories, and N is the case number. For example, SAC-9-3 represents column loss case #3 for SAC-9. The locations of the removed columns are shown in Figure 6 – 14 to Figure 6 – 16. It can be seen that every possible single column loss case is considered in this study considering the symmetry of the structural framing plan.

Table 6 - 12 List of column loss cases: SAC buildings

Column loss cases		Column location	Column type
SAC-3	SAC-3-1	C-A3-1	Exterior moment
	SAC-3-2	C-A4-1	Exterior moment
	SAC-3-3	C-A5-1	Corner moment
	SAC-3-4	C-B3-1	Interior gravity
	SAC-3-5	C-B4-1	Interior gravity
	SAC-3-6	C-B5-1	Exterior gravity
	SAC-3-7	C-C3-1	Interior gravity
	SAC-3-8	C-C4-1	Interior gravity
	SAC-3-9	C-C5-1	Exterior moment
	SAC-3-10	C-D3-1	Interior gravity
	SAC-3-11	C-D4-1	Interior gravity
	SAC-3-12	C-D5-1	Exterior moment
SAC-9	SAC-9-1	C-A4-1	Exterior moment
	SAC-9-2	C-A5-1	Exterior moment
	SAC-9-3	C-A6-1	Corner moment
	SAC-9-4	C-B4-1	Interior gravity
	SAC-9-5	C-B5-1	Interior gravity
	SAC-9-6	C-B6-1	Exterior moment
	SAC-9-7	C-C4-1	Interior gravity
	SAC-9-8	C-C5-1	Interior gravity
	SAC-9-9	C-C6-1	Exterior moment
SAC-20	SAC-20-1	C-A4-1	Exterior moment
	SAC-20-2	C-A5-1	Exterior moment
	SAC-20-3	C-A6-1	Exterior moment
	SAC-20-4	C-A7-1	Corner moment
	SAC-20-5	C-B7-1	Exterior moment
	SAC-20-6	C-C4-1	Interior gravity
	SAC-20-7	C-C5-1	Interior gravity
	SAC-20-8	C-C7-1	Exterior moment

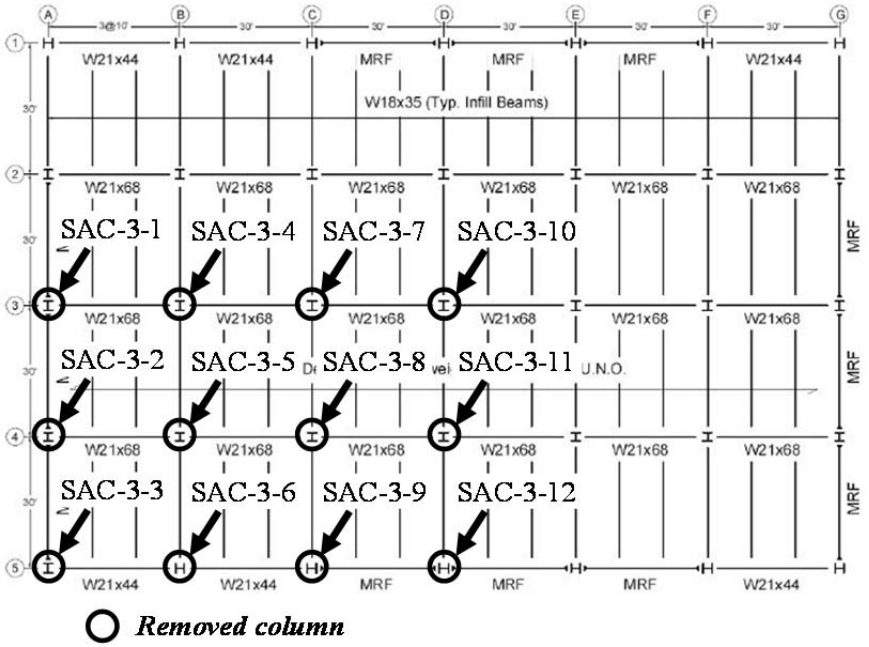

Figure 6 - 14 Removed columns: SAC-3 building

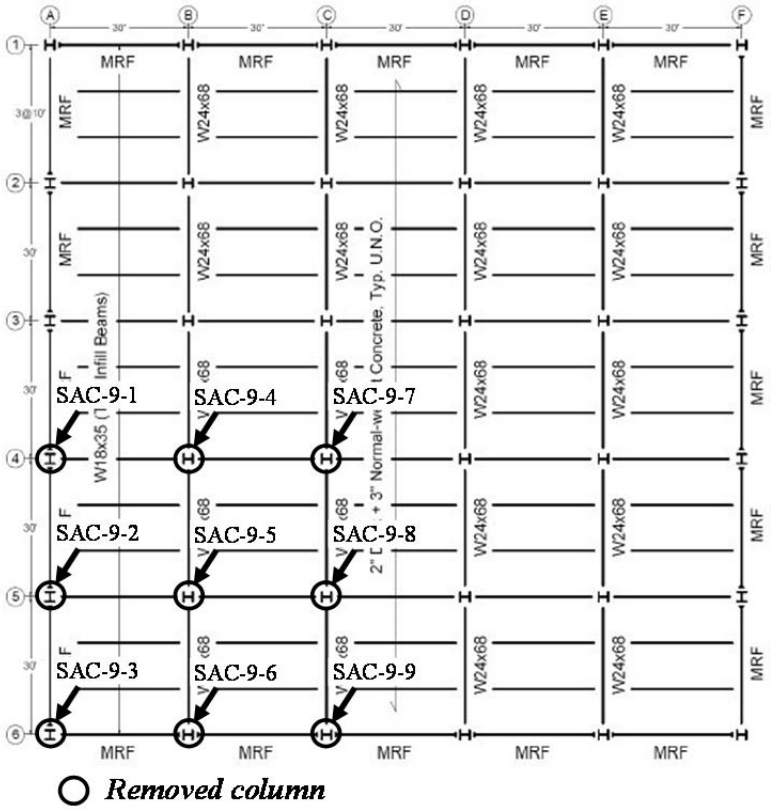

Figure 6 - 15 Removed columns: Boston 9-story building

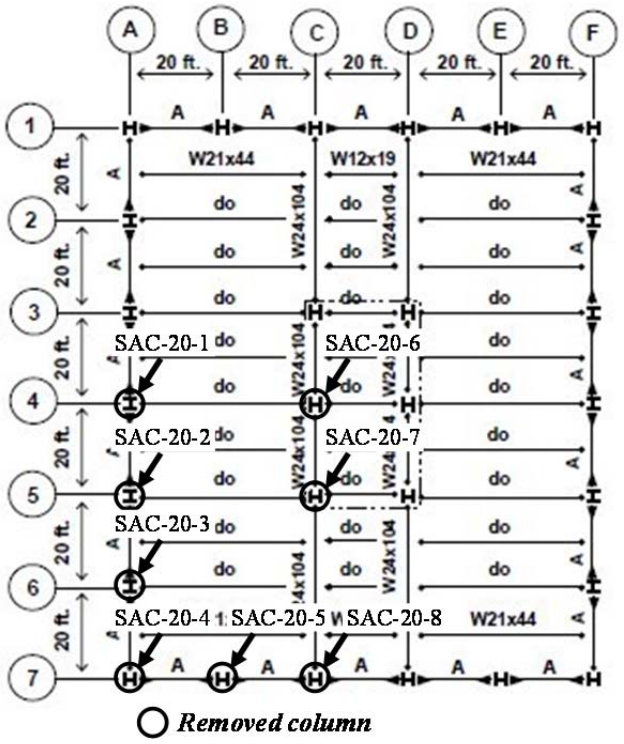

Figure 6 - 16 Removed columns: Boston 20-story building

The comparisons between permanent deformations obtained from model M2-SAC and M2-SAC-ATF for each of the buildings are compared in Table 6 – 13.

From Table 6 – 13, it is clear that the results are similar to those obtained for the NIST building. Model M2-SAC collapses in all gravity column loss cases except case SAC-20-6, in which the lost column has a small tributary area. Progressive collapse is prevented in all of the M2-SAC-ATF cases conducted. In the SAC-20-6 case, the deformation given by M2-SAC-20-ATF is 436 mm, which is 28% smaller than the one given by model M2-SAC-20 (608 mm). These results suggest that the additional reinforcement used for required tie forces contribute significantly to the system's collapse resistance after loss of a gravity column.

The situation is more complicated for the cases in which moment columns are lost. An interesting observation from Table 6 – 13 is that buildings with lower height are more

vulnerable after loss of a moment column. For example, in case SAC-3-1, the overall deflection of model M2-SAC-3 is 113 mm. While in case SAC-9-1 and SAC-20-1, the values are 29 mm and 19 mm for model M2-SAC-9 and M2-SAC-20, respectively. In all of these cases, the building considered is subjected to loss of an exterior column located in the middle of the moment frame it belonged to. This reduced vulnerability is directly attributed to system frame action discussed in Chapter 5.

Table 6 - 13 Comparison between M2 and M2-ATF: Boston buildings

Column loss cases	M2-SAC (mm)	M2-SAC-ATF (mm)	Difference (%)
SAC-3-1	113	97	14
SAC-3-2	112	102	9
SAC-3-3	254	191	25
SAC-3-4	***PC*[1]**	939	N/A
SAC-3-5	***PC*[1]**	900	N/A
SAC-3-6	***PC*[1]**	1191	N/A
SAC-3-7	***PC*[1]**	886	N/A
SAC-3-8	***PC*[1]**	848	N/A
SAC-3-9	648	495	24
SAC-3-10	***PC*[1]**	885	N/A
SAC-3-11	***PC*[1]**	828	N/A
SAC-3-12	121	95	21
SAC-9-1	29	27	7
SAC-9-2	30	28	7
SAC-9-3	34	30	12
SAC-9-4	***PC*[1]**	792	N/A
SAC-9-5	***PC*[1]**	829	N/A
SAC-9-6	43	40	7
SAC-9-7	***PC*[1]**	864	N/A
SAC-9-8	***PC*[1]**	864	N/A
SAC-9-9	29	28	3
SAC-20-1	19	18	5
SAC-20-2	20	19	5
SAC-20-3	24	22	8
SAC-20-4	26	24	8
SAC-20-5	11	10	9
SAC-20-6	608	436	28
SAC-20-7	***PC*[1]**	649	N/A
SAC-20-8	18	17	6

***PC*[1]**: Progressive collapse

A special case is case SAC-3-9. In this case, the deformation of model M2-SAC-3 is 648 mm after loss of exterior moment column C-C5-1, which is much larger than the other cases in which moment columns are lost. This is because this particular column has a moment connection on only one side of the column. The shear connections connected to the other side of the removed column fail immediately after loss of the column in both models M2-SAC-3 and M2-SAC-3-ATF. However, the tie forces reduce the deformation by 24% in M2-SAC-3-ATF. The failure mechanisms of M2-SAC-3 and M2-SAC-3-ATF are shown in Figure 6 – 17. For SAC-3, the maximum reduction in deformation for loss of moment columns attributed to the additional reinforcement occurs in case SAC-3-3 (25% increase). In that case (loss of corner moment column C-A5-1), the overall deflections of model M2-SAC-3 and M2-SAC-3-ATF are 254 mm and 191 mm, respectively.

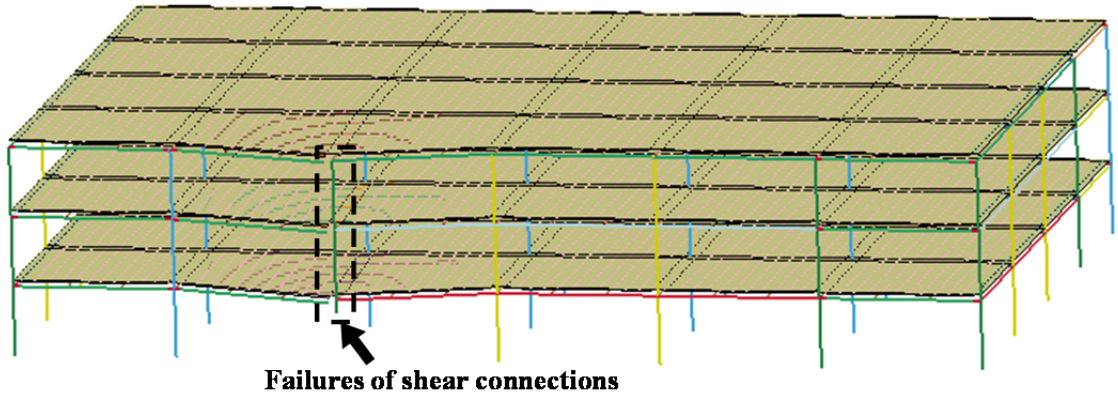

(a) Failure model of M2-SAC-3-ATF

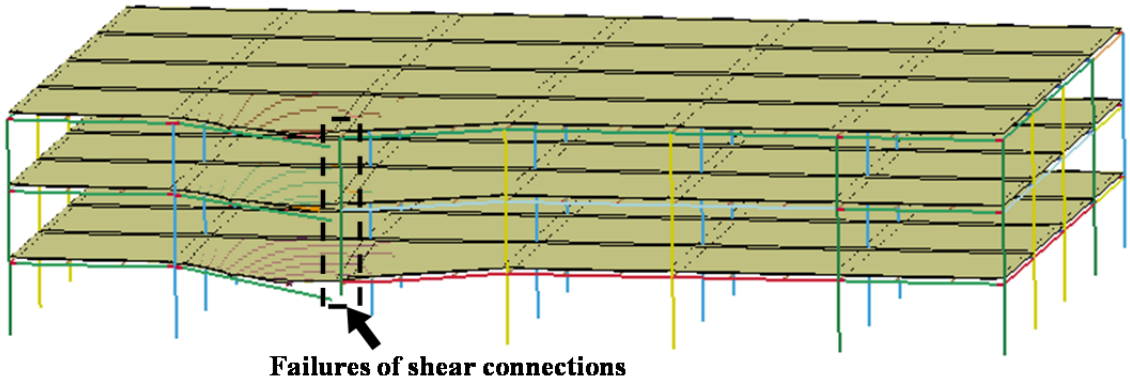

(b) Failure mode of M2-SAC-3

Figure 6 - 17 Comparison between failure modes M2-SAC-3 vs. M2-SAC-3-ATF: case SAC-3-9

For the 9-story and 20-story buildings, deformations given by both M2-SAC and M2-SAC-ATF after loss of any moment column are small. The reduction in deformation attributed to the additional tie reinforcement ranges between 3% and 12%.

6.6 Calculation of Dynamic Increase Factor

Static procedures do not capture the dynamic nature of the column removal problem. One convenient way to do so is to apply a Dynamic Increase Factor (DIF) to the results of static models to account for the response magnification associated with dynamic behavior. In GSA and older versions of the UFC criteria, DIF was taken as 2.0, based on the behavior of elastic systems. This number has been proved to be too conservative by several researchers (Ruth et al. 2006, Foley et al. 2008, Khandelwal 2007), primarily because system response is inelastic and not elastic. This recognition has promoted the latest UFC criteria to specify DIF as follows (for steel frame structures):

$$\Omega_N = 1.08 + \frac{0.76}{\theta_{pra}/\theta_y + 0.83} \qquad \text{(Equation 6 – 7)}$$

Where θ_{pra} is the plastic rotation angle given in the acceptance criteria tables in ASCE 41 for the appropriate structural response level (Collapse Prevention or Life Safety); and θ_y is the yield rotation according to Equation 5-1 in ASCE 41. It should be emphasized that θ_y is the yield rotation angle of the structural element that is being connected and θ_{pra} is for the connection. The DIF of the structure is determined by the smallest ratio of θ_{pra}/θ_y for any primary element, component, or connection in the model within the effective area of the removed column.

Equation 6 – 7 was obtained from curve fitting and thus lacks a theoretical basis. Furthermore, while three-dimensional models were used to formulate the equation (McKay et al. 2012), the models employed did not include slabs, which were shown in Chapter 5 to contribute significantly to collapse response. This is ironic since the UFC

criteria themselves, which promote the equation, specify that all primary components have to be considered in the computational model.

A series of cases studies using the NIST building in the context of APM are conducted in order to verify whether equation 6 – 7 is able to produce reasonable value of DIF. The M2-ATF model (case 4 as specified in Section 6.5.1) is used in these simulations since the DoD guidelines require that "for elements with inadequate horizontal tie force capacity, the Alternate Path method cannot be used". The column loss cases are listed in Table 6 – 15. To facilitate the following discussion, a similar naming scheme similar to the one used in Section 6.5.2 is used herein. The column loss cases are designated as N-X, where N represents the NIST building and X represents the case number. This naming scheme will also be used in the following sections. The locations of the removed columns are shown in Figure 6 – 18.

Table 6 - 14 Calculation of DIF: column loss cases

Column loss case	Column lost	Column type
N-1	C-A5-1	Exterior gravity column
N-2	C-D4-1	Interior gravity column
N-3	C-D6-1	Exterior moment column
N-4	C-E4-1	Interior moment column
N-5	C-E5-1	Interior gravity column
N-6	C-E6-1	Exterior moment Column
N-7	C-F6-1	Corner moment column
N-8	C-A5-5	Exterior gravity column
N-9	C-D4-5	Interior gravity column
N-10	C-D6-5	Exterior moment column
N-11	C-E4-5	Interior moment column
N-12	C-E5-5	Interior gravity column
N-13	C-E6-5	Exterior moment Column
N-14	C-F6-5	Corner moment column

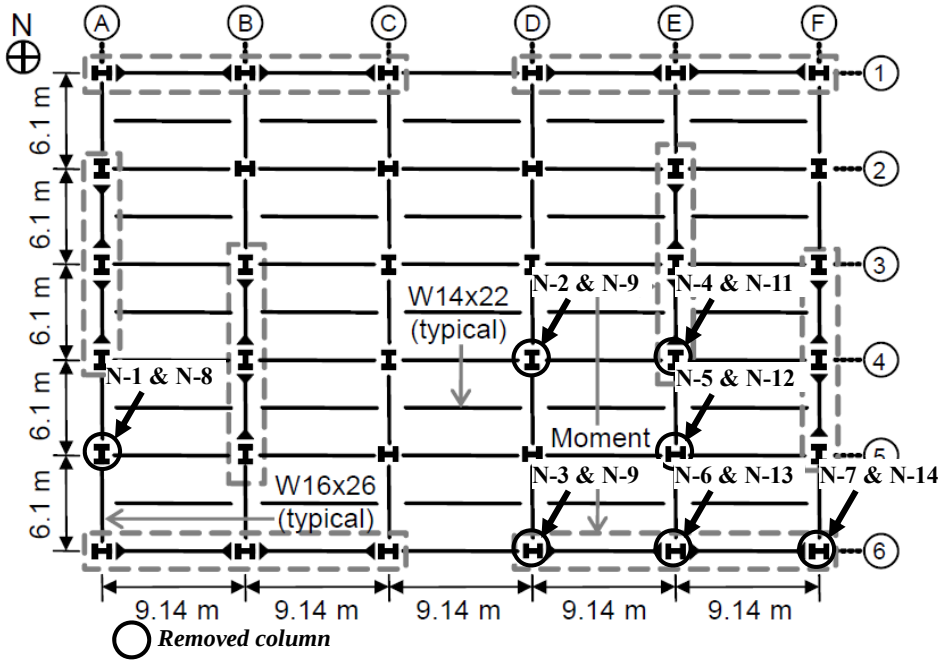

Figure 6 - 18 Calculation of DIF according to DoD guidelines for the NIST building: removed column

The values of DIFs for the column loss cases listed in Table 6 – 15 are calculated based on the equation given by the DoD guidelines and the results are shown in Table 6 – 16.

Table 6 - 15 DIF values according to DoD guidelines for the NIST building

Column loss case	Control member	Control member type	DoD DIF
N-1	B-AB5-1	E-W gravity beam	1.32
N-2	B-CD4-1	E-W gravity beam	1.32
N-3	B-CD6-1	E-W gravity beam	1.32
N-4	B-DE4-1	E-W gravity beam	1.32
N-5	B-DE5-1	E-W gravity beam	1.32
N-6	I-DE56-1	E-W gravity beam	1.32
N-7	I-EF56-1	E-W gravity beam	1.32
N-8	B-AB5-5	E-W gravity beam	1.32
N-9	B-CD4-5	E-W gravity beam	1.32
N-10	B-CD6-5	E-W gravity beam	1.32
N-11	B-DE4-5	E-W gravity beam	1.32
N-12	B-DE5-5	E-W gravity beam	1.32
N-13	I-DE56-5	E-W gravity beam	1.32
N-14	I-EF56-5	E-W gravity beam	1.32

In Table 6 – 16, 'control member' refers to the member or connection with the smallest value of θ_{pra}/θ_y, thereby controlling the maximum DIF. Table 6 – 16 reveals two other problems with the DoD guidelines: 1) θ_{pra}/θ_y is member dependent and not system dependent, and 2) certain members may dominate the DIF calculations. In other words, the members or connections with the smallest value of θ_{pra}/θ_y have the same member section and structural layouts for the different column loss cases, leading to the same DIF values. In all of the column loss cases, the control member is the gravity beam in East-West direction. Such beams are considered primary members and not neglected in this study because they are not considered to be pinned at both ends and the flexural strength of the shear connection is not neglected.

Nonlinear dynamic and static analyses are performed using model M2-ATF for the column loss cases listed in Table 6 – 15. Following McKay et al. (2012) and the procedure proposed in the DoD guidelines, the following steps are performed:

1. Nonlinear dynamic analysis is performed using the design loads. The alternate path method is employed and the peak deformation of the removed column is recorded.
2. Using the same model in Step 1, a nonlinear static analysis is performed. Increased loads with a trial DIF are applied in the effective area of the removed column.
3. Repeat step 2 until the deformation matches with the one computed in step 1.

The analysis results are shown in Table 6 – 17 and are compared with the values of DIF calculated using the DoD guidelines. In Table 6 – 17, DIF_{real} means the real dynamic increase factor obtained following the steps outlined above; DIF_{DoD} means the values of DIF calculated using equation 6 – 7.

Table 6 - 16 Comparison between DIF_{real} and DIF_{DoD}: NIST building: the NIST building

Column loss case	DIF_{real}	DIF_{DoD}	Difference
N-1	1.72	1.32	30%
N-2	1.70	1.32	29%
N-3	1.49	1.32	13%
N-4	1.30	1.32	-2%
N-5	1.53	1.32	16%
N-6	1.46	1.32	11%
N-7	1.45	1.32	10%
N-8	1.64	1.32	24%
N-9	1.71	1.32	30%
N-10	1.50	1.32	14%
N-11	1.30	1.32	-2%
N-12	1.53	1.32	16%
N-13	1.48	1.32	12%
N-14	1.48	1.32	12%

In Table 6 – 19, a positive difference means the DoD guidelines underestimate the values of DIF and a negative difference means the UFC overestimate the values of DIF. The table clearly shows that, except for cases N-4 and N-11, in which column C-E4-1 and C-E5-1 of the NIST building are removed, respectively, the values of DIF_{DoD} are all smaller than the DIF_{real}, which means the DoD guidelines are not conservative. The largest difference reaches 30%, which is significant.

This observed differences can be attributed to two possible reasons: (1) without modeling the slabs, McKay et al. (2012) misjudge the stiffness of the entire system significantly; and (2) McKay et al. did not consider a sufficient number of structural layouts; therefore their results may not be generally applicable.

To investigate whether neglecting the 3-D effects provided by the slabs is the only reason that Equation 6 – 7 does not provide accurate or conservative DIF, model M2-NS for the NIST building [used in Chapter 5] is employed herein. A series of column loss cases are conducted and the values of $DIF_{M2\text{-}NS}$, which represents the values of DIF obtained from the numerical simulations using model M2-NS, are compared with DIF_{DoD} , which are calculated according to Equation 6 – 7. The column loss cases include loss of C-D6-1, C-

D6-5, C-E6-1, C-E6-5, C-F6-1, and C-F6-5. The cases of loss of interior columns are not considered because the structure will collapse in these cases. The results are shown in Table 6 – 18.

Table 6 - 17 Comparisons between DIF_{DoD} and $DIF_{M2\text{-}NS}$

Column removed	DIF_{DoD}	$DIF_{M2\text{-}NS}$	Difference
C-D6-1	1.32	1.40	6
C-E6-1	1.30	1.96	51
C-F6-1	1.30	1.85	42
C-D6-5	1.32	1.25	-5
C-E6-5	1.30	1.97	52
C-F6-5	1.30	1.78	37

Table 6 – 18 illustrates that although slabs are ignored as in McKay et al. (2012), Equation 6 – 7 still does not produce reasonable results. Therefore, reason (1) is likely not the real cause for the deficiency of Equation 6 – 7.

To test reason (2), the SAC buildings are considered herein since these buildings have different structural layouts than the NIST building. As with the NIST building, models M2-SAC-ATF are employed and extensive case studies are conducted. Table 6 – 21 presents the values of DIF for various columns loss cases calculated on the basis of Equation 6 – 7 and Table 6 – 22 shows the comparison between the DoD DIF and real DIF. The same trends observed for the NIST building are seen, i.e. that the DoD guidelines are not accurate nor conservative.

Thus, in summary, as an empirical equation obtained from curve fitting and without any theoretical basis, Equation 6 – 7 provided by the DoD guidelines for calculating DIF is inaccurate.

Table 6 - 18 Comparison between DIF_{DoD} and DIF_{real}: SAC buildings

Column loss cases	Control section	DIF_{DoD}	DIF_{real}	Difference (%)
SAC-3-1	B-A23-3	1.38	1.48	7
SAC-3-2	B-A34-3	1.38	1.49	8
SAC-3-3	B-A45-3	1.38	1.45	5
SAC-3-4	B-B23-1	1.28	1.85	45
SAC-3-5	B-B34-1	1.28	1.82	42
SAC-3-6	B-B45-1	1.28	1.82	42
SAC-3-7	B-C23-1	1.28	1.85	48
SAC-3-8	B-C34-1	1.28	1.84	44
SAC-3-9	B-CD5-3	1.38	1.39	1
SAC-3-10	B-D23-1	1.28	1.87	46
SAC-3-11	B-D34-1	1.28	1.85	45
SAC-3-12	B-DE5-3	1.38	1.52	10
SAC-9-1	B-A34-9	1.33	1.50	13
SAC-9-2	B-A45-9	1.33	1.52	14
SAC-9-3	B-A56-9	1.33	1.46	10
SAC-9-4	B-AB4-1	1.28	1.83	43
SAC-9-5	B-AB5-1	1.28	1.79	40
SAC-9-6	B-BC6-9	1.33	1.46	10
SAC-9-7	B-BC4-1	1.28	1.80	41
SAC-9-8	B-BC5-1	1.28	1.79	40
SAC-9-9	B-CD6-9	1.33	1.41	8
SAC-20-1	B-A34-20	1.30	1.42	9
SAC-20-2	B-A45-20	1.30	1.38	6
SAC-20-3	B-A56-20	1.30	1.40	8
SAC-20-4	B-AB7-20	1.30	1.27	-2
SAC-20-5	B-BC7-20	1.30	1.34	3
SAC-20-6	B-AC4-1	1.30	1.66	28
SAC-20-7	B-AC5-1	1.30	1.74	34
SAC-20-8	B-CD7-20	1.30	1.28	-2

6.7 Energy-based Approach for Assessing Peak Dynamic Displacement

6.7.1 General Information

Section 6 – 6 showed that the DIF specified in the DoD guidelines is not accurate nor conservative. It was discussed that the approach suffers from several critical drawbacks and that it is based on empirical data. To resolve this problem, a new approach for assessing peak dynamic displacement is proposed herein.

A 4 slab-panel system with the mid-column removed as shown in Figure 6 – 19 is considered herein. It is assumed that the uniform load that is applied to the system is w. If the column is removed suddenly, according to Izzundin et al. (2007), the external work done by the system when peak dynamic displacement Δ_D is reached is

$$W_{ext} = \alpha w \Delta_D \qquad \text{(Equation 6 – 8)}$$

where α is a work-related factor that depends on the gravity load distribution and when w is identical everywhere, it is a constant which depends on the deformed shape of the floor system.

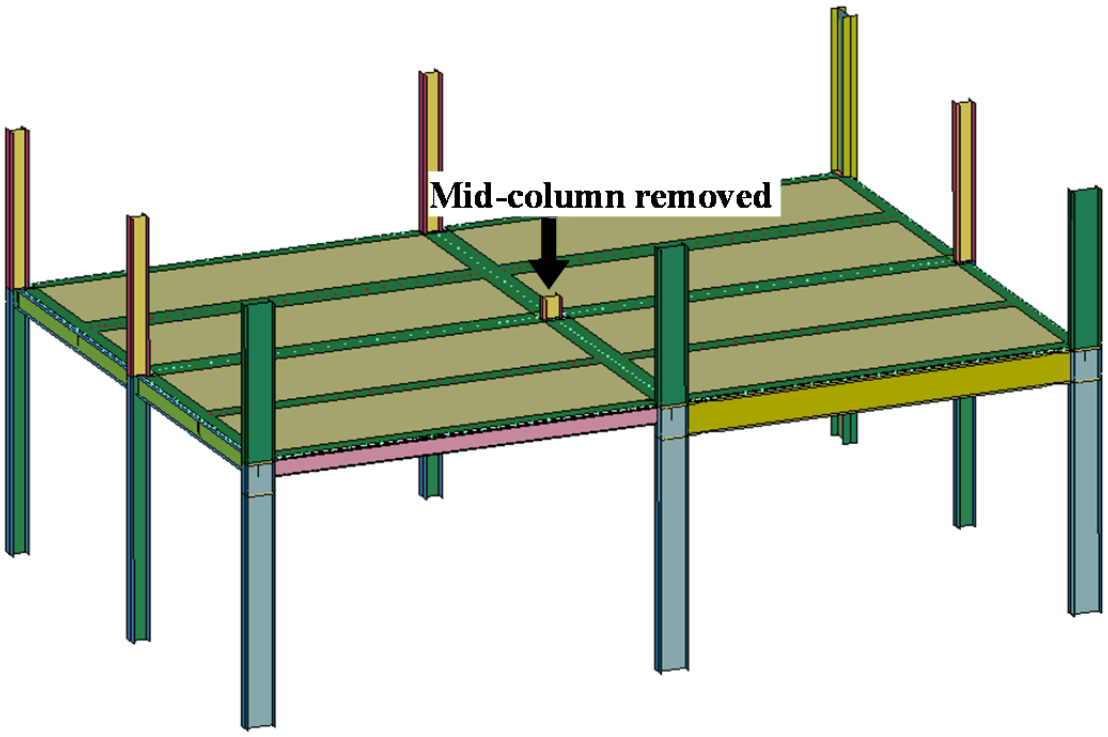

Figure 6 - 19 4 slab-panel system with mid-column removed

Assume that a load-deflection curve obtained from a static push-down analysis representing the relationship between the vertical displacement of the mid-column Δ and

the applied uniform load of the same system is as shown in Figure 6 – 20. In this case, the internal energy stored in the system can be expressed as

$$W_{int} = \int_0^{\Delta_D} \alpha w(\Delta) d\Delta \qquad \text{(Equation 6 – 9)}$$

Figure 6 - 20 Load-deflection curve

When peak dynamic deformation is reached, from the law of energy conservation, $W_{ext} = W_{int}$. The constant α can be eliminated, which indicates that the equality is not a function of the deformation mode of the system, as long as the deformation modes are the same under dynamic and static loading conditions.

Figure 6 - 21 Bi-linear approximation of the load-deflection curve

Assume that the relationship in Figure 6 – 20 can be simplified as a bi-linear relationship as shown in Figure 6 – 21. Further assume that the system response after loss of a column can be modeled as single degree of freedom mass-spring system as shown in Figure 6 – 22(a). The force-displacement relationship that describes the property of the spring is bilinear as shown in Figure 6 – 22(b). Sudden loss of a column is equivalent to a sudden application of the gravity load P_0. Therefore, the loads applied to the system (modeled as a SDOF system subjected to an excitation) can be described by the following equation and is shown in Figure 6 – 23.

$$P(t) = \begin{cases} 0, t \leq 0 \\ P_0, t > 0 \end{cases} \qquad \text{(Equation 6 – 10)}$$

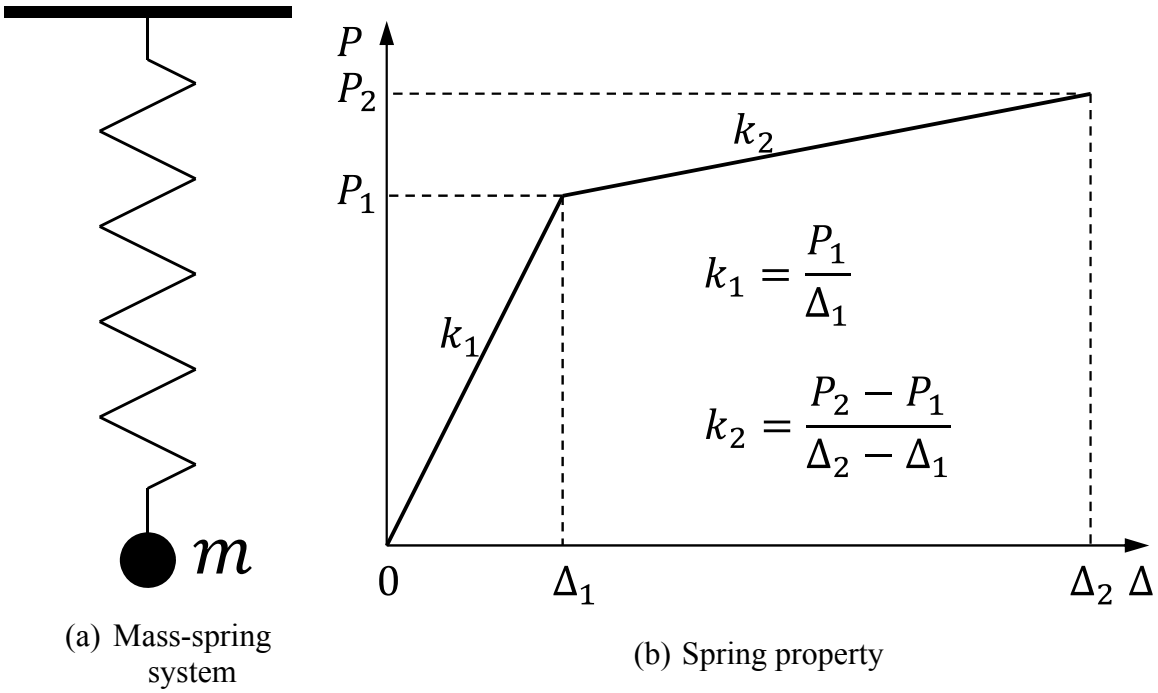

(a) Mass-spring system

(b) Spring property

Figure 6 - 22 Single degree of freedom (SDOF) system representing the response of a structural system

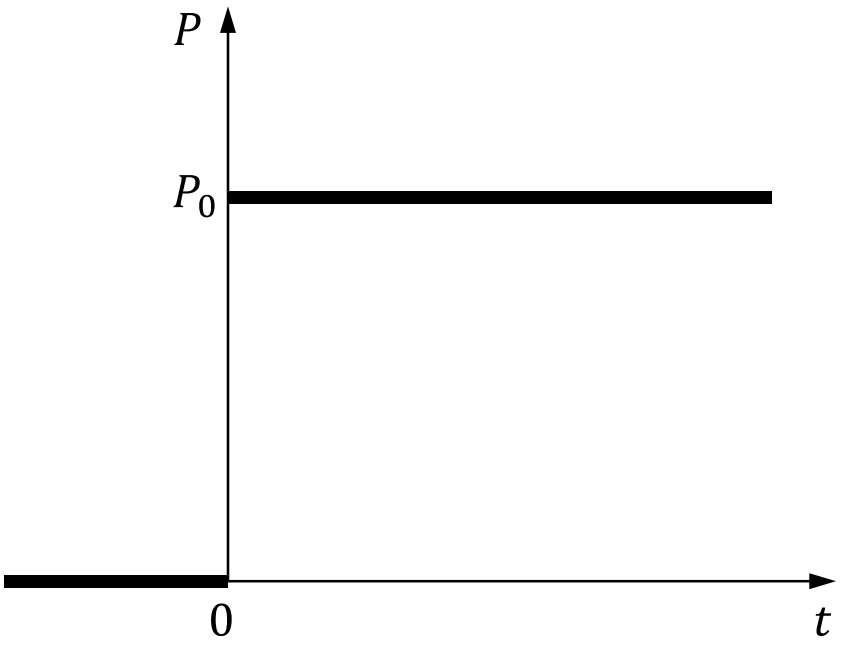

Figure 6 - 23 Loading scheme of the single degree freedom system

During vibration, the work done by the external force equals to kinetic energy of the mass plus the strain energy stored in the spring:

$$P_0\Delta(t) = \begin{cases} \frac{1}{2}m\left[\dot{\Delta(t)}\right]^2 + \frac{1}{2}k_1[\Delta(t)]^2, & \Delta(t) \le \Delta_1 \\ \frac{1}{2}m\left[\dot{\Delta(t)}\right]^2 + \frac{1}{2}k_1[\Delta_1]^2 + \frac{1}{2}k_2[\Delta(t)-\Delta_1]^2 + k_1\Delta_1[\Delta(t)-\Delta_1], & \Delta_1 < \Delta(t) \end{cases} \quad \text{(Equation 6 – 11)}$$

$\Delta(t)$ is the displacement at time t.

When the displacement of the SDOF system reaches the peak dynamic displacement, the velocity $\dot{\Delta(t)} = 0$ and therefore the kinetic energy of the system equals zero. At this instant,

$$P_0\Delta(t) = \begin{cases} \frac{1}{2}k_1[\Delta(t)]^2, & \Delta(t) \le \Delta_1 \\ \frac{1}{2}k_1[\Delta_1]^2 + \frac{1}{2}k_2[\Delta(t)-\Delta_1]^2 + k_1\Delta_1[\Delta(t)-\Delta_1], & \Delta(t) > \Delta_1 \end{cases} \quad \text{(Equation 6 – 12)}$$

Assume the peak dynamic displacement is Δ_D. Thus,

1. When $\Delta_D \le \Delta_1$

$$P_0\Delta_D = \frac{1}{2}k_1\Delta_D^2 \qquad \text{(Equation 6 – 10)}$$

$$\Delta_D = \frac{2P_0}{k_1} \qquad \text{(Equation 6 – 11)}$$

2. When $\Delta_D > \Delta_1$

$$P_0\Delta_D = \frac{1}{2}k_1[\Delta_1]^2 + \frac{1}{2}k_2[\Delta_D-\Delta_1]^2 + k_1\Delta_1[\Delta_D-\Delta_1] \qquad \text{(Equation 6 – 13)}$$

$$\Delta_D = \frac{P_0 + (k_2-k_1)\Delta_1 + \sqrt{P_0^2 + 2P_0\Delta_1(k_2-k_1) + k_1(k_1-k_2)\Delta_1^2}}{k_2} \qquad \text{(Equation 6 – 14)}$$

Alternatively, if the same displacement Δ_D is achieved by the same SDOF system statically, the final static load P_S applied to the system is as follows:

1. When $\Delta_D \leq \Delta_1$

   $$P_S = k_1 \Delta_D = \frac{2P_0}{k_1} k_1 = 2P_0 \qquad \text{(Equation 6 – 15)}$$

   And DIF $= \frac{P_S}{P_0} = \frac{2P_0}{P_0} = 2$ (Equation 6 – 15)

   This relationship also holds for the linear system.

2. When $\Delta_D > \Delta_1$

   $P_S = k_1 \Delta_1 + k_2(\Delta_D - \Delta_1) = P_0 + \sqrt{P_0^2 + 2P_0\Delta_1(k_2 - k_1) + k_1(k_1 - k_2)\Delta_1^2}$ (Equation 6 – 16)

$$\text{DIF} = \frac{P_S}{P_0} = 1 + \frac{\sqrt{P_0^2 + 2P_0\Delta_1(k_2 - k_1) + k_1(k_1 - k_2)\Delta_1^2}}{P_0} \qquad \text{(Equation 6 – 16)}$$

The above equations provide a theoretical basis for a new approach that can be used for assessing the peak dynamic displacement of a system Δ_D subjected to sudden column loss that can be used in a design office environment. In this approach, P_1 in the bi-linear relationship expressed in Figure 6 – 18(b) is taken as w_0, which is just the design load, thus Δ_1 is the overall deflection of the system under design load w_0, designated as u_1. Thus, $k_1 = \frac{w_0}{u_1}$. Let $P_2 = \alpha P_0$ $(\alpha > 1)$, and under this loading condition, $\Delta_2 = u_2$, and $k_2 = \frac{(\alpha - 1)w_0}{u_2 - u_1}$.

Since Δ_D must be larger than Δ_1 under this assumption, according to Equation 6 – 14:

$$\Delta_D = u_1 + \sqrt{\frac{u_1(u_2 - u_1)}{\alpha - 1}} \qquad \text{(Equation 6 – 17)}$$

Therefore, according to the proposed approach, two nonlinear static analyses are needed to estimate the peak dynamic displacement, one with normal loads and the other one with the normal load times a parameter α.

6.7.2 Verification of the Proposed Approach: Cases Studies

Numerical case studies are conducted using models M2-ATF representing the NIST building as well as the set of SAC buildings in order to verify the accuracy of the proposed approach. Nonlinear dynamic analyses are first performed to obtain the "true" peak dynamic displacement in a series of column loss cases. Then nonlinear static analyses are performed using the proposed approach for the same column loss cases. In each column loss case, a set of two static analyses are performed and the peak dynamic displacement is assessed using Equation 6 – 17. Next, nonlinear static analyses are performed based on the requirements of the DoD guidelines. Finally, the peak dynamic peak displacement obtained using the proposed approach and DoD guidelines are compared with the "true" peak dynamic displacement.

1. NIST building

The same column loss cases are conducted herein with Section 6.6. The results are shown in Table 6 – 21.

Table 6 - 19 Peak dynamic displacement obtained from various approaches: NIST building

Column loss case	True[1] (mm)	Method used	
		Proposed method (mm)	DoD guidelines (mm)
N-1	644	657	442
N-2	660	693	455
N-3	114	132	87
N-4	101	134	91
N-5	664	709	470
N-6	43	55	36
N-7	59	74	49
N-8	652	685	458
N-9	685	703	465
N-10	149	162	107
N-11	167	203	144
N-12	684	731	479
N-13	53	68	44
N-14	72	89	59

[1]True: True peak dynamic displacement obtained from nonlinear dynamic analysis

The displacements obtained according to DoD guidelines and the proposed method are normalized by the peak dynamic displacement obtained from the nonlinear dynamic analysis. A number smaller than unity means the result is underestimated and a number greater than unify means the opposite. The results are shown in Figure 6 – 24.

Table 6 - 20 Comparison between the unified peak dynamic displacements obtained from the DoD guidelines method and the proposed method: NIST building

Column loss case	Proposed method	DoD guidelines
N-1	1.02	0.69
N-2	1.05	0.69
N-3	1.16	0.76
N-4	1.33	0.90
N-5	1.07	0.71
N-6	1.27	0.84
N-7	1.24	0.83
N-8	1.05	0.70
N-9	1.03	0.67
N-10	1.09	0.72
N-11	1.21	0.86
N-12	1.07	0.70
N-13	1.28	0.84
N-14	1.23	0.81

It can be seen from Table 6 – 24 that the DoD guidelines underestimate the peak dynamic displacement in every case. For example, in case N-1, the peak dynamic displacement is underestimated by 30%. Therefore, the vulnerability of the system is significantly underestimated. On the other hand, the proposed method shows good accuracy. The peak dynamic displacements in the column loss cases are overestimated by 2% to 33%. For cases N-4, N-6, N-7, N-11, N-13, and N-14, the proposed method overestimates the peak dynamic displacement by over 20% and thus is conservative in these cases. However, in these cases, the deformation is fairly small and thus they are not critical column loss cases. However, in the critical column loss cases, such as case N-1, N-2, N-5, N-8, N-9, and N-12, the proposed method is accurate in estimating the peak dynamic displacement. The maximum difference between the proposed method and true dynamic peak displacement is 9% in those cases.

2. SAC buildings

More case studies are conducted using the SAC buildings. The true peak dynamic displacements and the ones obtained according to DoD guidelines and the proposed method are shown in Table 6 – 23. These peak dynamic displacements obtained by the proposed method and DoD guidelines are normalized by the true peak dynamic displacements in Table 6 – 24.

Table 6 - 21 Peak dynamic displacement obtained from various approaches: Boston buildings

Column loss case	True (mm)	Method used	
		Proposed method (mm)	DoD guidelines (mm)
SAC-3-1	124	145	104
SAC-3-2	129	147	108
SAC-3-3	229	256	191
SAC-3-4	989	1098	696
SAC-3-5	967	1094	693
SAC-3-6	1308	1400	890
SAC-3-7	937	1034	641
SAC-3-8	912	1006	663
SAC-3-9	531	602	527
SAC-3-10	933	974	628
SAC-3-11	887	894	623
SAC-3-12	123	128	103
SAC-9-1	36	47	31
SAC-9-2	39	50	34
SAC-9-3	37	50	34
SAC-9-4	858	907	588
SAC-9-5	887	918	588
SAC-9-6	53	71	48
SAC-9-7	914	961	621
SAC-9-8	916	976	628
SAC-9-9	35	49	33
SAC-20-1	20	28	18
SAC-20-2	20	28	19
SAC-20-3	23	30	23.78
SAC-20-4	26	29	18
SAC-20-5	11	16	10.64
SAC-20-6	463	513	341.09
SAC-20-7	688	790	513.59
SAC-20-8	19	27	19

Table 6 - 22 Comparison between the unified peak dynamic displacements obtained from the DoD guidelines method and the proposed method: NIST building

Column loss case	Proposed method	DoD guidlines
SAC-3-1	1.17	0.84
SAC-3-2	1.14	0.84
SAC-3-3	1.12	0.83
SAC-3-4	1.11	0.70
SAC-3-5	1.13	0.72
SAC-3-6	1.07	0.68
SAC-3-7	1.10	0.68
SAC-3-8	1.10	0.73
SAC-3-9	1.13	0.99
SAC-3-10	1.04	0.67
SAC-3-11	1.01	0.70
SAC-3-12	1.04	0.84
SAC-9-1	1.31	0.86
SAC-9-2	1.28	0.87
SAC-9-3	1.35	0.92
SAC-9-4	1.06	0.69
SAC-9-5	1.03	0.66
SAC-9-6	1.34	0.91
SAC-9-7	1.05	0.68
SAC-9-8	1.07	0.69
SAC-9-9	1.40	0.94
SAC-20-1	1.40	0.90
SAC-20-2	1.40	0.95
SAC-20-3	1.30	1.03
SAC-20-4	1.12	0.69
SAC-20-5	1.45	0.97
SAC-20-6	1.11	0.74
SAC-20-7	1.15	0.75
SAC-20-8	1.42	1.00

Similar to the NIST building, the proposed method tends to overestimate the peak dynamic displacement in the cases with small deformation. For example, according to Table 6 – 23, the peak dynamic displacement is overestimated by 45% by the proposed method in case SAC-20-5. However, since the true peak dynamic displacement obtained by the nonlinear dynamic analysis is 11 mm, and error is only 5 mm. The difference between the peak dynamic displacements obtained by the proposed method and the true peak dynamic displacements range from 5 mm to 20 mm. While the DoD guidelines underestimate the peak dynamic displacement by 3% in the same case. For the critical column loss cases in which large deflection is obtained, the proposed method performs

well, overestimating the peak dynamic displacement by 10% to 20%. However, the DoD guidelines underestimate the values of the peak dynamic displacement in these cases by 1% to 35%.

Based on a trial and error process, the value of α used in all of the cases studies described above is set to 1.3. The results suggest that this is a reasonable number to adopt.

6.7.3 Suitability of the Proposed Approach for Design Office Environment

The proposed method requires 2 nonlinear static simulations in lieu of a dynamic run. While this is more effort than a single nonlinear static run, it is certainly less effort than running a full dynamic simulation, with all of its complications in modeling and data processing. Many commercial software packages can now run nonlinear static simulations, tracking the inelastic response of frame elements and even shell elements. Therefore, conducting the requisite static simulations is certainly within the capabilities of most design offices at present, rendering the method practical and suitable for routine application.

6.8 Summary and Conclusions

In this chapter, several design requirements in the DoD guidelines are evaluated through numerical simulations. In particular, criteria for the tie force method and DIF are evaluated. Existing prototype structures that do not satisfy the tie force criteria are redesigned to satisfy the DoD guidelines and are used in a series of parametric studies. The studies suggest that the tie force method as implemented in the guidelines can effectively protect structures under column loss scenarios. Ensuring adequate tie strength reduces the overall deflection of the structural system significantly under large deformation conditions although this effect is limited when the deformations are small.

Additional simulations showed that the DIF model proposed by the DoD guidelines is deficient, consistently resulting in unconservative estimates of dynamic response. To address this issue, a new method is proposed to compute DIF. The new method is based on energy conservation and requires the results of two nonlinear static analyses. It is shown that the method results in reasonably conservative answers and is practical enough to be applied in a design office environment.

CHAPTER 7

SUMMARY AND CONCLUSIONS

7.1 Summary

This dissertation addressed key facets of structural robustness, focusing specifically on the collapse resistance of seismically-designed steel frame buildings subjected to sudden column loss. The study started with a survey of the literature on progressive building collapse research. Milestone events which motivated research related to this topic were described. Previous numerical and experimental studies on progressive collapse were also reviewed, followed by a description of the methods for assessment and quantification of structural robustness. Studies on probabilistic analysis of progressive collapse and enhancement of collapse resistance were also surveyed. Gaps in the literature were identified and used to formulate the goals of the research study.

One of the key objectives of this work was to investigate how different modeling approximations influence the outcome of collapse simulations. To this end, four types of models of a 10-story prototype building were developed. The models were: 1) a detailed micro model of the full 3-D system, termed M1; 2) a model of the full 3-D system comprised of macro-elements for beams, columns and connections and shell elements for the slab, termed M2; 3) a 3-D micro model of a single frame in the system, termed M3; and 4) a macro model of the frame modeled in M3, termed M4. M1 is the most sophisticated of the models, while M4 is the least complicated. Models M2 and M3 are

bracketed in between M1 and M4 in terms of complexity and their ability to accurately represent collapse response. The models were carefully calibrated and validated against available experimental test data and more refined finite element models. The validation studies showed that the models were able to adequately represent nonlinear dynamic behavior of collapsing buildings and they were therefore deemed reliable for use in the remaining parts of the study.

The effects of common modeling assumptions, such as macro versus micro modeling and planar versus 3-D modeling, were investigated using the four models. To achieve this objective, the responses of the various types of models were compared under similar column loss scenarios. Extensive studies showed that M2, the 3-D macro model, was able to reasonably represent the collapse behavior of the prototype structural system. Given its expediency and accuracy, M2 was then used to carry out a battery of simulations to gain insight into system behavior after loss of internal and external columns in the 1^{st}, 5^{th} and 10^{th} floors.

Parametric studies were conducted to quantify three-dimensional effects, especially those attributed to the slabs and efforts were made to identify the sources of collapse resistance, specifically composite action between the steel beams and composite floor system, slab membrane action and frame action in the moment resisting system. The global effect of the slabs was studied by comparing the responses of M2 and a modified M2 without the slab. The effect of flexural composite action was studied by comparing the responses of M2 and a variant in which slab-beam composite action was eliminated in the slab panels adjacent to the removed column(s). A flexural composite action factor was defined and used to quantitatively study flexural composite action. Incremental dynamic analysis was conducted to illustrate the role of composite action at the various stages of the collapse process. The effect of slab membrane action in resisting progressive collapse was investigated through a series of incremental dynamic analyses that focused on the responses of model variants with different slab tensile strengths. Frame action was investigated by evaluating the ability of planar model M4 to resist collapse.

In the last phase of this work, several design requirements in the Unified Facilities Criteria (UFC 2009) published by the US Department of Defense were evaluated, including Tie Force Method (TFM) and criteria for the calculation of the Dynamic Impact Factor (DIF). To ensure that the analytical results are generally applicable, numerical models for three additional prototype buildings were created using the same modeling approach employed in M2, leading to a pool of 4 buildings with different heights, layouts and designs. It was found the original design of these structures did not satisfy the Tie Force criteria and so the buildings were redesigned to ensure adequate tie strength. The responses of all four structures under column loss scenarios before and after the re-design were then compared to evaluate the efficacy of the TFM procedure in the UFC (2009) criteria. The DIFs of the prototype structures were obtained from the numerical simulations and compared with those computed using the DoD guidelines. It was found the DoD guidelines were not generally accurate nor conservative. To address this deficiency, a new, energy-based approach for assessing the peak dynamic displacement was proposed. In this approach, the results of two separate nonlinear static analyses are used to compute the DIF. Extensive studies were then conducted to assess the characteristics of the new method.

7.2 Conclusions

Within the scope of the studies conducted in this dissertation, the following conclusions can be drawn:

1) There are significant computational benefits to be gained by using models such as M2 or M4 in lieu of M1 and M3. The simulations in this work show that planar representations can lead to reasonable modeling of behavior, especially when failure is not predicted. However, the limitations and implications of their results must be thoroughly understood. For example, as highlighted in this dissertation, planar models tend to see higher deformations and greater force redistribution because the effect of the slab is not accounted for. Moreover, when failure is predicted, planar analysis

significantly overestimated the extent of the vulnerability for the case considered. It is, however, not possible to generalize this statement since, at the other extreme, planar analysis may also underestimate vulnerability, e.g. by predicting localized bay failure that could propagate to a progressive collapse in a 3-D model. These conclusions suggest that a full 3-D analysis, in spite of its computational cost, may be the only sure way to rigorously investigate system robustness.

2) Simulation results show that the prototype building could be more vulnerable to column loss in the upper stories than in the lower ones. This somewhat counter intuitive result stems from the fact that column loss in lower floors could mobilize more of the structure above it to survive than column loss in upper floors. Debris resulting from column loss in higher floors is damaging and was observed to precipitate progressive collapse.

3) Although the seismically designed prototype building could resist progressive collapse after loss of moment columns, it appeared to be particularly vulnerable to loss of interior gravity columns at all floor levels. For example, the simulation results showed that loss of interior gravity columns, such as C-D5-1, C-E5-5, and C-D5-10, precipitated progressive collapse of the structure.

4) Three-dimensional effects, especially those associated with the slabs, are critical in resisting progressive collapse and make significant contributions to structural robustness. Composite action between the slab and the underlying steel beams is particularly influential. The simulations show that composite action reduces deflections when collapse is not imminent and even wards off progressive collapse in one situation that would have led to collapse had composite action not been mobilized. However, composite action can be lost in the final stages of collapse as the slab is damaged due to large deformation demands. Under such conditions, membrane action takes over and becomes a dominant player in the final stages of collapse.

5) The simulations conducted herein suggest that membrane action is a double edged sword. It can help increase the resistance of the building to collapse, but once a threshold is exceeded and the building continues to collapse, membrane action can help promote progressive collapse by pulling on and damaging other components of the structure. Design for collapse accounting for membrane action therefore becomes a balancing act, weighing the potential benefits of membrane action on one hand, and its detrimental effects on the other.

6) Extensive parametric simulations suggest that the Tie Force Method as implemented in the UFC (2009) guidelines can effectively protect structures under column loss scenarios. Ensuring adequate tie strength reduces the overall deflection of the structural system significantly under large deformation conditions although this effect is limited when the deformations are small.

7) The proposed energy-based method for assessing the peak dynamic displacement of a structure after sudden column loss is reasonably accurate and conservative. Although the new method needs two separate nonlinear static analyses, its accuracy compared to the UFC (2009) method makes its attractive for use in a design office environment.

7.3 Recommendations for Future Research

The following research topics are recommended for further research to better understand the progressive collapse behavior of structural systems:

1) *Improved Modeling and Design Guidance:* Since test data on progressive collapse behavior is lacking, current design specifications, e.g. UFC (2009), are primarily adapted from seismic guidelines, in spite of the fact that structural behavior during collapse is different from that during a seismic event. As research results accumulate and with new test data, codification efforts will soon be necessary to: 1) specify minimum level of modeling required for accurate assessment of collapse potential, 2) provide guidance on

how to model structural behavior within linear and nonlinear simulation frameworks, and 3) specify appropriate performance criteria, addressing actions and structural responses that may not typically be considered in earthquake engineering, e.g. the potentially large tension generated by catenary action.

2) *The Role of Seismic Detailing*: It is widely thought that seismic detailing can play an important role in increasing collapse resistance. However, accumulating research evidence in Khandelwal and El-Tawil (2007) and Khandelwal et al. (2008) points to the fact that system layout and strength may play a more important role in mitigating the risks of collapse. In other words, it is more important to prevent the initiation of the collapse process itself rather than to try and control it once it starts. This suggests that stringent seismic detailing may not be as important as is widely believed, particularly for steel frame buildings. Given the additional expenses associated with seismic detailing, it is important to pursue research to determine the minimum level of detailing necessary for buildings at risk for progressive collapse initiating events.

3) *Treatment of Uncertainty*: As is evident from the state-of-the-art, much of the research on progressive collapse has focused on deterministic procedures. Additional work is imperative in incorporating the probabilistic nature of the problem, both from the loading and modeling perspectives.

4) *Economical and easy-to-implement rehabilitation strategies against progressive collapse*: It has been shown in this dissertation that membrane action in the slabs plays an critical role in resisting progressive collapse. Research is needed to investigate whether attaching FRP to the floor slabs can improve the structural robustness. New rehabilitation strategies against progressive collapse using FRP need to be proposed.

REFERENCE

ASCE 41-06. (2007). "Seismic Rehabilitation of Existing Buildings", *American Society of Civil Engineers*, Reston, Virginia.

Agarwal, J., Blockley, D. and Woodman, N. (2003). "Vulnerability of Structural Systems," *Structural Safety*, 25(3), 263-286.

Alashker, Y., El-Tawil, S., and Sadek, F. (2010). "Progressive Collapse Resistance of Steel-Concrete Composite Floors," *Journal of Structural Engineering*, 136(10), 1187-1196.

Alashker, Y. and El-Tawil, S. (2011). "A Design-oriented Model for the Collapse Resistance of Composite Floors Subjected to Column Loss," *Journal of Constructed Steel Research*, 67(1), 84-92.

Alashker, Y., Li, H. and El-Tawil, S. (2011). "Approximations in Progressive Collapse Modeling," *Journal of Structural Engineering*, 137(9), 914-924.

ANSI/AISC 341-10. (2010). "Seismic Provisions for Structural Steel Buildings." *American Institute of Steel Construction*, Chicago, IL.

Arora, J.S., Haskell, D.F., and Govil, A.K. (1980), "Optimal Design of Large Structures for Damage Tolerance," *AIAA Journal*, Vol. 18, No. 5, 563-570.

Astaneh-Asl, A., Jones, B., Zhao, Y. and Hwa, R. (2001). "Progressive Collapse Resistance of Steel Building Floors", *Report Number UCB/CEE-Steel-2001/03*, Dept. of Civil and Environmental Engineering., University of California, Berkeley.

Asprone, D., Jalayer, F., Prota, A. and Manfredi, G. (2010). "Proposal of A Probabilistic Model for Multi-Hazard Risk Assessment of Structures in Seismic Zones Subjected To Blast for the Limit State of Collapse," *Structural Safety*, 32(1), 25-34.

Asprone, D., Jalayer, F., Prota, A. and Manfredi, G. (2011). "Performance of Different Seismic Retrofitting Techniques in Case of Blast Induced Progressive Collapse," *Applied Mechanics and Materials*, v 82, p 485-490.

Bae, S. W., LaBoube, R. A., Belarbi, A. and Ayoub, A. (2008). "Progressive Collapse of Cold-Formed Steel Framed Structures," *Thin-Walled Structures*, 46(7-9), 706-719.

Baker, J. W., Schubert, M. and Faber, M. H. (2008). "On the Assessment of Robustness," *Structural Safety*, 30(3), 253-367.

Bazant, Z. P. and Verdure, M. (2007), "Mechanics of Progressive Collapse: Learning from World Trade Center and Building Demolitions," *Journal of Engineering Mechanics*, 133(3), 308-319

Bazant, Z. P., Le, J., Greening, F. R., and Benson, D. B. (2008). "What Did and Did Not Cause Collaspe of World Trade Center Twin Tower in New York," *Journal of Engineering Mechanics*, 134(10), 892-906.

Bazant, Z. P. and Zhou, Y. (2002). "Why Did the World Trade Center Collapse?- Simple Analysis," *Journal of Engineering Mechanics*, 128(3), 369-370.

Bao, Y., Kunnath, S. K., El-Tawil, S. and Lew, H. S., (2008). "Macromodel-Based Simulation of Progressive Collapse: RC Frame Structures," *Journal of Structural Engineering*, 134(7), 1079-1091.

Bao, Y. and Kunnath, S. K. (2010). "Simplified Progressive Collapse Simulation of RC Frame-Wall Structures," *Engineering Structures*, 32(10), 3153-3162.

Bennett, R. M. (1988). "Formulations for Probability of Progressive Collapse," *Structural Safety*, 5(1), 66-77.

Braverman, J. I., Miller, C. A., Hofmayer, C. H., Ellingwood, B. R., Naus, D. J., and Chang, T. Y. (2004). "Degradation Assessment of Structures and Passive Components at Nuclear Power Plants," *Nuclear Engineering and Design*, 228(1), 283-304.

Byfield, M. P. (2006). "Behavior and Design of Commercial Multistory Buildings Subjected to Blast," *Journal of Performance of Constructed Facilities*, 20(4), 324-329.

Casciati, F., and Faravelli, L. (1984). "Progressive Failure for Seismic Reliability Analysis", *Engineering Structures*, Vol. 6, No. 2, 97-103.

Chao, S-H, Khandelwal, K., and El-Tawil, S. (2006), "Ductile Fracture Initiation in Shear Link Webs," *Journal of Structural Engineering*, ASCE, 132(8), pp. 1192 – 1200.

Cherepanov, G. P. (2006). "Mechanics of WTC Collapse," *International Journal of Fracture*, 141(1-2), 287-289.

Chiaia, B. M. and Masoero, E. (2008). "Analogies between Progressive Collapse of Structures and Fracture of Materials," *International Journal of Fracture*. 154(1-2), 177-193.

Corley, W. G. and Mlakar Sr., P. F., Sozen, M. A. and Thornton, C. H. (1998). "Oklahoma City Bombing: Summary and Recommendations for Multihazard Mitigation," *Journal of Performance of Constructed Facilities*, 12(3), 100-112.

Ellingwood, B., and Leyendecker, E.V. (1978). "Approaches for design against progressive collapse," *Journal of the Structural Division*, ASCE, 104(3), 413-423.

Ellingwood, B. R. (2006). "Mitigating Risk from Abnormal Loads and Progressive Collapse," *Journal of Performance of Constructed Facilities*, 20(4), 315-323.

El-Tawil, S., Vidarsson, E., Mikesell, T., & Kunnath, S. K. (1999). "Inelastic Behavior and Design of Steel Panel Zones," *Journal of Structural Engineering*, 125(2), 183-193.

Ferahian, R. H. (1972). "Buildings: Design for Prevention of Progressive Collapse", *Civil Engineering- ASCE*, February 1972, pp. 66-69.

Foley, C. M., Martin, K., and Schneeman, C. (2009). "Robustness in Structural Steel Framing Systems," *Report MU-CEEN-SE-07-01*, Marquette University, Milwaukee, WI.

Fu, F. (2009). "Progressive Collapse Analysis of High-rise Building with 3-D Finite Element Modeling Method," *Journal of Constructional Steel Research*, 65(5), 1269-1278.

Fu, F. (2010). "3-D Nonlinear dynamic progressive collapse analysis of multi-storey steel composite frame buildings- parametric study," *Engineering Structures*, 32(12), 3974-3980.

Galal, K. and El-Sawy, T. (2010) "Effect of retrofit strategies on mitigating progressive collapse of steel frame structures," *Journal of Constructional Steel Research*, 66(4), 520-531.

Gracia, J., Bayo, E., Ferrario, F., Bursi, O., Braconi, A., and Salvatore, W. (2010). "The Seismic Performance of a Semi-Rigid Composite Joint with a Double-Sided Extended End-Plate. Part I: Experimental Research," *Engineering Structures*, 32(2), 385-396.

Grierson, D. E., Xu, L. and Liu, Y. (2005). "Progressive-Failure Analysis of Buildings Subjected to Abnormal Loading," *Computer-Aided Civil and Infrastructure Engineering*, 20(3), 155-171.

Griffiths, H., Pugsley, A., and Saunders, O. (1968). "Report of Inquiry into the Collapse of Flats at Ronan Point, Canning Town". *Ministry of Housing and Local Government*, London, England.

Gross, J.L., and McGuire, W. (1983). "Progressive Collapse Resistant Design," *Journal of Structural Engineering*, ASCE, 109(1), 1-14.

Gross, J.L. (1998). "A Connection Model for the Seismic Analysis of Welded Steel Moment Frames," *Engineering Structures*, Volume 20, Issues 4-6, pp 390-397.

Gurson, A. L. (1977). "Continuum theory of ductile rupture by void nucleation and growth. Part I: Yield criteria and flow rules for porous ductile media," *Journal of Engineering Materials and Technology*, 99(1), 2-15.

Heidarpour, A. and Bradford, M. A. (2011). "Beam-Column Element for Non-Linear Dynamic Analysis of Steel Members Subjected to Blast Loading," *Engineering Structures*, 33(4), 1259-1266.

Hoffman, S. T. and Fahnestock, L. A. (2011). "Behavior of Multi-Story Steel Buildings under Dynamic Column Loss Scenarios," *Steel and Composite Structures*, 11(2), 149-168.

Hoffman, S. T. (2010). "Behavior and Performance of Steel Moment-Framed Buildings subjected to Dynamic Column Loss Scenarios," *Master thesis*, University of Illinois at Urbana-Champaign, Urbana, Illinois.

House Armed Services Committee (1996). "The Khobar Towers Bombing Incident," *House Armed Services Committee*, Washington, DC.

Hsiao, P. C., Lehman, D. E., & Roeder, C. W. (2012). "Improved Analytical Model for Special Concentrically Braced Frames," *Journal of Constructional Steel Research*, Volume 73, 80-94.

Isobe, D. and Tsuda, M. (2003). "Seismic Collapse Analysis of Reinforced Concrete Framed Structures Using the Finite Element Method," *Earthquake Engineering and Structural Dynamics*, 32(13), 2027-2046.

Izzuddin, B. A., Vlassis, A. G., Elghazouli, A. Y. and Nethercot, D. A. (2008). "Progressive Collapse of Multi-Storey Buildings Due to Sudden Column Loss - Part I: Simplified Assessment Framework," *Engineering Structures*, 30(5), 1308-1318.

Jin, J. and El-Tawil, S. (2005). "Evaluation of FEMA-350 Seismic Provisions for Steel Panel Zones," *Journal of Structural Engineering*, 131(2), 250-258.

Kaewkulchai, G. and Williamson, E. B. (2003). "Dynamic behavior of planar frames during progressive collapse" *Proceedings of 16th engineering mechanics conference*, 2003.

Kaewkulchai, G. and Williamson, E. B. (2004). "Beam Element Formulation and Solution Procedure for Dynamic Progressive Collapse Analysis," *Computer & Structures*, 82(7-8), 639-651.

Kanvinde, A. M. and Deierlein, G. G. (2006), "Void Growth Model and Stress Modified Critical Strain Model to Predict Ductile Fracture in Structural Steels." *Journal of Structural Engineering*, 132(12), 1907-1918.

Kaplan, S., Perla, H. F., and Bley, D. C. (1983). "A Methodology for Seismic Risk Analysis of Nuclear Power Plants," *Risk Analysis*, 3(3), 169-180.

Karns, J. E., Houghton, D. L., Hall, B. E., Kim, J. and Lee, K., (2006) "Blast Testing of Steel Frame Assemblies to Assess the Implications of Connection Behavior on Progressive Collapse," *Proceedings of the Structures Congress: Structural Engineering Research Frontiers*, Long Beach, California, United States, ISBN (print): 978-0-7844-0944-2, Publisher: American Society of Civil Engineers

Karns, J. E., Houghton, D. L., Hall, B. E., Kim, J. and Lee, K., (2007) "Analytical Verification of Blast Testing of Steel Frame Moment Connection Assemblies," *Proceedings of the Structures Congress: Structural Engineering Research Frontiers*, Long Beach, California, United States, ISBN (print): 978-0-7844-0944-2, Publisher: American Society of Civil Engineers

Karns, J. E., Houghton, D. L., Kim, J. and Hong J. K. (2008). "GSA Steel Frame Bomb Blast & Progressive Collapse Test Progressive Report," *General Services Administration*, Washington, DC.

Kennedy, R. P., Cornell, C. A., Campbell, R. D., Kaplan, S., and Perla, H. F. (1980). "Probabilistic Seismic Safety Study of an Existing Nuclear Power Plant," *Nuclear Engineering and Design*, 59(2), 315-338.

Kennedy, R. P., & Ravindra, M. K. (1984). "Seismic Fragilities for Nuclear Power Plant Risk Studies," *Nuclear Engineering and Design*, 79(1), 47-68.

Khandelwal, K., and El-Tawil, S. (2007). "Collapse behavior of steel special moment resisting frame connections," *Journal of Structural Engineering*, 133(5), 646-655.

Khandelwal, K. (2008). "Multi-Scale Computational Simulation of Progressive Collapse of Steel Frames," *PhD Thesis*, University of Michigan, Ann Arbor, MI.

Khandelwal, K., El-Tawil, S., Kunnath, S. K., and Lew, H. S. (2008). "Macro-model based simulations of progressive collapse: steel frame structures," *Journal of Structural Engineering*, 134(7), 1070-1078.

Khandelwal, K., El-Tawil, S., and Sadek, F. (2009). "Progressive Collapse Analysis of Seismically Designed Steel Braced Frames," *Journal of Constructional Steel Research*, 65(3), 699-708.

Khandelwal, K. and El-Tawil, S. (2011). "Pushdown resistance as a measure of robustness in progressive collapse analysis," *Engineering Structures*, 33(9), 2653-2661.

Kim, J. and An, D. (2009). "Evaluation of Progressive Collapse Potential of Steel Moment Frames Considering Catenary Action," *Structural Design of Tall and Special Buildings*, 18(4), 455-465.

Kim, H. S., Kim, J. and An, D. W. (2009). "Development of Integrated System for Progressive Collapse Analysis of Building Structures Considering Dynamic Effects," *Advances in Engineering Software*, 40(1), 1-8.

Kim, T. and Kim, J. (2009a). "Progressive Collapse-Resisting Capacity of Steel Moment Frames Considering Panel Zone Deformation," *Advances in Structural Engineering*, 12(2), 231-240.

Kim, T. and Kim, J. (2009b). "Collapse analysis of steel moment frames with various seismic connections," *Journal of Constructional Steel Research*, 65(6), 1316-1322.

Kim, J., and Kim, T. (2009c). "Assessment of progressive collapse-resisting capacity of steel moment frames," *Journal of Constructional Steel Research*, 65(1), 169-179.

Kim, T., Kim, J. and Park, J. (2009). "Investigation of Progressive Collapse-Resisting Capability of Steel Moment Frames Using Push-Down Analysis," *Journal of Performance of Constructed Facilities*, 23(5), 327-335.

Kim, J., Lee, Y. and Choi, H. (2011a). "Progressive Collapse Resisting Capacity of Braced Frames," *Structural Design of Tall and Special Buildings*, 20(2), 257-270.

Kim, J., Lee, S. and Choi, H. (2011b). "Progressive Collapse Resisting Capacity of Moment Frames with Viscous Dampers," *Structural Design of Tall and Special Buildings*, 11(5), Article in Press.

Kim, J. and Jung, M. (2011). "Progressive Collapse-Resisting Capacity of Modular Mega-Frame Buildings," *Structural Design of Tall and Special Buildings*, doi: 10.1002/tal.697.

Kim, J., Park, J. H. and Lee, T. H. (2011). "Sensitivity Analysis of Steel Buildings Subjected To Column Loss," *Engineering Structures*, 33(2), 421-432.

Krawinkler, H. (1978). "Shear in Beam-Column Joints in Seismic Design of Steel Frames," *Engineering Journal*, 15(3), 82-91.

Kwasniewski, L. (2010). "Nonlinear dynamic simulations of progressive collapse for a multistory building," *Engineering Structures*, 32(5), 1223-1235.

Lavan, O., Sivaselvan, M. V., Reinhorn, A. M. and Dargush, G. F. (2009). "Progressive Collapse Analysis through Strength Degradation and Fracture in the Mixed Lagrangian Formulation," *Earthquake Engineering and Structural Dynamics*, 38(13), 1483-1504.

Lee, K. and Foutch, D. A. (2002), "Performance evaluation of new steel frame buildings for seismic loads," *Earthquake Engineering & Structural Dynamics*, 31(3), 653–670. doi: 10.1002/eqe.147.

Lewicki, B. and Olesen, S.O. (1974). "Limiting the Possibility of Progressive Collapse," *Building Research & Practice*, 2(1), 10-13.

Leyendecker, E.V. and Ellingwood, B.R. (1977). "Design to reduce the risk of progressive collapse," *Building Science Series 98*, National Bureau of Standards, Washington, D.C.

Li, H. and El-Tawil, S. (2013). "Three-Dimensional Effects and Collapse Resistance Mechanisms in Steel Frame Buildings". *Journal of Structural Engineering*. doi: 10.1061/(ASCE)ST.1943-541X.0000839

Liu, Y., Xu, L. and Grierson, D. E. (2010). “Influence of Semi-rigid Connections and Local Joint Damage on Progressive Collapse of Steel Frameworks,” *Computer-Aided Civil and Infrastructure Engineering*, 25(3), 184-204.

Main, J. A. (2009). "Development of 3D models of steel moment-frame buildings for assessment of robustness and progressive collapse vulnerability,” *Proceedings of the 2009 Structures Congress*, Austin, Texas.

Main, J. and Sadek, F. (2012). “Robustness of Steel Gravity Frame Systems with Single-Plate Shear Connections,” *NIST Technical Note 1749*, National Institute of Standards and Technology, Gaithersburg, MD.

Masoero, E., Wittel, F. K., Herrmann, H. J., and Chiaia, B. M. (2010). “Progressive Collapse Mechanisms of Brittle and Ductile Framed Structures,” *Journal of Engineering Mechanics*, 136(8), 987-995.

McGuire, W. (1975). “Prevention of progressive collapse,” presented at the Jan., 1975, *ASCE International Association for Bridge and Structural Engineering Regional Conference on Tall Buildings*, Asian Institute of Technology, Bangkok, Thailand.

McConnel, R.E. and Kelly, S.J. (1983). “Structural Aspects of Progressive Collapse of Warehouse Racking,” *The Structural Engineer*, Vol. 61A, No.11, 343-347.

Mlakar Sr., P. F., Corley, W. G., Sozen, M. A. and Thornton, C. H. (1998). “Oklahoma City Bombing: Analysis of Blast Damage to the Murrah Building,” *Journal of Performance of Constructed Facilities*, 12(3), 113-119, 1998.

Mohamed, O. A. (2009). “Assessment of progressive collapse potential in corner floor panels of reinforced concrete buildings,” *Engineering Structures*, 31(3), 749-757.

Mulas, M. G. (2004). A Structural Model for Panel Zones in Non-Linear Seismic Analysis of Steel Moment-Resisting Frames. Engineering structures, 26(3), 363-380.

Naji, A. and Irani, F. (2011). "Simplified Procedure for Progressive Collapse Analysis of Steel Structures," *Advanced Materials Research*, v 255-260, p 482-486.

National Institute of Standards and Technology (NIST). (2005). "Final Report on the Collapse of the World Trade Center Towers," S. Shyam Sunder, Lead Investigator, *National Institute of Standards and Technology*, Gaithersburg, MD. (248 pgs.).

Nie, J., Qin, K., and Cai, C. S. (2008). "Seismic Behavior of Connections Composed of Cfsstcs and Steel–Concrete Composite Beams—Finite Element Analysis," *Journal of Constructional Steel Research*, 64(6), 680-688.

Park, J. and Kim, J. (2010). "Fragility Analysis of Steel Moment Frames with Various Seismic Connections Subjected To Sudden Loss of a Column," *Engineering Structures*, 32(6), 1547-1555.

Pearson, C. and Delatte, N. (2005). "Ronan Point Apartment Tower Collapse and Its Effect on Building Codes," *Journal of Performance of Constructed Facilities*, 19(2), 172-177.

Pirmoz, A. (2011). "Performance of Bolted Angle Connections in Progressive Collapse of Steel Frames," *Structural Design of Tall and Special Buildings*, 20(3), 349-370.

Pretlove, A.J. (1986). "Dynamic Effects in Fail-Safe Structural Design," In: *Proceedings, International Conference on Steel Structures: Recent Advances and their Application to Design*, Budva, Yugoslavia, 749-757.

Ruth, P., Marchand, K. A., and Williamson, E. B. (2006). "Static equivalency in progressive collapse alternate path analysis: reducing conservatism while retaining structural integrity," *Journal of Performance of Constructed Facilities*, 20(4), 349-364.

Sadek, F., El-Tawil, S. and Lew, H. S. (2008). "Robustness of Composite Floor Systems with Shear Connections: Modeling, Simulation, and Evaluation," *Journal of Structural Engineering*, 134(11), 1717-1725.

Sadek, F., Main, J. A., Robert, S. D., Chiarito, V. P. and El-Tawil, S. (2010). "An Experimental and Computational Study of Steel Moment Connections under a Column Removal Scenario," *NIST Technical Note 1669*, National Institute of Standards and Technology, Gaithersburg, MD.

Sadek, F., Main, J. A., Lew, H. S. and Bao, Y. (2011). "Testing and Analysis of Steel and Concrete Beam-Column Assemblies under a Column Removal Scenario," *Journal of Structural Engineering*, 137(9), 881-892.

Scott, M. H. and Fenves, G. L. (2010). "Krylov Subspace Accelerated Newton Algorithm: Application to Dynamic Progressive Collapse Simulation of Frames," *Journal of Structural Engineering*, 136(5), 473-480.

Seffen, K. A. (2008). "Progressive Collapse of the World Trade Center: Simple Analysis," *Journal of Engineering Mechanics*, 134(2), 125-132.

Shen, J., and Astaneh-Asl, A. (2000). "Hysteresis Model of Bolted-Angle Connections", *Journal of Constructional Steel Research*, 54(3), 317-343.

Sozen, M. A., Thornton, C. H., Corley, W. G., and Mlakar Sr., P. F. (1998). "Oklahoma City Bombing: Structure and Mechanics of the Murrah Building," *Journal of Performance of Constructed Facilities*, 12(3), 113-119.

Song, B. I. and Sezen, H. (2009). "Evaluation of an existing steel frame building against progressive collapse," *Proceedings of the 2009 Structure Congress*, 1878-1885, Austin, Texas.

Starossek, U. (2007). "Typology of Progressive Collapse," *Engineering Structures*, 29(9), 2302-2307.

Starossek, U. and Haberland, M. (2008), "Measures of Structural Robustness-Requirements & Applications," *Proceedings of the 2008 Structures Congress*, v 314, Vancouver, Canada.

Szuladzinski, G. (2008). "Discussion of 'Mechanics of Progressive Collapse: Learning from World Trade Center and Building Demolitions' by Zdenek P. Bazant and Mathieu Verdure," *Journal of Engineering Mechanics*, 134(10), 913-915.

Szyniszewski, S. (2009). "Probabilistic approach to progressive collapse prevention. Physics based simulations," *Proceedings of the 2009 Structures Congress*, Austin, Texas.

Tsitos, A. (2009). "Experimental and Numerical Investigation of the Progressive Collapse of Steel Frames," *PhD Thesis*, Department of Civil, Structural and Environmental Engineering, University at Buffalo, State University of New York. Buffalo, NY.

UFC (2009). "UFC 4-023-03: Design of Buildings to Resist Progressive Collapse," *Department of Defense*, Washington, DC.

U.S. General Service Administration (GSA) (2003). Progressive collapse analysis and design guidelines for new federal office building and major modernization project", *U.S. General Service Administration*, Washington, D.C.

Weigand, J. M., Meissner, J. E., Francisco, T., Berman, J. W., Fahnestock, L. A., and Liu, J. (2012). "Overview of AISC/NSF Structural Integrity Research and Preliminary Results". *Proceedings of Structures Congress 2012*. 135-145, Chicago, IL.

Williamson, E. B. and Stevens, D. J. (2009). "Modeling Structural Collapse including Floor Slab Contributions," Proceedings of the 2009 Structures Congress, 2046-2054, Austin, Texas.

Xu, G. and Ellingwood, B. R. (2011a). "An Energy-Based Partial Pushdown Analysis Procedure for Assessment of Disproportionate Collapse Potential," *Journal of Constructed Steel Research*, 67(3), 547-555.

Xu, G. and Ellingwood, B. R. (2011b). "Disproportionate Collapse Performance of Partially Restrained Steel Frames with Bolted T-stub Connections," *Engineering Structures*, 33(1), 32-43.

Xu, G. and Ellingwood, B. R. (2011c). "Probabilistic Robustness Assessment of Pre-Northridge Steel Moment Resisting Frames," *Journal of Structural Engineering*, 137(9), 925-934.

Yang, B., & Tan, K. H. (2012). "Robustness of Bolted-Angle Connections against Progressive Collapse: Experimental Tests of Beam-Column Joints and Development of Component-Based Models," *Journal of Structural Engineering*. Article in press.

Yu, M., Zha, X. and Ye, J. (2010). "The Influence of Joints and Composite Floor Slabs on Effective Tying of Steel Structures in Preventing Progressive Collapse," *Journal of Constructed Steel Research*, 66(3), 442-451.

Zhang, X., and Ricles, J. M. (2006). "Seismic Behavior of Reduced Beam Section Moment Connections to Deep Columns," *Journal of Structural Engineering*, 132(3), 358-367.